FACULTY OF ENGINEERING AND APPLIED SCIENCE

INSTITUTE OF SOUND & VIBRATION RESEARCH

A PARAMETRIC STUDY OF IMPACT NOISE

by

J.M. CUSCHIERI

A Thesis submitted for the Degree

of

Doctor of Philosophy

University of Southampton

April 1983

ABSTRACT

FACULTY OF ENGINEERING AND APPLIED SCIENCE

INSTITUTE OF SOUND AND VIBRATION RESEARCH

Doctor of Philosophy

A PARAMETRIC STUDY OF IMPACT NOISE

by

Joseph M. Cuschieri

The noise radiated due to impact can be divided into two parts, that part which is radiated only during the impact, that is, during the forced movement of the structure and that part which is radiated after the impact has occured, and is due to the local vibrations of the structure. The former part is termed acceleration noise because it originates from the sudden acceleration or deceleration of the structure. The part, radiated after the impact has occured, is due to the vibrational energy that escapes into the structure during the impact. This is termed as ringing noise.

The vibrational energy can be either radiated as noise (ringing noise) or else dissipated as heat in the structure due to the structural damping. If a balance is set up between the input energy and the radiated and dissipated energies, the noise energy radiated can be expressed in terms of the structural response at the point of impact, the structural loss factor and the radiation efficiency of the structure and the inpact force spectrum.

This thesis investigates this relationship with special emphasis on the structural response and force pulse terms. The response of some common structures is presented to show the effect of stiffening and other structural changes on the response. Since, it is not always

possible to estimate the response, a relation is given between the point response and the ratio of spatial average velocity squared to the excitation force.

Since generally in noise energy measurements, no distinction is made between the acceleration noise and the ringing noise, the spectral content of the acceleration noise is investigated. It is shown that the acceleration noise energy spectrum is independent of the exact details of the structure shape and the impact force pulse, and is only related to the contact duration of the impact, the total size of the structure and the averaging time over which the noise is being measured.

These parametric relations for noise due to impact are investigated for a flat plate structure and a diesel engine structure. The modification of the structural response for large noise reductions is shown in the case of the plate. Using this insight on the relation between noise radiated and structure response, ideas for the reduction of noise from a diesel engine by structural changes are suggested.

The final part looks at the applicability of active force cancellation in the case of impact excitation and comments on the effect of bending moment excitation if the cancelling forces are not coincident with those involved in the machine work process. A test-rig is constructed to study the limitations and the controlling parameters on the total noise reduction by the application of an active force system.

ACKNOWLEDGEMENTS

The author gratefully acknowledges the guidance, encouragement and constructive criticism of Professor E.J. Richards during the work on this project. His practical insight in this field was a great help in the solution of many problems encountered during this thesis.

Thanks are due to all the author's colleagues in the Structures and Machinery Group for their constant encouragement and fruitful discussions, and to all the I.S.V.R. technicians for their help. The author would also like to thank the Science and Engineering Research Council for the financing of this work.

Finally, special thanks to my wife, Liliana for typing this thesis and for her patience during the long hours of work.

CONTENTS

LIST OF FIGURES

TABLES

CHAPTER I

INTRODUCTION

I. 1. Review of Literature

Noise generated from all types of industrial machines is receiving a great deal of attention since legislation limiting the maximum levels of noise energy that an operator and other nearby machine operators can be exposed to daily is becoming more imminent. The prime cause of industrial noise is the short duration contact of machine parts; such as the impact of the hammer and anvil in drop forges, the punching in punch presses, the combustion and piston slap in diesel engines, backlash in ball bearings, the clashing of bottles and cans in bottling lines, the hammering of pile drivers and other rock drilling etc. These result in impact excitation of the machine structure and the workpiece. Some of the impacts that occur in industry are not always necessary. Punch presses and forge hammer impacts do useful work and these impacts are the operation of the machine. However, impacts from transfer of material when thrown down shutes or into stillages are unnecessary but they still contribute to the factory noise level. The elimination of these unnecessary noise sources and of the machinery noise is to be of importance because of the coming legislation.

The noise radiated from a structure, including the structural damping and the radiation loss factor has been investigated by a number of researchers in this field, especially in the case of continuous excitation. Cremer et al [1] investigated the nature and propagation of structure-borne sound and the effect of modifications in the structure on the transmission of vibrational energy. Also included is the development of structural damping with an investigation of the different damping mechanisms to increase the structural loss factor. Ver and Holmer [2] did similar work and related the noise radiated from a plate structure to that from a piston of the same size to obtain a radiation efficiency curve for the plate. Also a relation is developed between the sound power radiated and the input vibrational

power to the structure. Another investigation is the control of noise from impacts by softening of the blow. Maidanik [3] also investigates the radiation efficiency of structures, and uses the assumption of an average level of response in the case of large complex structures, similar to machine structures, where a large number of modes are present.

Morse and Ingard [4] study the interaction between acoustic waves and the vibrating structure in very great detail, involving high level mathematics. This is both an advantage and a disadvantage; it gives very accurate estimates of the noise radiated from a structure, but generalisations are not very easy to deduce. An important section in this reference is the interaction of acoustic waves with the vibrating structure in the case where fluid loading cannot be ignored like in the case of underwater excitation.

Identification of noise sources and noise control measures at source have been developed over the past few years. However, most of these investigations resulted in ad-hoc empirical relations between the noise generated and the operation of the machine. The noise control measures suggested, usually take the form of enclosures around the machine structure, which while they may temporarily solve the problem, they can hardly be thought of as permanent solutions. This is because of the number of problems that enclosures create; access to the machine is restricted, the operator is reluctant to fit the enclosure back on after maintenance, parts of the enclosure do not stand up for long periods due to the extreme conditions that certain machine operators create, and in any case they are expensive.

Other investigations suggest methods to reduce the noise radiated from machine structures by relating the noise radiated to the machine operation. Evensen studied the noise radiated from a punch press during blanking [5] and related the radiated noise to changes in the force pulse shape and to the shape of the unloading of the press during fracture when blanking. There is no relation other than with the force shaping and nothing is given on how other parameters which affect the noise radiated can be modified for noise control. The

tailoring of the shape of the force pulse is not always desired by either the operator or the manufacturer because of lower production.

The noise radiated from plates due to impact has been investigated by Benedetto et al [6], where he gives an expression for the sound radiated from a thin square plate when impacted by a sphere. Bolgov and Nikiforov [7] also studied the noise radiated from flexural vibrations of an infinite plate when transversely impacted. In both these papers, the relation between the noise radiated and the parameters of the plate are very complicated to extract and nothing at all can be deduced from such relationships, except to estimate the radiated noise from a particular plate. Machine structures are seldom only of plate-like constructions and such complicated equations cannot therefore be extensively used.

Endo et al [8] investigates the noise radiated from circular cylinders when impacted both longitudinally and transversely by an elastic sphere. This paper gives experimental results backed by theory which can only be used for the specific cases of impacts in cylinders. Although some of the results can be applied to other types of structures, hardly any quantitative measures can be given to modifications of the structure to control the radiation of noise. The parameters of the structure that effect the noise energy radiated are not specified and only changes due to impact velocities and size of structure are given.

The reduction in noise energy radiated by a plate structure due to the addition of damping is investigated in the paper by Holmer & Lagace [9]. This investigation goes some way in determining the different parameters involved in the radiation of sound from a plate but there are no generalisations to other forms of structures. The theory and experimental results presented are only applicable to a plate and are tested for a hopper, and most of the results are directed at the effect that damping will have on the radiation of noise energy. One result which is worth mentioning is that if the addition of damping does not appreciably change the stiffness and surface density of the structure, then the reduction in the noise energy radiated is directly dependent on the increase of damping.

The work by Goyder and White [10] and Pinnington and White [11] on the flow of energy from the point of excitation to the rest of a structure goes some way in specifying the parameters that influence the vibrational energy that escapes into a structure. Their work investigated the relation between the flow of power into a structure and the excitation force and structural response. In the work by Pinnington, it is shown that the exact detail of the response of the structure is not important; only the mean and peak levels of vibration are needed. This leads to the study of more complicated systems in the estimation of power flow from one system to the other. The work mainly deals with continuous or random excitation, but it can be easily adopted for the case of impulsive excitation to estimate the flow of energy for each impact. Also other investigations are done on the flow of power when the excitation point is not just a single point but a number of different points.

Another important work in the field of structural response and mean levels of response is by Skudrzyk [12] who investigates the mean levels of vibration for different types of structures under different types of excitation. His work does not deal with the power flow at all but there is a direct relationship since the average power flow is directly dependent on the mean value of the structure response if the excitation force in the frequency domain is constant. This work, together with the work by Goyder & White and Pinnington and White provide some generalisation in the solution of the vibration levels in complicated structures.

As one can see, little work has been done on the relation of noise radiated by a structure and the structural response, except perhaps relating radiated noise to the surface velocity of a structure. Richards et al in his series of papers [13-15] on the prediction of impact noise from machine structures goes a long way in bringing together structural response and radiated noise. Previously, a lot of work has been done on structures and on acoustics; the propagation of sound waves in different media, but never has the relation between structural response and noise radiated been investigated. The work

by Richards does not only make a good attempt at obtaining a relation between noise radiated and structural response, but also by the elimination of minute details, he obtained generalised results which are very useful in practice. These results can be used by engineers without deep knowledge of acoustics or structures. The noise radiated is related to a single impact which thus permits the investigation of pulse shaping, repetition rate and the machine process. In its present form, the noise radiated can be estimated in broad bands, that is, an average over all modes in a bandwidth, but this can be further developed to estimate the noise radiated in narrow band analysis. This made possible the tackling of noise at source where high noise reduction can be obtained without keeping the operator away from his machine.

I. 2. Development of the Energy Accountancy Concept

The ringing noise energy radiated from a structure when excited by an impact can be estimated using an energy accountancy concept [15]. Some of the energy developed by the machine in the work process goes into the work done and some escapes into the machine structure and workpiece which are left in a state of vibrational motion.

$$E_{in} = E_{work} + E_{escape} \qquad (1.1)$$

where E_{in} is the energy developed by the machine;
E_{work} is the work done by the machine; and
E_{escape} is the energy that escapes into the machine structure.

E_{escape} is either radiated as noise (E_{rad}) or dissipated as heat due to the structural damping ($E_{structure}$). It is assumed that the foundation and workpiece can be considered as being part of the machine structure with their own radiation efficiency. Thus

$$E_{escape} = E_{rad} + E_{structure} \qquad (1.2)$$

The noise radiated from a structure is given by

$$E_{rad} = \rho_o c_o A \sigma_{rad} \overline{\langle V^2 \rangle} \qquad (1.3)$$

where $\rho_o c_o$ is the acoustic impedance of the surrounding medium, air;

A is the surface area of the structure;

σ_{rad} is the radiation efficiency of the structure; and

V is the normal velocity of the structure surface.

$\langle\ \rangle$ and $\overline{\ }$ denote spatial and time averaging respectively. From the definition of structural loss factor, the energy lost due to the structural damping is given by

$$E_{structure} = \pi f \eta_s \rho_m A d \overline{\langle V^2 \rangle} \qquad (1.4)$$

where η_s is the structural loss factor;

d is the bulkiness or thickness of the structure;

ρ_m is the material density of the structure; and

f is the frequency of radiation.

From equations (1.2), (1.3) and (1.4) an expression for the noise energy radiated can be obtained, viz.

$$E_{rad}(f) = \frac{E_{escape}(f)\, \sigma_{rad}}{\sigma_{rad} + \frac{\pi f \eta_s d \rho_m}{\rho_o c}} \qquad (1.5)$$

For machine structures which have a high structural damping, because of the many parts which are bolted together, σ_{rad} in the denominator of equation (1.5) can be neglected. However, this is

not essential in the understanding of the different parameters that influence the noise energy radiated.

The energy that escapes into the structure during the impact is equal to the integration of the product of impact force and the velocity of the structure at the impact point and in the same direction of the impact, over the time of impact. In the frequency domain, this can be expressed as

$$E_{escape} = \int_0^\infty \frac{|\dot{F}(f)|^2}{2\pi f} \cdot \text{Im}\,[H(f)]\, df \qquad (1.6)$$

where $|\dot{F}(f)|$ is the modulus of the force derivative spectrum and $\text{Im}\,[H(f)]$ is the structural response at the point of impact defined as the ratio of the velocity in the direction of the force $V(f)$, to the force derivative $\dot{F}(f)$. If we are interested in that in a bandwidth Δf centred on frequency f, we can write

$$E_{escape}\,(f,\Delta f) = \frac{1}{2\pi} |\dot{F}(f)|^2 \cdot \text{Im}\,[H(f)] \cdot \frac{\Delta f}{f} \qquad (1.7)$$

This expression for E_{escape} holds for both narrow band and wide band analysis. In the case of the latter, an average value over several modes for $\text{Im}\,[H(f)]$ can be assumed, while in narrow band analysis, the details of $\text{Im}\,[H(f)]$ have to be known.

Expressing the radiated noise energy from a machine structure in an equivalent power level, assuming one impact per second, the A-weighted radiated noise in frequency band Δf with central frequency f

$$L_{eq}(A,f,\Delta f) = 10 \log |\dot{F}(f)|^2 + 10 \log \text{Im}\,[H(f)] + 10 \log \left(\frac{A\sigma_{rad}}{f} \right)$$

$$- 10 \log \eta_s - 10 \log d + 10 \log \left(\frac{\rho_o c}{2\pi^2 \rho_m} \cdot \frac{\Delta f}{f} \right) \qquad (1.8)$$

If N impacts occur per second, then another term 10 log N is included in equation (1.8). The $L_{eq}(A)$ is the average A-weighted level of noise radiated. It is a summation over all frequency bands and number of impacts occuring during the time of averaging. If this represents the energy received by the machine operators, it should not exceed 90 dBA in total over an eight-hour period by the present code of practice. The equivalent level is used because of the impulsive nature of the noise.

Equation (1.8) shows that the energy radiated by a structure can be expressed in terms of such structure parameters as: structural response, structural damping, bulkiness and radiation efficiency, and the operation of the machine (if the structure is a machine structure) or the mechanics of the impact. Therefore, this equation gives the contribution that each of these parameters has on the noise radiated. The change in the radiated noise due to modifications of more than one parameter can be computed by estimating the effect due to each parameter and then summing all these contributions linearly to obtain the total noise reduction. Therefore, from this equation, we can estimate which parameters will give the highest noise reduction and by how much.

I. 2.1. Relevant Parameters in Impact Noise

In the expression for the noise energy radiated in a bandwidth Δf, we can assume $|\dot{F}(f)|^2$ to be constant and take an average value of $\text{Im}\,[H(f)]$, which need not take into account the frequency variations of the term in each resonant mode. Needless to say, the higher the modal density in the band, the more justifiable will be this approach.

This is an added advantage when using the accountancy equation in the design stage because the exact point response of the structure is not needed, but it may be approximated to by an infinite structure of the same plate thickness, the mean response of which is known. The driving point mobilities of structures and corresponding point mobilities for similar structures but of infinite extent are given

in [10] and [12] with a more in depth study in Chapter II. The term H(f) is related to mobility by the factor $1/j\omega$, $(1/j2\pi f)$. The same response as that for continuous excitation can be used, and the change between continuous and single impacts is incorporated in the shape of the force derivative spectrum.

Sometimes, the structure which is the most efficient radiator is not excited directly but through some other structure or series of structures. Examples are the dies and die holder mounted on the anvil for a drop hammer, and the bearing caps bolted onto the engine frame of a diesel engine. At medium frequencies, the dies and holder are very poor radiators, but the anvil is a good radiator. This applies also for the bearing caps in engines; the caps are inefficient radiators, while the engine frame is a good radiator. Close covers wrapped around engine frames via a resilient interlayer present further examples.

Under such conditions, the system can be considered to be made up of a source structure (in the preceding examples, the dies and holder), a receiver structure (the anvil), and a form of isolator in between, which itself may consist of other types of structures. This system can be represented schematically by a source, isolator, receiver (figure 1.1). The energy escape into the receiver structure has been computed in terms of the transfer mobilities and point mobilities of the system components [11] for various combinations of the source structure and receiver structure. The point response for a source-isolator-receiver system is given by (figure 1.1)

$$\text{Im}\,[H(f)] = \frac{1}{2\pi f}\,\frac{|M_{12}|^2}{\left|M_2 + M_R + \frac{2\pi f}{k}(j + \eta_s)\right|^2}\,\text{Real}\,[M_R] \qquad (1.9)$$

where

M_{12} - transfer mobility between points 1, excitation point and 2, attachment point of the source structure;

M_2 - point mobility at the point of attachment of source structure;

M_R - point mobility of receiver;

$\frac{2\pi f}{k}(j + \eta_s)$ - mobility of isolators;

η_s - loss factor; and

k - stiffness of isolator.

Each of these terms varies with frequency and exhibits peaks and troughs at the structure's resonances and anti-resonances. However, a mean average value similar to the mean response for direct excitation can be computed, in this case by frequency averaging this expression. This value for $\text{Im}\,[H(f)]$ is used in the accountancy equation to estimate the noise energy radiated from a structure which is not directly excited.

This equation can also be used to estimate the response when the structure is modified for noise control. From equation (1.8), one method to reduce the noise radiated is to reduce the E_{escape} term, which can be done by lowering the response level of the structure. If the structure is made more rigid, less energy is transferred on impact, and the energy will remain in the impactor.

The next parameter to consider is that of the force pulse. As in the frequency domain, the force term can be expressed easily in terms of any of its derivatives, we prefer to study a derivative that is effectively flat at the dominant frequency of the noise. As the radiation efficiency is zero at zero frequency, a static (zero frequency) force gives rise to no noise: thus, it is more sensible to work in terms of $\dot{F}(f)$ or $\ddot{F}(f)$ or any other derivative that is flat with frequency; thus the prediction of the first derivative is emphasised.

The shape of the force pulse and magnitude in the time domain can be easily measured or computed, but to obtain the energy spectrum of such an impulse it will necessitate the use of a frequency analyser. In Appendix A a method is given on how the spectrum shape and magnitude can be approximated using the force pulse and its derivatives in the time domain. This method will allow the spectrum of the pulse to be computed from time measurements. The operation of a machine can only be described in the time domain, therefore by relating the spectrum to measurements in this domain, possible tailoring of the pulse to achieve a desired spectrum can be worked out more easily. In the experimental tests done, the true spectrum and the calculated approximate spectrum obtained using the method in Appendix A are both presented on the same figures. However, for estimating the sound energy radiated the approximate spectrum is used.

Another reason for using the approximate envelope for the force derivative spectrum is that in [7], it is shown that the pulse from a rigid body (sphere) hitting a plate in an elastic impact, has a finite slope at t=0. From measurements, all pulses have a zero starting slope. The Fourier transform of a pulse will consist of a main lobe and a series of side lobes and the rate of decay will depend upon the number of derivatives that are possible within the interval of the pulse (see Appendix A). Thus, if theoretically it is proved that the slope at t = 0 is not zero, then the zero slope in the measurement may be due to a computer transient, and if this is eliminated, but keeping the maximum slope constant, the Fourier transform at the high frequency increases in level. By using the maximised envelope , this problem is eliminated, but with the result that there is an overestimate at the high frequency end. At the region of maximum force derivative spectrum, the envelope is within 1 dB of the Fourier transform, figure (1.2.) shows the change in level due to the small correction in the pulse shape at t = 0, and also a comparison between the Fourier transform as computed using a digital frequency analyser and the approximation method. In the region of the

maximum level, the approximation is within 1dB of the computed results.

Another characteristic of the $|\dot{F}(f)|^2$ spectrum is that, if the impact is softened, the maximum of this spectrum is shifted towards the low frequencies. This is shown in the results for the plate experiments in Chapter V. Thus, if the response of the structure is not altered, the vibrational energy that escapes into the structure in the case of a soft impact is at a lower frequency range. Also, with a longer contact duration, the maximum impact force is reduced for the same impact velocity which results in a lower level for the $|F(f)|^2$ spectrum. That is, less energy escapes into the structure. This can be explained as follows: the contact time is increased by placing a resilient insert at the point of impact. During the impact, the resilient pad is compressed and stores the energy lost by the impactor in coming to rest. Some of this stored energy is transferred to the structure and the rest is transferred back to the impactor which rebounds. Thus, the structure is left with a lower energy as compared to a direct impact.

The remaining parameters to be discussed are those of the structural loss factor η_s and of the modified radiation efficiency $10 \log \frac{A\sigma_{rad}}{f}$. The loss factor η_s is the ratio of the energy lost in heat in the structure per cycle to the maximum strain energy of the structure, and can be measured or estimated in the case of simple structures. In reference [14], various curves for σ_{rad} against frequency are presented for different structures in various forms of vibrational motion.

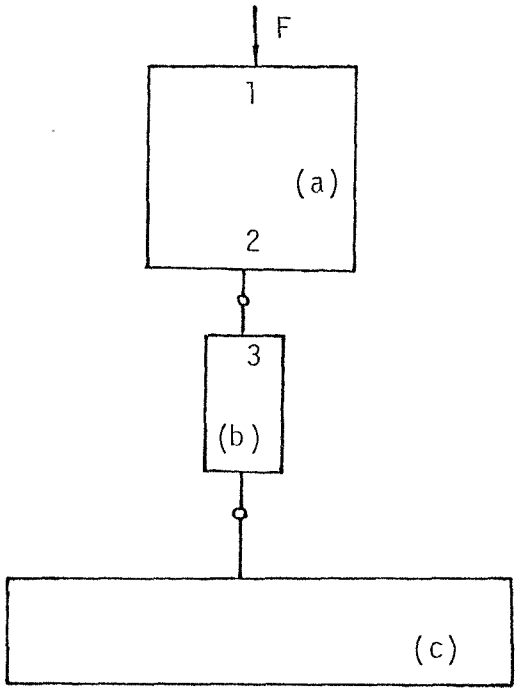

figure 1.1. Source-Isolator-Receiver system, Point force excitation; (a) source, (b) isolator with complex stiffness $k(1 + j\eta)$, (c) receiver.

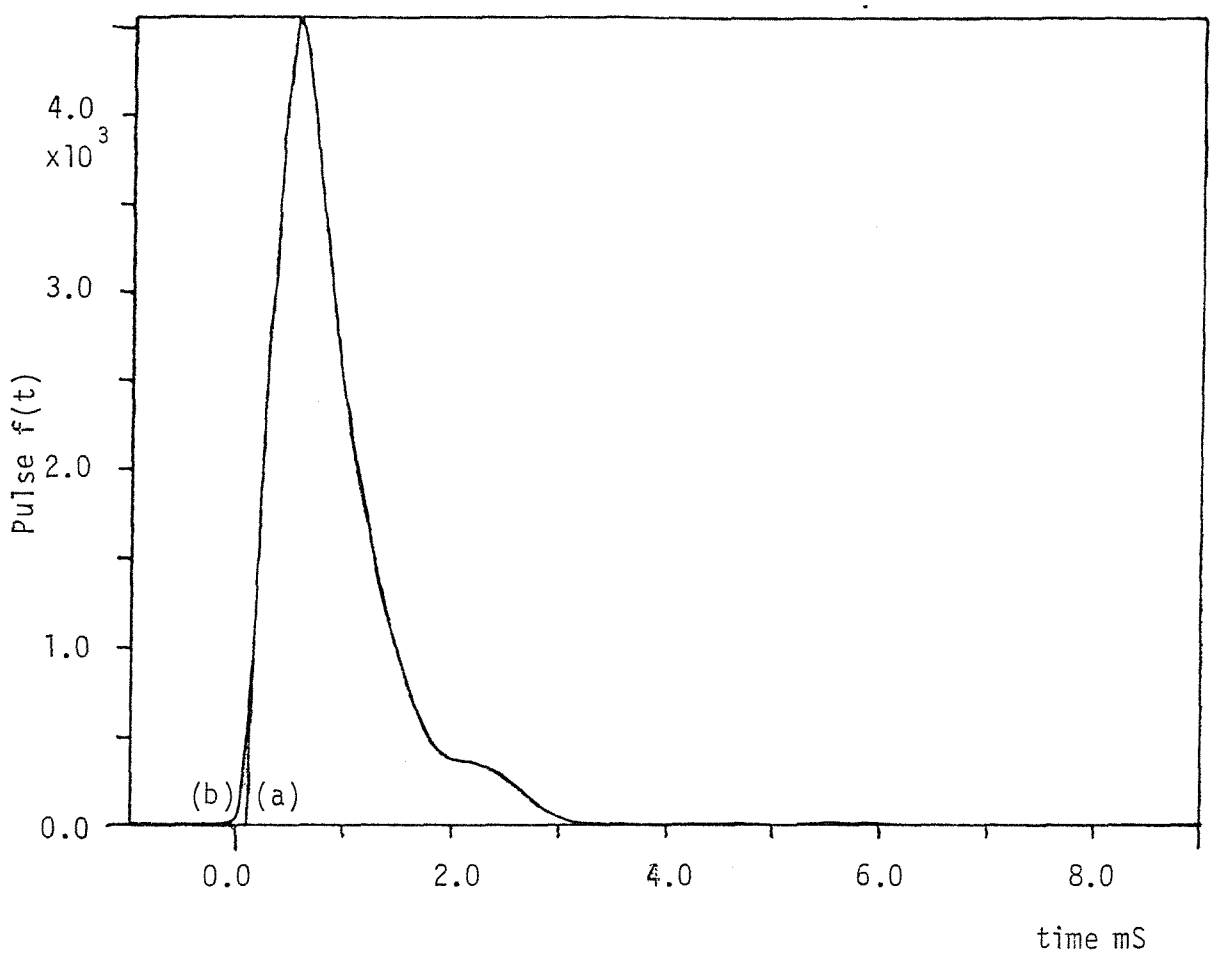

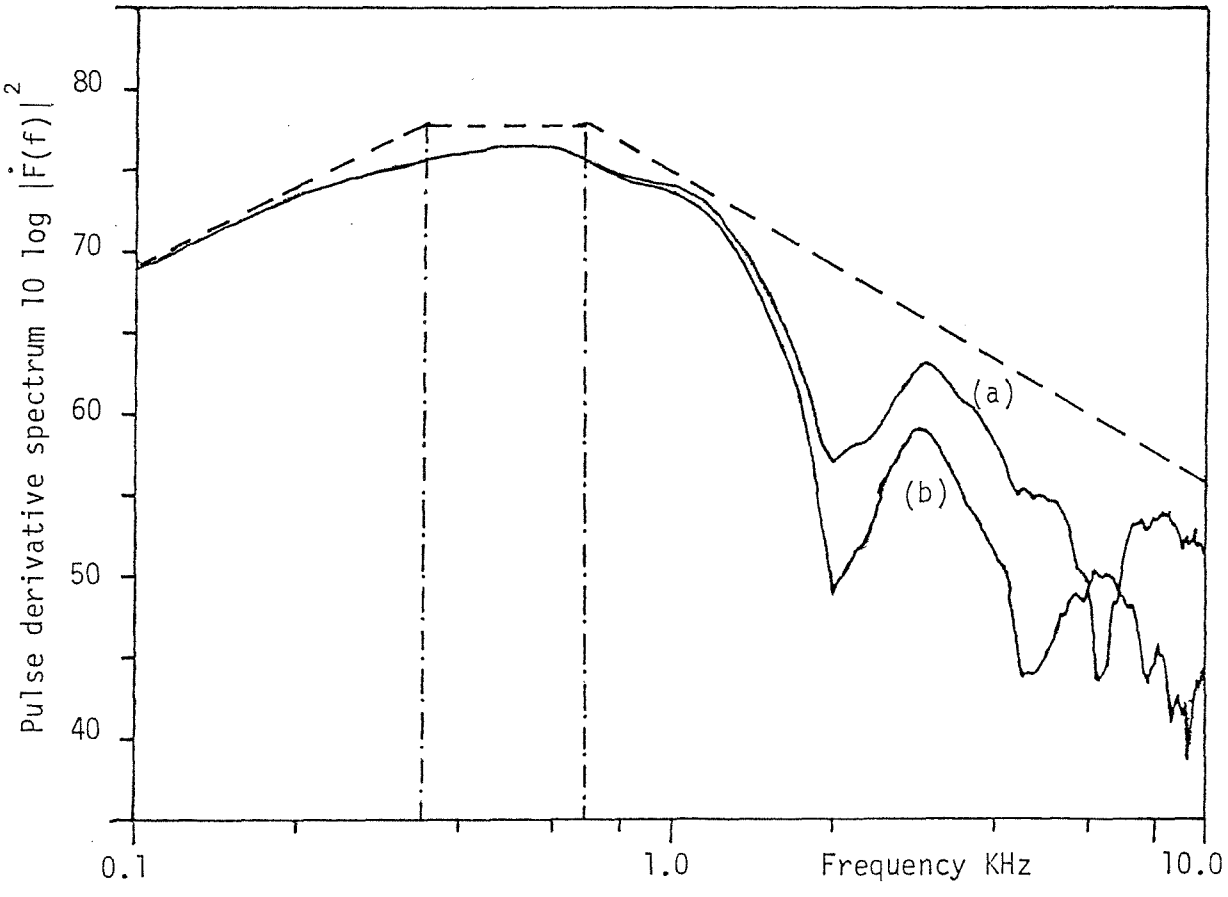

figure 1.2. Pulse correction and resulting change in level of the $10 \log |\dot{F}(f)|^2$ curve.

CHAPTER II

THE STRUCTURAL RESPONSE OF MACHINE COMPONENTS

II.1. Introduction

It was shown in the previous chapter that the noise radiated from a structure, as a result of an impact, can be expressed generally as a summation of a series of terms, one of which is the structural response term which is the ratio of the velocity, at a given frequency, and at the point of excitation to the rate of change of force at the same frequency ($V(f)/\dot{F}(f)$). Thus the noise radiated can be controlled by lowering the level of the structural response, to a given excitation force.

This chapter is therefore concerned with the response of structures to excitations at frequencies which radiate efficiently. Such frequencies are often well above those which excite the structure in its most basic modes, and the well known methods of calculating natural frequencies and investigating the response in each of these modes is not particularly profitable; there may well be several modes in a single third octave band and each of these modes may well incur large movements in completely different parts of the structure. We therefore search for more generalised response methods using statistical power flow, leading to the use of a mean value for the response of the structure. Using these statistical power flow methods we need to recognise when a structure is under force or moment excitation and when, and at what frequency ranges, can the structure be treated as a plate, flat or cylindrical, or as a beam, etc. In this chapter the mean level of the response for some typical structures, under different forms of excitation are analysed and compared. Thus one can choose the optimum structure with the minimum response for a particular application.

The structural response level can be reduced by including some resilience in the structure, say, by the introduction of resilient material in the construction of the machine structure. However, in many machines, there are limitations placed on the acceptability of excessive resilience, even though this reduces the response at the higher frequencies. The impacting element, whether it be a hammer, shuttle, cam, geartooth or, for that matter, the housing which holds

it, or the structure it strikes, needs to provide positive positioning and a lack of flexibility, so that the following impact meets the machine structure with great accuracy and timing. In some machines such as drop stamps, slow punch presses, and slowly repetitive systems, this resilience may not matter, but on others involving very high speeds, such as gears, cams etc., the resilience needs to be strictly controlled to prevent excessive bounce and malfunctioning. Under these circumstances, the structural responses have to be calculated more carefully and resiliences chosen to be acceptable at the low frequencies described by the repetition rate, but so designed to reduce response at the higher frequencies associated with the maximum noise output.

II. 2. Structural Response

The point response Im [H(f)] for a structure can be obtained by four different methods. They are, (1) the classical method which determines the natural frequencies and associated mode shapes of the structure. The structure is compared to a multi-degree of freedom system and the solution is the infinite sum of the contributions from all modes, (2) a statistical method by which the most important modes are determined and then only these modes of vibration containing the highest energy contents are considered, (3) the finite element method in which the structure is broken into a number of cells and the solution is arrived at numerically by connecting each individual cell by the boundary conditions, (4) the integral transform method, where a complete solution is found to the differential equation of motion for the structure, using the boundary conditions of the system.

All these methods give the precise response which may not always be necessary. To determine the noise energy radiated from a machine structure in frequency bands, only the mean value or characteristic response is needed throughout the whole frequency range.

The total escape energy, repeating equation (1.6) is given by

$$E_{escape} = \int_{-\infty}^{\infty} \frac{|\dot{F}(f)|^2}{2\pi f} \cdot \text{Im}\,[H(f)]\, df \qquad (2.1)$$

and if the term $|\dot{F}(f)|^2 / 2\pi f$ does not change very rapidly with frequency, then this term can be taken outside the integral. Therefore, the total escape energy will depend on the integral of [Im H(f)]. This is the same as the integral of a mean line, the geometrical mean value between the peaks and troughs, passing through the curve for Im [H(f)]. Thus in considering the energy in percentage frequency bands, instead of taking into account the frequency variations of the response, a mean value, frequency averaged can be used for Im [H(f)], provided there is more than one mode in each band. This mean value is the response of a similar structure but of infinite extent. There are no resonances and the structure has no mode shapes. For finite structures this condition is satisfied if the structure is either highly damped or for high frequencies when the modal density is high. For a highly damped structure, the bandwidth associated with each mode is less than the bandwidth separating successive modes, and also the stress waves in the structure moving away from the excitation point will decay to very low amplitudes by the time they reach the edge of the structure and thus the reflected wave is very weak, thus there are no reflected waves as if the structure is infinite. However, this frequency averaged response gives the escape energy in frequency bands and not at a particular frequency. Therefore, using this method, the noise energy radiated from a structure cannot be estimated at discrete frequencies. This is not a limitation on this method because machine structures usually have a high modal density and a relatively high loss factor. Also, even for structures with low modal density a reasonably good estimate for the energy escape leading to noise radiated can be obtained [16] .

Figure (2.1) shows a comparison of the different slopes of the mean value for the structure response for plates and beams for either force or torque excitation.

In some cases the first ringing frequency of the structure is within the frequency range of high noise levels. Below the fundamental frequency the statistical energy method and modal density treatment break down and we have to look at other methods to estimate the level of the response. This may be obtained using the method of summation of modes but only the first mode need be considered. This approximation

can be used up to a frequency of one-half the fundamental frequency. At frequencies just above the fundamental ringing frequency, the statistical mean level is not very satisfactory because of the low modal density, but the general levels of impact energy can still be obtained using this level.

Therefore, the response of a structure can be divided into three regions. The first region is below one-half the fundamental frequency. The level in this frequency range is usually loss factor dependent. The second region is between one-half the fundametnal frequency and the fundamental. In this frequency range there is a sudden increase in the response level. This sudden jump is structural damping dependent. At frequencies above the fundamental, the third region, the level is given by the statistical method and is independent of damping.

II. 3. Low Frequency Response

Using the summation of modes method, the response of a structure is given by

$$\text{Im}\,[H(f)] = \sum_{n=1}^{\infty} \frac{\eta_{s_n}}{\pi^2 m_n} \cdot \frac{f_n^2}{(f_n^2 - f^2)^2 + \eta_{s_n}^2 f_n^4} \qquad (2.2)$$

where m_n and η_{sn} are the mass and the structural loss factor respectively associated with the nth mode. $m_1 = M$, the total mass of the structure.

For $f << f_1$ (frequencies below the first resonance) only the first term of the series needs to be considered and η_{s_1} is the structural loss factor for the first mode. Therefore

$$\text{Im}\,[H(f)] = \frac{\eta_{s_1}}{M\pi^2 f_1^2(1 + \eta_{s_1}^2)} \simeq \frac{\eta_{s_1}}{\pi^2 M f_1^2} \qquad (2.3)$$

Thus, the structural response at frequencies well below the first ringing frequency (f_1) of the structure will have a constant level

given by equation (2.3). At a frequency of one-half the first ringing frequency, the response varies from the constant level response at the very low frequencies by about 2dB. Thus up to this frequency the low frequency approximation for the response can be assumed to apply. The low frequency approximation is dependent on damping while above the first ringing mode the response is independent of damping. Therefore, the sudden increase between the first ringing frequency and one-half this frequency is inversely dependent on the loss factor of the first mode. Figure 2.2. shows the measured imaginary part of the structural response of a bottle excited on the side for two different values of damping. The damping of the bottle was increased by fixing viscoelastic material on the outside. The theoretical representation of the structural response is shown in the same figure. The low frequency agreement is particularly promising, especially when considering the difficulty in obtaining these results because of the low amplitudes i.e. high noise to signal ratio at off resonances.

II. 4. Cylindrical Shell Structures

A very important parameter in shell theory is the radial or circumferential resonance frequency given by $f_r = c_\ell/(2\pi a)$ Hz where c_ℓ is the longitudinal wave speed and 'a' the radius of the shell. Thus the response characteristics of a shell structure can be separated into two regimes or regions (figure 2.3). Below this circumferential resonance, the vibrations of the shell are controlled by membrane forces while above this frequency the vibrations are controlled by bending forces, i.e. the shell will behave like a flat plate of the same thickness. The response of a shell for point force excitation at any frequency is given by

$$\text{Im}\,[H(f)] = \frac{J(f/f_r)}{16\pi f\sqrt{B\rho_s}} \qquad (2.4)$$

where $J(f/f_r)$ is a function of the ratio of any frequency to the circumferential resonance frequency, and is given by

$$J(f/f_r) = \sqrt{f/(2f_r)}\ , \qquad f < f_r$$

$$= \frac{\log_e \left\{ \frac{\sqrt{48}\, a}{h} \right\}}{\sqrt{2}\,\pi}\ , \qquad f = f_r$$

$$= 1\ , \qquad f < f_r \qquad (2.5)$$

where h is the thickness of the shell wall;
B the bending stiffness given by $B = EI/(1-\nu^2)$;
E is Young's Modulus;
I the second moment of area about an axis in the neutral plane;
ν is Poisson's Ratio and
ρ_s is the surface density.

Therefore the mean value of the response of a cylindrical structure is lower than that of a plate of the same thickness below the circumferential resonance frequency while at this frequency the response takes a discrete value which is greater than that for a flat plate. Above this frequency the response is exactly like that of a plate.

II.5. Stiffened Structures

II.5.1. Point Force Excitation

Other types of structures, very common in machine construction are rib-stiffened shells and plates. If the point excitation is between two ribs, these act like imperfect reflectors, but the ribs have a very small effect on the mean value of the response from that of a plate [12]. Although in this case some of the input energy is used in torsional vibrations of the ribs, these are poor radiators, and therefore, the noise radiated would only be slightly reduced. When the excitation point coincides with one of the ribs, to a first approximation, the response will be the addition of the individual point responses for the rib and shellor plate, as if the two systems

are in parallel. Since they are rigidly fixed both have the same displacement. For a better approximation, we have to take into account the reaction between the rib and the plate. Since the rib is much stiffer in the direction along its axis, the bending wavelength along the rib is not different from that of the rib alone. However, normal to the rib, the bending wavelength will be that of the plate. Hence the plate behaves as if it is orthotropic and the response for the plate is given by

$$H(f) = \frac{j}{16\pi f \left(\frac{B_p \rho_{s_p}^3 B_b}{\rho_{\ell_b}} \right)^{\frac{1}{4}}} \qquad (2.6)$$

where $B_b = E_b I_b$ for rib and ρ_{ℓ_b} is the mass per unit length of the rib. For the reaction of the plate on the rib, the density of the resonances in the rib is increased by a factor $\sqrt{\delta}$ which is the ratio of increased mass due to the addition of plate, to the rib mass, i.e.

$$\delta = \frac{M_b + M_p/2}{M_b} \qquad (2.7)$$

where M_b is the total mass of the rib and M_p is the total mass of the plate. Thus the characteristic admittance of the rib becomes

$$H(f) = \frac{1+j}{8\pi f \, (B_b \rho_{\ell_b}^3)^{\frac{1}{4}} \sqrt{\frac{2\pi f}{\delta}}} \qquad (2.8)$$

These two equations for the response of the plate and the beam (2.6 and 2.8) must be added (parallel additions) to get the more accurate response for the ribbed plate. The level of the response changes as compared to a plate on its own because of the introduction

of the ribs, i.e., the level is lowered. However, for the point excitation of rib-stiffened plates with the point excitation coinciding with one of the ribs, the response does not change at all if the number of ribs in the structure is increased (figure 2.4(a)). The response is highly dependent on the stiffness of the beam as compared to that of the plate. From figure (2.4(b)), it can be observed that if the rib is less stiff than the plate, the response is that of the beam, and it goes down at 15dB per frequency decade and is higher at low frequencies. Also, the level of the response is reduced with the increase of the rib stiffness. At high frequencies, the response of the combined structure approaches that of the beam [10].

In the case of ribbed shells, the response of the shell is used instead of the response of the plate.

II.5.2. Torque Excitation

In the case of torque excitation the energy escape term in the accountancy equation does not change at all, from the case of point force excitation. The structure response for torque excitation is used instead of the response for force excitation, and the spectrum of the torque derivative instead of the force derivative. That is

$$E_{escape}(f) = \frac{|\dot{T}(f)|^2}{2\pi f} \cdot \mathrm{Im}\,[H(f)] \qquad (2.9)$$

where T is the applied torque and H(f) is the ratio of the angular velocity $\dot{\theta}(f)$ to the rate of change of torque at the same point and frequency ($\dot{\theta}(f)$ / $\dot{T}(f)$).

Torque excitation of a ribbed structure may be either symmetrical or asymmetrical. In the symmetrical case, the torque is applied perpendicular to the rib, that is, no torsional waves are induced in the rib. The motion of the structure in this case is symmetrical on either side of the rib. From the power flow equation [6] the point response is given by

$$\text{Im}\,[H(f)] = \frac{(1-c)}{4(B_b{}^3\,\rho_{\ell_b})^{\frac{1}{4}}\,\sqrt{2\pi f}} \qquad (2.10)$$

where

$$c = \frac{\left[2B_p\,\rho_{\ell_b} + (B_p\,\rho_{s_p}\,B_b\,\rho_{\ell_b})^{\frac{1}{2}} + B_b\,\rho_{s_p}\right]}{2\sqrt{2\pi f}\,\left[(B_b\,\rho_{s_p})^{\frac{1}{2}} + (B_p\,\rho_{\ell_b})^{\frac{1}{2}}\right]^{\frac{1}{2}}} \cdot \left[\frac{B_p}{B_b{}^3}\right]^{\frac{1}{4}} \frac{1}{\rho_{\ell_b}} \qquad (2.11)$$

where B_b is the beam (rib) bending stiffness;

B_p is the plate bending stiffness;

ρ_{s_p} is the mass per unit area of the plate and

ρ_{ℓ_b} is the mass per unit length of the beam.

This response depends on the coupling term $\frac{B_p}{\sqrt{2\pi f}\,(B_b{}^3\,\rho_{\ell_b})^{\frac{1}{4}}}$

and at high frequencies this term is small and the response is similar to that of a beam with torque excitation, the beam vibrating in flexural wave motion. At low frequencies, the coupling is strong and the response level is reduced and approaches that of an orthotropic plate under torque excitation.

Figure (2.5) shows a comparison between the level of the response for a plate under torque excitation and the same plate rib-stiffened with different stiffeners. It can be observed that the response of the combined structure reduces with the increase of the stiffness of the beam. The largest reduction in the level of the response occurs at high frequencies. The shape of the response curve changes and instead of being independent of frequency as in the case of a flat plate, the response has a slope of 5dB per frequency decade due to the influence of the rib.

As shown in figure (2.6) an increase in the number of ribs does not alter the response of the structure at all when excited on one of the ribs.

In the asymmetrical case, the torque is in the same direction as the beam, that is, torsional waves are induced in the beam and the

stress waves in the plate, on either side of the beam, are completely out of phase. The point response for the structure in this case is given by

$$\text{Im}\,[H(f)] = \frac{1}{2\pi f\,(GQJ\rho)_b} \cdot \left(\tfrac{1}{2} + \frac{A - B}{4\pi^2 f^2} \right) \qquad (2.12)$$

where

$$A = \left(\frac{B_p\, \rho_{s_p}\, G_b\, Q_b}{4\, \rho_b{}^3\, J_b{}^3} \right)^{\frac{1}{2}} \qquad (2.13)$$

and

$$B = \left(\frac{B_p{}^2}{(GQJ\rho)_b} \right) \qquad (2.14)$$

where the suffix b denotes properties of the rib;

G_b is the shear Modulus of the rib;

J_b is the polar second moment of area of the beam;

Q_b is the torsional stiffness factor to allow for the fact that the rib is seldom circular; and

ρ_b is the material density of the beam.

This equation is the same as that for a beam, except for additional terms due to the influence of the plate. At high frequencies, the bending stiffness of the plate is small compared to that of the beam and the response approaches that of a beam under torsional excitation. At low frequencies, the torsional stiffness of the beam and its inertia are small and therefore the response of the combined structure approaches that of an orthogonal plate.

This relation of the response applies only above the frequency at which the torsional waves in the beam have the same velocity as the flexural waves in the plate. The torsional wave velocity is proportional to the square root of the frequency. Thus at some frequency these two wave velocities are equal. Below this frequency,

no relation for the response can be obtained. In most modern structural constructions using I-beam sections, this frequency is lower than 100 Hz.

The response in this case is also much lower than that for a plate (figure 2.7) and in this case, it has a slope of 10 dB per frequency decade corresponding to the slope of torsional vibrations in the beam. Figure (2.8) shows that the response is influenced by the plate if the stiffness of the rib is of the same order of magnitude as the bending stiffness of the plate. However, if the beam is made with a high torsional stiffness factor, apart from high stiffness, the response level is even lower.

II. 6. Line Excitation of Flat Plates

The point response of an infinite plate under line force excitation, can be obtained from the expression for the power flow per unit length as given by Nayak [17] and Skudrzyk [18]

$$\text{Im}\,[H(f)] = \frac{1}{4\sqrt{(2\pi f)^3}\,(B_p\,\rho_{s_p}^{\,3})^{\frac{1}{4}}} \qquad (2.15)$$

This expression for the response is for an infinite plate and the line force acts constantly along one direction. Therefore, for a finite line of excitation, the response as given by equation (2.15) is multiplied by the length of the line of excitation, i.e.

$$\text{Im}\,[H(f)] = \frac{L}{4\sqrt{(2\pi f)^3}\,(B_p\,\rho_{s_p}^{\,3})^{\frac{1}{4}}} \qquad (2.16)$$

where L is the length of the line force.

The escape energy into the plate structure is then given by the product of this response and $|\dot{F}(f)|^2$ where F is the force per unit length. Since the force is constant along a straight line, the vibration pattern is unidirectional, perpendicular to the line of

excitation. Thus the plate behaves like a beam and the response is the same as that of a beam. For a finite structure, the beam has a mass per unit length of M/L, where M is the total mass of the plate and L is the length of the plate in the direction perpendicular to the line of excitation [18].

Similarly, the response of a plate when excited by a line torque can be obtained by considering the plate to be a beam, since the waves only propagate along one direction. The response for an infinite plate under torque excitation is thus given by

$$\text{Im}\,[H(f)] = \frac{1}{4\sqrt{2\pi f}\,(B_p^{\,3}\,\rho_{s_p})^{\frac{1}{4}}} \qquad (2.17)$$

and the response for a structure with a finite line (L) of torque excitation is given by

$$\text{Im}\,[H(f)] = \frac{L}{4\sqrt{2\pi f}\,(B_p^{\,3}\,\rho_{s_p})^{\frac{1}{4}}} \qquad (2.18)$$

Similar to the case of force excitation, the escape energy into a structure under this type of excitation is given by the product of this response, equation (2.18), and $|\dot{T}(f)|^2$ where T(f) is the torque per unit length applied to the structure.

II.7. Double Beam Structures

Another type of structure common in machine construction is a double beam system, with only structural damping, and interconnected by several webs which can be considered as several springs. The response of this type of structure has been investigated by Irie et al [19] and the response curves for some typical examples from this reference are shown in figures (2.9) and (2.10).

The point impedance of a double beam system with a spring configuration in between is lower than the impedance for a beam of the

same thickness as the combined thickness of the two beams in the double beam configuration. For both of the cases investigated - the end excitation of a cantilever beam and the mid-point excitation of a simple supported beam - at low frequencies the mean response is the same as that for a beam of equal thickness. In figure (2.9) comparison is made between the mean response of a single beam and the response for the double beam system with highest structural damping, since this will approximate closely the mean impedance of the system. In the figures n subscript denotes n=1 for one beam and n=2 for the other beam, b_n is the width of the beam, h_n the depth, ν_n Poisson's ratio, ρ_n the density, EI_n the bending stiffness, A_n the cross-sectional area, L the length, S_n the slenderness ratio given by $(AL^2/I)_n$, κ_n is the shear coefficient due to the shape of the cross-section of the beams, N the number of springs, K_n is a dimensionless spring stiffness, where the stiffness is given by $K_n(EJ/L^3)$, δ_K is the loss factor of the structurally damped springs, δ_E the elasticity loss factor of the beams and δ_G the shear loss factor of the beams.

At high frequencies the point response is higher (lower impedance), which suggests that double beam systems are worse off as regards to power flow for high frequencies.

If the two beams are of different material, considering the curve for the driving point impedance of the simply supported double beam system excited at the centre, the mean level of the impedance is again lower than the mean level of impedance of a single composite beam.

From these results, it can be observed that double beam systems are worse off as compared to single beams for noise radiation. When the beam is divided to accomodate the springs in between,the stiffness is reduced especially in the case of out of phase vibration of the two beams. For in phase vibration, the stiffness of the composite system is nearly the same as for a single beam.

II.8. Honeycomb Structures

A new type of structure which is increasingly being used nowadays, especially in space vehicle construction are honeycombed structures.

These are constructed from two face plates which are usually very thin compared to the core. The core is of the honeycomb construction and is usually steel or some other metal. The core is glued to the face plates (figure(2.11)). This type of construction makes these structures very stiff, with a high stiffness to weight ratio. Honeycombed plates have been investigated in I.S.V.R. [20] for the modal density and its relation with area and weight. From these relations for the modal density, an expression for the point response of the structure can be obtained.

This expression for the point response of a honeycombed plate is given by

$$\text{Im}\,[H(f)] = \frac{h_2}{8d^2\sqrt{G_x G_y}}\left\{1 + \frac{m\omega^2 + 2g^2Y(1-\nu^2)}{\left[m^2\omega^4 + 4m\omega^2 g^2 Y(1-\mu^2)\right]^{\frac{1}{2}}}\right\} \quad (2.19)$$

and

$$Y = d^2E\left(\frac{h_1 h_3}{h_1 + h_3}\right) \quad (2.20)$$

$$d = h_2 + \frac{h_1}{2} + \frac{h_3}{2} \quad (2.21)$$

$$g = \frac{\sqrt{G_x G_y}}{Eh_2}\left(\frac{1}{h_1} + \frac{1}{h_3}\right) \quad (2.22)$$

$$m = \rho_2 h_2 + \rho_1 h_1 + \rho_3 h_3 \quad (2.23)$$

where G_x and G_y are the shear moduli of the plate in the same plane at perpendicular directions;

h_2 is the core thickness;

h_1 and h_3 are the face plates thicknesses;

E is Young's Modulus of the material;

ρ_1, ρ_2, ρ_3 are the densities of the face plates (1,3) and the core (2); and

ν is Poisson's Ratio

If we compare a honeycombed plate to a solid plate with the same bending stiffness, assuming that the face plates are of the same thickness, then

$$\frac{Eh^3}{12\,(1-\nu^2)} = \frac{Eh_f}{2}\,(h_c + h_f) \qquad (2.24)$$

where h_f is the face plate thickness;
h_c is the core thickness; and
h is the thickness of the solid plate.

If $h_f = h/x$, then from equation (2.24)

$$h_c = \sqrt{x/6} - 1/x \qquad (2.25)$$

Figure (2.12.) shows the response of a honeycombed plate for different values of h_c and h_f, these being related by equation (2.25). It can be observed that the general level of the response is higher than that of a solid plate, and also that the level is dependent on the h_c/h_f ratio. At low frequencies the level is lower the smaller the core thickness, while at high frequencies it is the contrary; the lower the response the larger the thickness of the core.

The response can be divided into two parts, the low and high frequency regimes. At low frequency the second term in the brackets, equation (2.19) is very high (>>1), and the response is proportional to the reciprocal of the frequency. However, at high frequencies, this second term is small and the response becomes independent of frequency.

Although the response of honeycombed structures is much higher, implying that more noise energy will be radiated if all other parameters of the structure remain constant, the loss factor of this type of structure is much higher than that of normal plates, due to the different parts that are glued together and due to the high level of damping in the resin used to hold the core and face plates together. Thus this high damping may offset the disadvantage of the higher

response to give a lower radiated noise energy. Since honeycombed structures are very high in stiffness to weight ratio, these types of structures are very useful where weight is one of the limiting factors. However, they can be improved by rib-stiffening and the mass per unit length of the rib need not be high to give large reductions in the response because of the low mass of the structure.

II.9. Approximation for the Structural Response

If a structure is similar to a beam or a plate, then it can be approximated to an infinite structure and expressions for the structure response can be easily obtained. For other complicated structures it is difficult to calculate or find expressions for the mean structure response without going through complex mathematical procedures. However, if measurement on the structure is possible then there is no problem and the structural response can be found experimentally. The problem arises when the structure is not available for measurement and approximate values must then be used. The imaginary part of the structure response can [10, 21] be approximated to

$$\text{Im}\,[H(f)] = |H(f)| \cos\left(\frac{\varepsilon\pi}{2}\right) \qquad (2.26)$$

where ε is the exponent of the frequency response $H(f) \sim \omega^{\varepsilon-1}$

and $$H(f) = \begin{cases} 1/(4\pi^2 f^2 \rho S \ \text{Min.}\ (\ell, \lambda/5)) & \text{one dimensional} \\ 1/(4\pi^2 f^2 \rho h \ \text{Min.}\ (S_p, \pi(\lambda/5)^2)) & \text{two dimensional} \end{cases}$$

where S is the cross sectional area, for a one dimensional structure, and ℓ the length of the structure. Min. $(\ell, \lambda/5)$ is the lesser of the length of the structure or one-fifth of the bending wavelength from the point of excitation, whichever is shorter. For a two dimensional structure, h is the thickness and S_p the surface area. Again min. $(S_p, \pi(\lambda/5)^2)$ is the lesser of the surface area of the structure or the area enclosed by a circle of radius one-fifth of a

wavelength.

Similar expressions are given for moment excitation. In this approximation, the point response is that of the mass within one-fifth of the bending wavelength from the point of excitation. If the structure is free and has dimensions less than $\lambda/5$, then it will behave like a rigid mass. Thus for any structure, an approximate value can be obtained. If this is compared to known responses for plates and beams, the two results are different but in dB terms the error is very small.

II. 10. Concluding Remarks

From the noise point of view, there is room for improvement in most machine structures by the modification of the structure for lower response. The whole concept is to try to block or otherwise reduce the vibrational energy as it propagates from where it is generated to the radiating surfaces. The changes in the response is to reflect back a significant amount of the escape energy. For the same impact force, a lower response will imply that the escape energy is reduced, resulting in a lower radiated noise level. The above sections dealt with the response of different forms of structures and it can be concluded that improvement in most machine structures for noise control is possible, by changes in the mobility (or impedance) along the path of energy flow to obtain great attenuation in structure-borne sound.

At medium and high frequencies, lumped masses are very effective to block most of the vibrational energy flow. A mass attached to a structure at the point of impact will act as a mobility change and reflect most of the vibrational energy. A complete discussion of lumped masses will be dealt with in Chapter V. Other changes in the structure to produce a mobility change can be either due to material or to structural configurations, such as elastic interlayers, bends, changes in structural cross-section, etc. However, restricting the flow of vibrational energy may not result in a

reduction of the radiated noise. To reduce the noise energy radiated by structural discontinuities, i.e., by reflecting part of the vibrational energy, that part of the structure containing the energy must have some mechanism to dissipate this energy, otherwise the same amount of energy will be transmitted due to multiple reflections.

For the two conditions of the ribbed plate, the attenuation of the vibrational energy flow is due to such a change in impedance. For the condition of excitation in the space between the two ribs, there is a change in the structure impedance where the ribs are attached and energy is restricted from flowing away from the section between the two ribs. A typical example is the hull of a ship. Since it is of one single construction, one would expect the vibrational energy to flow readily from bow to stern. However, this is not the case, the ribs included in the ship structure act as an impedance change and reduce the flow of vibrational energy. If the excitation point coincides with a rib, there is an impedance mismatch at the point of excitation, or else the point mobility of the combined structure is reduced at this point.

The low frequency response of a structure, below the fundamental mode is also investigated and it is shown that the response at this low frequency is dependent on the structural loss factor of the first mode and the mass or static stiffness of the structure ($f_1 = \sqrt{K_S/M}$, where K_S and M are the static stiffness and mass of the structure respectively). The static stiffness of the structure is related to the cross-sectional shape and area. This is very useful when the first resonant mode is within the frequency range of interest. One method to reduce the radiated noise in this case is to stiffen the structure to increase the frequency of the first mode, thus making more effective use of the very low response below the first mode.

The results obtained for the response of the different types of structures also suggest which type of structure is best suited for a particular application. It is not possible to offer a general solution to a noise problem and give the optimum type of structure that should always be used, but each problem has to be studied individually to find the best type to be used in that

particular case. The decision of which is the best type of structure to be used can only be made by the designer of that particular machine because he knows which are the important factors. Hence, the above results present to the designer a large selection of structures which he can choose from to have the desired parameters plus giving a low level of radiated noise from the structure.

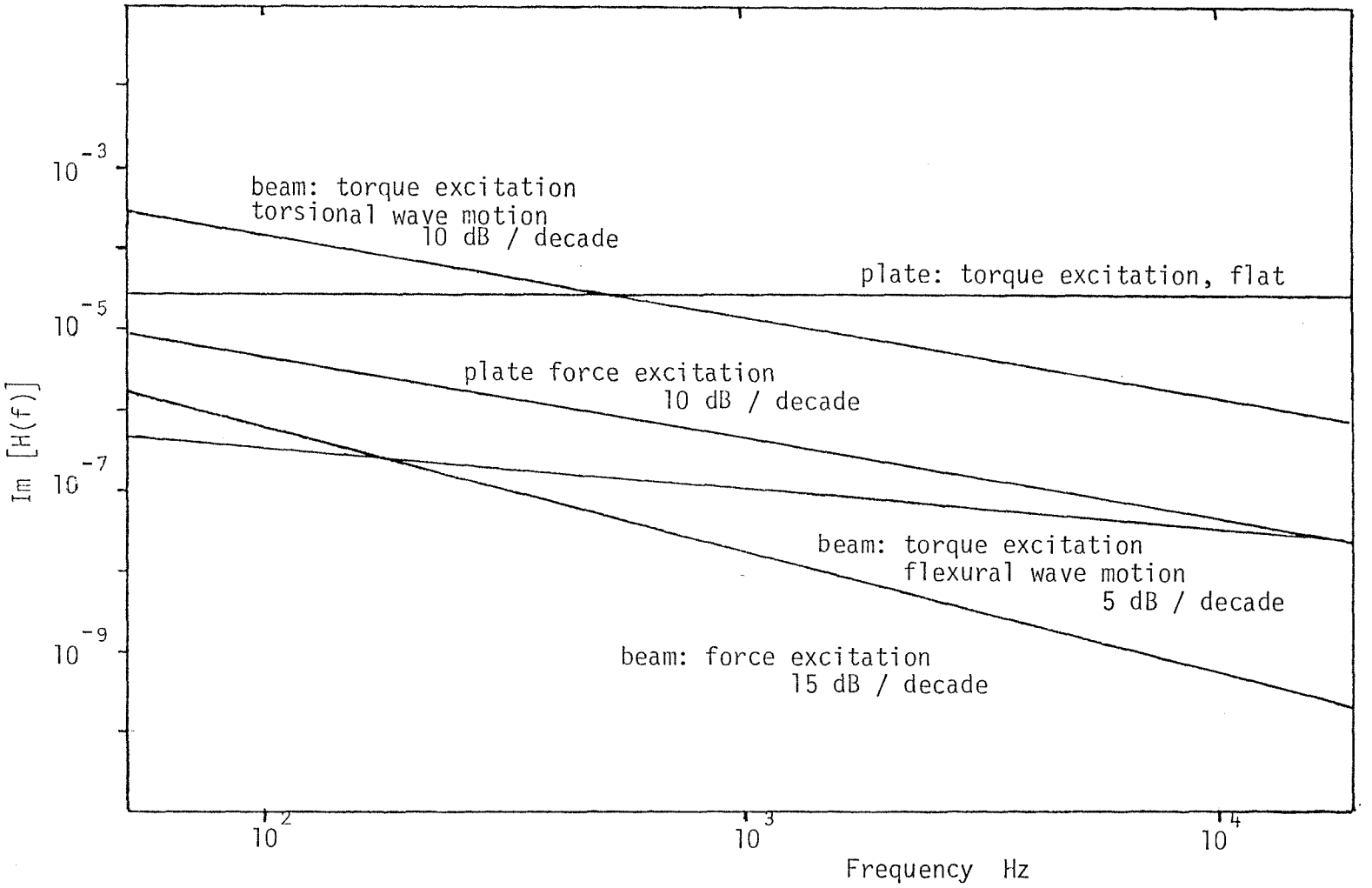

figure 2.1. Mean value for the point response for plates and beams with force or torque excitation.

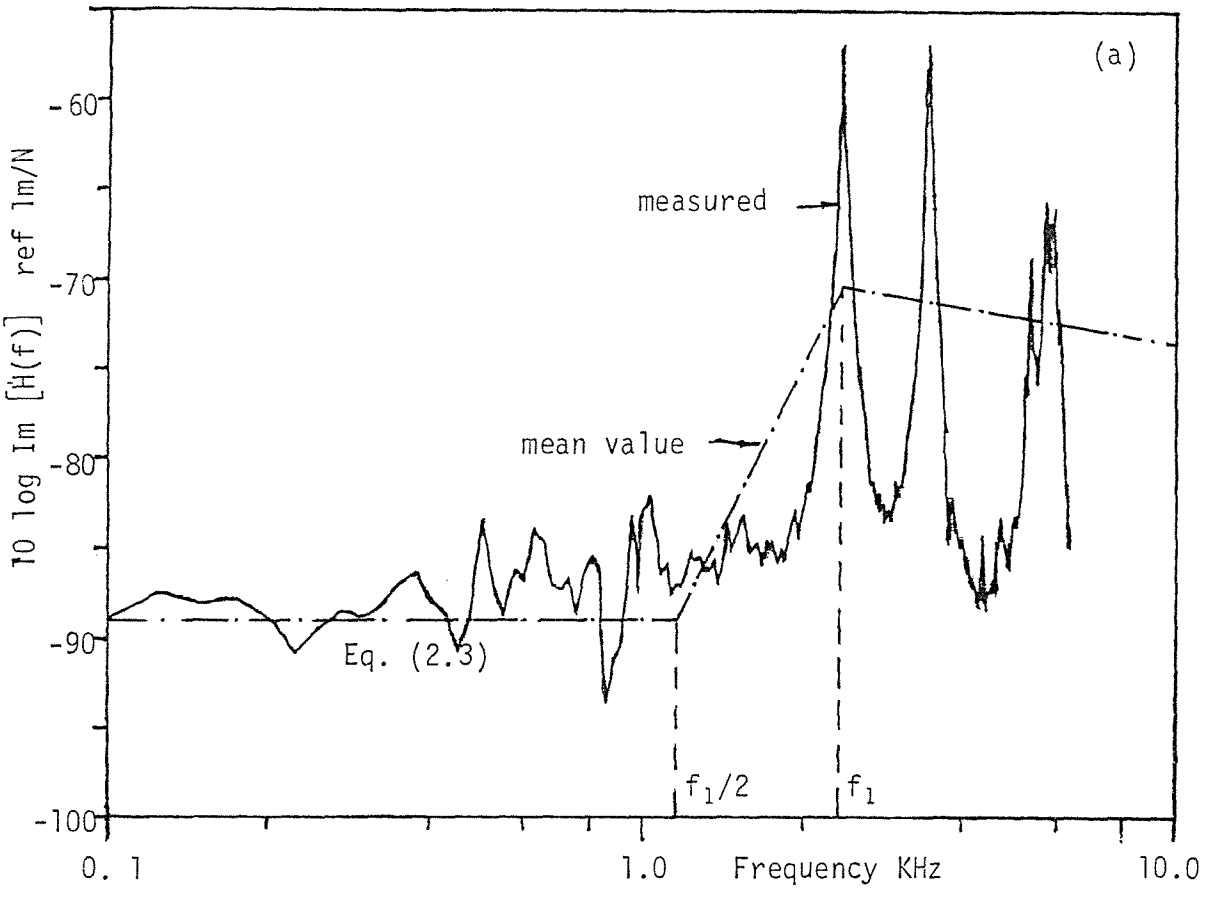

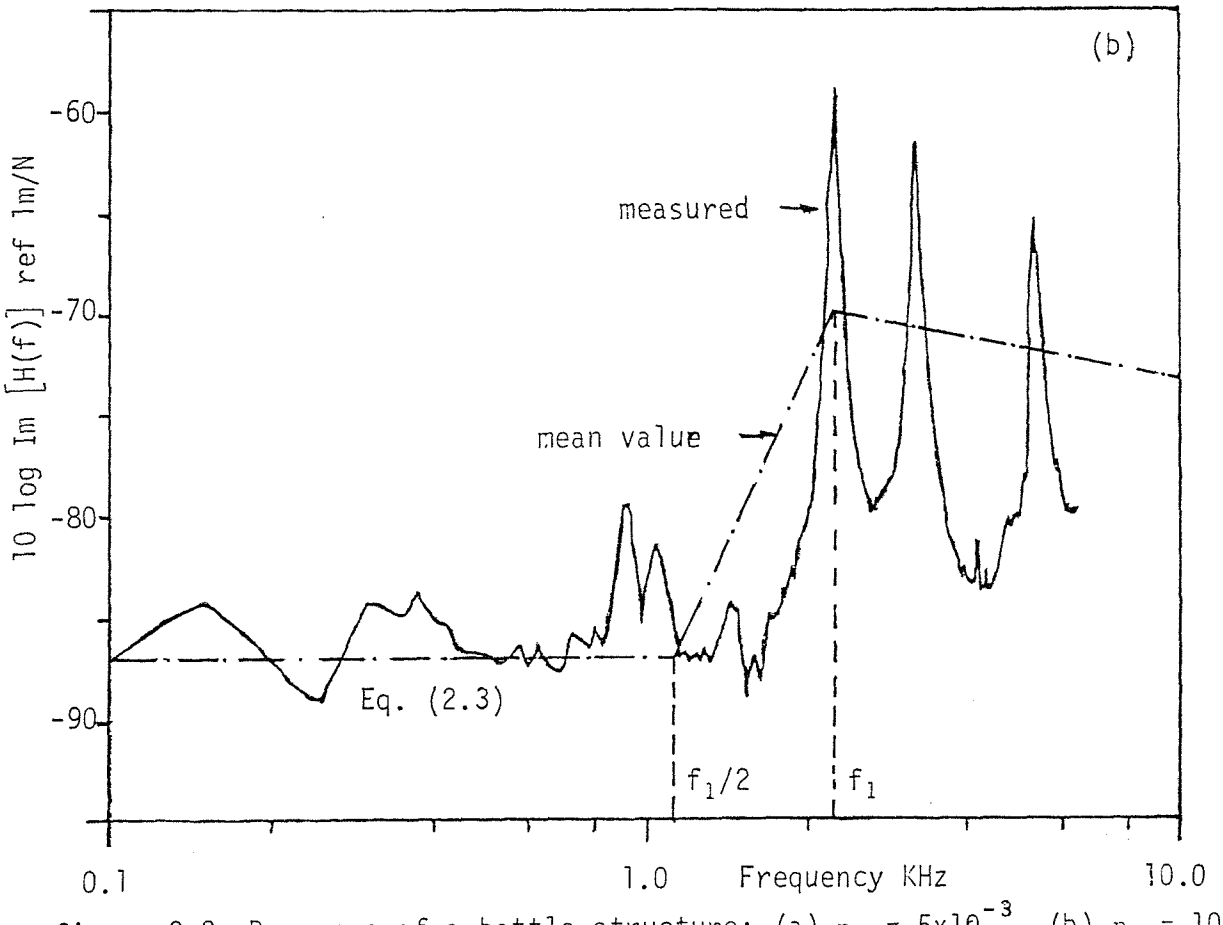

figure 2.2. Response of a bottle structure; (a) $n_s = 5x10^{-3}$,(b) $n_s = 10^{-2}$

The measured curves have a frequency resolution of 25 Hz.

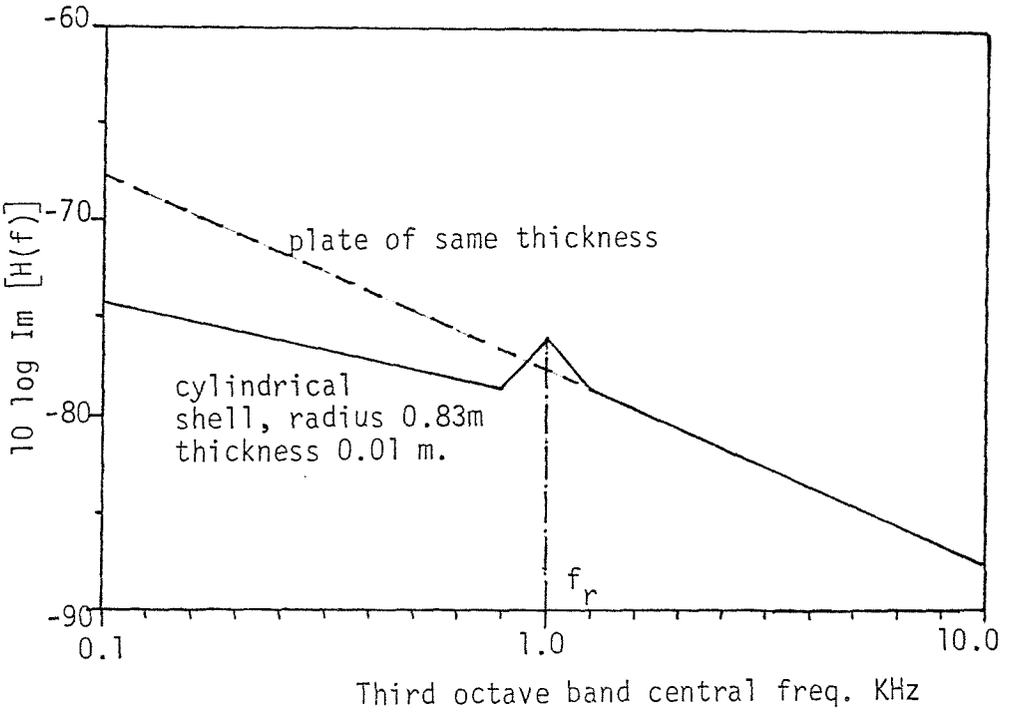

figure 2.3. Response of a cylindrical shell

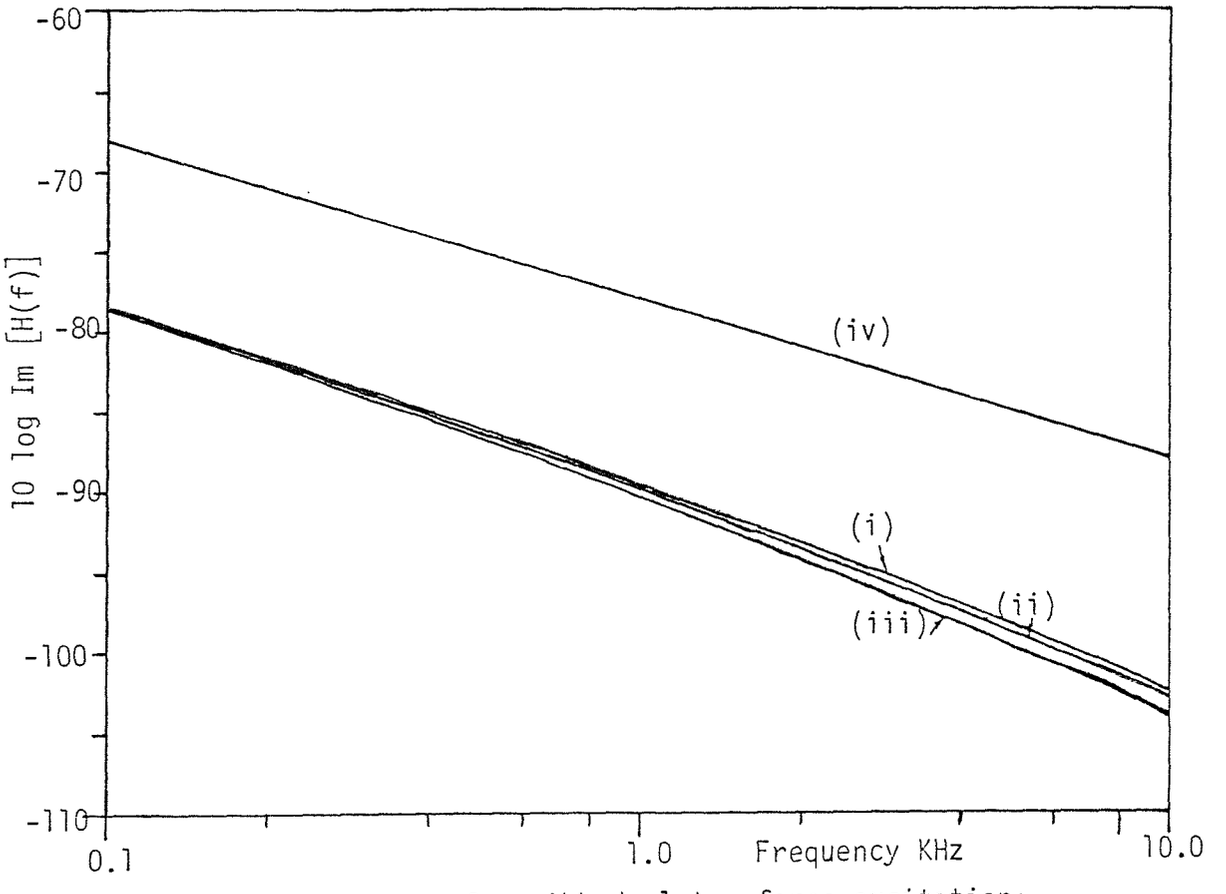

figure 2.4(a). Response of a ribbed-plate, force excitation;
(i) δ = 70, (ii) δ = 50, (iii) δ = 30, (iv) plate.

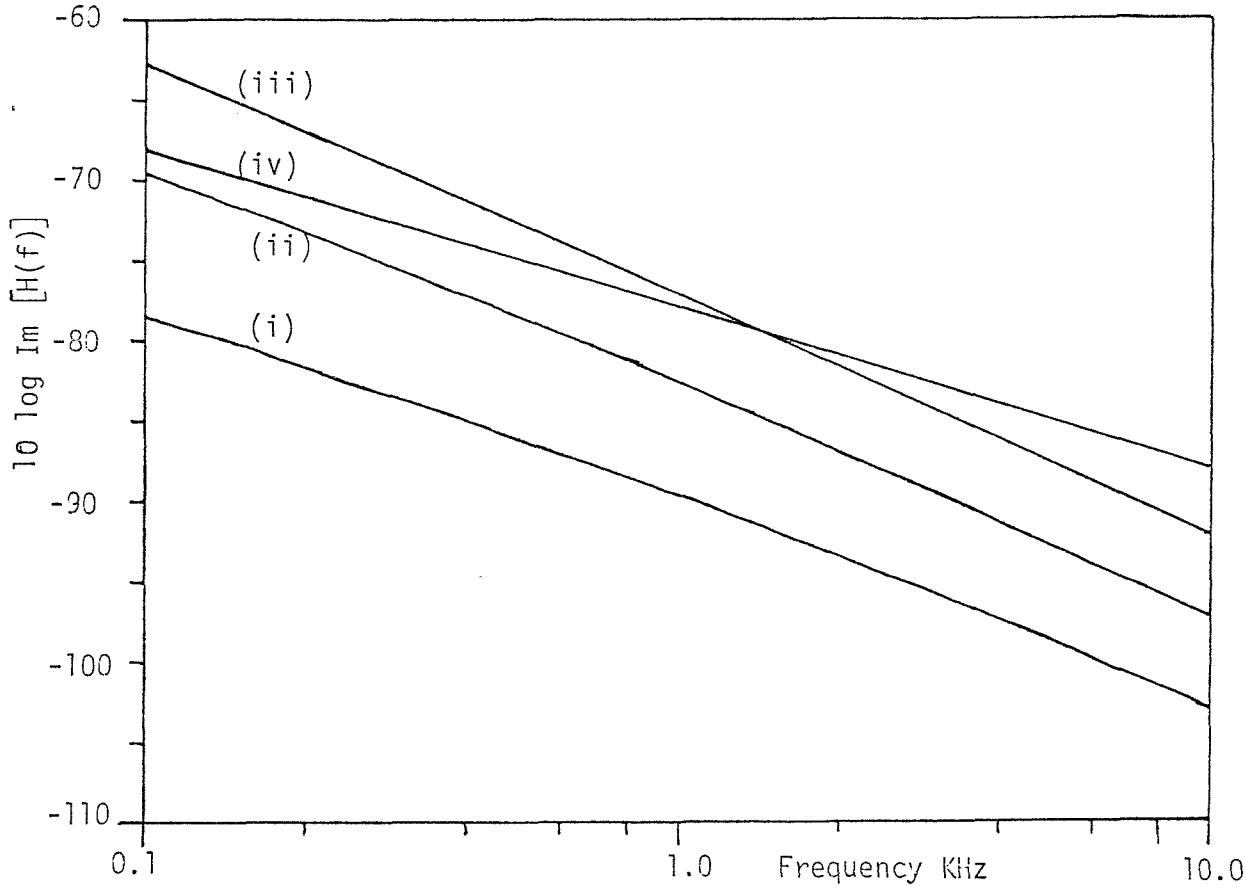

figure 2.4(b). Change of response with rib stiffness for a ribbed-plate, force excitation, δ=50; (i) B_b=1x10^8 Nm^2 ; (ii) B_b=1x10^6 Nm^2 ; (iii) B_b=1x10^{4}Nm^2 (iv) plate.

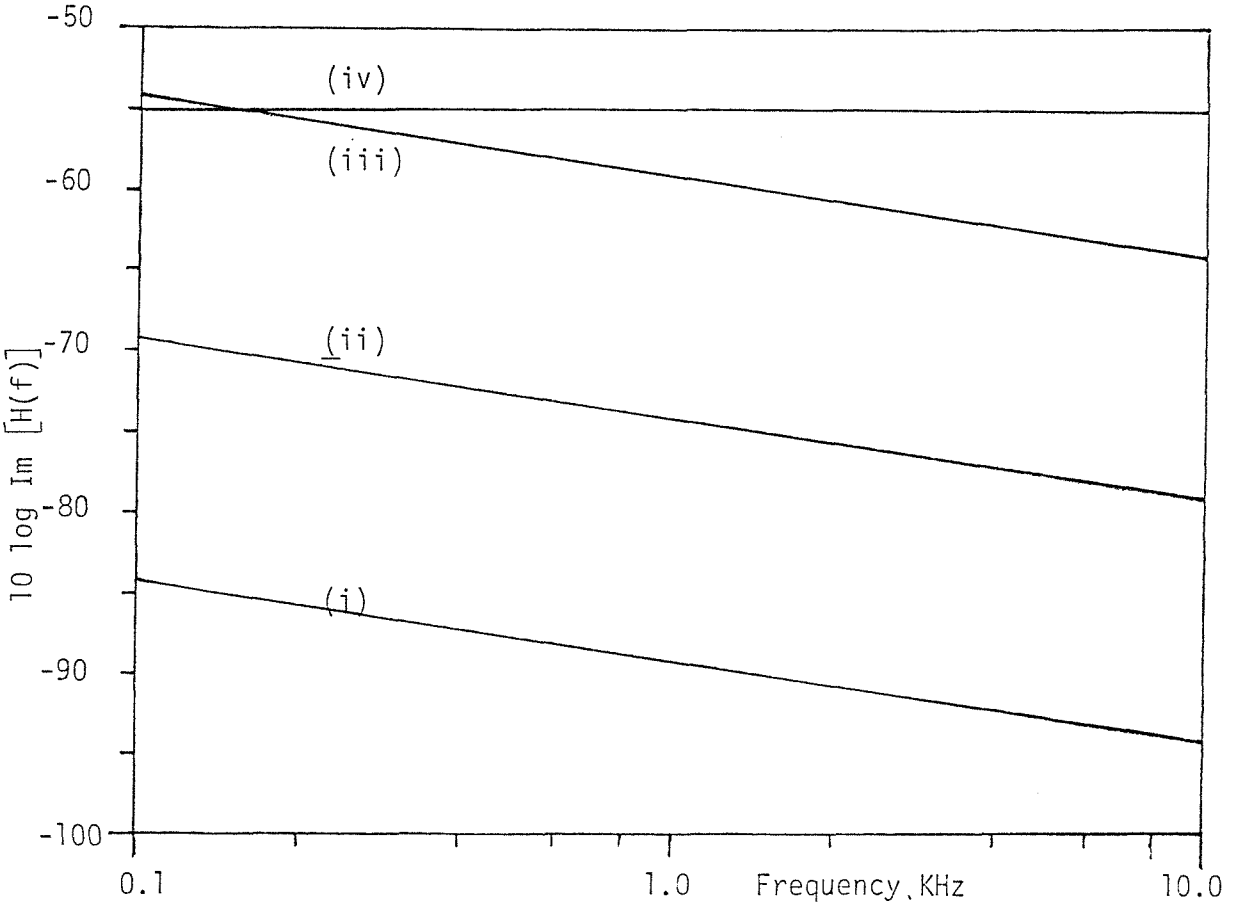

figure 2.5. Response of ribbed-plate, symmetrical torque excitation (i) B_b=1x10^{8}Nm^2 ;(ii) B_b=1x10^{6}Nm^2 ; (iii) B_b=1x10^{4}Nm^2; (iv)plate

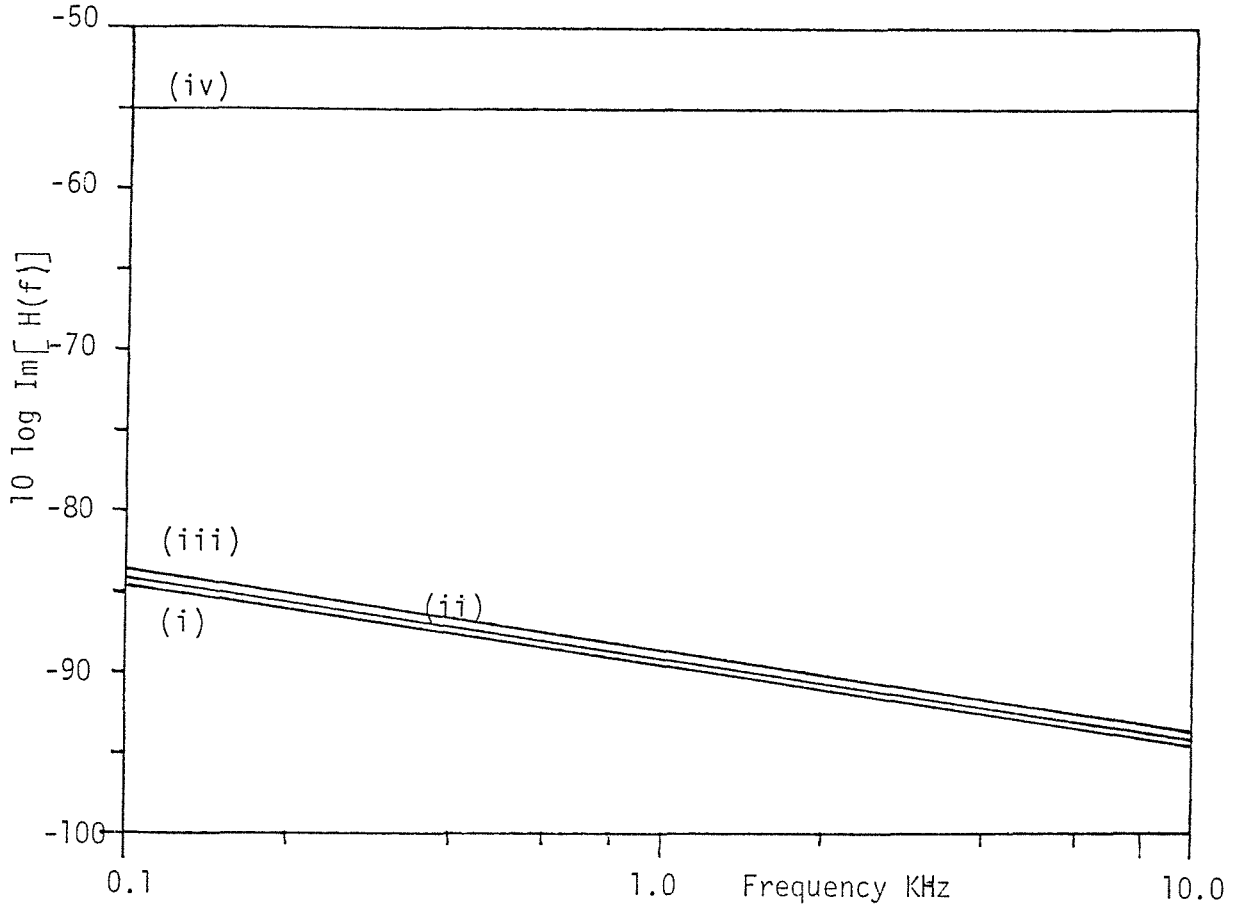

figure 2.6. Response of ribbed-plate, symmetrical torque excitation; (i) $^{\rho}\ell_b$=70 Kg/m; (ii) $^{\rho}\ell_b$=50 Kg/m; (iii) $^{\rho}\ell_b$=30 Kg/m; (iv) plate

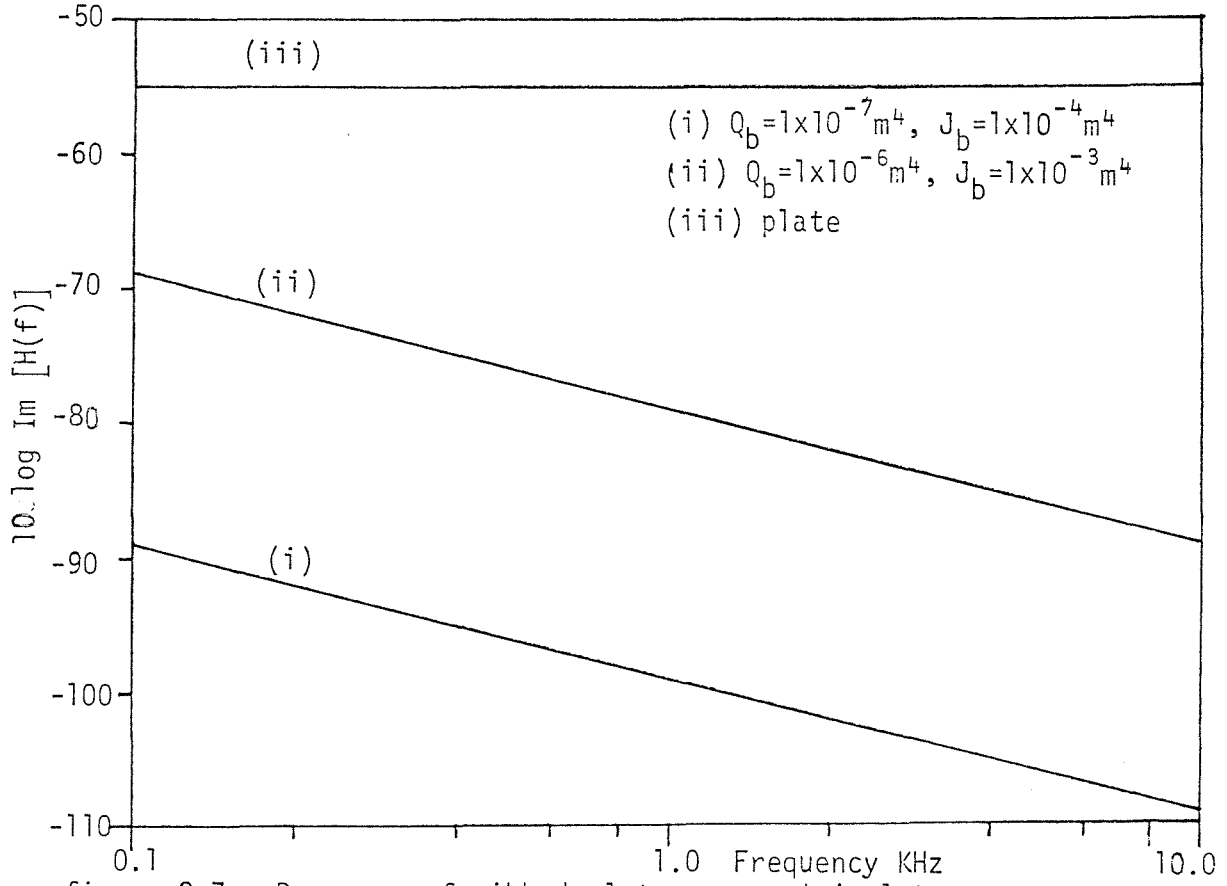

figure 2.7. Response of ribbed-plate, asymmetrical torque excitation;

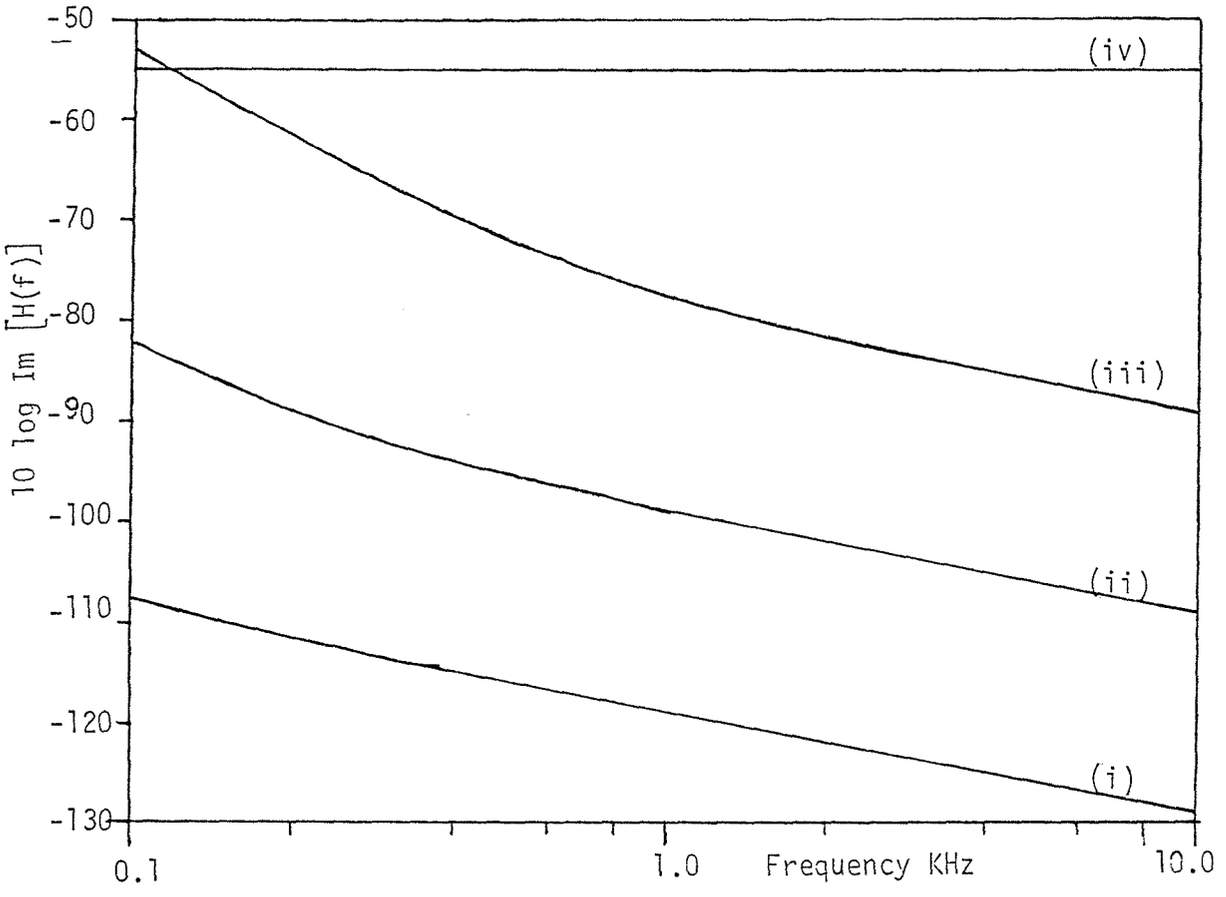

figure 2.8. Response of a ribbed-plate with different rib stiffness, asymmetrical torque excitation; (same rib shape , but with different mass per unit lenght). (i)$Q_b=1x10^{-4}m^4$, $J_b=1x10^{-3}m^4$; (ii) $Q_b=1x10^{-5}m^4$, $J_b=1x10^{-4}m^4$; (iii) $Q_b=1x10^{-6}m^4$, $J_b=1x10^{-5}m^4$; (iv) plate.

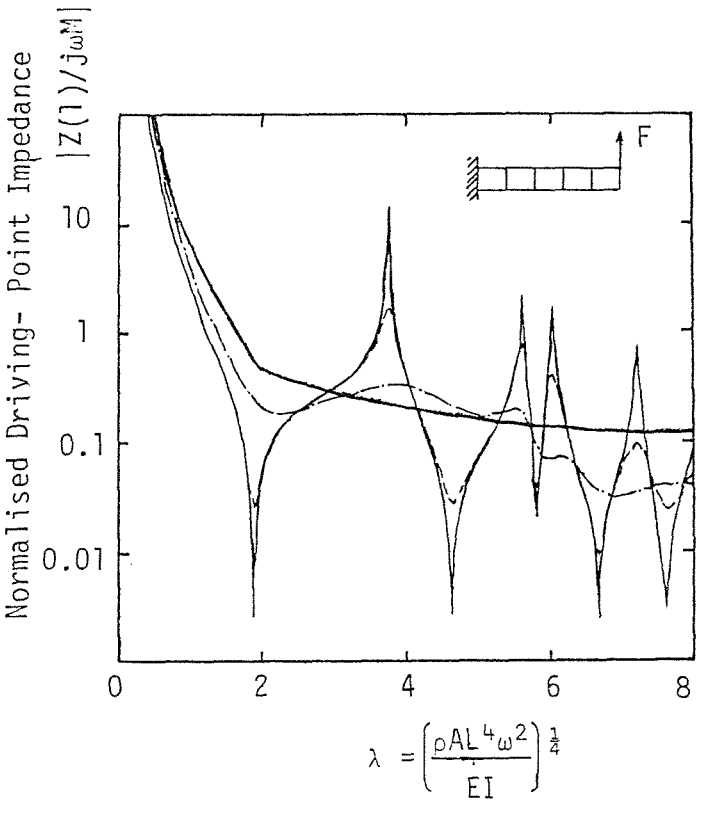

figure 2.9. Normalised driving-point impedance of a double-cantilever system; $(\rho A)_1/(\rho A)_2=1$; $(EI)_1/(EI)_2=1$; $\nu_p=0.3$; $s_p=50$; $\kappa_p=0.85$; N=5; $k_p=100$; $\delta_k=0.01$; $\delta_E=\delta_G$:
—— 0.01, --- 0.1, — - — 1.

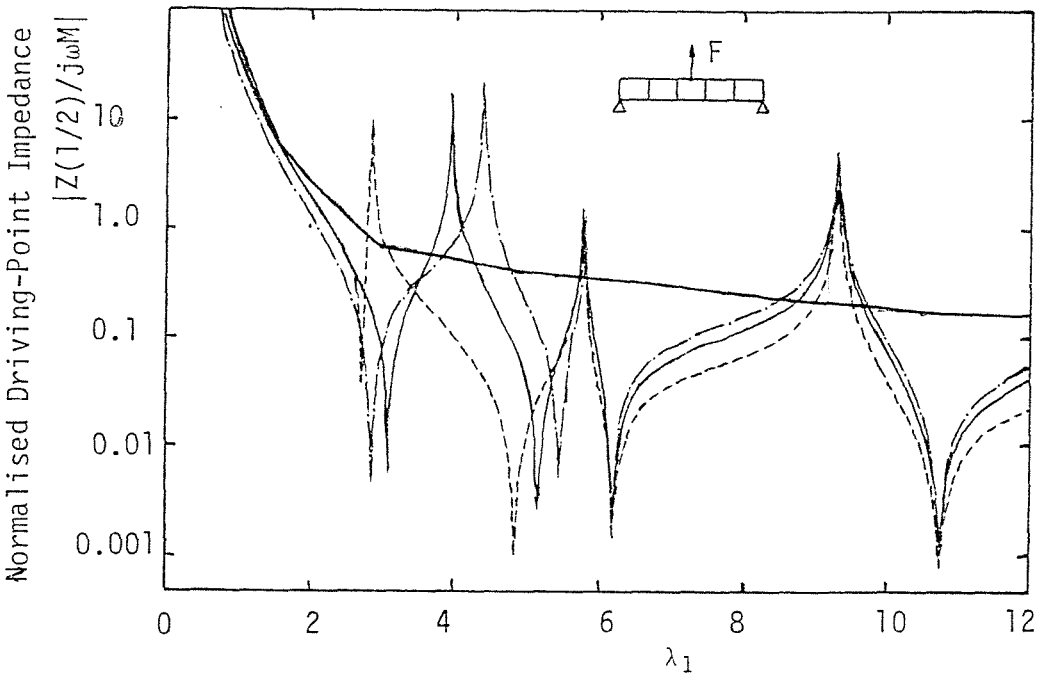

figure 2.10. Normalised driving-point impedance of a simply supported double beam system; $\rho_1/\rho_2=2.7/7.8$; $b_1/b_2=1$; $E_1/E_2=7.2/21.0$; $\nu_p=0.3$; $s_1=50$; $\kappa_p=0.85$; $\delta_E=\delta_G=\delta_k=0.01$; N=6; $k_1=100$; h_1/h_2: —— 1, --- ½, — - — 3/2.

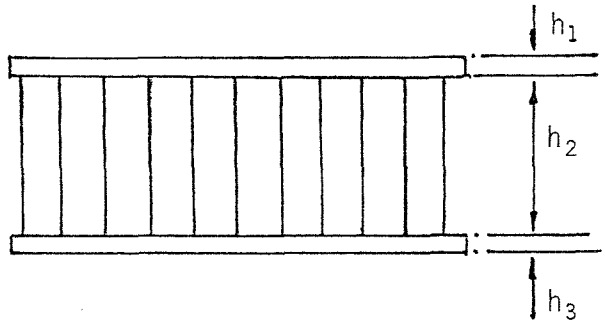

figure 2.11. Construction of a Honeycombed Panel.

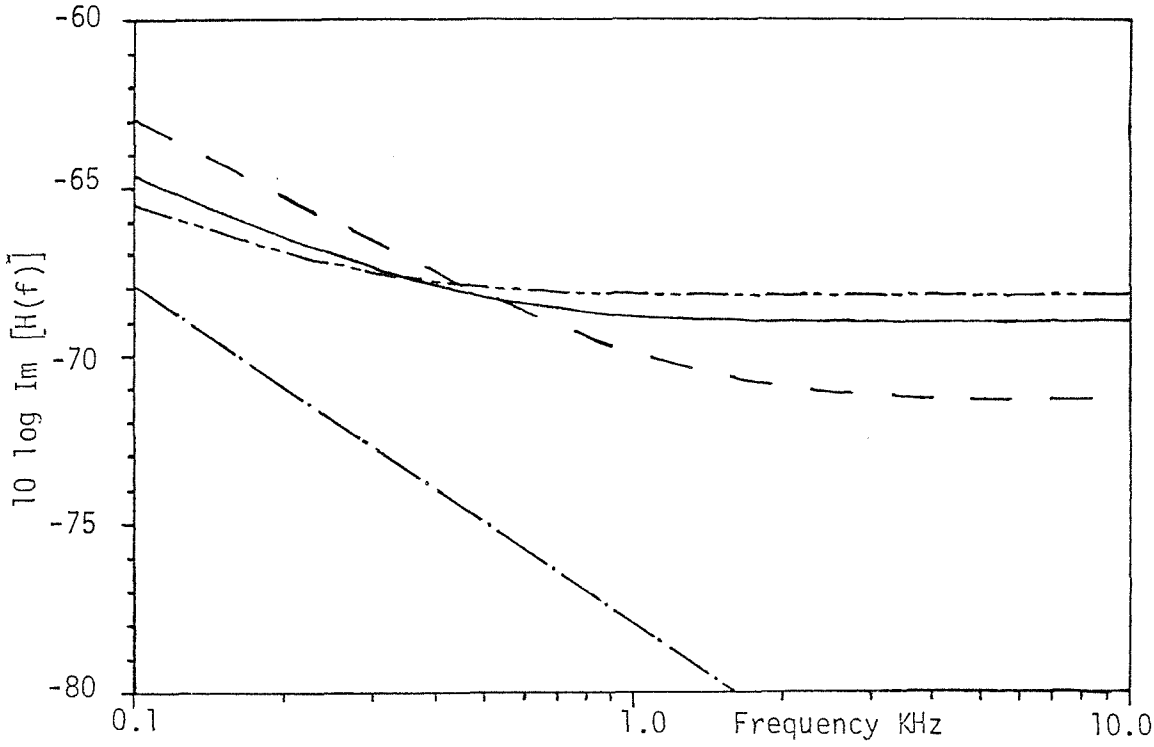

figure 2.12. Point response of Honeycombed plates with the same bending stiffness, force excitation ; —— h_2=1.19cm; — — — h_2=7.1 mm; ---- h_2=2.33 cm; — · —·— steel plate 1 cm thick.

CHAPTER III

AN ALTERNATIVE METHOD OF ESTIMATING THE STRUCTURAL RESPONSE

III. 1. Introduction

In Chapter II the frequency averaged point response of most types of structures is given in the form of an expression relating the response to structure parameters. However, in some circumstances an expression to estimate the structure response is not available, and to develop such an expression will be too complicated. For example, the structure may consist of a series of components which cannot be individually measured or modelled. In this case, the structural response term must be estimated using some other method. For diagnostic purposes, it will be an advantage if when using this alternative method, the result is related to the response term in the accountancy equation so that the same method of analysis can follow.

A very convenient method to estimate the structural response term is to establish a relation between the point response of a structure and the surface spatial average transfer response, which is the ratio of the average surface normal velocity to the excitation force. This relation is obtained both mathematically and experimentally in the case of a cantilever beam. This is similar to relating the noise radiated from a structure to the surface average velocity, but interpreting this relation in terms of the energy accountancy concept and thus retaining the diagnostic capabilities of this concept.

Another way of looking at this alternative method is that instead of measuring the input vibrational energy, the initial energy distributed within the structure is measured. This level of initial energy will depend on both the structural loss factor and the radiation loss factor, since the distribution of the energy will be affected by the losses of the structure.

The structural point response is independent of any losses, because the energy input at a point is not influenced by the rate of energy dissipation of the structure. This is why when using the point response to calculate the escape energy, the structural loss factor term comes in as a seperate term in the expression for the noise energy radiated. Since the spatial average response is dependent on the total loss factor of the structure, the relation between the point response and the spatial average response must contain a loss factor term so that this term does not appear twice in the noise energy estimate. If the same assumption as before is made, that is, the structural loss factor is much larger than the radiation loss factor, then the contribution to the total loss factor will only be from structural losses.

III. 2. Theoretical Analysis

The response of a structure at any point, excited by a force acting perpendicular to the structure surface is given in modal form by

$$y^2 = \frac{1}{S\rho_s} \sum_{n=1}^{\infty} |V_n|^2 \int_s \rho_s \psi_n^2 \, ds \qquad (3.1)$$

for a surface of varying surface density, where V is the total normal surface velocity at the point, and V_n is the contribution to this velocity from the nth mode. ψ_n is the mode shape, due to the form of excitation. Let

$$\phi_n = \int_s \rho_s \psi_n^2 \, ds \qquad (3.2)$$

where ϕ_n is the modal mass, ds an elemental area of the structure and s the total surface area. In each mode, the structure behaves like a one dimensional system, and V_n at each point is given by [1]

$$V_n = \frac{j\omega}{[\omega_n^2(1 + j\eta) - \omega^2]\phi_n} \int_{s'} p\psi_n \, ds' \qquad (3.3)$$

where p is the excitation pressure acting over an area s' and η is the total loss factor (both structural and radiational). In the case where the structural loss factor is much higher than the radiation loss factor, then η will represent the structural loss factor. For a point source, ψ_n inside the integral can be considered a constant ψ_{n_c} and also

$$\int_{s'} p \, ds' = F \qquad (3.4)$$

where F is the point excitation force. Substituting in equation (3.3) and then into equation (3.2)

$$V^2 = \frac{F^2}{S\rho_s} \sum_{n=1}^{\infty} \frac{\omega^2 \psi_{n_c}^2}{[(\omega_n^2 - \omega^2)^2 + \eta^2\omega_n^4]\phi_n} \qquad (3.5)$$

Averaging equation (3.5) over the surface of the structure to obtain the value for the spatial averaged velocity squared, or alternatively by the law of recprocity averaging for any point of excitation on the structure surface, an expression for the spatial averaged velocity is obtained viz.

$$\langle V^2 \rangle = \frac{4F^2\omega^2}{S^2\rho_s^2} \sum_{n=1}^{\infty} \frac{1}{[(\omega_n^2 - \omega^2)^2 + \eta^2\omega_n^4]} \qquad (3.6)$$

where $\langle \; \rangle$ denote spatial averaging.

Frequency averaging this expression over frequency band Δf from frequency f_1 to frequency f_2 ($\omega = 2\pi f$), to compare with the frequency averaged point response in chapter II,

$$\langle V^2 \rangle = \frac{F^2}{\pi^2(\Delta f)S^2\rho_s{}^2} \sum_{n=1}^{\infty} \int_{f_1}^{f_2} \frac{f^2\, df}{[(f_n{}^2 - f^2)^2 + \eta^2 f_n{}^4]} \qquad (3.7)$$

If f is the central frequency in the frequency band Δf i.e. $f_1 < f < f_2$, equation(3.7) becomes

$$\langle V^2 \rangle = \frac{F^2}{S^2\rho_s{}^2} \cdot \frac{1}{\pi 2\eta f}\left(\frac{\Delta N}{\Delta f}\right) \qquad (3.8)$$

where $\Delta N/\Delta f$ is the number of modes per Hertz, i.e. the modal density. However the modal density is also given by [18]

$$\left(\frac{\Delta N}{\Delta f}\right) = 2M\pi f \; \mathrm{Im}\,[H(f)] \qquad (3.9)$$

where $M = S\rho_s$, which is the total mass of the structure. Combining equations (3.8) and (3.9)

$$\mathrm{Im}\,[H(f)] = M\,\eta\left(\frac{\langle V^2 \rangle}{F^2}\right) \qquad (3.10)$$

However, this relation only applies for frequencies above the first resonant frequency, because below, the modal density has no meaning. However, below the fundamental frequency the same approximation method as given in Chapter II for low frequencies may be used. This discrepancy below the fundamental is also observed in the theoretical results for the response of a cantilever beam. These results are shown later on in this chapter.

The above relation (equation (3.10)) holds for both transient and steady state excitation. The effect of the mode of excitation

being included in the $|F(f)|^2$ term in the accountancy equation which is still retained in the same form. Like Im $[H(f)]$, $\langle V^2 \rangle / F^2$ is characteristic of the structure irrespective of whether the structure is subjected to transient or continuous excitation.

From equation (3.10) the proportionality constant between the Im $[H(f)]$ term and the spatial average response as obtained from modal analysis, contains a loss factor term. The level of the spatial average response, or the level of the initial energy will be inversely proportional to the loss factor of the structure. By multiplying the spatial response with the loss factor, as in equation (3.10), the result will be independent of the loss factor. Thus, when using this term in the energy accountancy equation (which contains a separate loss factor term), instead of the point response term, the loss factor will only be included once in the estimation of the noise energy radiated by the structure.

III. 3. Verifying the Response Relation for a Cantilever Beam

The purpose of this experimental and theoretical analysis for a cantilever beam is to obtain curves for the imaginary part of the point response and the spatial average transfer response, and compare them to the theoretical relation for the response obtained above. The theoretical response of the cantilever beam is obtained by completely solving the fourth order differential equation governing the motion of the beam.

Some problems were encountered in obtaining the experimental results because of the limitations in the electronic gear used in the experiment. The main problem was that the beam tested was 1m long giving the lowest natural frequency in bending of about 5Hz. This frequency is outside the frequency range of most electronic devices. The results at low frequencies are not very accurate even above the fundamental frequency. However, the mean level can still be located. The response of the beam at the fundamental frequency is missing for the same reason as above, and therefore data below this frequency could not be verified experimentally.

The mean value of the imaginary part of the response for a beam force excited in flexural vibrations has a slope of -15 dB per

frequency decade [10]. This is shown in both the theoretical and experimental results. There is also good agreement between the theoretical results obtained by direct solution of the equations of motion and the modal solution at low frequencies, showing that the approximation used in chapter II for low frequencies is acceptable.

III. 3.1. Theoretical Analysis

The equation of motion for transverse vibrations of a beam, with its axis in the positive x-direction is given by

$$EI \frac{\partial^4 \xi}{\partial x^4} + \rho A \frac{\partial^2 \xi}{\partial t^2} = p(x) \qquad (3.11)$$

where ξ is the transverse displacement of the beam;
E is Young's Modulus of elasticity;
I is the second moment of area of the beam cross section about an axis in the neutral plane;
ρ is the density;
A is the cross sectional area; and
p(x) is the pressure distribution on the beam.

A solution to this D.E. can be obtained either in closed form, that is by completely solving the D.E. or else using the modal method, as in the first part of this chapter. The closed form solution of equation (3.11) has the form

$$\xi = A_1 \cosh k^*x + A_2 \sinh k^*x + A_3 \cos k^*x + A_4 \sin k^*x \qquad (3.12)$$

where A_n are constants determined from the end conditions; and
k^* the complex wave number.

If $x = 0$ is the fixed end, and $x = \ell$ the end where the force is applied, then the end conditions are:

$$\xi_{x=0} = 0 \qquad \left.\frac{\partial \xi}{\partial x}\right]_{x=0} = 0$$

$$\left.\frac{\partial^2 \xi}{\partial x^2}\right]_{x=\ell} = 0 \qquad \left.\frac{\partial^3 \xi}{\partial x^3}\right]_{x=\ell} = \frac{F_0}{EI} \qquad (3.13)$$

Using these equations it can be shown that

$$\xi = \frac{j\omega F_0}{2EI(k^*)^3} \left\{ \frac{(\cosh k^*x - \cos k^*x)(\sinh k^*\ell + \sin k^*\ell) - (\sinh k^*x - \sin k^*x)(\cosh k^*\ell + \cos k^*\ell)}{(1 + \cosh k^*\ell \cos k^*\ell)} \right\} \qquad (3.14)$$

and the driving point response, $[H(f)]$, that is $\dot{\xi}/\dot{F}_0\Big]_{x=\ell}$ is given by

$$\frac{\dot{\xi}}{\dot{F}_0} = \frac{1}{EI(k^*)^3} \left\{ \frac{\cosh k^*\ell \sin k^*\ell - \sinh k^*\ell \cos k^*\ell}{1 + \cosh k^*\ell \cos k^*\ell} \right\}. \qquad (3.15)$$

The spatial average squared admittance is given by

$$\left[\frac{\xi}{\dot{F}_0}\right]^2 = \frac{1}{\ell}\left[\frac{k^*\ell}{2\omega M}\right] \int_0^{\ell} \left\{ \frac{(\cosh k^*x - \cos k^*x)(\sinh k^*\ell + \sin k^*\ell) - (\sinh k^*x - \sin k^*x)(\cosh k^*\ell + \cos k^*\ell)}{(1 + \cosh k^*\ell \cos k^*\ell)} \right\} dx$$

(3.16)

Equations (3.15) and (3.16) are plotted using the university main computer, to obtain the response curves with frequency. The programmes used are listed in Appendix B. The value of the integration, equation (3.16), is obtained by replacing the integral sign by a summation taken over N points in the range, that is dx becomes $\Delta x = \ell/N$ and $x = r\ell/N$ and summing over r. Thus equation (3.16) becomes

$$\frac{\langle V^2\rangle}{F^2} = \frac{\langle \dot{\xi}^2\rangle}{F^2} = \frac{1}{\ell}\left(\frac{k^*\ell}{2\omega M}\right)^2 \frac{\ell}{N}\sum_{r=1}^{N}\left\{\left\{(\cosh\frac{k^*r\ell}{N} - \cos\frac{k^*r\ell}{N})\right.\right.$$

$$(\sinh k^*\ell + \sin k^*\ell) - (\sinh\frac{k^*r\ell}{N} - \sin\frac{k^*r\ell}{N})$$

$$\left.\left.(\cos k^*\ell + \cosh k^*\ell)\right\} \Big/ (1 + \cosh k^*\ell \cos k^*\ell)\right\}^2 \qquad (3.17)$$

or

$$\frac{\langle V^2\rangle}{F^2} = \frac{1}{N}\left\{\frac{k^*\ell}{2\omega M(1 + \cosh k^*\ell \cos k^*\ell)}\right\}^2$$

$$\sum_{r=1}^{N}\left\{(\cosh\frac{k^*r\ell}{N} - \cos\frac{k^*r\ell}{N})(\sinh k^*\ell + \sin k^*\ell) - \right.$$

$$\left.(\sinh\frac{k^*r\ell}{N} - \sin\frac{k^*r\ell}{N})(\cos k^*\ell + \cosh k^*\ell)\right\}^2 \qquad (3.18)$$

These results are shown in figures (3.1) to (3.4) for two different values of the damping loss factor of 2×10^{-3} and 2×10^{-2}. In the case of the transfer admittance, the value of N used is 40. The physical dimensions of the beam investigated are 6mm thick, 0.944m long and 31.75mm wide.

III. 3.2. Experimental Analysis

Tests were done on two cantilever beams 0.944m long and 31.75mm wide with different thicknesses of 6mm and 9.5mm. The set-up for the rig and equipment is shown in figure (3.5). The difference in thickness allowed the investigation of the effect of structural bulkiness on the response. The damping of the beams was increased by

sticking viscoelastic damping tape on both faces of the beam. The loss factor of the beams was measured by the decay method and the results obtained are shown in figure (3.6). Because of the uncertainty regarding loss factor measurements, and because of the fact that there were only slight variations with frequency, a mean value for the loss factor is assumed, (shown by broken line in figure (3.6)). This mean value for the loss factor is the value used when comparing results.

Both the point response and the spatial averaged response were measured. The beam was excited by a transient signal from a sweep oscillator, scanning from 10 to 350 Hz in 2.5 seconds. The signal was then fed to the electrodynamic vibrator via a power amplifier. The point response of the beam was measured by an impedance head, and the transfer admittance measured by the use of a force transducer and an accelerometer. The signals from these transducers were analysed by means of a digital computer with a sampling rate of 750 samples per second and with 8192 data points. This gave an acquisition time of over ten seconds, that is both the transient and the ringing vibration of the structure were recorded. To obtain the spatial averaged response, the accelometer was transversed along the whole length of the beam. The separation between the consecutive positions of the accelometer was determined from the wavelength of the highest frequency of interest. It can be shown that to measure the mean square value of a sinusoidally varying parameter by measurements at discrete points, three or more equally spaced points randomly placed over one wavelength have to be taken. Then the squared average of these measurements will give the mean square value. At a frequency of 500 Hz, which is the highest frequency of interest in this case, the bending wavelength is 33cm for the 6mm thick beam and 40cm for the 9.5mm thick beam. Therefore to obtain a measure of the spatial averaged velocity squared, the accelometer positions were 8cm apart for both beams. The results obtained for the $Im[H(f)]$ and spatial average admittance for the 6mm , with two different values of loss factor, and the 9.5mm beams are shown in figures (3.7) to (3.12) respectively.

III. 3.3. Comparison of Results

The modal density for a beam excited at one end is given by [1]

$$\left(\frac{\Delta N}{\Delta f}\right) = \frac{k_b \ell}{2\pi f} \tag{3.19}$$

where k_b is the bending wave number given by

$$k_b = \left(\frac{4\pi^2 \rho A f^2}{EI}\right)^{\frac{1}{4}} \tag{3.20}$$

and substituting in equation (3.8),

$$\frac{\langle V^2 \rangle}{F^2} = \frac{1}{Mn}\left(\frac{1}{EI(\rho A)^3}\right)^{\frac{1}{4}} \frac{1}{(2\pi f)^{3/2}} \tag{3.21}$$

Equation (3.21) gives the mean value of the spatial average admittance, for frequencies above the fundamental frequency. This equation shows that the mean level decreases at 15 dB per frequency decade. Since the relation between Im [H(f)] and the spatial average admittance is independent of frequency (equation (3.10)), this same slope should apply for the point response. In fact, the mean level of the curves obtained both theoretically and experimentally agree with this value, for frequencies above the fundamental. Also the exact position of the mean level is given by equation(3.21) for the spatial average admittance. For the imaginary part of the point response, the exact position of the level, using the response relation, is given by,

$$\text{Im } [H(f)] = \left(\frac{1}{EI(\rho A)^3}\right)^{\frac{1}{4}} \frac{1}{(2\pi f)^{3/2}} \tag{3.22}$$

Comparing the theoretical and experimental curves for the spatial average admittance and for Im [H(f)], it can be observed that there is good agreement not just for the mean level but also for the detailed shape of each curve. The theoretical curves have the same axes and can be compared directly. The change in level between the curves for Im [H(f)] and the spatial averaged admittance is equivalent to the product of the mass of the structure, in this case the beam and the loss factor. This is the theoretical result obtained in the first section of this chapter.

In the theoretical results, when comparing the curves for the response, it can also be observed that while the mean level remains the same in the case of the curves for Im [H(f)] with different values of damping, the mean level of the spatial averaged admittance curves changes. With a tenfold increase in damping, the level decreases by 10 dB. Thus the level for the spatial averaged admittance is directly dependent on the loss factor while the level of Im [H(f)] is not. The relation between the two responses is dependent on damping, to compensate for the difference between the relation of each response with the loss factor. The same can be observed from the experimental results, which show a 2 dB change in level corresponding to the equivalent change in the loss factor. However, in this case, the curves cannot be directly compared because of the poor quality of the exact details of the results.

In the experimental results, the noise to signal ratio at the troughs is very high and this distorts the curves. This is why there are sharp drops and discontinuities at some points in the experimental curves. The Im [H(f)] of a structure should be all positive, but because of the low signal to noise ratio , at low values of the response, the noise distorts the signal and the curves become negative. When taking the logarithm of these curves, the negative values are neglected by default. This is not so evident in the spatial average response, and the reasons are that the values are all positive because of the squaring of the measurements and also, because of the number of averages taken. The only problem created because of these discontinuities is that the exact position of the troughs cannot be located and this is therefore assumed.

The influence of the thickness of the beam on the level of the response can be obtained by comparison of the Im [H(f)] curves, (figures (3.7) and (3.9)). Since the level is independent of the loss factor, the difference between the curves for the 6mm and 9.5mm thick beams is entirely due to the change in thickness. The change in the level between these two curves is of 3 dB, that is, the Im [H(f)] is inversely proportional to the square of the thickness or bulkiness of the structure, (20 log (9.5/6)). Consequently, the spatial average admittance will inversely depend on the cube of the thickness. The change in level of the spatial average admittance, (figures (3.8) and (3.12)), is of 8 dB, 3 dB of which are due to the change in damping and 5 dB due to the change in thickness, (30 log (9.5/6)).

The experimental results do not show any information for frequencies below the fundamental. The first resonance was at a very low frequency and is therefore not included in the results. However, from the theoretical results, it can be observed that there is a marked difference between the curves for Im [H(f)] and the curves for the spatial average admittance. At low frequencies, Im [H(f)] is dependent on damping, while the curve for $\langle V^2 \rangle / F^2$ is independent of the damping. Also the Im [H(f)] is constant with frequency, while $\langle V^2 \rangle / F^2$ increases at 20 dB per frequency decade. However, this difference does not affect the estimation of the structural response because the curve of Im [H(f)] below the first resonance can be estimated using the relation for low frequencies given in chapter II. In fact, figures (3.1) and (3.3) verify this low frequency response for a cantilever beam.

III. 4. Conclusion

A relation between Im [H(f)] and the spatial average admittance has been obtained and verified for the case of a cantilever beam. Although one particular type of structure with excitation at only one point is investigated, this does not limit the extent of the general relationship obtained for Im [H(f)] and $\langle V^2 \rangle / F^2$, which shows that they are directly proportional, with the constant of proportionality

being the product of the mass of the structure and the damping loss factor. This relation is proved both theoretically and experimentally.

This result is very useful when it is not possible to directly measure or estimate the point response of a structure. This response relation is used in chapter VI of this thesis, in the case study of the noise energy radiated from a diesel engine structure.

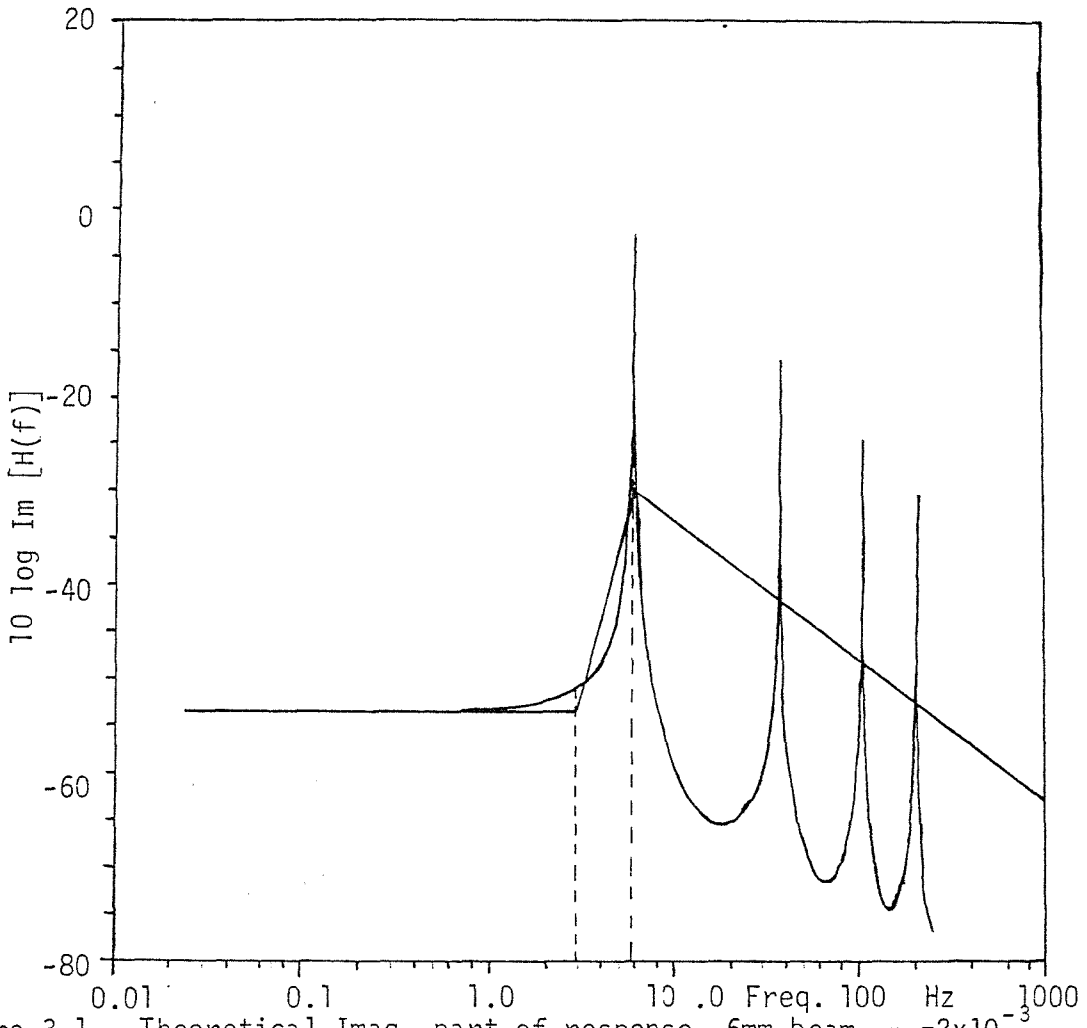

figure 3.1. Theoretical Imag. part of response, 6mm beam, $\eta_s = 2 \times 10^{-3}$

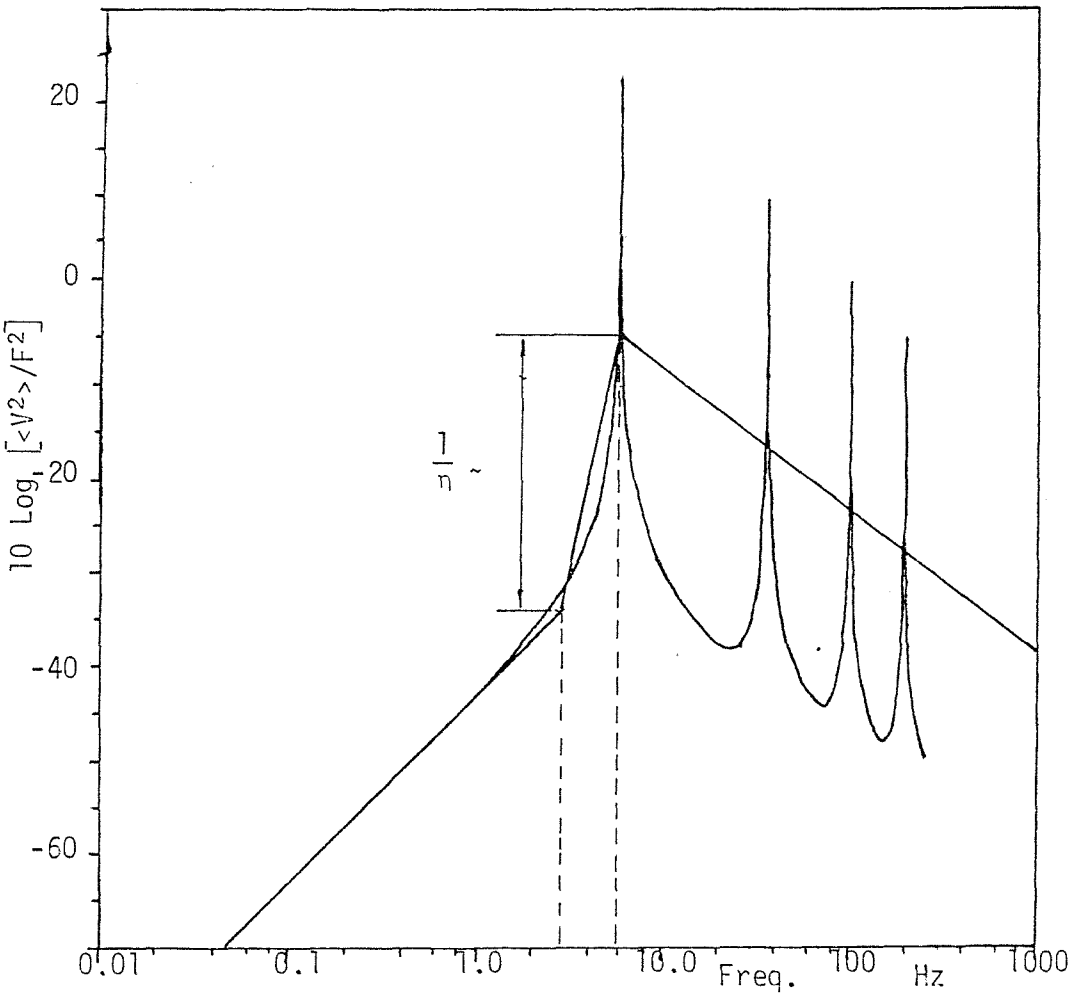

figure 3.2. Theoretical spatial mean transfer admittance , h=6mm, $\eta_S = 2 \times 10^{-3}$

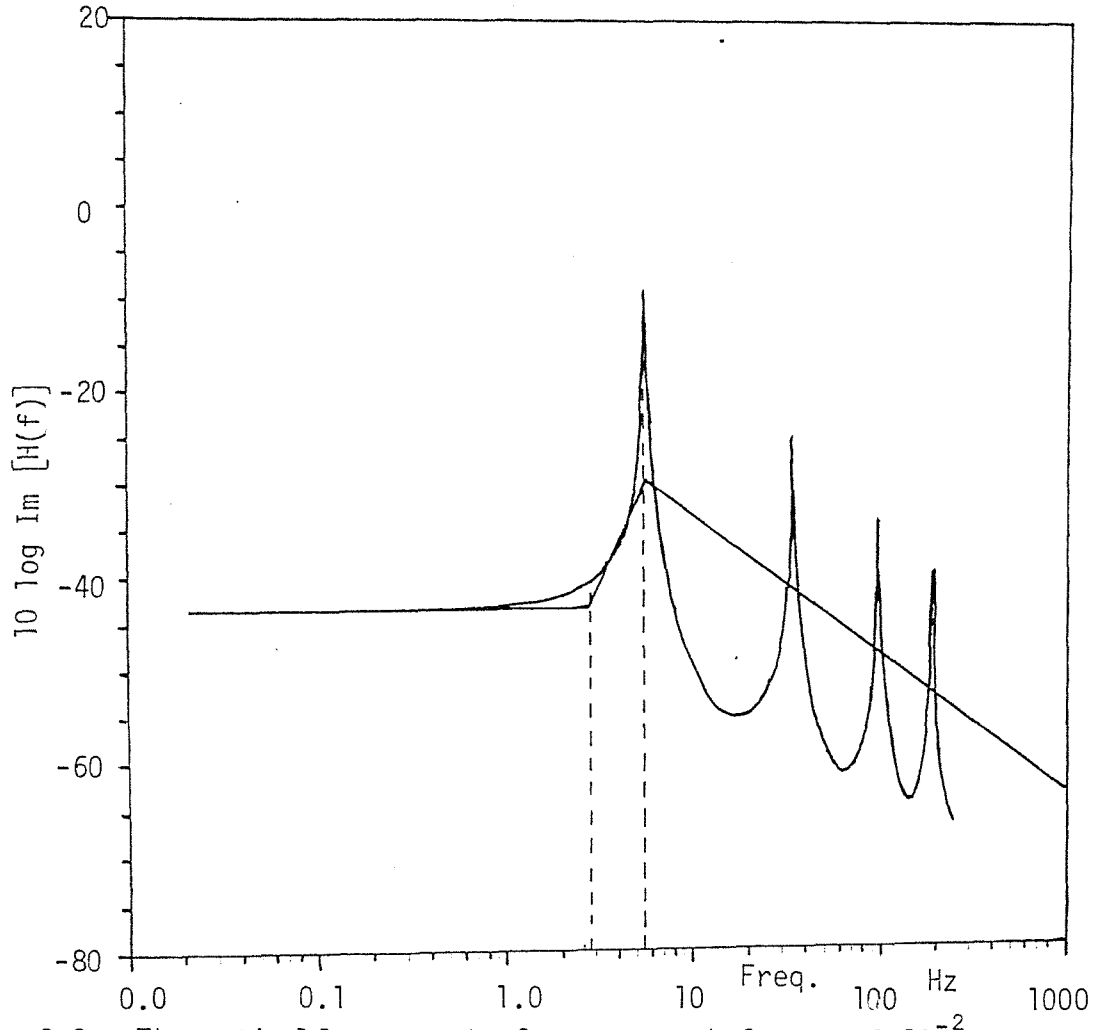

figure 3.3. Theoretical Imag. part of response, h=6mm, $\eta_s=2\times10^{-2}$.

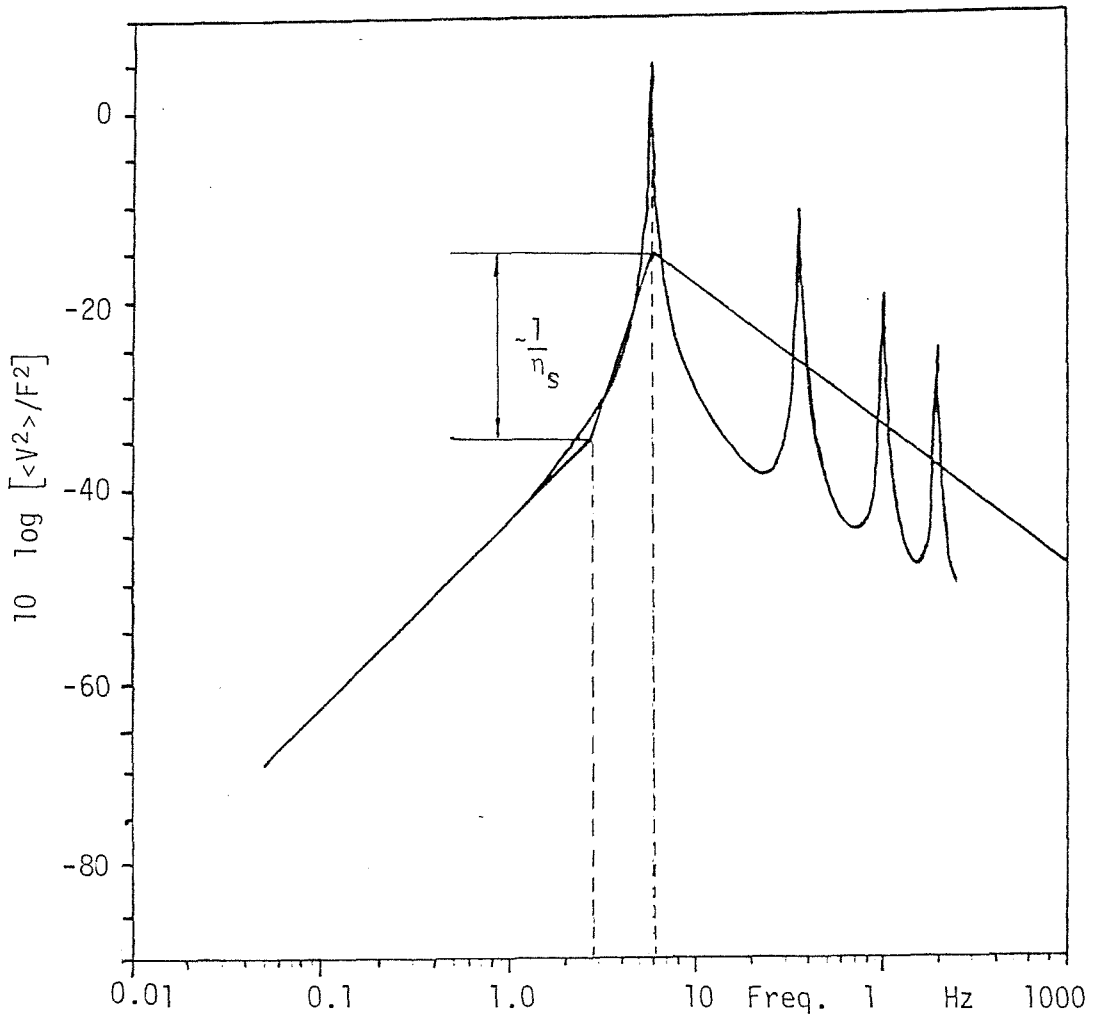

figure 3.4. Theoretical spatial mean transfer admittance, h=6mm, $\eta_s=2\times10^{-2}$

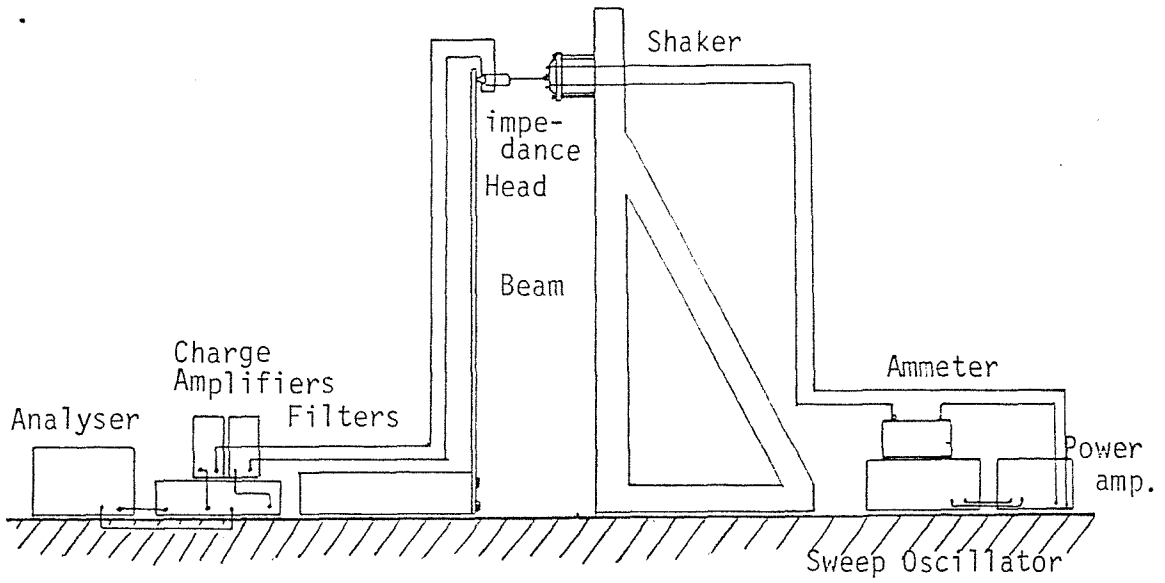

figure 3.5. Cantilever beam set up.

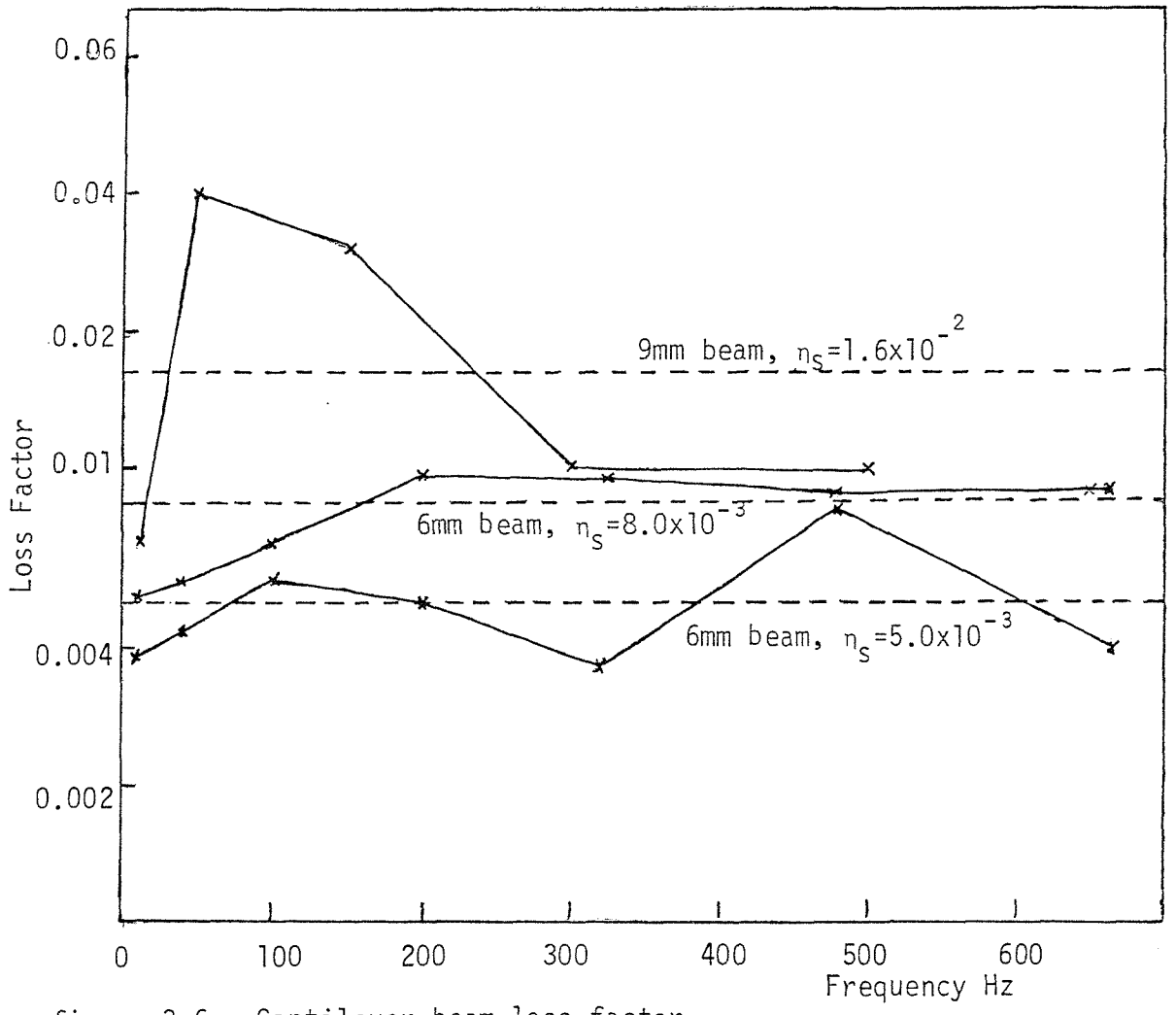

figure 3.6. Cantilever beam loss factor.

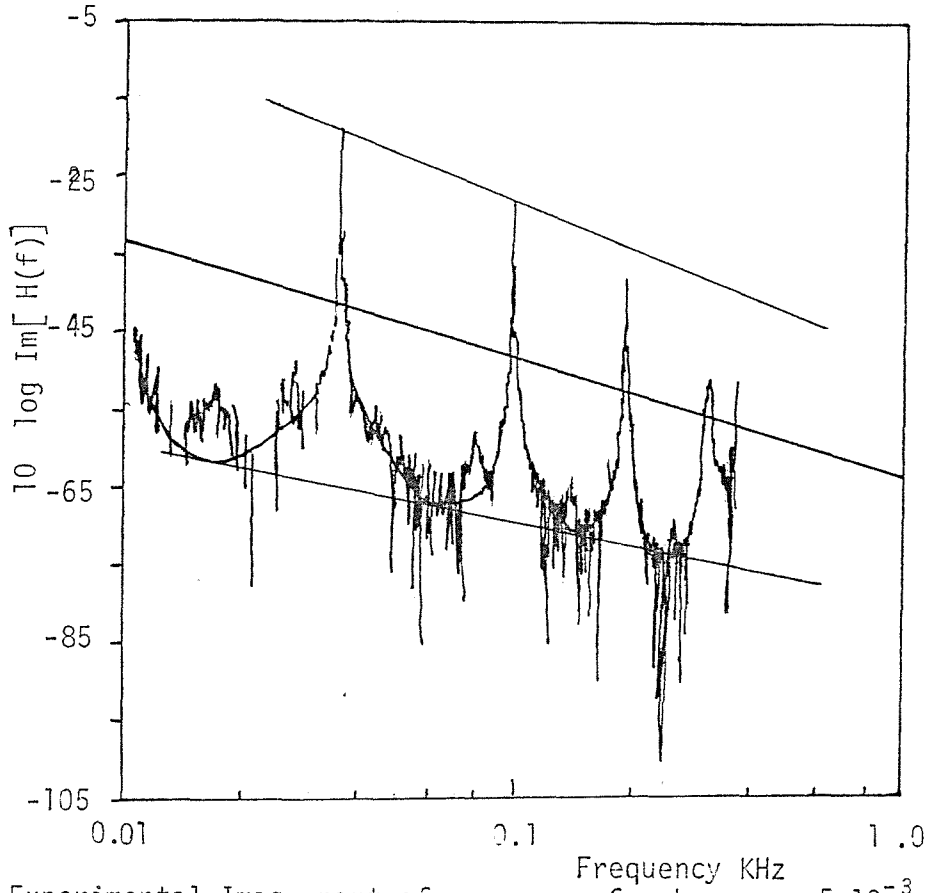

figure 3.7. Experimental Imag. part of response, 6mm beam, $n_s=5x10^{-3}$

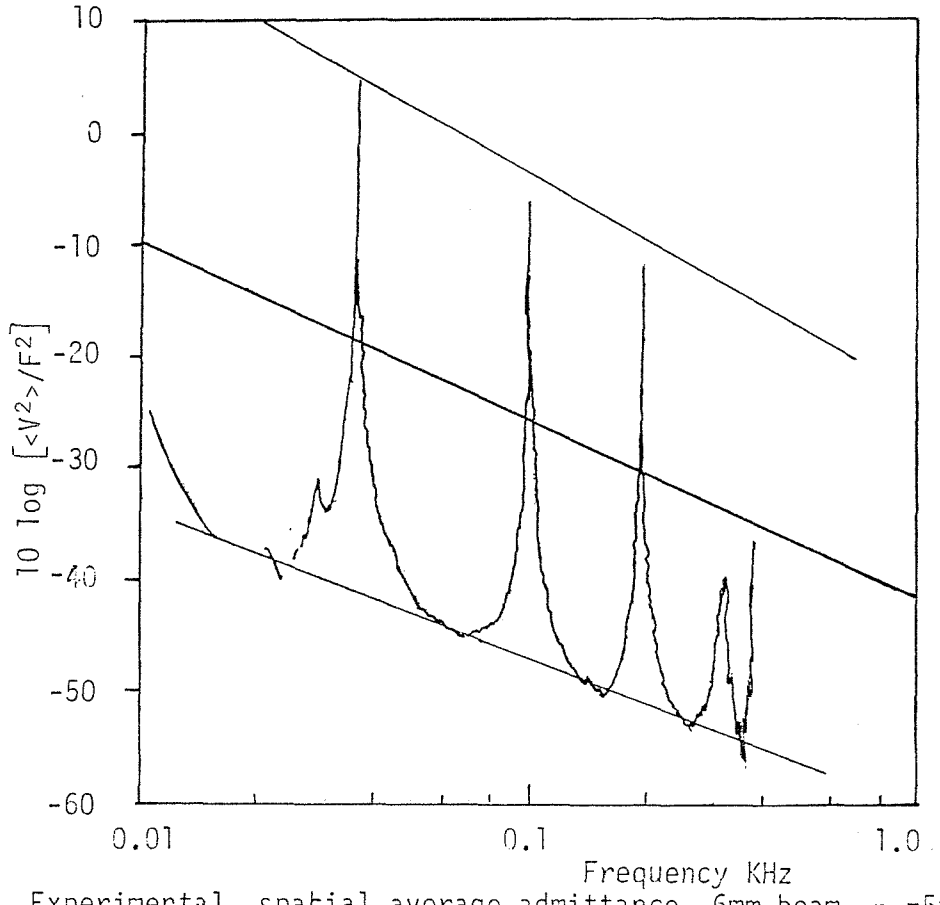

figure 3.8. Experimental spatial average admittance, 6mm beam, $n_s=5x10^{-3}$

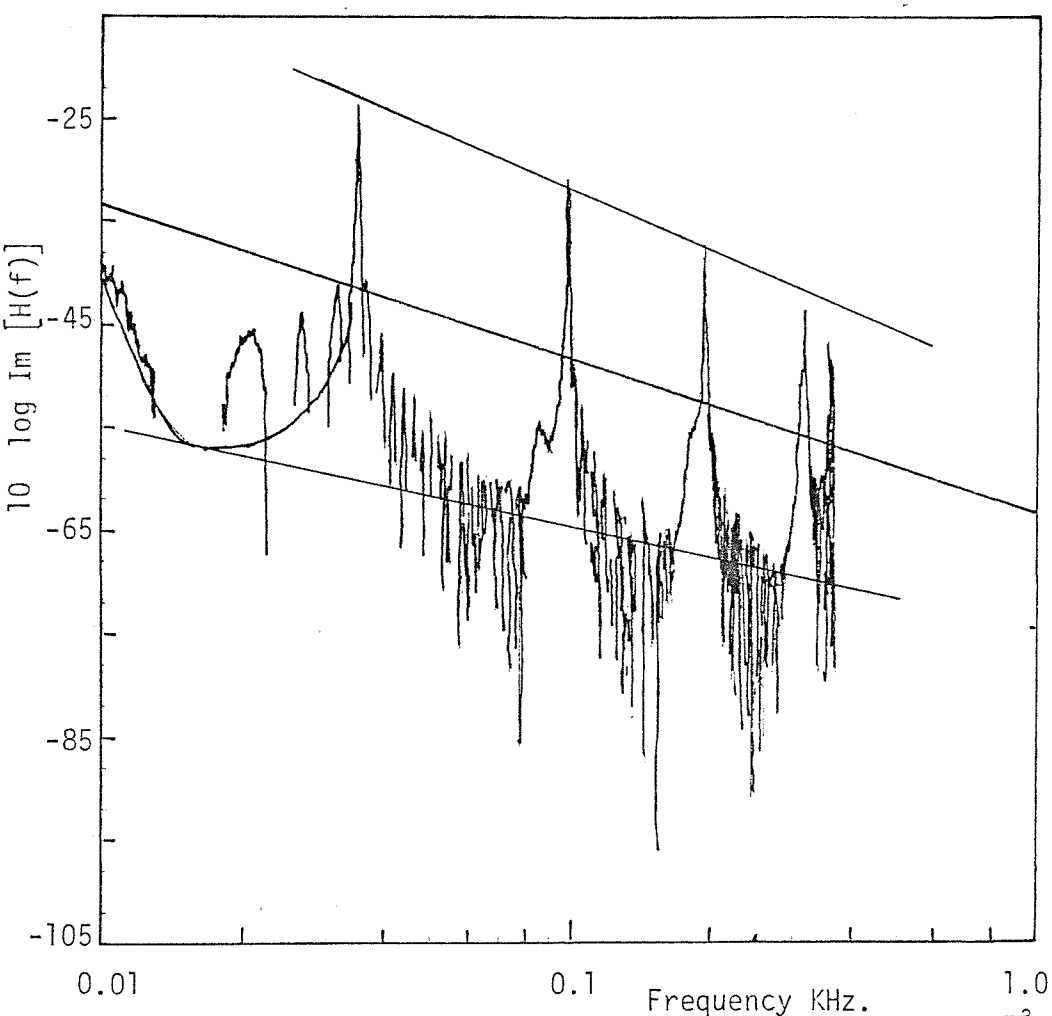

figure 3.9. Experimental Imag. part of response, 6mm beam, $\eta_s = 8 \times 10^{-3}$

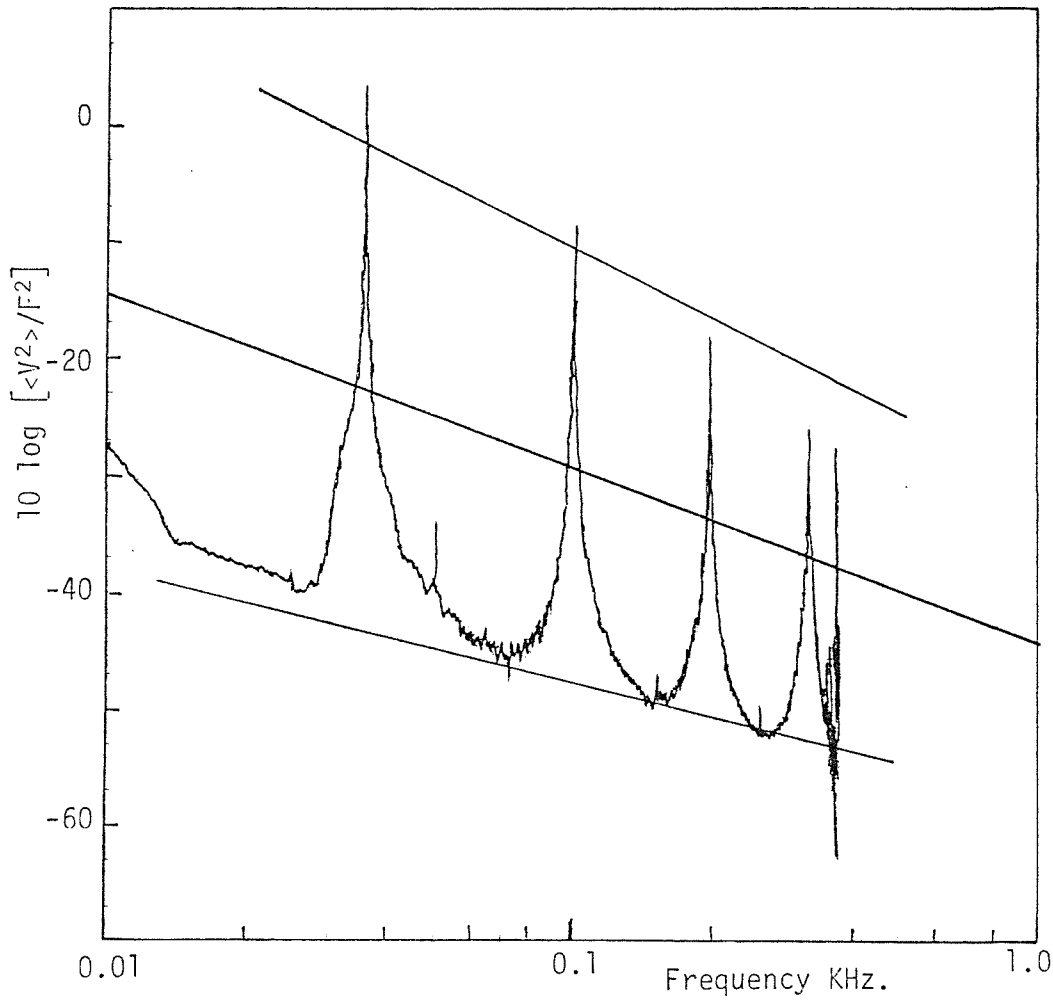

figure 3.10. Experimental spatial average admittance, 6mm beam, $\eta_s = 8 \times 10^{-3}$

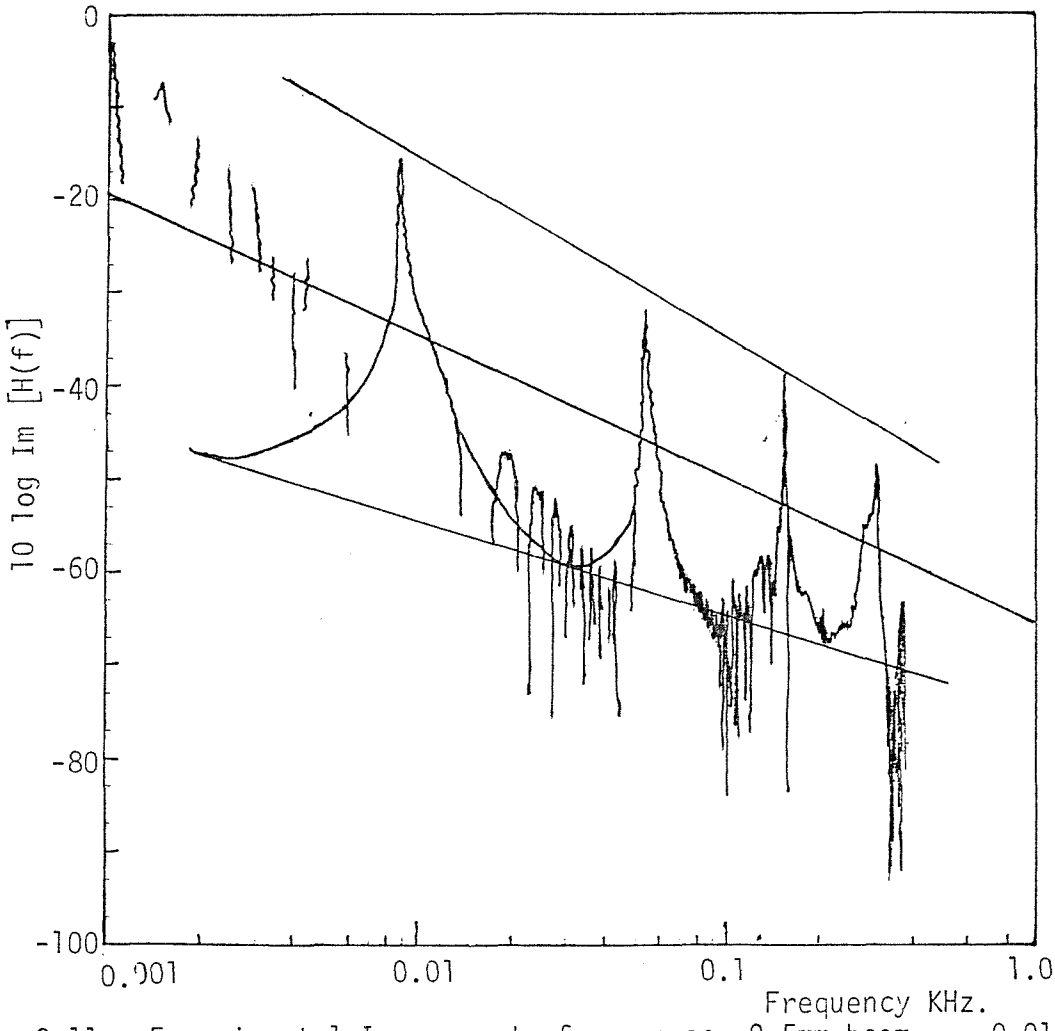

figure 3.11. Experimental Imag. part of response, 9.5mm beam, n_s=0.016.

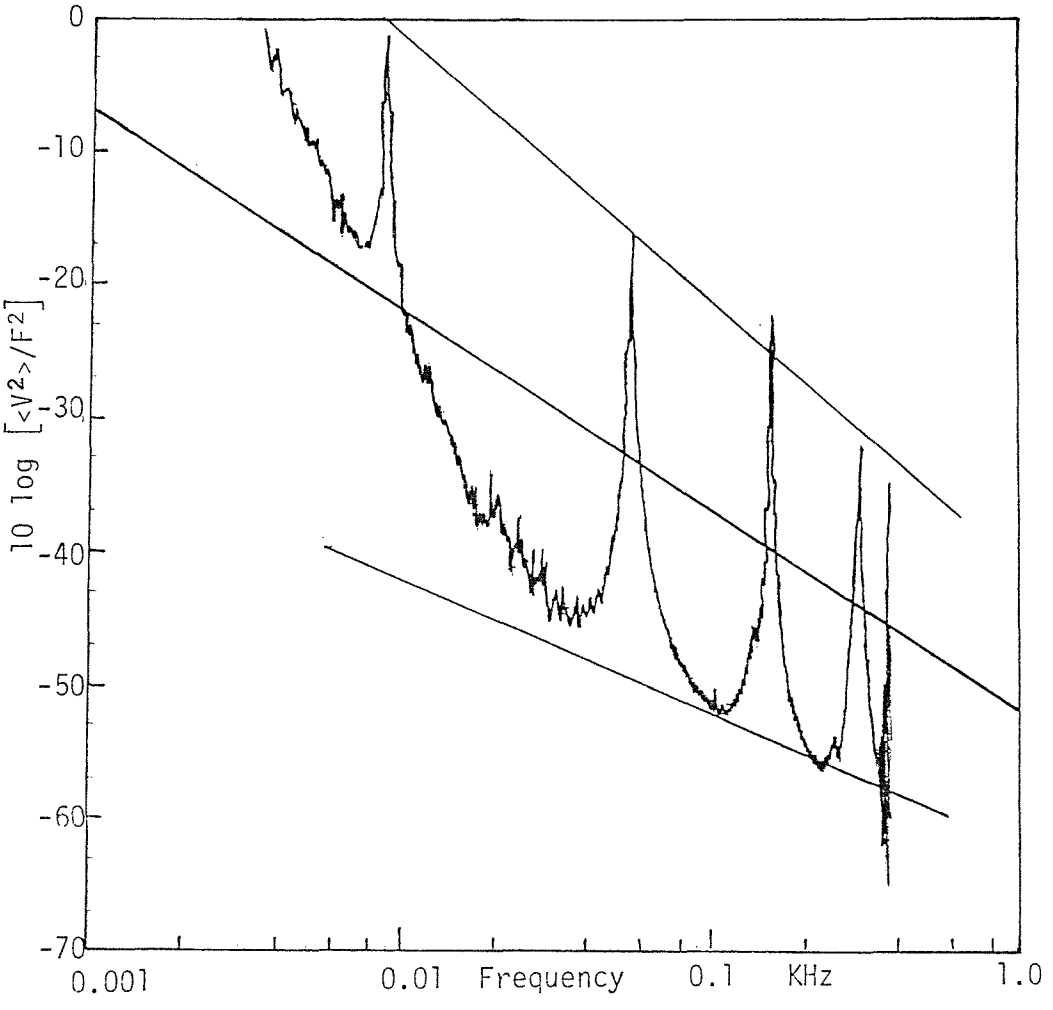

figure 3.12. Experimental spatial average admittance, 9.5mm beam, n_s=0.016

CHAPTER IV

THE SPECTRAL DISTRIBUTION OF ACCELERATION NOISE

IV. 1. Introduction

The noise radiated from an impact can be divided into two parts: the part radiated only during the impact and the part radiated after the impact has occurred. The latter type of noise is termed the ringing of the structure and its parameters are investigated in the previous chapters. The noise that is radiated during the impact is termed acceleration noise and is defined as the noise made by a body (treated as rigid) coming to rest, or accelerating rapidly from one velocity to another in a very short time t_o of such a duration as to cause the air adjacent to it to be compressed or expanded so that some part of the pressure perturbation close to the body will be in phase with the particle velocity. This noise does not depend on the distortion of the impacted structure but only on the whole bodily movement. Even so, it contributes to the total L_{eq} from each impact and has a spectral distribution which depends upon the details of the pulse shape and the size of the body. In this chapter, this acceleration noise which is investigated for a large number of cases in reference [13], is investigated for its frequency content.

If the ringing noise is sufficiently reduced or if the first resonant frequency of the structure under investigation is relatively high, so that the response of the structure below this first resonance is very low and little vibrational energy is contained in this frequency range, (implying a low level of noise radiated due to ringing), then the noise due to the transient deceleration during the impact may be the dominant source of noise in this frequency range. It is therefore necessary for predictive purposes to be able to present the acceleration noise energy in spectral form from knowledge of the impact time and size of the impactor.

The spectral distribution of the acceleration noise will give the frequency bands in which this noise contributes to the total L_{eq}

radiated by the machine structure. The spectral distribution can be obtained by either the consideration of the far field pressure equations which are given in reference [13] or by using the spatial average surface velocity of the impacting body together with a 'steady state' radiation efficiency. Both of these methods give the same result for the frequency distribution of the acceleration noise.

IV. 2. Acceleration Noise Spectrum from the Pressure Signature

To obtain the spectral distribution from Part I [13], assuming that the acceleration transient is in the form of a half-sine pulse, it is necessary to go back to the two far-field equations (7) and (8) [13], for the pressure at a point along or at any specified angle to the axis of acceleration. These equations are expressed as functions of the non-dimensionalised retarded time τ. To obtain the acceleration noise energy spectral density per unit area enclosing the body, flowing past a point in space following the impact, the pressure signature equations are transformed into the frequency plane, the total energy then being the integral over frequency and space (enclosing the source). This follows from Parceval's theorem.

A value for $L_{eq}(A, f, \Delta f)$, can be derived by integrating the pressure spectrum over frequency bands and space, and then A-weighting. For the $L_{eq}(A, f, \Delta f)$ the period over which the acceleration noise is averaged must be stated. If a repetition rate of one occurance per second is assumed, then $L_{eq}(A, f, \Delta f)$ will be the A-weighted total acceleration noise energy, radiated in frequency band Δf, with central frequency f.

Rewriting equations (7) and (8) from Part I, [13]

$$P_o(r, \tau) = \frac{\rho_o a c v_o}{2r\sqrt{4\delta^4 + 1}} \left[\cos(\pi \tau - \gamma) + \sqrt{2}\, e^{-\pi\delta\tau}\cos(\pi\delta\tau + \chi)\right], \quad \tau \leq 1 \tag{4.1}$$

and

$$P_o(r,\tau) = \frac{\rho_o a c v_o}{\sqrt{2} r \sqrt{4\delta^4 + 1}} \left[e^{-\pi\delta(\tau-1)} \cos[\pi\delta(\tau - 1) + \chi] + e^{-\pi\delta\tau} \cos(\pi\delta\tau + \chi) \right], \quad \tau > 1 \qquad (4.2)$$

(please note editorial errors in the original expressions in reference [13])

where $\tau = t'/t_o$, t' being the retarded time and t_o the contact time;

$\delta = ct_o/(\pi a)$;

c = speed of sound in air;

a = radius of the sphere;

$v_o = \frac{2A_o t_o}{\pi}$, the velocity of impact, assuming a half sine pulse for the acceleration, with amplitude A_o;

r = distance of measuring point from point of acceleration of sphere;

$$\gamma = \sin^{-1}\left(\frac{2\delta}{\sqrt{4\delta^4 + 1}} \right) ;$$

$$\chi = \sin^{-1}\left(\frac{2\delta^2 + 1}{\sqrt{2}(4\delta^4 + 1)} \right) ;$$

ρ = density of the medium surrounding the sphere.

The pressure at any angle θ from the acceleration axis is given by: $p(r,t',\theta) = P_o(r,t') \cos\theta$.

Fourier transforming the pressure signature equations (4.1) and(4.2)

$$P_o(r, f) = t_o \int_{-\infty}^{\infty} P_o(r, \tau) e^{-j2\pi f\tau} d\tau \qquad (4.3)$$

$$P_o(r, f) = t_o \left[\int_o^1 P_o(r, \tau) e^{-j2\pi f\tau} d\tau + \int_1^{\infty} P_o(r, \tau) e^{-j2\pi f\tau} d\tau \right] \qquad (4.4)$$

Using equation (4.1) for the first integral and equation (4.2) for the second, will give the expression for the normalised pressure spectrum along the axis of acceleration, $\dfrac{|P_o(r, f)|^2}{\left(\dfrac{\rho_o c a v_o t_o}{r}\right)}$ as follows:

$$\frac{|P_o(r, f)|^2}{\left(\dfrac{\rho_o a c v_o t_o}{r}\right)} = \frac{1}{2\pi^2} \frac{f^2 t_o^2 (1 - \cos 2\pi f t_o)}{(1 - 4f^2 t_o^2)^2 (\delta^4 + 4f^4 t_o^4)}, \quad f \neq \frac{1}{2t_o} \qquad (4.5)$$

$$= \frac{1}{16(4\delta^4 + 1)}, \qquad f = \frac{1}{2t_o} \qquad (4.6)$$

The normalised energy in a bandwidth Δf centred on frequency f, $\mu_{acc}(f, \Delta f)$ where

$$\mu_{acc}(f, \Delta f) = \frac{E_{acc}(f, \Delta f)}{\frac{1}{2}\rho_o (vol) v_o^2} \quad ; \qquad (4.7)$$

$E_{acc}(f, \Delta f)$ is the acoustic energy radiating from the sphere; and

(vol) is the volume of the sphere;

is given by :

$$\mu_{acc}(f, \Delta f) = \frac{1}{\frac{1}{2}\rho(vol)\, v_o^2} \frac{4\pi r^2}{3\rho c} \int_{f - \frac{\Delta f}{2}}^{f + \frac{\Delta f}{2}} |P_o(r, f)|^2 df, \quad (4.8)$$

After integrating over a sphere enclosing the source, taking into account the directionality (cos θ) .

$$\mu_{acc}(f, \Delta f) = \frac{2\delta}{\pi} \left(\frac{\Delta f}{f}\right) \frac{(ft_o)^3 (1 + \cos 2\pi f t_o)}{(1 - 4f^2 t_o^2)^2 (\delta^4 + 4f^4 t_o^4)}, \quad f \neq \frac{1}{2t_o} \quad (4.9)$$

$$= \frac{\pi}{8} \left(\frac{\Delta f}{f}\right) \left(\frac{\delta}{4\delta^4 + 1}\right), \quad f = \frac{1}{2t_o} \quad (4.10)$$

where ($\Delta f/f$) is a constant if percentage frequency bands (e.g., one third octave bands) are being considered.

IV. 3. Acceleration Noise using the Spatial Average Surface Velocity

Another method to express the acceleration noise energy in frequency bands is to use the spatial average of the velocity on the surface of the body and then attaching to this movement a 'steady state' vibrational radiation efficiency of a body in oscillatory bodily movement.

Considering again a sphere of the same volume as the body under transient acceleration and assuming that the shape of the acceleration transient is a half sine pulse with duration (contact time) t_o. The surface velocity on the sphere, if angles are measured from the axis of acceleration or impact is given by;

$$v_s = v \cos \theta \quad (4.11)$$

where v_s is the normal surface velocity; and

v is the velocity of the sphere along the axis of bodily movement.

The spatial average velocity squared is then given by:

$$\langle v_s^2 \rangle = \frac{2v^2}{4\pi a^2} \int_0^{\pi/2} 2\pi a^2 \sin\theta \cos^2\theta d\theta = \frac{v^2}{3} \qquad (4.12)$$

where $\langle\ \rangle$ denotes spatial averaging.

The radiated noise energy from a vibrating surface is given by:

$$E_{rad} = \int_{-\infty}^{\infty} P(t)dt \qquad (4.13)$$

where $P(t)$ is the average radiated power given by:

$$P(t) = \rho c A \overline{\langle v^2 \rangle} \sigma_{rad} \qquad (4.14)$$

where $\rho c A$ is the air impedance;

A is the surface area of the body;

$\overline{\ \ }$ indicates time averaging of the velocity squared; and

σ_{rad} is the radiation efficiency.

Expressing equation (4.13) in the frequency domain;

$$E = \rho c A \sigma_{rad} \int_{-\infty}^{\infty} \langle |V(f)|^2 \rangle df \qquad (4.15)$$

where $V(f)$ is the Fourier transform of the surface velocity.

Or, expressing the energy in frequency bands with central frequency f,

$$E(f, \Delta f) = 2\rho c A \sigma_{rad} \int_{f - \frac{\Delta f}{2}}^{f + \frac{\Delta f}{2}} \langle |V(f)|^2 \rangle \, df \qquad (4.16)$$

but $A = 4\pi a^2$ for a sphere, and the acceleration transient is assumed to have a half-sine pulse, then

$$V(f) = \frac{A_o t_o}{j2\pi^2 f} \left[\frac{1 + e^{-j2\pi f t_o}}{1 - 4f^2 t_o^2} \right] \qquad (4.17)$$

or

$$\langle |V(f)|^2 \rangle = \frac{v_o^2}{24\pi^2 f^2} \frac{(1 + \cos 2\pi f t_o)}{(1 - 4f^2 t_o^2)^2} \qquad (4.18)$$

therefore

$$E(f, \Delta f) = 2\rho c \left[\frac{\Delta f}{f} \right] f \sigma_{rad} \frac{4\pi a^2}{3} \left[\frac{v_o^2 (1 + \cos 2\pi f t_o)}{8\pi^2 f^2 (1 - 4f^2 t_o^2)^2} \right] \qquad (4.19)$$

and

$$\mu_{acc}(f, \Delta f) = \frac{\delta}{2\pi} \left[\frac{\Delta f}{f} \right] \frac{\sigma_{rad}}{f t_o} \frac{(1 + \cos 2\pi f t_o)}{(1 - 4f^2 t_o^2)^2} \qquad (4.20)$$

The radiation efficiency for an oscillating body is given by [14];

$$\sigma_{rad} = \frac{(ka)^4}{4 + (ka)^4} \qquad (4.21)$$

for a dipole system, where k is the acoustic wave number, or

$$\sigma_{rad} = \frac{4f^4 t_o^4}{\delta^4 + 4f^4 t_o^4} \quad . \tag{4.22}$$

Substituting this expression for σ_{rad} in equation (4.20)

$$\mu_{acc} = \frac{2\delta}{\pi}\left(\frac{\Delta f}{f}\right)\frac{(ft_o)^3(1 + \cos 2\pi f t_o)}{(\delta^4 + 4f^4 t_o^4)(1 - 4f^2 t_o^2)^2} \qquad f \neq \frac{1}{2t_o} \tag{4.23}$$

$$\simeq \frac{\pi}{8}\left(\frac{\Delta f}{f}\right)\frac{\delta}{(4\delta^4 + 1)} \qquad f = \frac{1}{2t_o} \tag{4.24}$$

Equations (4.23) and (4.24) are the same as those obtained by considering the pressure waveform equations (4.9) and (4.10) . Thus the acceleration noise energy can be estimated either using the pressure signature over a surface enclosing the body, or using the average velocity squared of the body. In retrospect, this result is not surprising, since the only difference between the two methods is the stage in the argument when the transfer from real time to frequency is carried out. It means that measurements of body velocities during and after the impact can lead to the prediction of 'acceleration' noise of the body, from the components of the velocities during the impact, as well as the ringing noise from the components of the velocities after the impact. This finding is used practically in reference [22] which deals with the noise from a drop hammer.

IV. 4. Determining the Shape and Magnitude of the Spectrum

Equations (4.5), (4.6), (4.9) and (4.10) can be written in

logarithmic form. Equation (4.9) becomes:

$$10 \log \left[\mu_{acc}(f, \Delta f)\right] = 10 \log \left[\frac{(ft_o)^3(1 + \cos 2\pi ft_o)}{(1 - 4f^2t_o{}^2)^2}\right]$$

$$+ 10 \log \left[\frac{1}{\delta^4 + 4f^4t_o{}^4}\right] + 10 \log \left[\frac{2\delta}{\pi}\left(\frac{\Delta f}{f}\right)\right] .$$

$$f \neq \frac{1}{2t_o} \qquad (4.25)$$

The first term in this equation depends only on the parameter ft_o, while the second term depends solely on the dimensions of the sphere.

There are other forms into which equation (4.25) can be written, depending upon the interpretation that is required. If we introduce a base frequency f_o which is the reciprocal of twice the contact time t_o , $(f_o = 1/2t_o)$, and using a non-dimensionalised frequency f' , where $f' = f/f_o$, then equation (4.25) becomes (from equation (4.19))

$$10 \log \left[\mu_{acc}(f, \Delta f)\right] = 10 \log \left[\frac{\delta}{\pi}\left(\frac{\Delta f}{f}\right)\right] + 10 \log \left[\frac{(1 + \cos \pi f')}{f'(1 - f'^2)^2}\right]$$

$$+ 10 \log \left(\sigma_{rad}(f)\right) , \quad f' \neq 1 \qquad (4.26)$$

In this expression, the first term determines the general level of the curve and is dependent only on 'δ'. The second term is dependent on the ratio of the frequency f to the conceptual frequency f_o $\left(= \frac{1}{2t_o}\right)$ and is not influenced by body size.

Comparing this second term with the approximation of the spectrum of a pulse in Appendix A, this term represents the general shape of the spectrum of any pulse with duration t_o. There is a term f' missing in the denominator, but this has been included in the first term. Only one break frequency is present here as compared to the two break frequencies in Appendix A and the small frequency range between these two break frequencies has been ignored for the sake of simplicity, but without any loss of accuracy. This shows that this acceleration noise spectrum will hold for all shapes of pulses.

The third term depends solely on the steady-state radiation efficiency of the body, which is dependent on body size for the coincidence frequency. The radiation efficiency relates the distance around the body to the wavelength of sound, thus it will be independent of the exact shape of the body. Therefore from these last two terms, it can be concluded that this spectrum for the acceleration noise will hold for all body shapes, a conclusion also reached in [13] when measurements of acceleration noise peak pressures and total energies were made.

The first term is independent of frequency, while the second term has a break frequency at $f' = 1$. Below this frequency, this term has a slope of -10 dB per decade, and above it decreases at 50 dB per decade (figure 4.1). The third term has a break frequency at $f' = \sqrt{2}\,\delta$ (this is a normalised frequency). This term has a slope of 40 dB per decade below this break frequency and a slope of 0 above this frequency (figure 4.2). Therefore the shape of the spectrum can be constructed without plotting equations (4.9) and (4.10), by adding the contributions at each frequency from the three terms.

The shaping will depend on the value of δ. For $\delta > 1$, it follows from above that the spectrum will have a slope of 30 dB per decade at the low frequency end, then a slope of -10 dB per decade between the two corner frequencies $f'_{a1} = 1$ and $f'_{a2} = \sqrt{2}\delta$, and then a roll-off of -50 dB per decade at the high frequency end. At $f' = 1$ which is the maximum of the curve, the value for this point is independent of frequency and is given by $\dfrac{\pi\delta}{8(4\delta^4 + 1)}\left(\dfrac{\Delta f}{f}\right)$.

The shape of the energy spectrum in frequency bands using equations (4.9) and (4.10) for the acceleration noise is compared with the constructed curve (figure 4.3). The agreement is good and the maximum error which occurs at the corner frequencies is within 2 dB.

For $\delta \lesssim 1$, the curve for the acceleration noise is constructed slightly differently. A new corner frequency is introduced, given by:

$$f'_{a1} = \delta \left[\frac{1 + \cos \sqrt{2}\pi\delta}{(1 - 2\delta^2)^2\sqrt{2}} \right]^{1/3} , \qquad (4.27)$$

but still retaining the other two; $f'_{a2} = \sqrt{2}\delta$ and $f'_{a3} = 1$. In this case the curve has a different shape. Above frequency f'_{a1} there is a flat portion which is equal in magnitude to the maximum acceleration noise energy given by

$$\mu_{acc_{max}} = \frac{1}{\sqrt{8}\pi} \left(\frac{\Delta f}{f} \right) \left[\frac{1 + \cos \sqrt{2}\pi\delta}{(1 - 2\delta^2)^2} \right] . \qquad (4.28)$$

This flat portion extends until it meets the curve as drawn for values of $\delta > 1$. The shape of the acceleration noise energy spectrum as obtained using equations (4.9) and (4.10) is compared with the constructed curve (figure 4.4). The agreement again is within 2 dB. Curves for $\delta = 1$ using the same method of construction as for values of $\delta < 1$, are compared with the plotted curves and the agreement is similar to the other cases (figure 4.5).

IV. 5. L_{eq} from μ_{acc}

If the acceleration noise transient dies down, after its occurence in less than the averaging time T, then with T averaging time,

$$L_{eq}(f, \Delta f) = 10 \log \left[\mu_{acc}(f, \Delta f)\right] + 10 \log \left[\tfrac{1}{2}\rho_o(vol)v_o^2\right] - 10 \log T \qquad (4.29)$$

and $L_{eq}(A, f, \Delta f)$ can be obtained by A-weighting these results.

The A-weighted acceleration noise energy spectrum, measured in one-third octave bands for a sphere subject to an acceleration transient of magnitude 16.34×10^3 m/s^2 over a period of 0.18 ms, is compared with the estimated spectrum (figure 4.6) using the above method. The agreement between the two curves is within ± 3 dB.

Figure (4.7(b)) shows the estimated and measured total acceleration noise energy spectrum (linear) for the impact between a drop stamp tup and a 152mm diameter steel cylinder. The acceleration pulse is shown in figure (4.7(a)). This acceleration signal also includes the ringing of the cylinder, but this ringing is above our frequency range of interest, although it shows on the acceleration noise energy spectrum at the high frequency end; the measured noise has an upward trend unlike the estimated noise. Both the cylinder and the tup are subjected to a transient motion, therefore both will radiate acceleration noise. The agreement between the measured and estimated, based on spheres of equal volume is good even though the shapes of the cylinder and tup are far from spherical. This brings out the point that acceleration noise is independent of the detailed shape of the impacting body, but only dependent on its volume or a typical body size, and the duration of the transient.

Other examples on the use of this method to estimate the spectral content of the acceleration can be found in reference [16], the noise radiated from bottle clashing.

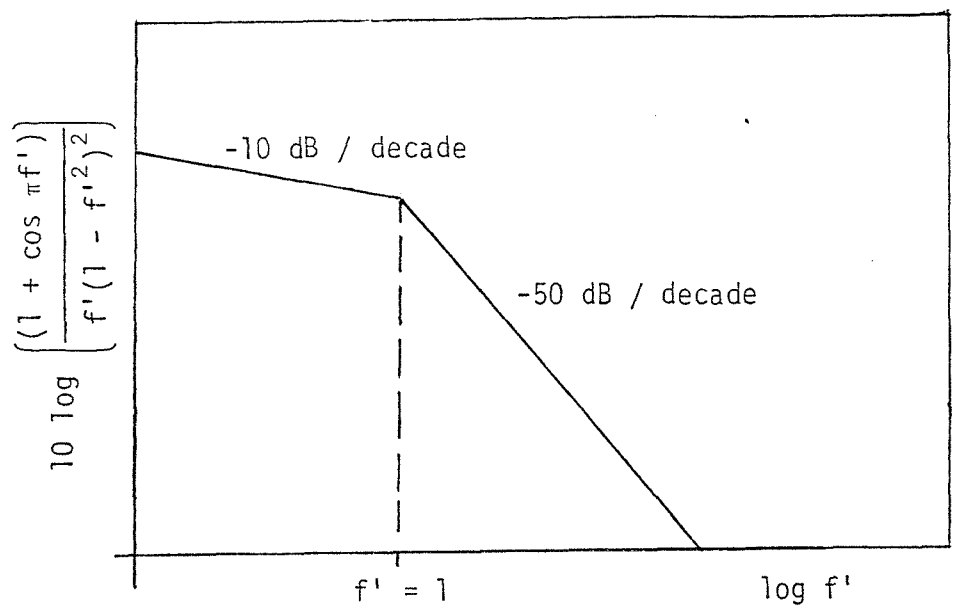

figure 4.1. Variation of the 10 log $\left[\frac{(1 + \cos \pi f')}{f'(1 - f'^2)^2}\right]$ component with frequency f'

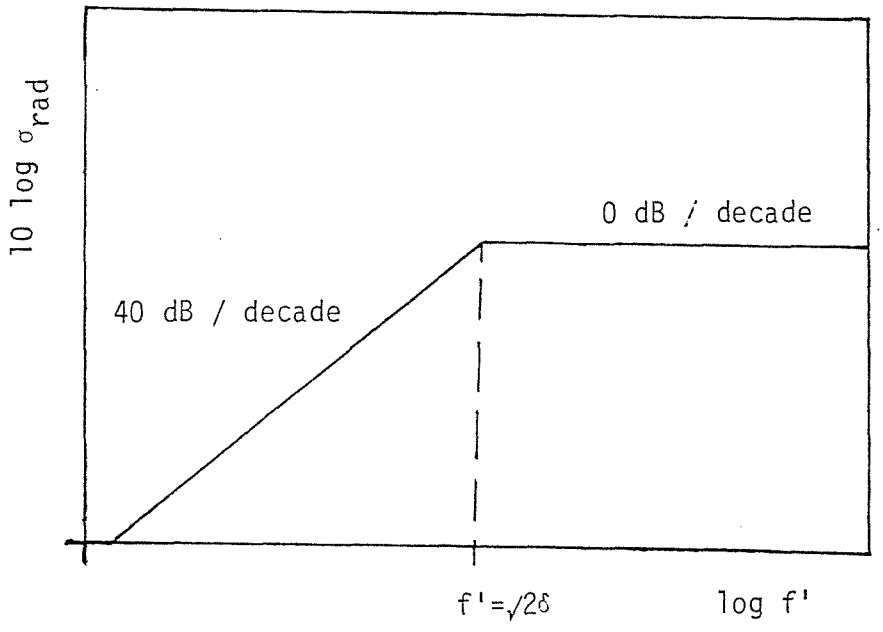

figure 4.2. Variation of 10 log σ_{rad} with frequency f'

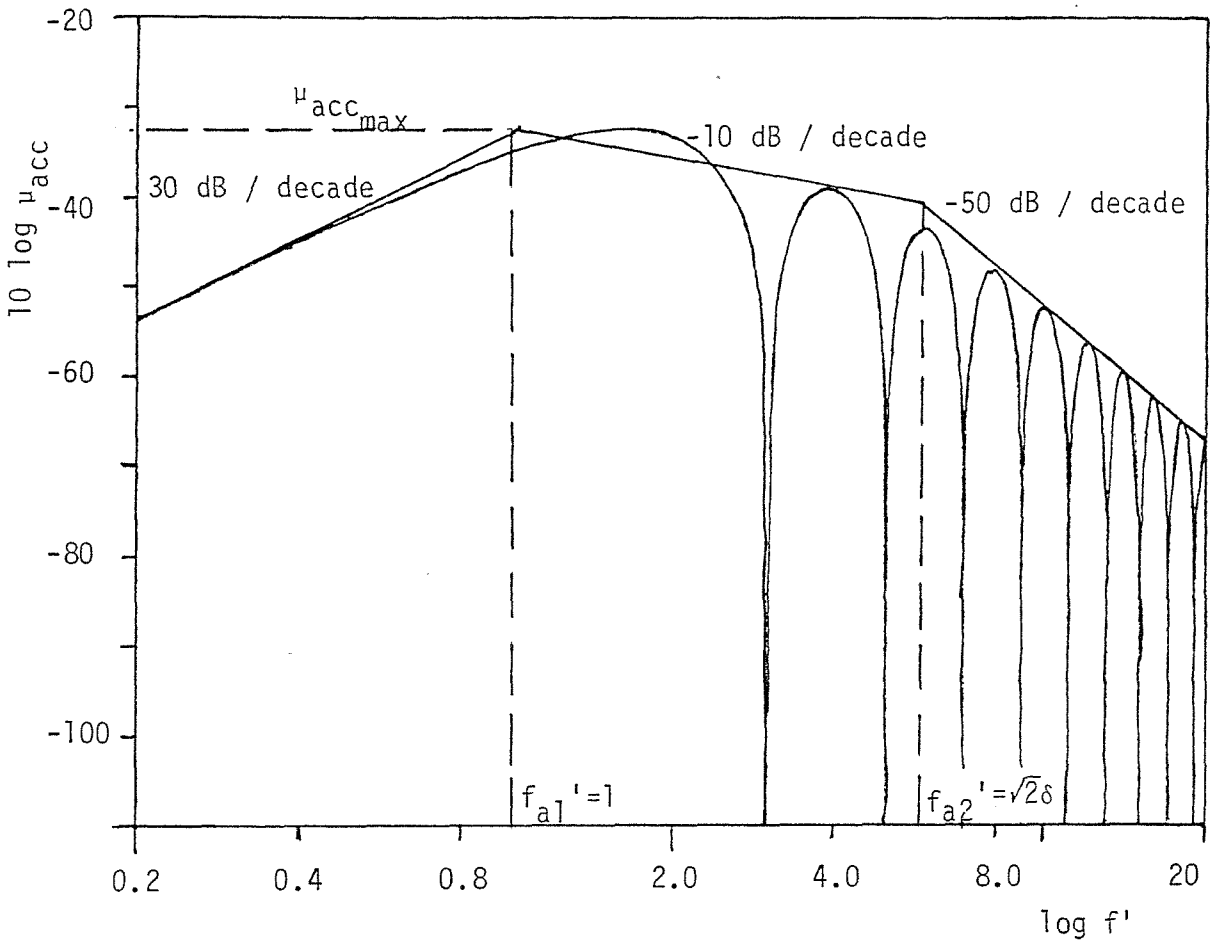

figure 4.3. Normalised acceleration noise, μ_{acc} in one-third octaves, for sphere radius 0.025m, $\delta = 4.135 > 1$.

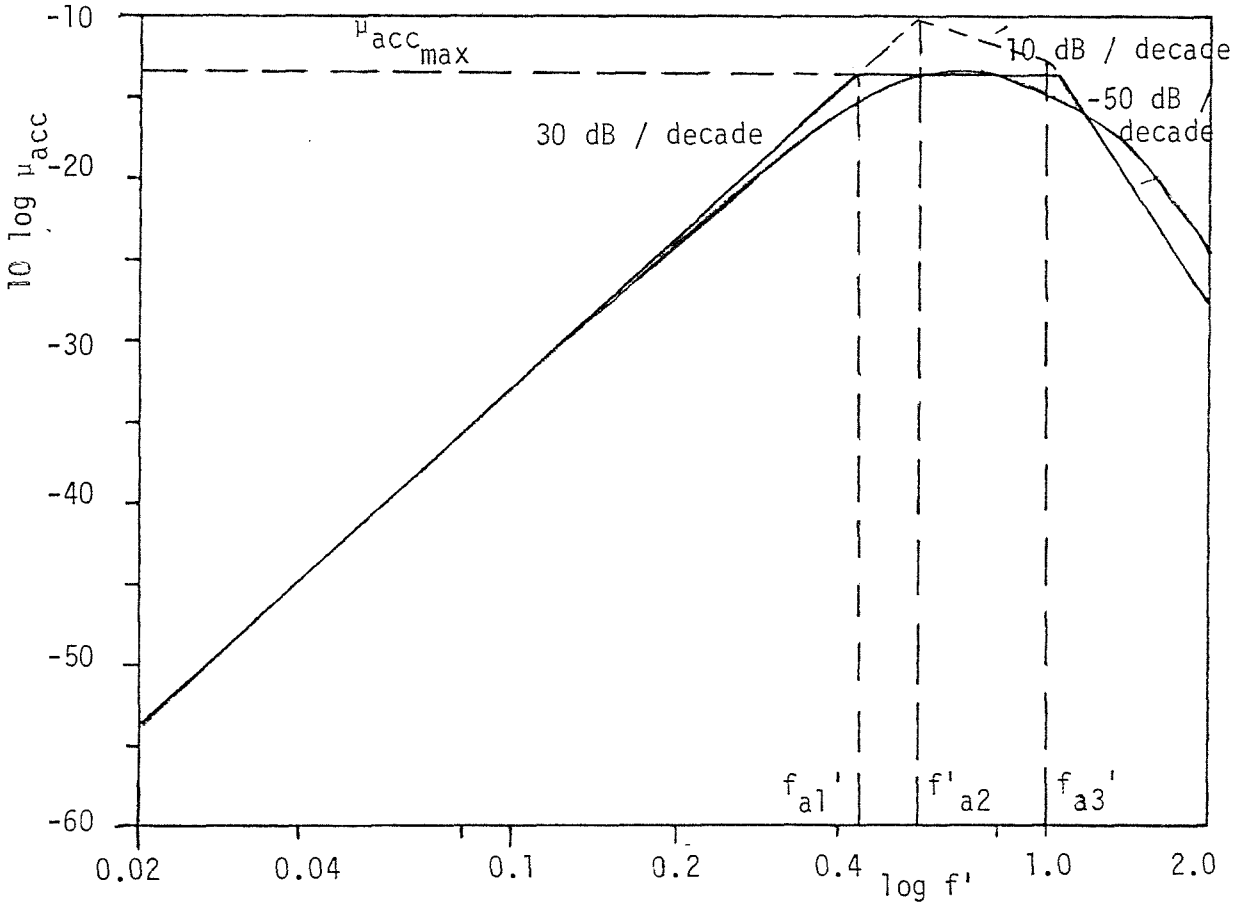

figure 4.4. Normalised acceleration noise, μ_{acc} in one-third octaves, for sphere 0.025m radius, $\delta = 0.41 < 1$

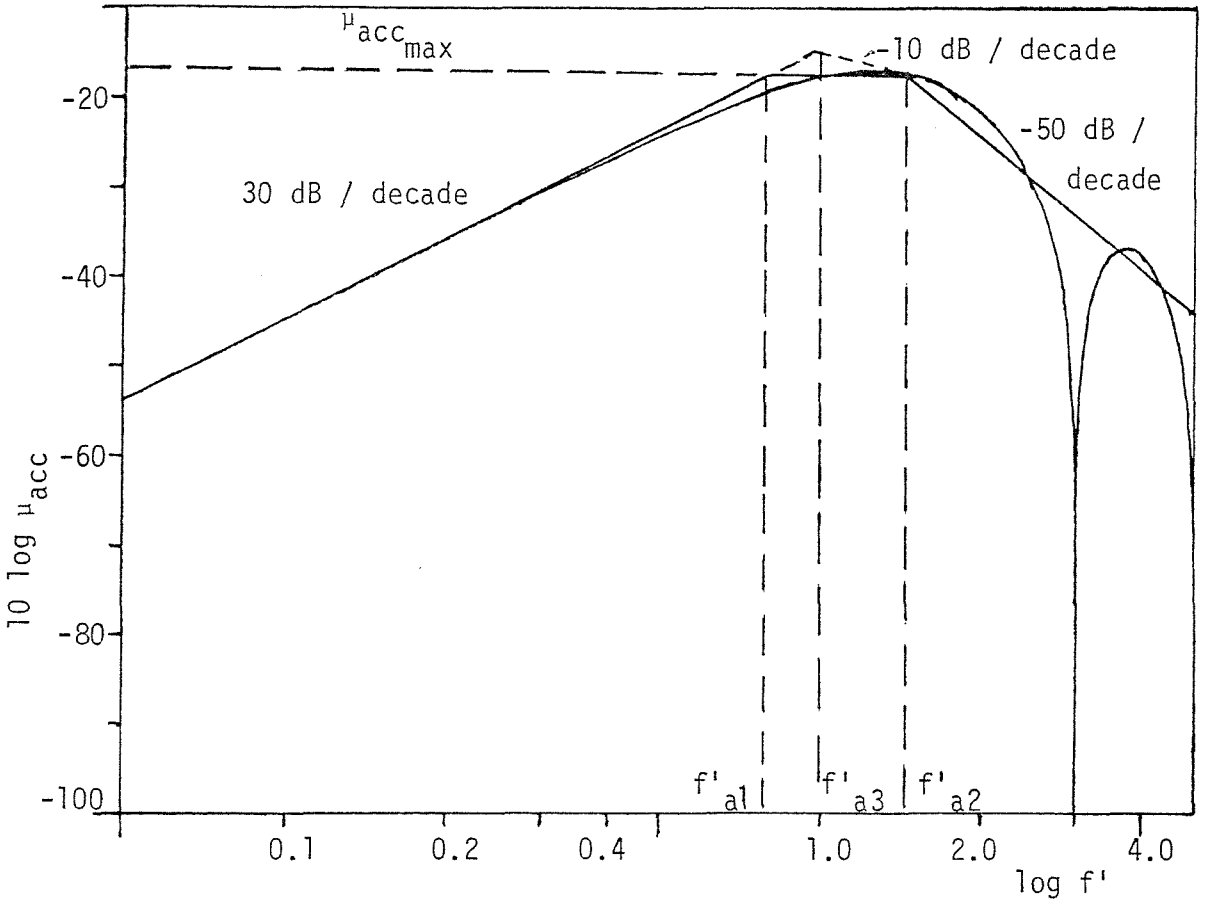

figure 4.5. Normalised acceleration noise, μ_{acc}, in one-third octaves for sphere radius 0.025m, δ = 1.

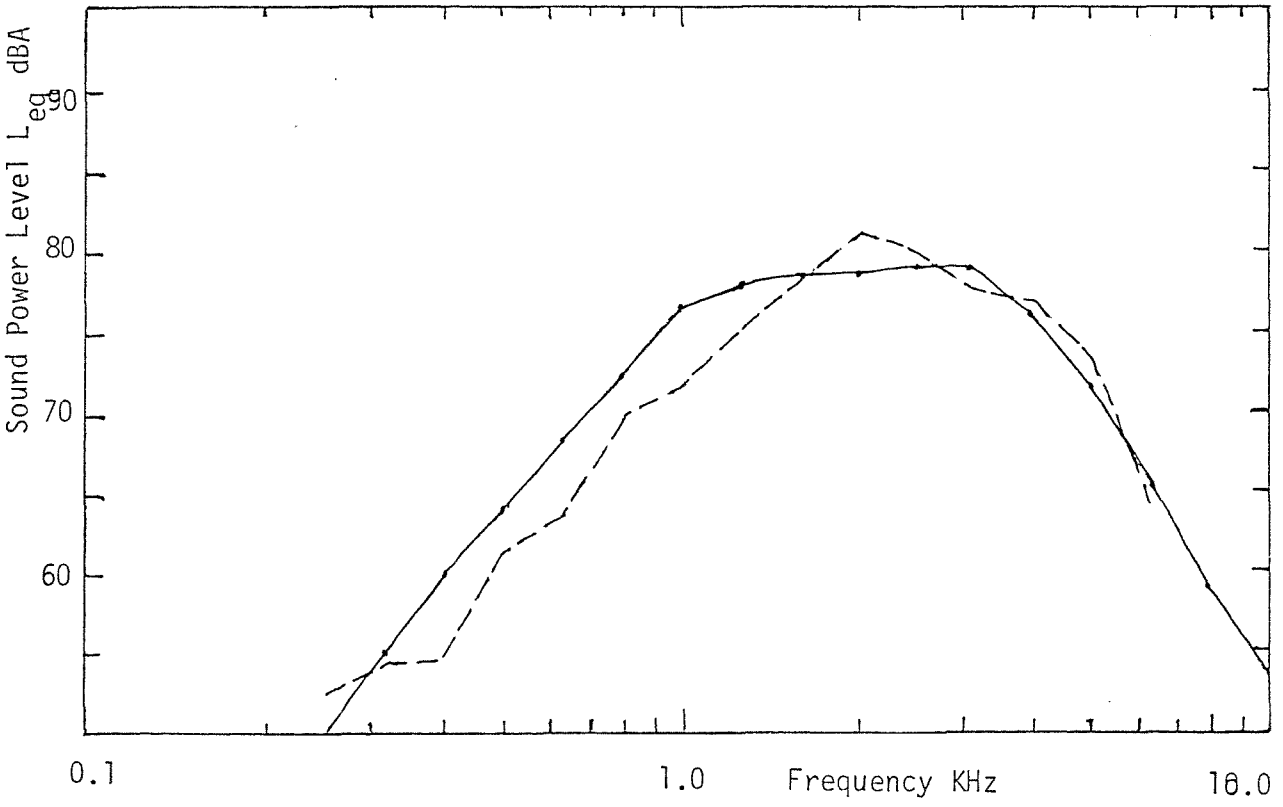

figure 4.6. Acceleration noise energy spectrum in one-third octave bands for a 100mm diameter sphere, δ = 0.372 (<1).——— estimated ----- measured.

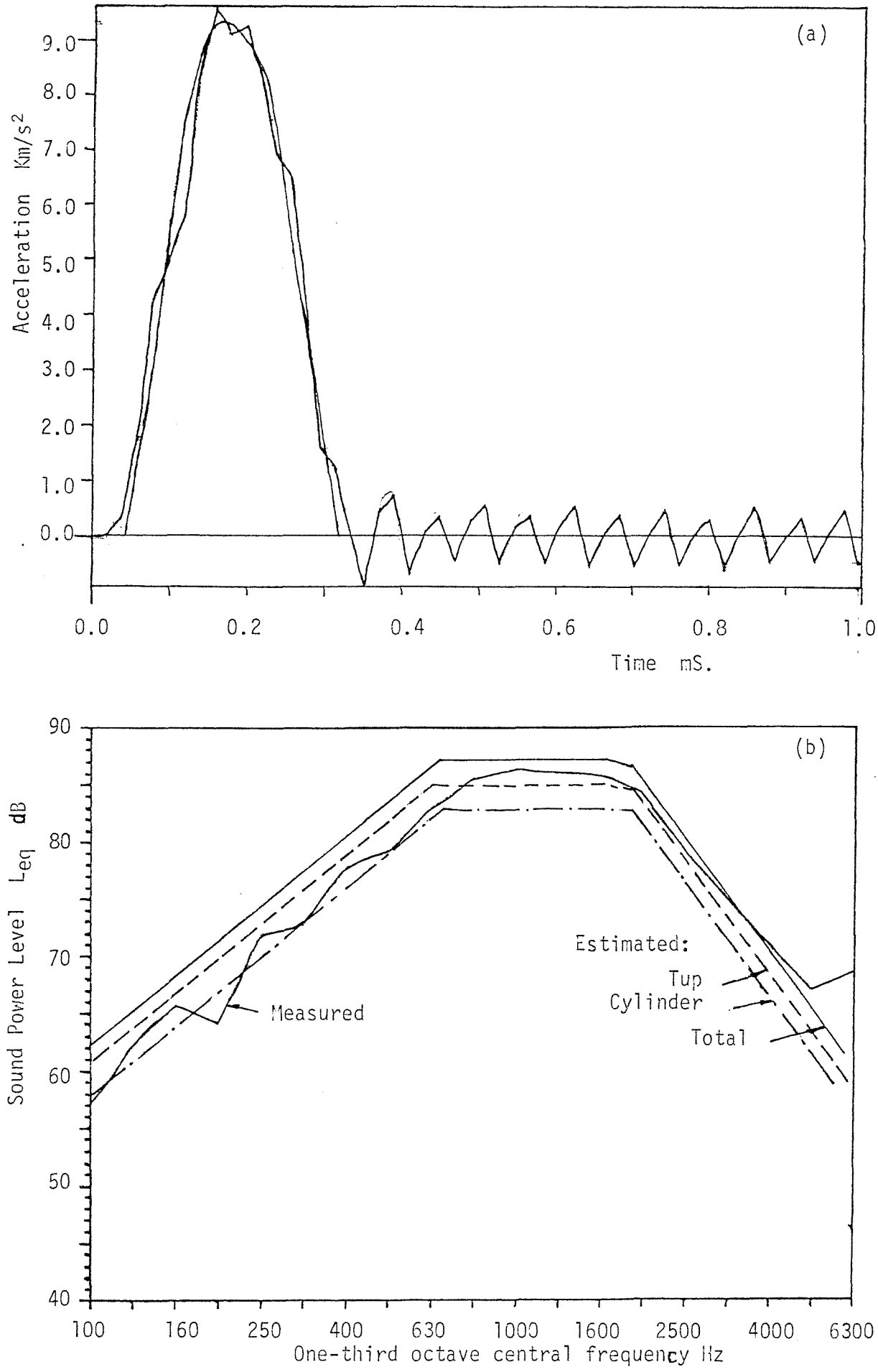

figure 4.7. Measured and Estimated acceleration noise energy for a drop stamp tup: (a) acceleration pulse; (b) radiated acceleration noise.

CHAPTER V

ESTIMATION OF RADIATED NOISE ENERGY BY IMPACT EXCITATION OF A PLATE STRUCTURE

V. 1. Introduction

The energy accountancy method as described in Chapter I gives the designer a good diagnostic tool with which to work, and to estimate the noise energy radiated from his designed structure; if estimated levels are unacceptably high, he is presented with a diagnostic equation that will indicate the available possibilities he may use to reduce his noise problem, and optimise his structure so that the different peaks in different terms will not coincide in frequency.

This method is best suited to calculate one-third octave noise rather than the exact narrow band spectra that a plate or structure surface will radiate. This still has wide applications, since actual machine structures are highly damped due to interaction between different parts which are bolted together so that resonant modes are well damped out. At frequencies where acoustic radiation is high, the spectrum of the machine surface vibrations will in general have a high modal density, and the point mobility curves with frequency will approximate to uniform mean lines or curves rather than to a multitude of peaks and troughs. As the noise regulations do not in general include crest factors, the exact tonality of the noise is not important.

A further point to bear in mind is that the radiated noise signature is related to the shape of the individual force pulses even though the subjective effect of the noise, by virtue of the high repetition rate, sounds continuous to the ear; as this tailoring of the impact is of greater design interest, than is the continuous noise spectrum, more design insight is provided by a study of a single pulse than by orthodox noise analysis.

In this chapter, the noise energy radiated by a flat plate under a single impact is both predicted, using the energy accountancy concept, and measured. This serves as a validification process for the energy accountancy concept and of the use of the mean value for the response

in estimating the vibrational energy escape into the structure.

V. 2. Experimental Verification of the Accountancy Equation

V. 2.1. Noise Estimate

It is obvious that so many approximations are implied in the noise prediction process, using the accountancy concept, that it has to be validated by experiment. The noise dose being measured directly from an array of microphones, and also predicted from measured or calculated value of the variance parameters, for a range of impact times and pulse shapes, for different damping factors, and for impacts which are applied directly to a plate and via lumped masses with resilient and damped inserts. These experiments have been carried out on the plate as shown in figure (5.1).

The total radiated sound from a one metre square plate, 0.01 metre thick, is estimated in one-third octave bands when excited at its centre, both directly and through a lumped mass. Having the excitation point at the centre provides the added experimental stringency as it is a nodal point for many modes and therefore these modes are not excited, making the bandwidth separating succesive modes wider. In practice, we find that the location of the excitation point is not important provided that it is away from an edge.

The term $10 \log \frac{A\sigma_{rad}}{f}$ is computed, assuming the plate to be in a baffle, the radiation efficiency is calculated using reference [14] where, the efficiency for other machine structures apart from plates are presented. A-weighting this curve and dividing by the central frequency of each third octave band gives the $10 \log \frac{A\sigma_{rad}}{f}$ (figure 5.2).

The effect of leaving out the baffle plate is to reduce the radiation efficiency at low frequencies well below the coincidence frequency as edge and corner modes will not radiate if cancellation occurs from one surface to the other.

The plate is excited by impacting it with a 50mm diameter sphere

of hardened steel. Because of the repetitive impacts, the plate work-hardened at the impact point. Therefore, while measurements were being taken, there was no plastic deformation either on the sphere or on the plate. The force pulse delivered to the plate is thus measured by having an accelerometer stuck to the steel sphere to measure the acceleration and then applying Newton's laws of motion. The spectrum of the pulse is obtained using a frequency analyser and comparing it with the spectrum obtained by the approximation method, Appendix A.

Since the accountancy equation (1.4) is for relatively highly damped structures, the plate loss factor is increased by bolting another thin metal sheet to the plate as a damping panel. The loss factor varied with the thickness of this damping panel (figure 5.3). The loss factor of the plate is computed by measuring the rate of decay of vibration in one-third octave bands. Since the modal density is high, it is impossible to use other methods, such as the bandwidth method. It is found that the loss factor varies with frequency and decreases at the high frequency end. However, since the accountancy equation in its simplest form is built up on the assumption of a constant loss factor with frequency, an average value relevant to the peak radiating frequencies is used for each damping panel, this is also shown in figure (5.3). This is not an essential element in the formulation of the prediction process, it being perfectly reasonable to take the measured or estimated loss factor as varying from one frequency to another. Since from [24] measurements on damping are not very consistent when performed on different conditions, the average value would be a much better representation. For the estimation procedure the average value is used.

V. 2.2. Direct Impact on the Plate

The experiments performed may be divided into two phases. In the first phase, the plate is excited directly and possible modifications in the other terms for noise reduction considered. In the second phase

the plate is excited through a lumped mass rigidly fixed or mounted on a resilient pad, to obtain possible noise control through the modification of the structural response term.

When the plate is directly excited, comparing it to an infinite plate structure, the response is given by:

$$\text{Im}\,[H(f)] = \frac{1}{16\pi f\sqrt{B\rho_s}}; \qquad B = \frac{EI}{1-\nu^2} \tag{5.1}$$

where ρ_s is the mass per unit area of the plate;

I is the second moment of area of the plate per unit width about an axis in the neutral plane;

ν is Poisson's ratio; and

E the Young's modulus.

Measurements of the response are made by the use of a force transducer, accelerometer and a phase-matched charge amplifier. The response $\text{Im}\,[H(f)]$ is found by dividing the transfer function of the force and acceleration at point of excitation by $1/\omega^2$ ($\omega = 2\pi f$). The measured response and the frequency averaged mean line are plotted on the same graph for every condition. It is noticed that this mean point response is independent of the plate damping. The lower the damping, the larger the deflections of the peaks and troughs from the mean curve and at high damping the curve approaches the mean line. The effect of damping on the radiated noise is included in a separate term, $10 \log \eta_s$, in the energy accountancy equation.

V. 2.3. Modification of the Structural Response Term

When the plate is excited through a lumped mass rigidly fixed to the plate, using equation (1.5), the stiffness of the isolator is very large $(k \to \infty)$ and $M_{12} = M_2 = 1/(j2\pi fm)$; where m is the mass

which is fixed onto the plate. The frequency averaged expression for the response is then given by

$$\text{Im}\,[H(f)] = \frac{1}{8\pi^3 f^3 m^2} \cdot \frac{Q}{Q^2 + \left[Q + \frac{1}{2\pi f m}\right]^2} \qquad (5.2)$$

where f is the centre frequency and Q is the mean or frequency-averaged mobility of the receiving structure, which is the same as $2\pi f$ times the structural response had the structure been excited directly. In this case the receiver structure is a plate, then

$$Q = \frac{1}{8\sqrt{B\rho_s}} \quad . \qquad (5.3)$$

When the mass is coupled to the plate via a resilient pad, the 'frequency averaged' response function is given by

$$\text{Im}\,[H(f)] = \frac{1}{8\pi^3 f^3 m^2} \cdot \frac{Q}{Q^2 + \left[\eta \frac{2\pi f}{K}\right]^2 + \left[\frac{2\pi f}{K} - \frac{1}{2\pi f m} - Q\right]^2 + \eta^2 \frac{\pi f \hat{Q}}{K}} \qquad (5.4)$$

where η is the loss factor of the resilient pad and K its stiffness, and $\hat{Q}$ is the peak value of the mobility of the receiver; since the mobility curve for the receiver exhibits a number of peaks [11] $\hat{Q}$ is given by the curve passing through the peak points in this curve. $\hat{Q} = 2Q/\cos\beta$ and $\cos\beta = \eta_s k\ell/2$, where η_s is the structural loss factor of the receiver, ℓ a typical length and k the wave number. For an infinite structure, $\cos\beta = 1$.

V. 2.4. The Constant Term

All that remains for the estimation of the noise from such a plate is the constant. The terms in this constant are

$\frac{\Delta f}{f} \cdot \frac{\rho_o c}{2\pi^2 \rho_m}$. The analysis are being done in one-third octave bands and $\frac{\Delta f}{f}$ has a constant value of -6.4 dB. Values [25] for air density, ρ_o = 1.21 kg/m^3; c = 340 m/s; material density of steel ρ_m = 7.7 x 10^3 kg/m^3; will give the constant as -32 dB for a steel structure.

Adding all these terms together will give the estimated A-weighted noise energy that the plate will radiate with reference to 1 Joule of energy. In acoustics the reference of power is 10^{-12} Watts. If there is one impact per second, that is, in equation (1.4), N = 1, then the energy radiated is per second and thus can be referred to 10^{-12} Watts. That is, adding 120 dB to the computed sum will give the sound intensity as would be measured by an L_{eq} meter, averaging over one second. The estimated curves are shown on the same graph as the measured noise energy for comparison.

V. 3. Noise Measurements and Other Considerations

Noise measurements were made using a B & K 2218 L_{eq} meter, at nine points on a parallelpiped envelope (figure 5.4). The reason for using a nine point measuring surface is that this gives a low error if the source is directional (in the order of 0.7 dB). The L_{eq} meter signals from the nine measuring positions are fed into a frequency analyser where they are averaged and multiplied by the enclosed area, then Fourier transformed to give the sound energy density. The energy in frequency bands is the integral of the energy density within the bands' limits. Since the sound measurements are made in semi-reverberant conditions, apart from the usual measurement errors (nearfield, finite number of measuring points and experimental errors) another error is incurred as compared

to freefield measurements. The measured sound power includes a term which is the contribution from the reverberant sound field. This contribution can be determined if sound power level measurements are made on concentric enveloping surfaces at a greater and lesser distance from the source [26]. The contribution will then be the lesser of the difference between the sound power levels measured on the lesser or greater surface and the primary surface.

V. 3.1. Sound Measurement for Direct Impact

For the first phase of the experiment, that is when the plate is directly excited, sound measurements are done for three different conditions. The first condition is taking arbitrary values for the force pulse duration (metal to metal) and for the loss factor ($\eta_s = 0.02$). The sound is estimated and measured using A-weighting. For metal-to-metal impact the steel ball does not rebound, all the potential energy of the ball being transferred into vibrational energy in the plate. To estimate the noise energy radiated from the plate in this phase of the investigation, knowledge of the force pulse shape and magnitude is needed. For comparison, the measured force pulse in the time domain for metal-to-metal impact and the frequency transform of its derivative are recorded (figure 5.5 , (a) and (b) respectively). On the same graph of the force derivative spectrum, the approximate spectrum is shown, the latter being used in the estimate. Figure (5.5 (c)) shows the measured and geometric mean curves for Im [H(f)] for the plate at the point of impact.

The narrow band analysis and the one-third octave spectrum of the measured sound together with the estimated curve are shown in figure (5.5 (d) and (e)) respectively. Corrections have been applied to the measured curve to account for reflections in the semi-reverberant conditions; other corrections include that due to the shape of the envelope, and that due to the finite number of measuring points. As can be seen from the curves of the measured and the estimated sound energy, there is good agreement between the two to within $\pm$ 3 dB. This suggests that this method provides a powerful method of estimating the sound energy radiated. The

departure of the measured curve from the estimated curve at the high frequency is due to two reasons. One, because of the lower loss factor at high frequencies, lower than the average value used in the estimation process; and two, because of the acceleration noise. The second reason becomes more apparent in later experiments when the sound radiated by the plate is reduced and the acceleration noise becomes dominant at the high frequencies.

As a second condition, the plate is less damped, but the force pulse duration is kept constant, giving the same force derivative spectrum (figure 5.6 (a) and (b)). The measured and calculated results are shown in figure (5.6 (d)) for A-weighted noise energy. Again the same corrections as before are applied. In this case, strictly speaking, the accountancy equation cannot be used to estimate the noise energy radiated, because of the low damping. However, it can still be used as a diagnostic tool to estimate the effect that each parameter will have on the noise energy radiated.

In the original derivation of the accountancy equation [15], it was suggested that σ_{rad} could be neglected in the term

$\sigma_{rad} + \frac{2\pi\rho_m}{\rho_o c} f\eta_s$ at medium and higher frequencies for damping factors obtained in fabricated structures, and that even at low frequencies the error was small. That this is true in the present experiments, even though the damping factor η_s (= 0.006) is low is indicated in Table 5.I , the error amounting to no more than a fraction of a decibel even in the lowest frequency band.

As can be seen from a comparison of figures (5.5 (e)) and (5.6 (d)), which show estimated and measured sound power levels, the noise energy radiated by the same plate but with the damping decreased threefold in the second case, is in keeping with the expected prediction throughout the frequency range. A direct comparison of the two curves is shown in figure (5.7), and if the total energy is summed up, for a loss factor of 0.006, this is 113 dB(A) and for a loss factor of 0.02 it is 108 dB(A), a 5 dB reduction which corresponds

to the change in loss factor from 0.006 to 0.02.

The results (figures 5.5 (e) and 5.6 (d)) show that this accountancy equation predicts noise energy from plate structures with acceptable accuracy; for high damping, one can use the equation directly, but at low damping the approximation in neglecting σ_{rad} (equation (3) in reference [15]) has to be checked and the error (if any) evaluated.

V. 3.2. Impact Lengthening via Resilient Inserts

The third condition in the validation experiments consisted of examining the introduction of a soft or resilient insert between the impactor and the plate, the insert itself being too small to radiate noise significantly. This can be done in many practical processes, and some of these have been referred to in reference [15]. The unfortunate characteristic which was observed in these experiments is the increase in low frequency noise, and the possibility it raised, of the overall noise level not falling. As it is very difficult to increase structural damping by more than a factor of three in fabricated structures, a better understanding of the exact mechanism in tailoring of the pulse was felt to be essential. Therefore in this case the pulse duration is increased, such that the peak of the force derivative spectrum will not coincide with the peak of the

$10 \log \frac{A\sigma_{rad}}{f}$ curve. The reason why the term $10 \log |\dot{F}(f)|^2$ if changed may in some cases give a reduction in noise while in some it does not, is that the reduction is only possible if the maximum of this spectrum does not coincide with the maximum of the radiation efficiency term. In the first two conditions, these two terms maximised almost in the same frequency band.

When performing this experiment with the same set-up as before, i.e., putting the same amount of energy, the noise energy radiated was so much reduced it was comparable to the background noise and therefore too low to be measured. Thus a different set-up has been used, using a larger impactor, thus putting in a lot more energy

(increasing E_{escape}) by increasing the exciting force relative to the set-up with the previous mass. Figure (5.8 (a)) shows the force pulse shape and figure (5.8 (b)) the spectrum of the force pulse derivative. It may be seen that the peak in the force derivative spectrum is shifted to the low frequency end.

The curves for the measured and estimated A-weighted sound energy are shown in figure (5.8 (c)). Again the agreement is good thus proving that the method is quite powerful and gives an insight into how different parameters will affect the total noise energy radiated from a structure excited impulsively. The curve for Im [H(f)] does not change, since the mean level of the curve is independent of damping.

Normalising the results to have the same momentum-change or same energy transfer, (figure 5.9 (a)),(there is no change in structural response), in conditions one and three, the reduction in noise energy radiated is very high, especially at high frequencies (figure 5.9 (b)). Most of the input energy is at low frequencies where there is the combined effect of low radiation efficiency and A-weighting, to minimise the importance of the sound radiated during the time the vibration dies out.

The characteristic increase at low frequencies referred to earlier is clearly seen in figure (5.9 (b)). In this case it is small, and the total noise radiated, indicated by the summation of the energies in each one-third octave is considerably lower and in keeping with the $L_{eq(A)}$ reductions of up to 20 decibels recorded in reference [15]. It must be concluded therefore that the procedure of softening impacts, wherever possible is a far more effective noise control measure than is that of adding damping.

In our experiments, it was noticed that some energy was transferred back into the impactor and some rebound occurred. This may not matter in many practical installations but where accuracy of timing is required in repetitive processes, the need for a controlled rebound becomes important.

The accountancy equation suggests that similar and even better results can be obtained by shortening the impact (less contact duration) so that the force derivative spectrum will have a maximum in a higher

frequency band than will that of the modified radiation efficiency curve [15]. In this case, A-weighting will not be a mechanism in the noise reduction process, but rather that for high frequencies the structural response term Im [H(f)] will decrease, implying that less energy escapes into the radiating structure which will in any case not ring for so long a period. The problem is to have sharper impacts than those between metals.

V. 3.3. Impact Shortening

For standard materials, metal-to-metal impacts are the shortest from consideration of impact mechanics. During impact the material may act in two ways, either elastically or plastically. If during impact the material plastically deforms, the impulse duration can be reduced by hardening the material. However, further hardening will not decrease the pulse duration once the impact becomes elastic.

For an elastic impact the duration will depend on the elasticity of the structure. If the structure is solid, the relevant elasticity is Young's modulus and hardening the structure will not change the Young's modulus; it will only increase the yield point. Metals have some of the highest moduli of elasticity, and this is why metal-to-metal impact is one of the shortest possible. However, for plate-like structures, say, impacted by some kind of bulk structure, then the impact will depend on the elasticity of the plate. Therefore the impulse duration may be decreased if the elasticity constant of the structure is increased, by stiffening it. For a plate this may be achieved by, say, having a rib at this point. One provision here is that it may be that the duration will not change because the plate is already stiff and it is acting like a solid structure. Other methods of reducing the pulse duration shown in reference [27] are by using a smaller radius of impactor. However, considering the impact of a sphere with a certain velocity, if the diameter of the sphere is reduced, the energy of impact will be reduced by the cube of the diameter. For elastic impacts, the impulse will depend on the elasticity which in turn depends on the area of contact or the square of the diameter; the pulse duration will therefore be reduced only because the energy transfer is less. For the same amount of energy

the pulse duration will be longer.

V. 3.4. Structural Response Tailoring

Increasing the impulse duration may create some problems to the designer. Usually the pulse would depend on some process of the machine and by softening the impact, accuracy of the sequential impact may be lost. Thus it is sometimes quite difficult to change this parameter.

To reduce the noise energy radiated from the structure, therefore, the parameters which are left to be altered are the point response and the average plate thickness.

This leaves the designer with the only option to tailor the response of the structure or in physical terms to find ways of restricting the energy flow from the point of application of the force to the rest of the structure while maintaining the same characteristics of the pulse.

This leads to the second phase of the present experiments in which the plate is excited through another structure. For the first condition in this second phase the plate is excited through a mass rigidly fixed to the plate. Substituting for Q in equation (5.2) by using equation (5.3), an expression for the structural response for this condition is obtained (figure 5.10 (a)). Using the same set-up as in condition 3, phase 1, both the force pulse (figure 5.10 (b) and (c)) , (for the noise energy estimate), and the A-weighted noise energy radiated are maesured (figure 5.10 (d)). The area under the force pulse is unaltered as compared to the first condition (in phase one) but because of the mass, the energy flow is restricted. With the lower response less energy escapes into the plate, giving a lower radiated noise energy (figure 5.11)

The mean mobility (Q) for the plate suggests that the plate acts like a damper. Therefore for a mass rigidly fixed to a plate the equivalent system will be a mass and a dash pot. This will result in the system having no resonant frequencies, and no tuning is needed to reduce the escape energy into the plate. Had there been a resonant frequency, that is, a high structural response, it would imply that

at that particular frequency more energy escapes into the structure. The larger the mass fixed to the plate, the higher will be the reduction in the escape energy. The only limitation on size being what is possible to be incorporated in the structure.

For the second condition in this second phase, the plate is excited via a lumped mass coupled to the plate by a damped spring, or resilient pad. The loss factor and stiffness of the resilient pad are measured, by exciting at one end, measuring the acceleration at this end and the blocking force at the other end (figure 5.12). The stiffness of the resilient pad changes with frequency (figure 5.13), but the loss factor remains constant at about 0.25. No standing waves occur in this frequency range. Using these values in equation (5.4) with Q given by equation (5.3) and $\cos \beta = 1$, $\mathrm{Im}\,[H(f)]$ is obtained (figure 5.14).

For this condition because of the very low structural response at the high frequencies, the acceleration noise becomes dominant at these high frequencies (> 2 kHz). The acceleration noise is measured by a simple experiment where the steel sphere is made to hit the mass fixed on to a rigid structure so that no sound is radiated from the latter. Since the natural frequencies of both sphere and block are very high and were above the frequency range of interest, the measured noise is the acceleration noise (figure 5.15). The force pulse did not change from the previous condition (blocking mass directly fixed on plate). The estimated and measured A-weighted sound energy curves are shown in figure (5.16). For the estimated noise level, the estimate from the energy accountancy equation is added to the measured acceleration noise. Because of the lower structure response term, the escape energy is lower, resulting in a lower radiated energy (figure 5.17).

Below 315 Hz there is a difference between the estimated and measured noise energy levels. When the plate is excited through the lumped mass via the isolator, most of the energy entering the plate is at low frequencies. In computing the radiation efficiency term for the plate it has been assumed that the plate is in a baffle and at low frequencies the edge and corner modes do not cancel. This

approximation is acceptable for the free plates set-up in this experiment for high frequencies near and above the coincidence frequency, but in this case because of the importance of the low frequency end, this error is more visible. According to [14], it is very difficult to compute the radiation efficiency for free standing plates below the coincidence frequency, because it is not possible to estimate to what extent edge and corner modes are cancelled around the edges. This accounts for the large differences below the 315 Hz band. However, if the measured curves for the radiation efficiency for free hanging plates are used (viz. figures 26 and 27 in reference [14]), and the estimates from the accountancy equation based on these curves, then these estimates will have the same values at high frequencies (above coincidence), but lower values at low frequencies. The estimates follow the dotted line of curve (iii) in figure (5.17) which are much closer to the measured values.

The structural response given by equation (5.4) has a fall-off rate which depends on the third term in the denominator. That is, if the second part of the expression is plotted against frequency, it will have a maximum point when $Q = \frac{2\pi f}{K} - \frac{1}{2\pi fm}$. This is the combined natural frequency for the mass, isolator and receiver structure. For a stiff structure, small Q, this resonance is the mass-isolator natural frequency. For frequencies above the combined natural frequency the fall-off rate is 50 dB/decade. Therefore, the structural response can be detuned for optimum noise control by choosing this combined natural frequency to be below the frequency range of interest, thus making full use of the high fall-off rate, or at least the coincidence frequency for the radiating structure. In the experiment, the combined natural frequency is below 100 Hz.

Near the natural frequency, the point response will depend on $\hat{Q}$, equation (5.4), or the damping of the receiver (the receiver is not infinite). When the receiver damping decreases ($\cos \beta$ approaches 0),

$\hat{Q}$ increases, and the structural response decreases (figure 5.18). Therefore, if the combined natural frequency falls within the frequency range of interest, then there is a trade-off between a lower structure response, by decreasing the receiver damping - less energy escapes to the receiver - to a higher value for, $-10 \log \eta_s$ in the energy accountancy equation. That is, although the receiver takes longer to ring down for the same amount of energy, less energy escapes into the receiver, therefore less energy can be radiated compensating for the decrease in damping.

V. 4. Conclusion and Other Comments

The two main conclusions from this set of experiments are: (1) that the energy accountancy equation for the estimation of noise energy radiated from a plate-like machine structure is good, with the second phase of the experiments suggesting that the energy accountancy equation is very versatile and can be used in a wide range of cases; (2) that two of the terms in the equation which are the most important are the force derivative and structural response terms. Noise control procedures can be adopted to reduce both these terms, which imply a reduction in the amount of energy that escapes to the structure.

As observed in the results, large attenuation in structure-radiated and structure-borne sound is possible by a mobility mismatch along the path of energy flow and most of the incident energy is reflected back. This is shown in the reduction of noise energy radiated when the plate is excited through the lumped mass. At moderate and high frequencies an attached mass to a structure will act as an effective discontinuity, producing a change in the mobility along the energy flow path. The mass impedance will block the propagation of the vibrational energy and is referred to as a blocking mass. The sound radiated by the plate when excited through the blocking mass is much less than when the plate is directly excited. With the insertion of resilient material between the blocking mass and the structure a high attenuation is achieved in the energy flow. However, this only occurs above the combined natural frequency. The natural frequency can be reduced by either

increasing the softness of the resilient pad or increasing the blocking mass. If the resilient pad is too soft, the structure may lose its stability and the size of the blocking mass determines the acceleration noise.

It is thus impossible to give a general solution to all noise problems from industrial machines, but each structure type has to be studied individually. The point of impact or energy input into the structure has to be established before noise control measures are applied. In the case of a drop hammer, the energy escapes at the point where the two dies come in contact, and in this case a possible noise control measure may be to either increase the mass of the dies and holder or insert resilient material between the interfaces of the dies and holder and anvil. This should not decrease the operational capabilities of the machine process, because by the increase of mass there is a higher inertia at the operation point. In other structure types, impacts may occur at more than one point. During the combustion explosion in a diesel engine cylinder, a transient force acts on the piston top and consequently impacts occur between the piston and crank shaft linkages, and the crank shaft and bearing caps, at which the vibrational energy is transferred to the engine frame. In this case the bearing caps may be increased in mass or resilient material included in the bearing rings [28], (see Chapter VI).

In restricting energy flow, a problem arises because more energy is left in the impactor, which will result in rebound. This was observed in the experiments when the plate was impacted through the blocking mass, with and without the resilient pad. In rebound, the impactor may hit other structure parts and the same amount of energy will be transferred to the structure. Also, subsequent impact precision may be lost. Similar observations happen when the impact is softened. The energy is transferred to the structure at a lower frequency and because the contact duration is long the receiver structure will transfer back some of the impact energy.

These problems have to be considered in redesigning a machine structure using mobility changes in the energy flow path, the application of such structural changes to standard machine structures, to assess the predicted noise control measures will be investigated in the following chapter.

TABLE 5.I

Effect of neglecting the σ_{rad} term for a relatively low practical value of loss factor η_s(=0.006)

One-third octave central frequency	10 log $\left(\frac{2\pi\rho_m f\eta_s d}{\rho_o c}\right)$	10 log $\left(\sigma_{rad} + \frac{2\pi\rho_m f\eta_s d}{\rho_o c}\right)$
100	-1.5	-1.1
125	-0.4	-0.2
160	0.6	0.4
200	1.5	1.8
250	2.5	2.7
315	3.5	3.7
400	4.5	4.7
500	5.5	5.7
630	6.5	6.7
800	7.5	7.8
1000	8.5	9.1
1250	9.5	11.3
1600	10.5	11.3
2000	11.5	12.0
2500	12.5	12.8
3150	13.5	13.8
4000	14.5	14.7
5000	15.5	15.6
6300	16.5	16.6
8000	17.5	17.6
10000	18.5	18.6

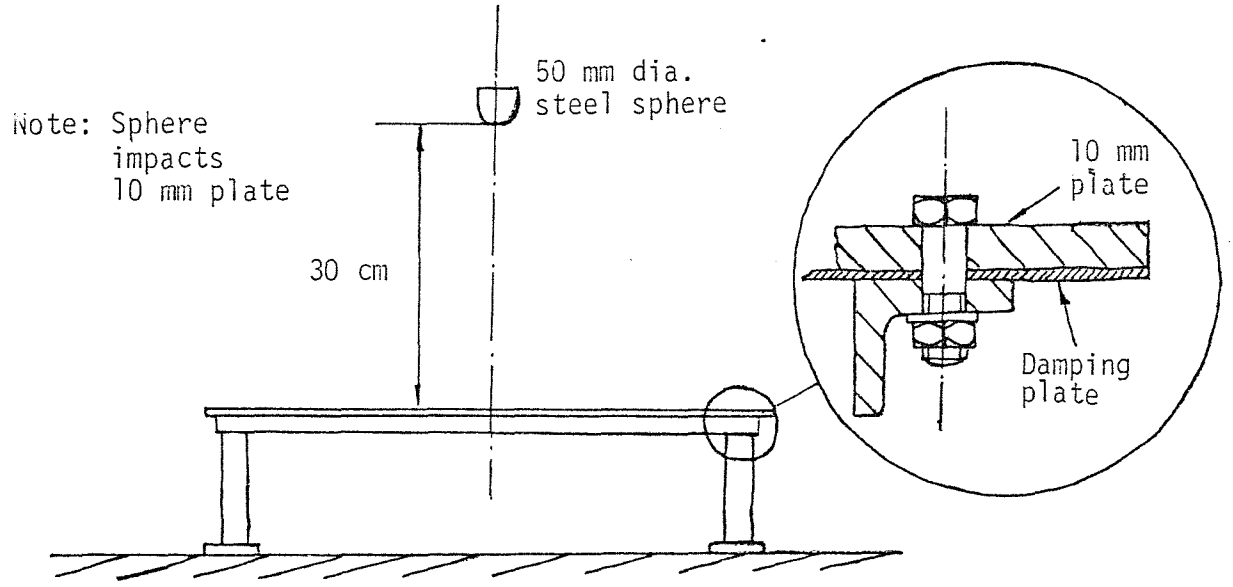

figure 5.1. Experimental set-up.

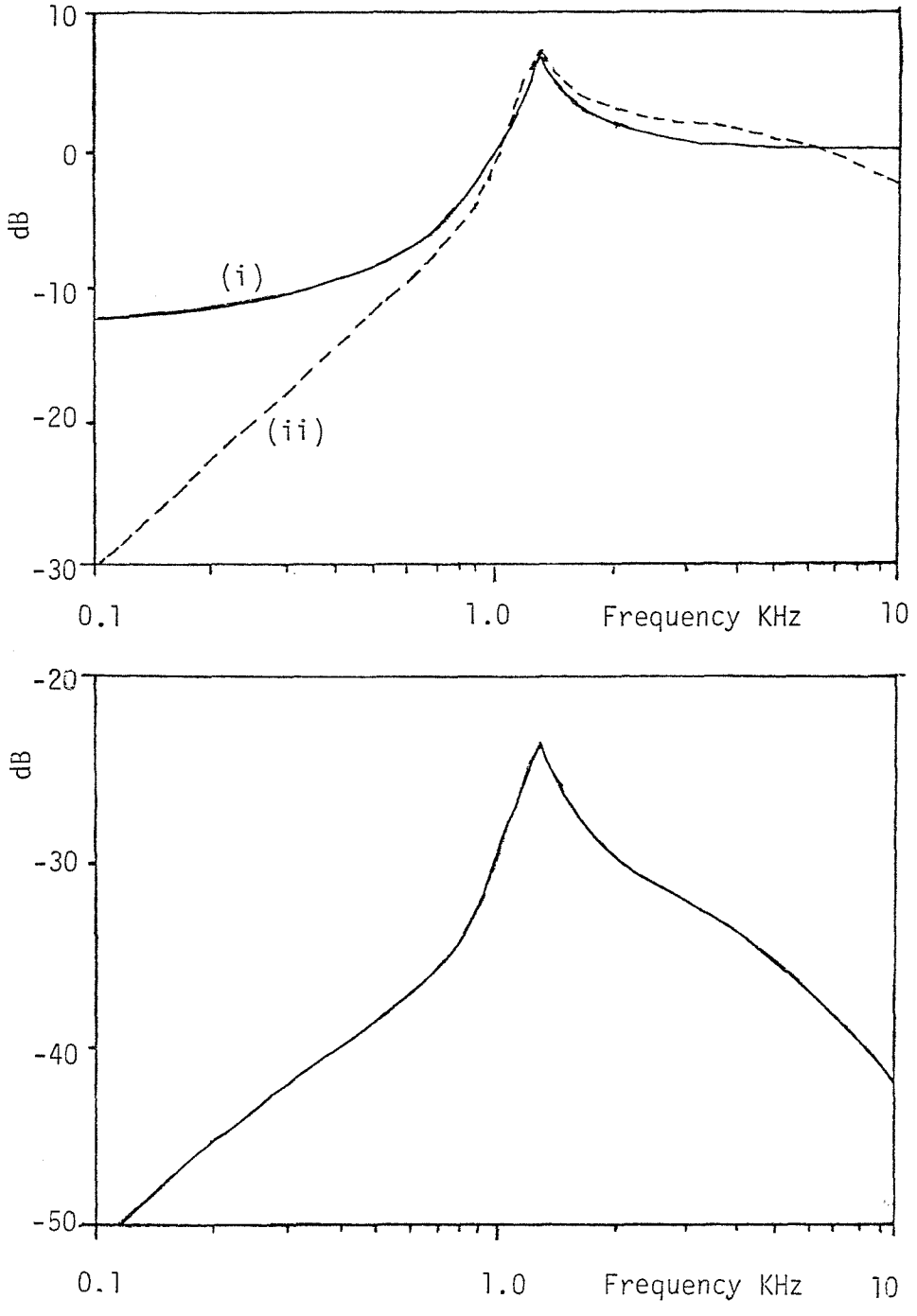

figure 5.2. Radiation efficiency curves for test plate. (i) 10 log σ_{rad}; (ii) 10 log ($A\sigma_{rad}$); (iii) 10 log ($A\sigma_{rad}/f$).

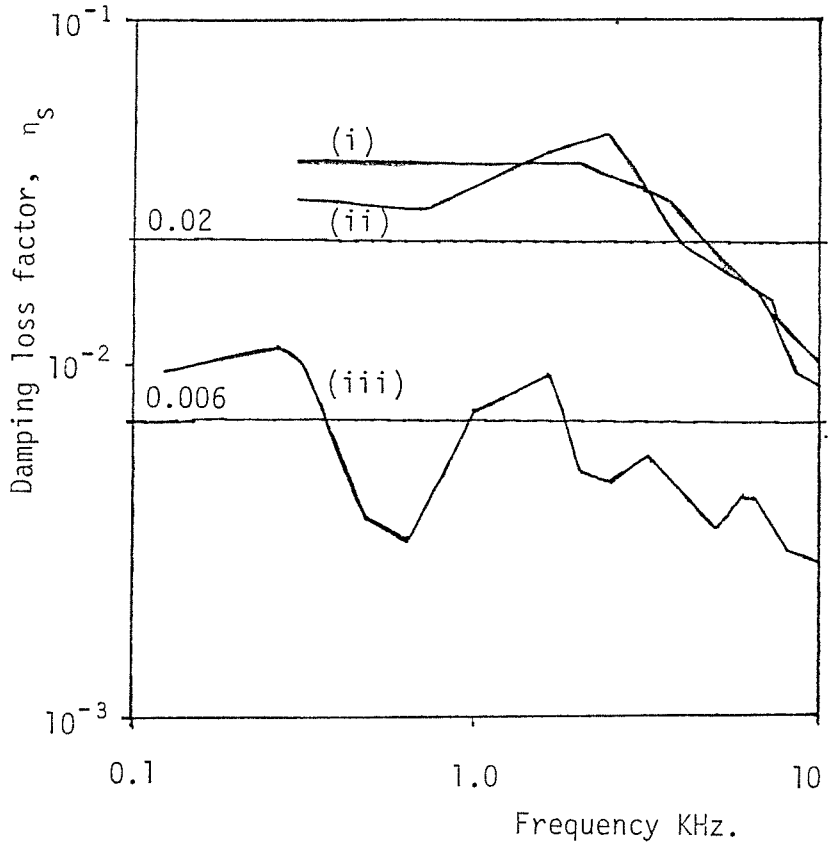

figure 5.3. Loss factor of plate with different damping panel thickness. (i) Damping panel 2mm thick; (ii) 1.2mm; (iii) no damping panel.

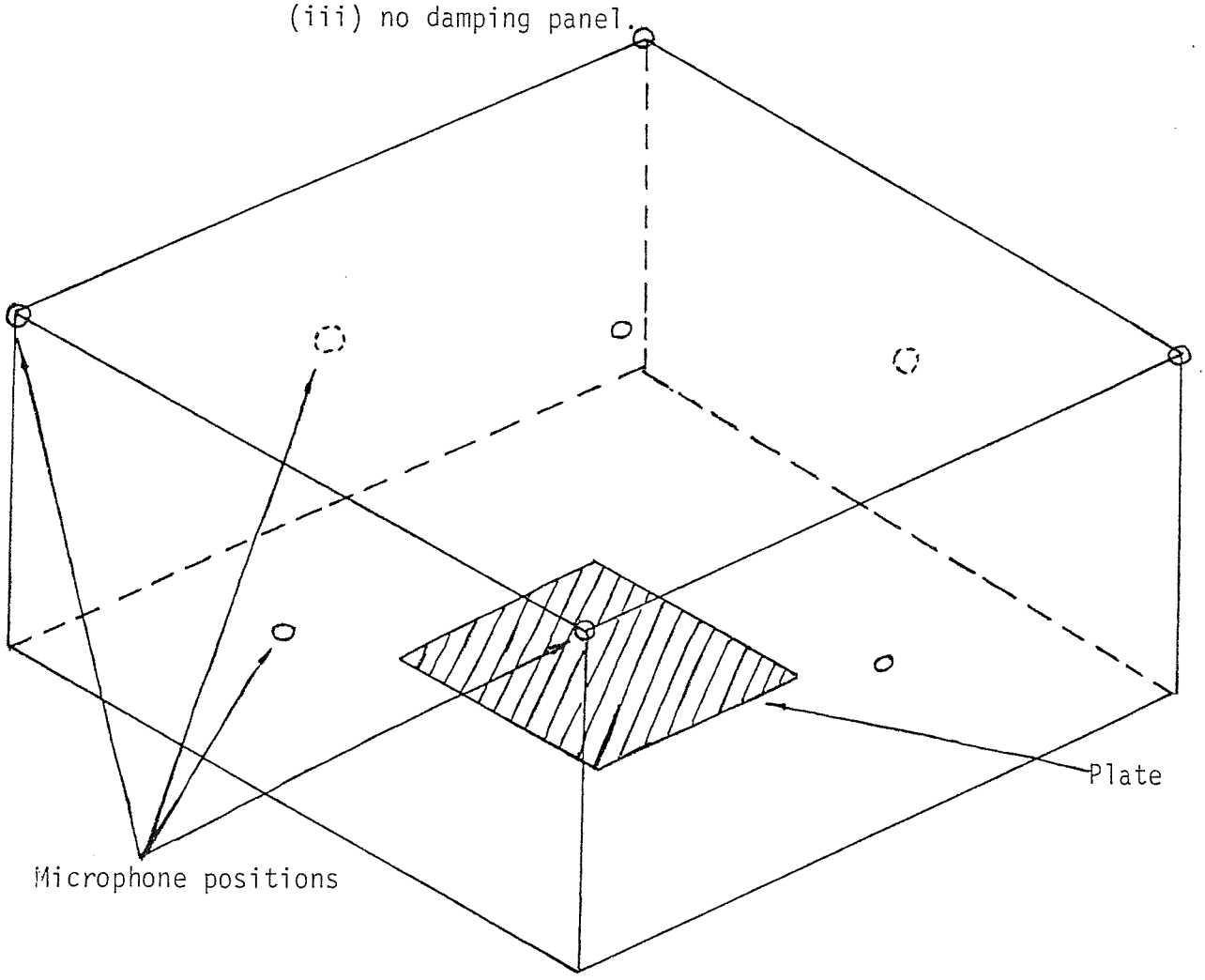

figure 5.4. Sound measuring positions.

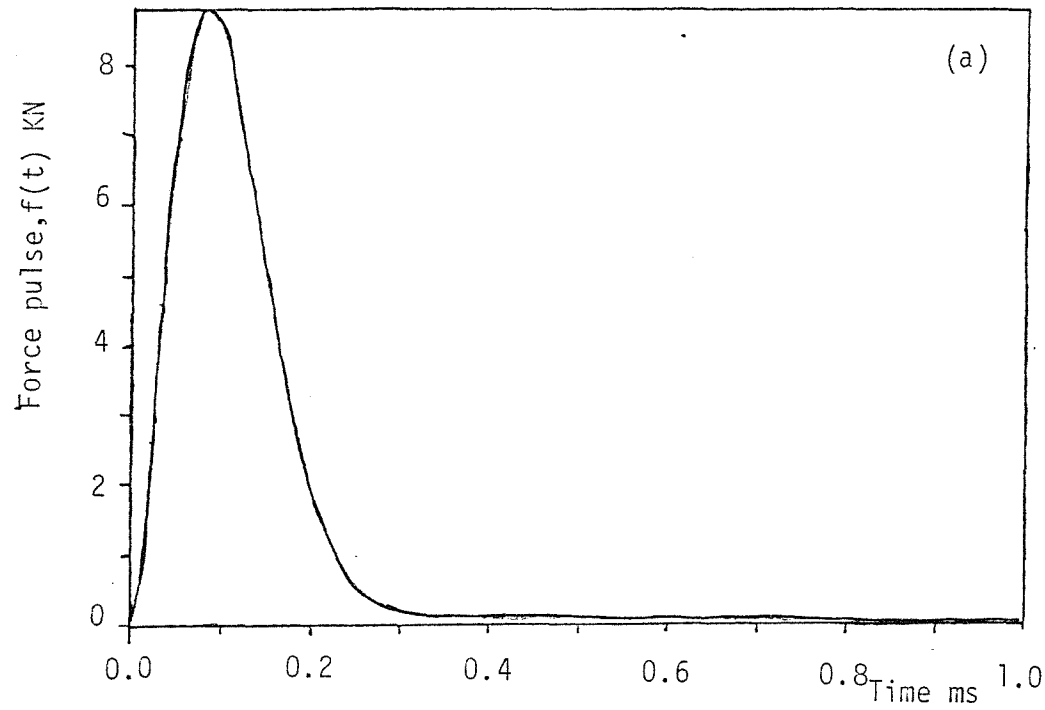
(a)
Force pulse, f(t) KN
8
6
4
2
0
0.0
0.2
0.4
0.6
0.8
Time ms
1.0

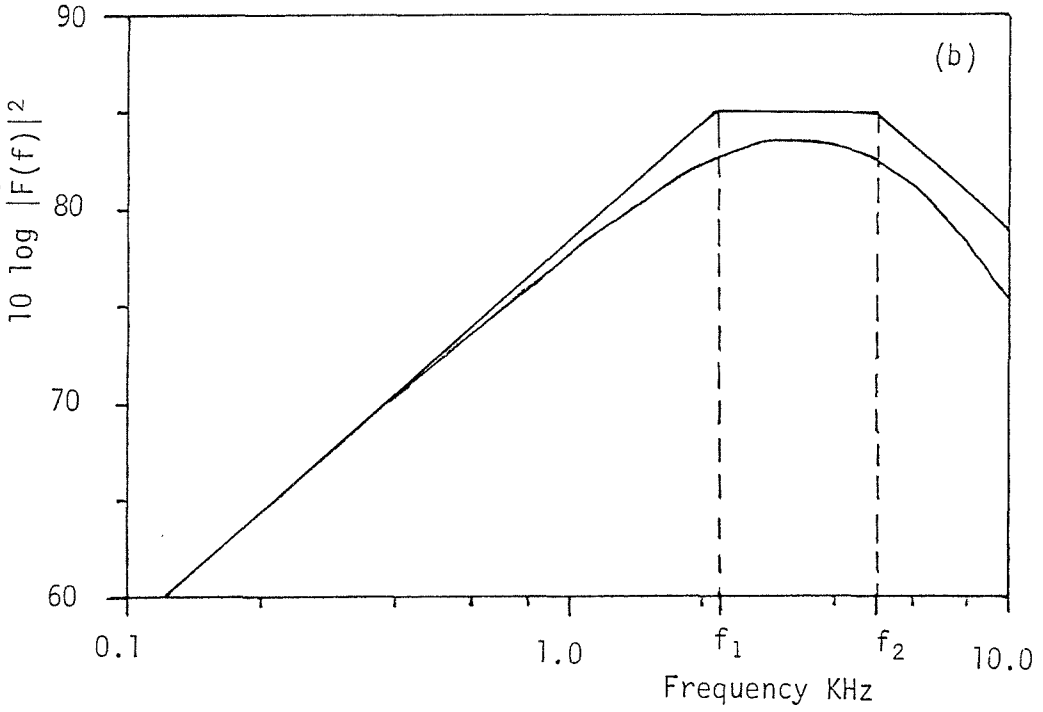
(b)
10 log |F(f)|²
90
80
70
60
0.1
1.0
f1
f2
10.0
Frequency KHz

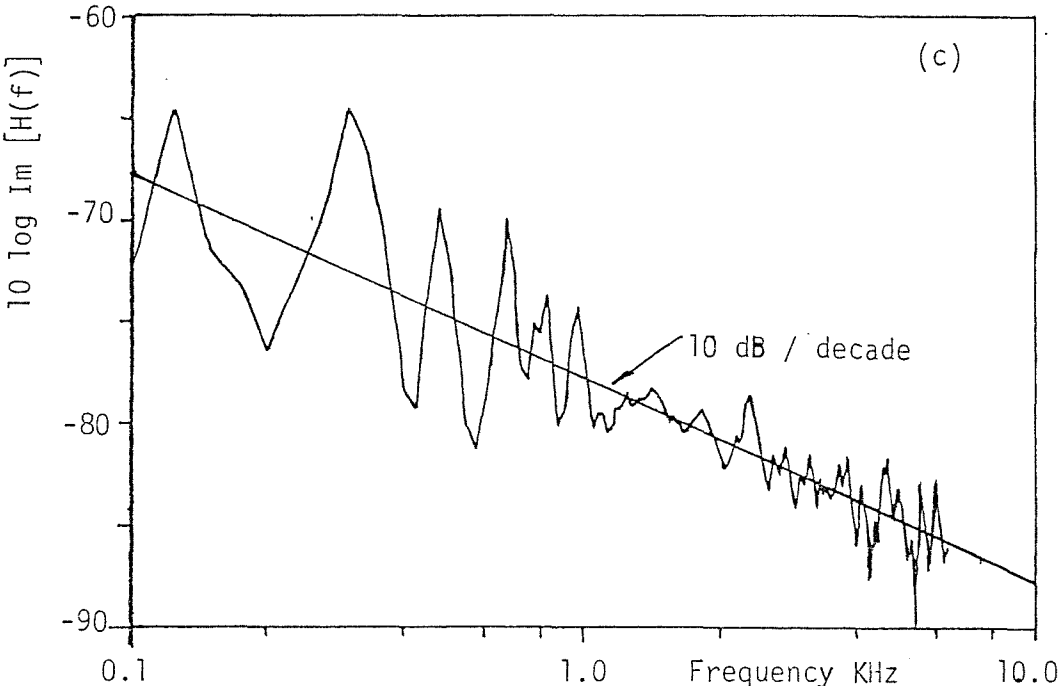
(c)
10 log Im [H(f)]
-60
-70
-80
-90
10 dB / decade
0.1
1.0
Frequency KHz
10.0

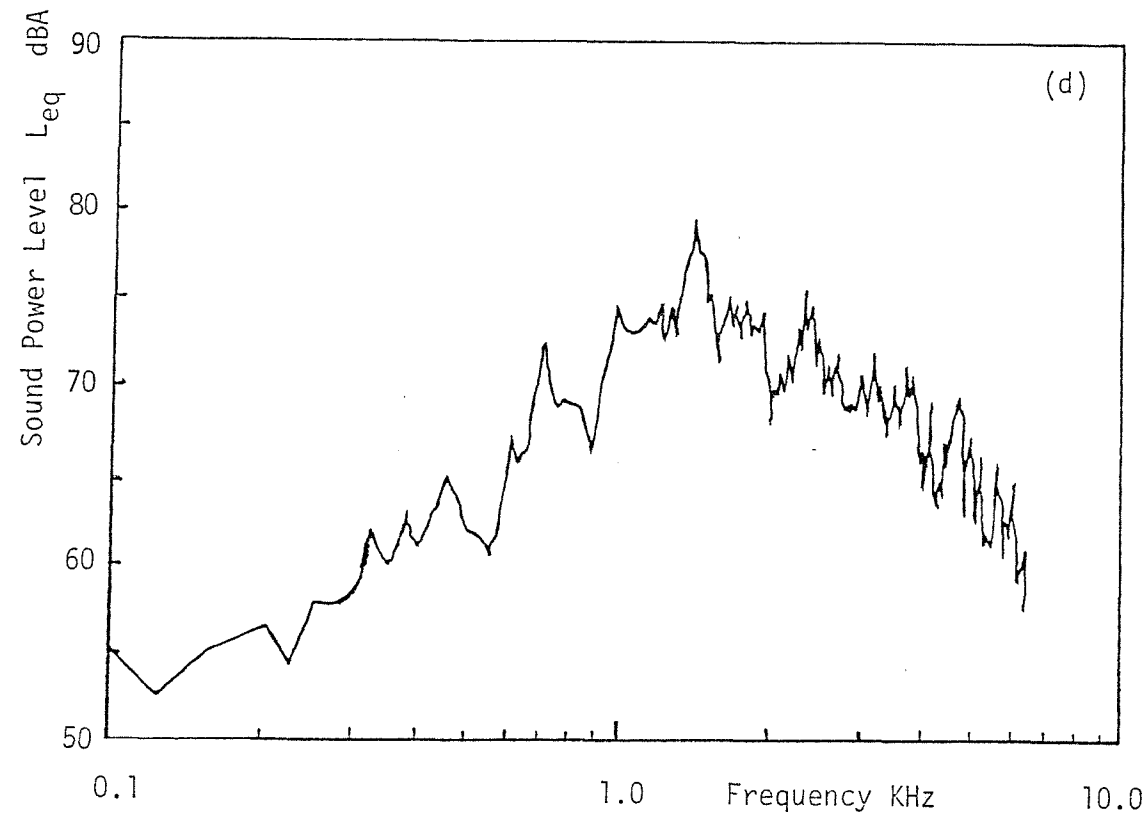

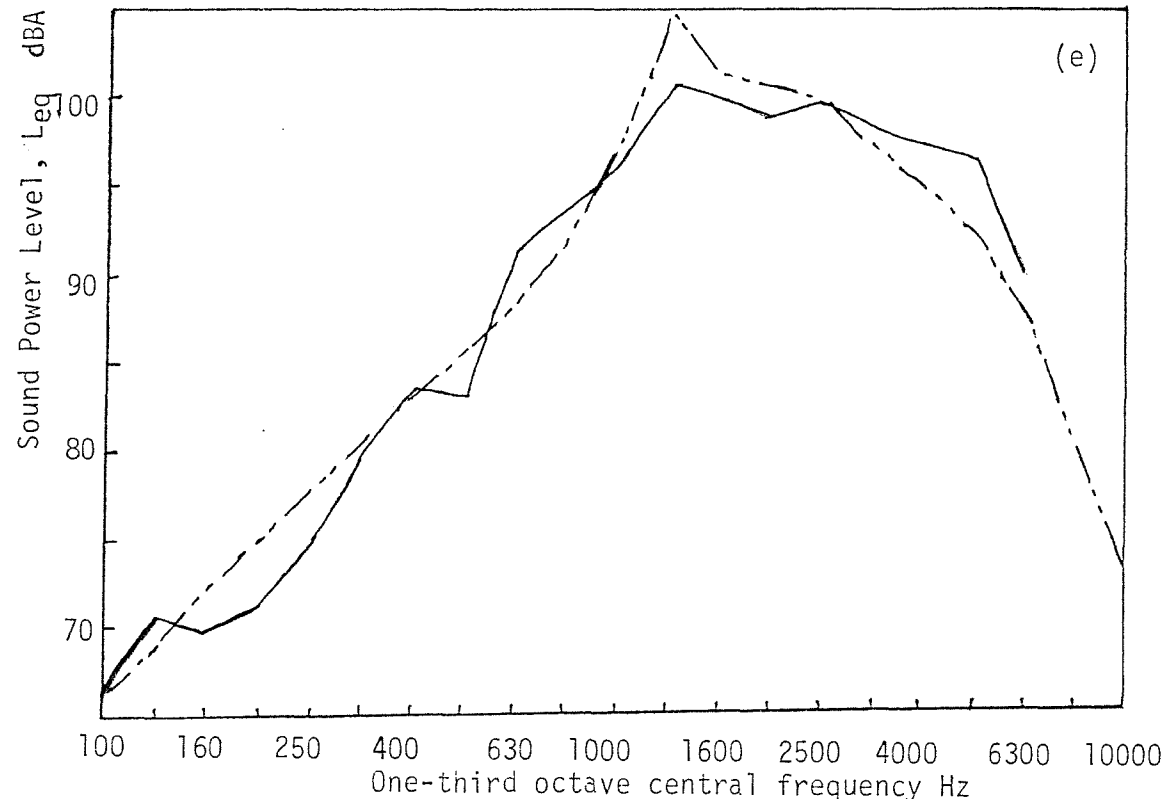

figure 5.5. Condition 1, phase 1: metal-to-metal impact, η_S =0.02. (a) Force pulse; (b) force derivative spectrum; (c) structure point response; (d) measured narrow band sound spectrum; (e) A-weighted noise energy radiated from plate. ———, Measured; — ·· —, estimated.

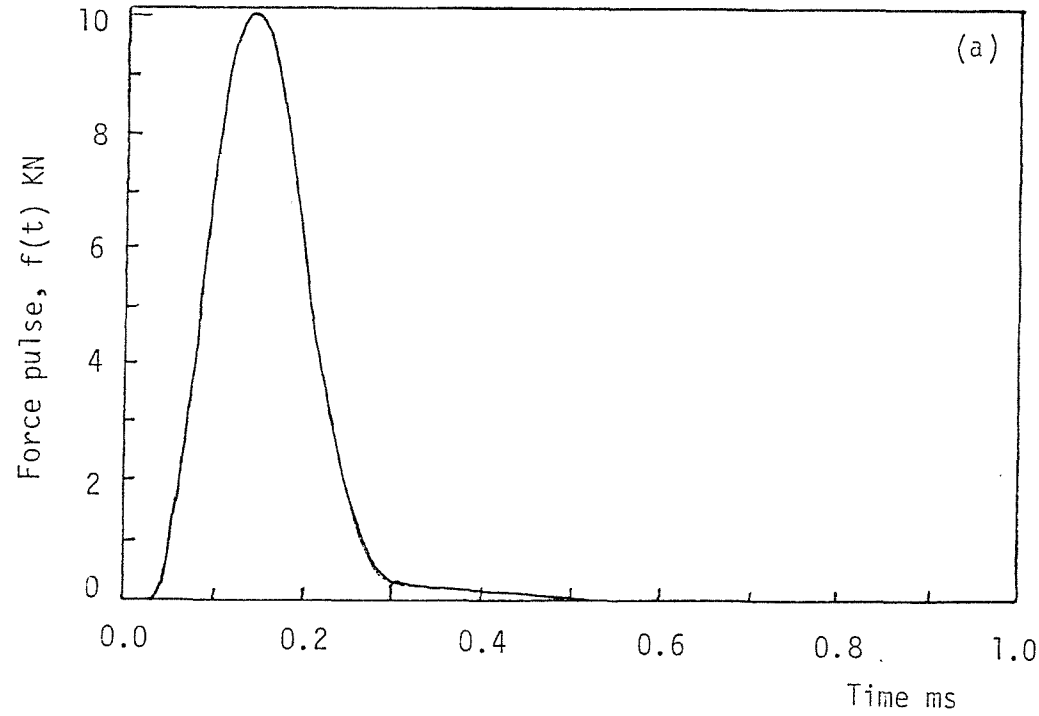
(a)
Force pulse, f(t) KN
10
8
6
4
2
0
0.0
0.2
0.4
0.6
0.8
1.0
Time ms

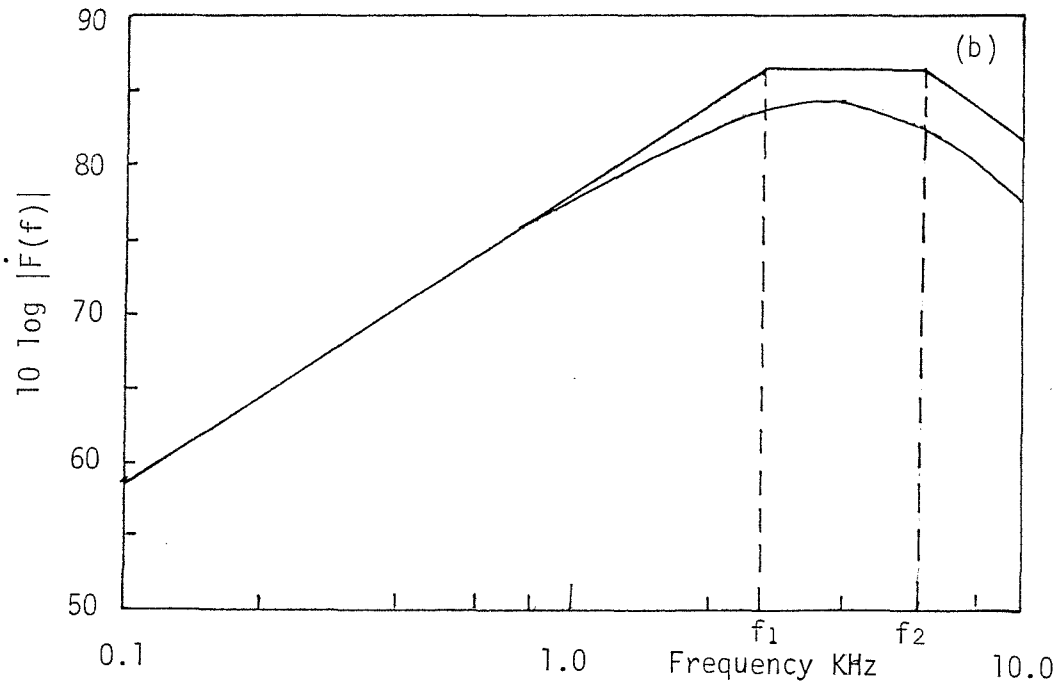
(b)
10 log |F(f)|
90
80
70
60
50
0.1
1.0
Frequency KHz
10.0
f1
f2

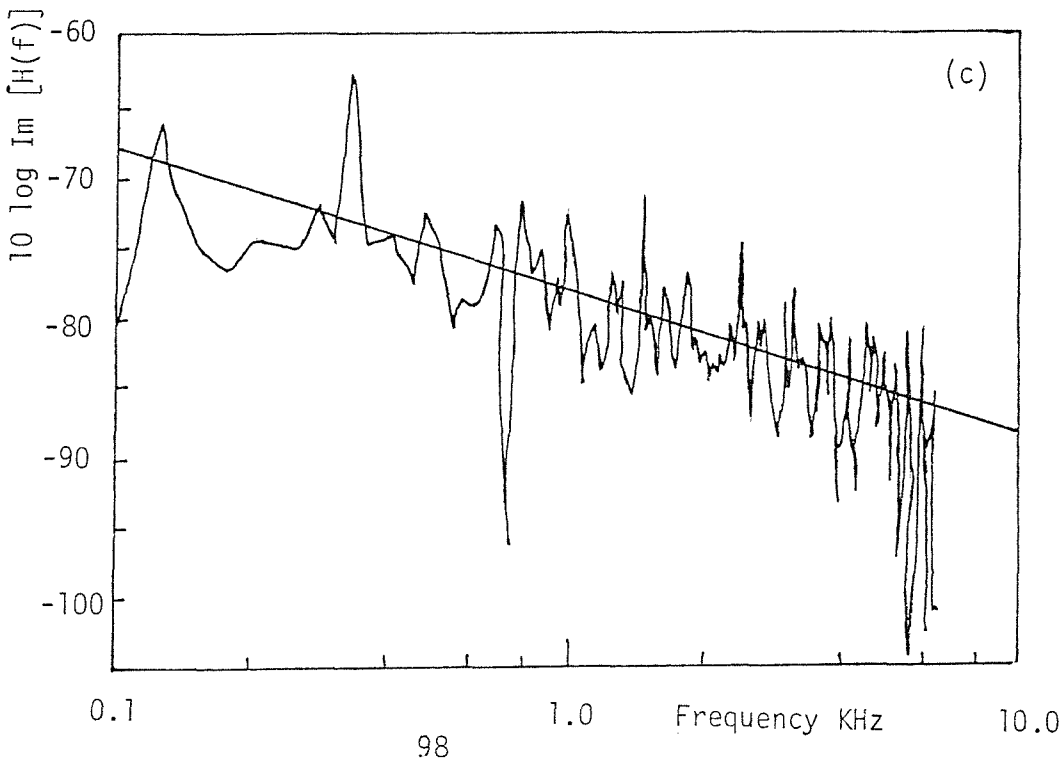
(c)
10 log Im [H(f)]
-60
-70
-80
-90
-100
0.1
1.0
Frequency KHz
10.0

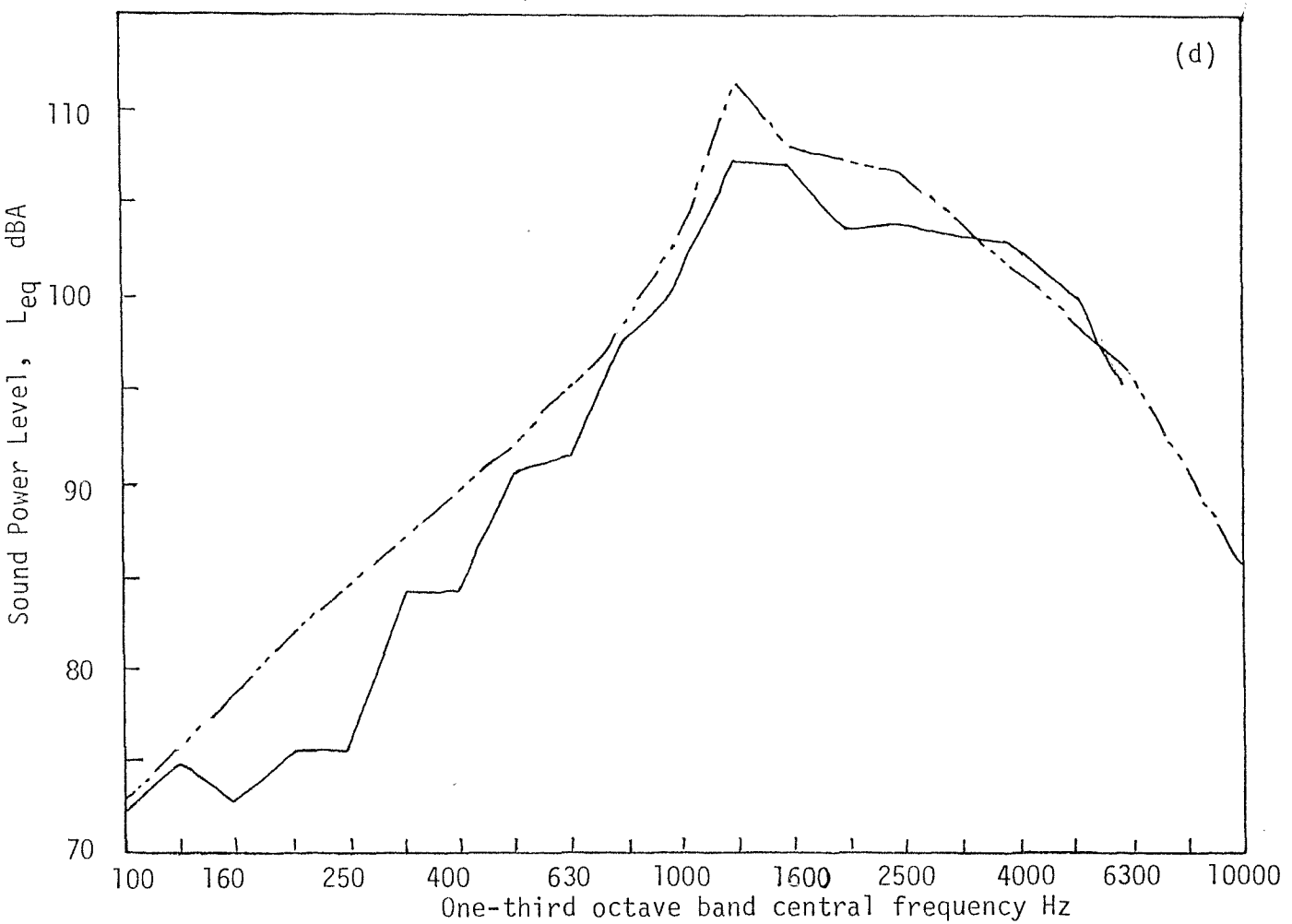

figure 5.6. Condition 2, phase 1: metal-to-metal impact, η_s = 0.006. (a) Force pulse; (b) force derivative spectrum; (c) structure point response; (d) A- weighted noise from plate.
———, Measured; —— ·· —, estimated.

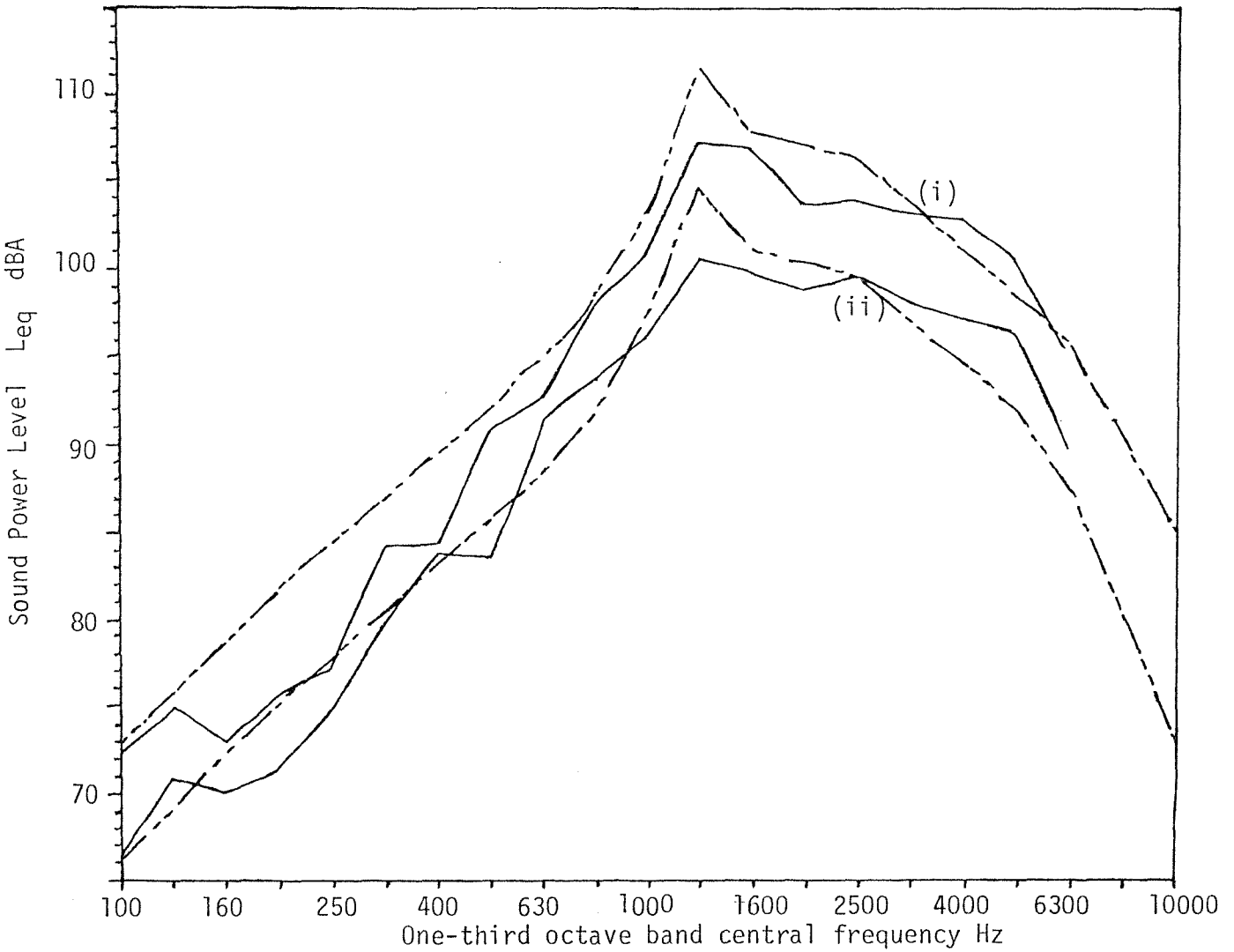

figure 5.7. Metal-to-metal impact for different plate damping. (i) η_S = 0.006; (ii) η_S = 0.02. ———, Measured; —— ·· —, estimated.

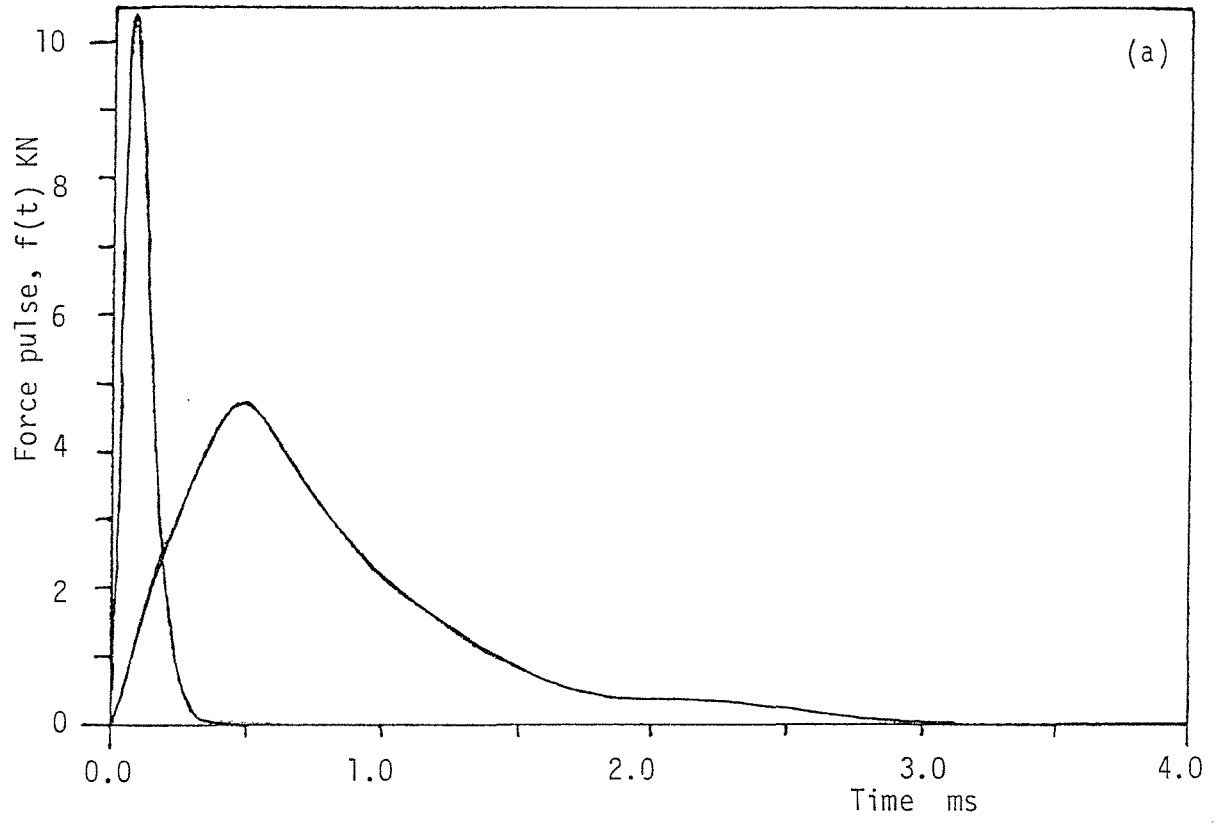
(a)
Force pulse, f(t) KN
10
8
6
4
2
0
0.0
1.0
2.0
3.0
4.0
Time ms

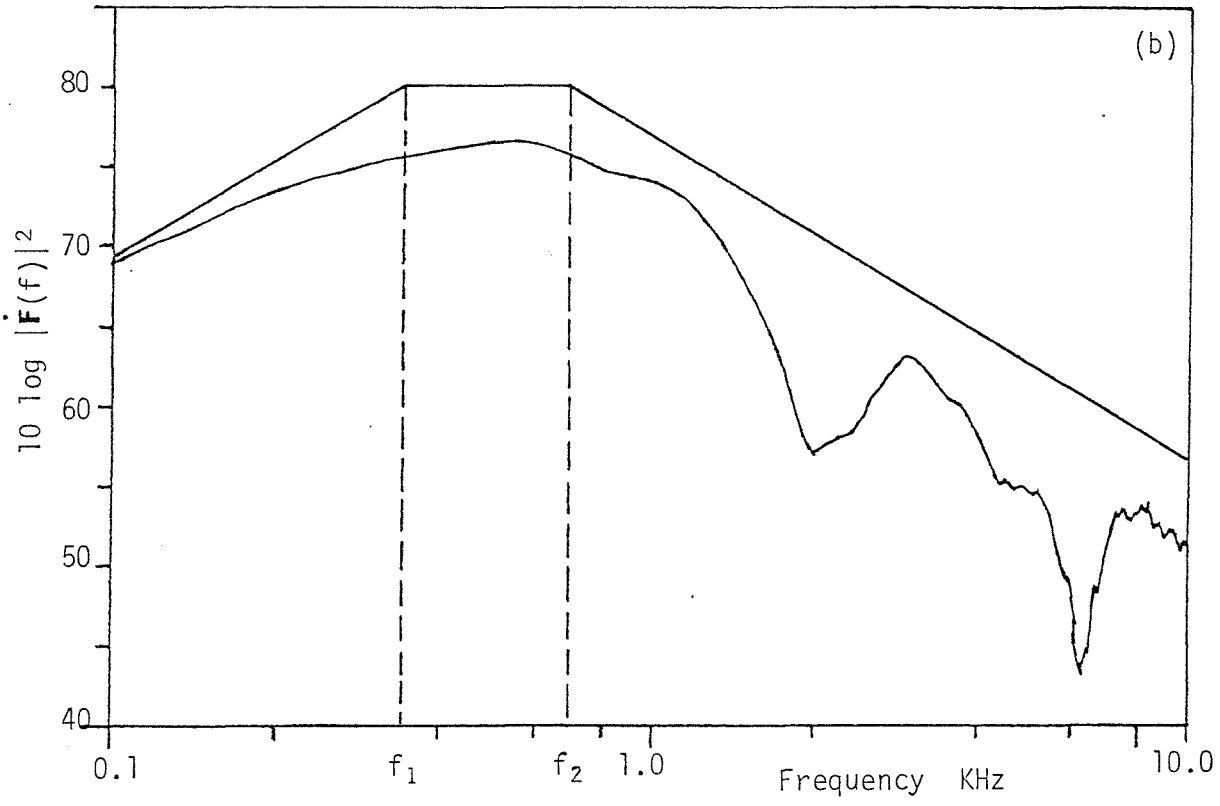
(b)
10 log |F̈(f)|²
80
70
60
50
40
0.1
f1
f2
1.0
10.0
Frequency KHz

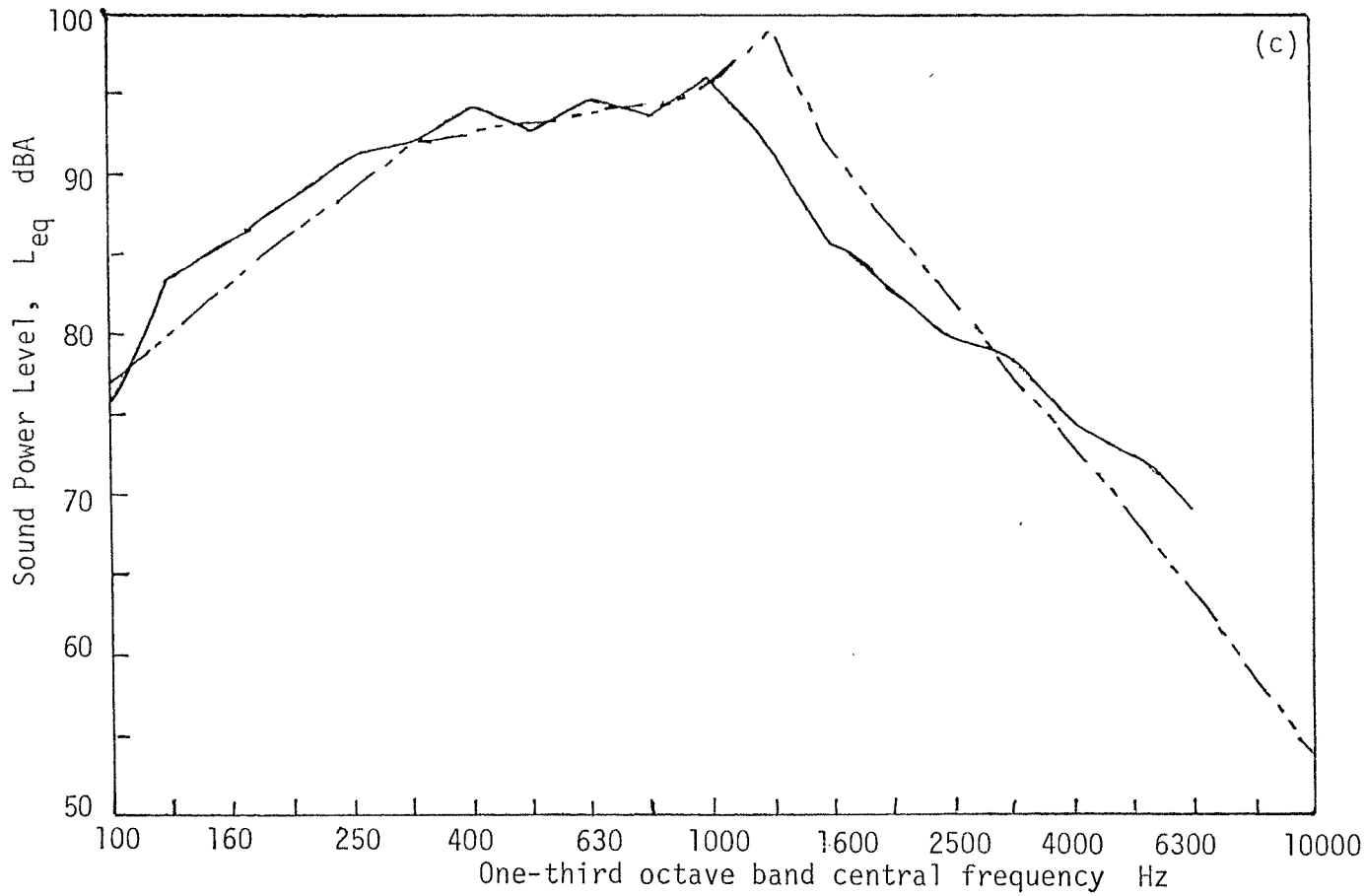

figure 5.8. Condition 3, phase 1: soft blows with rubber insert, n_s = 0.02. (a) Force pulse; (b) force derivative spectrum; (c) A-weighted noise radiated from plate. Note shift to low frequency. ———, Measured; —— ·· —, estimated.

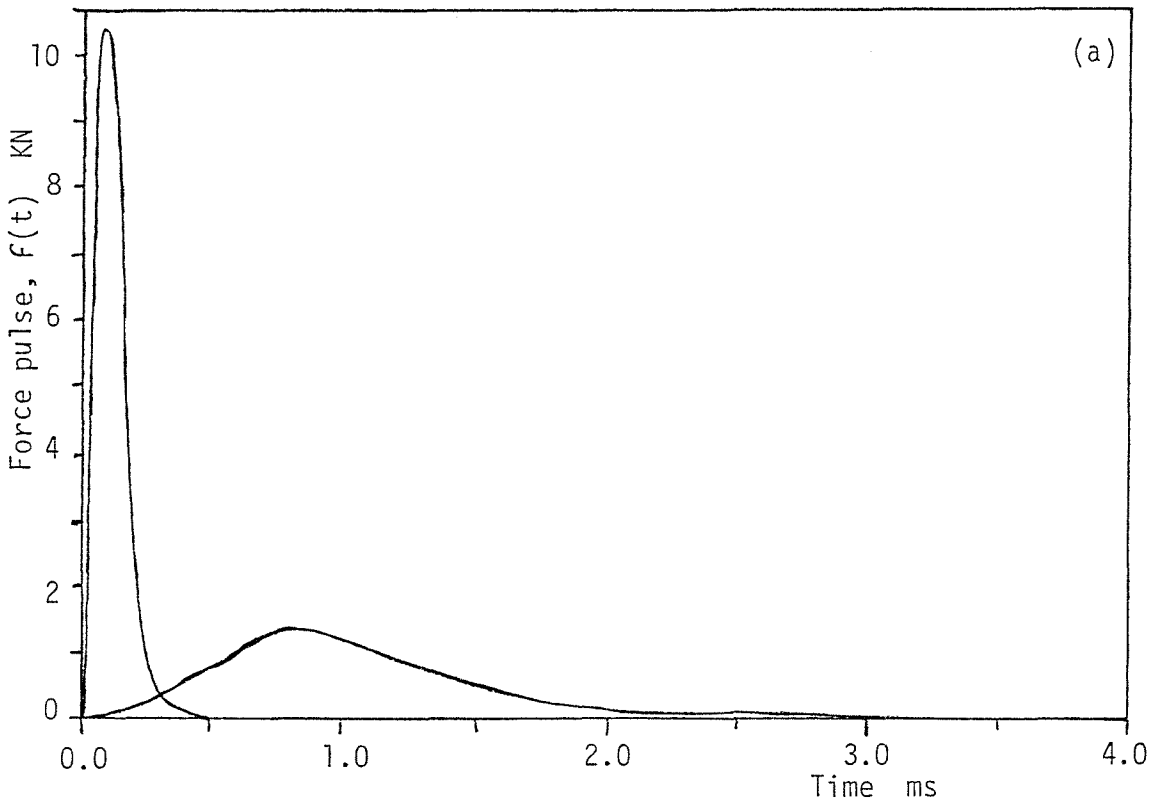

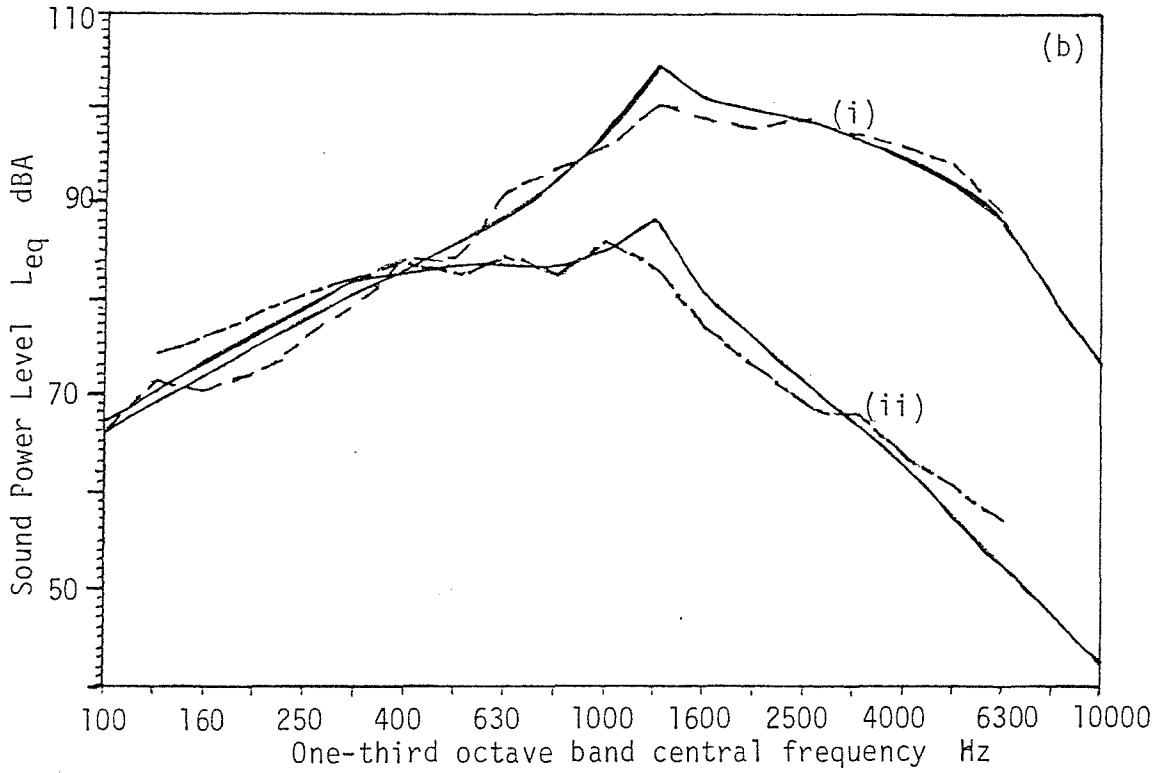

figure 5.9. Equal energy force pulse (a) of different duration; (b) reduction in noise radiated due to impulse tailoring for equal energy impact: (i) short pulse, (ii) long pulse. ———, Measured; ----, estimated.

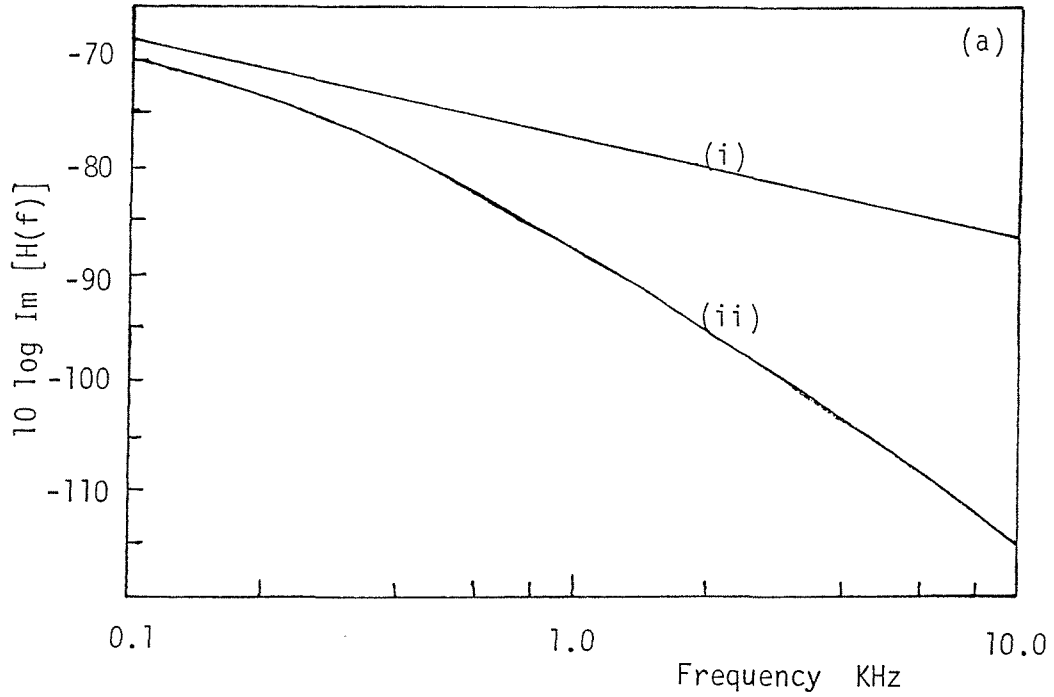
(a)
-70
-80
-90
-100
-110
10 log Im [H(f)]
(i)
(ii)
0.1
1.0
10.0
Frequency KHz

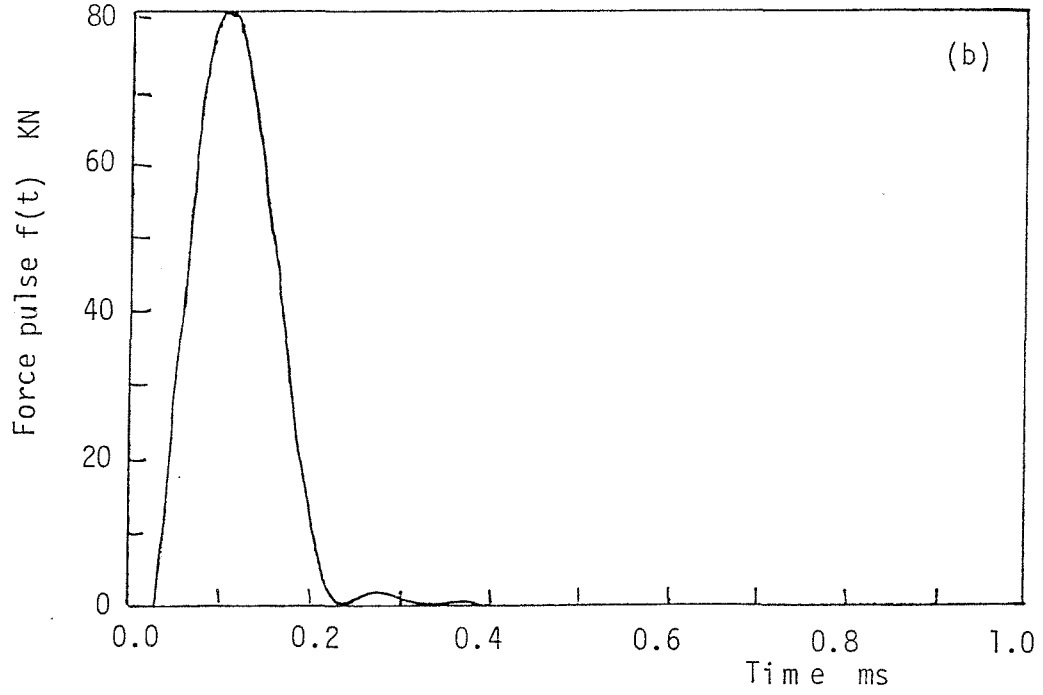
(b)
80
60
40
20
0
Force pulse f(t) KN
0.0
0.2
0.4
0.6
0.8
1.0
Time ms

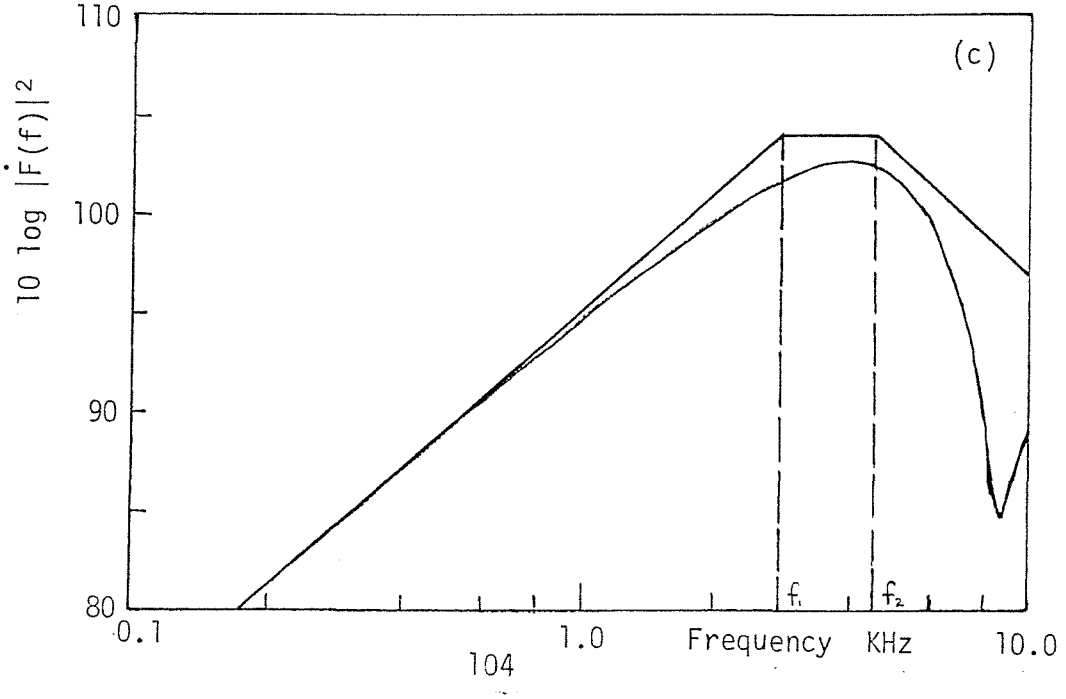
(c)
110
100
90
80
10 log |F(f)|²
f₁
f₂
0.1
1.0
10.0
Frequency KHz

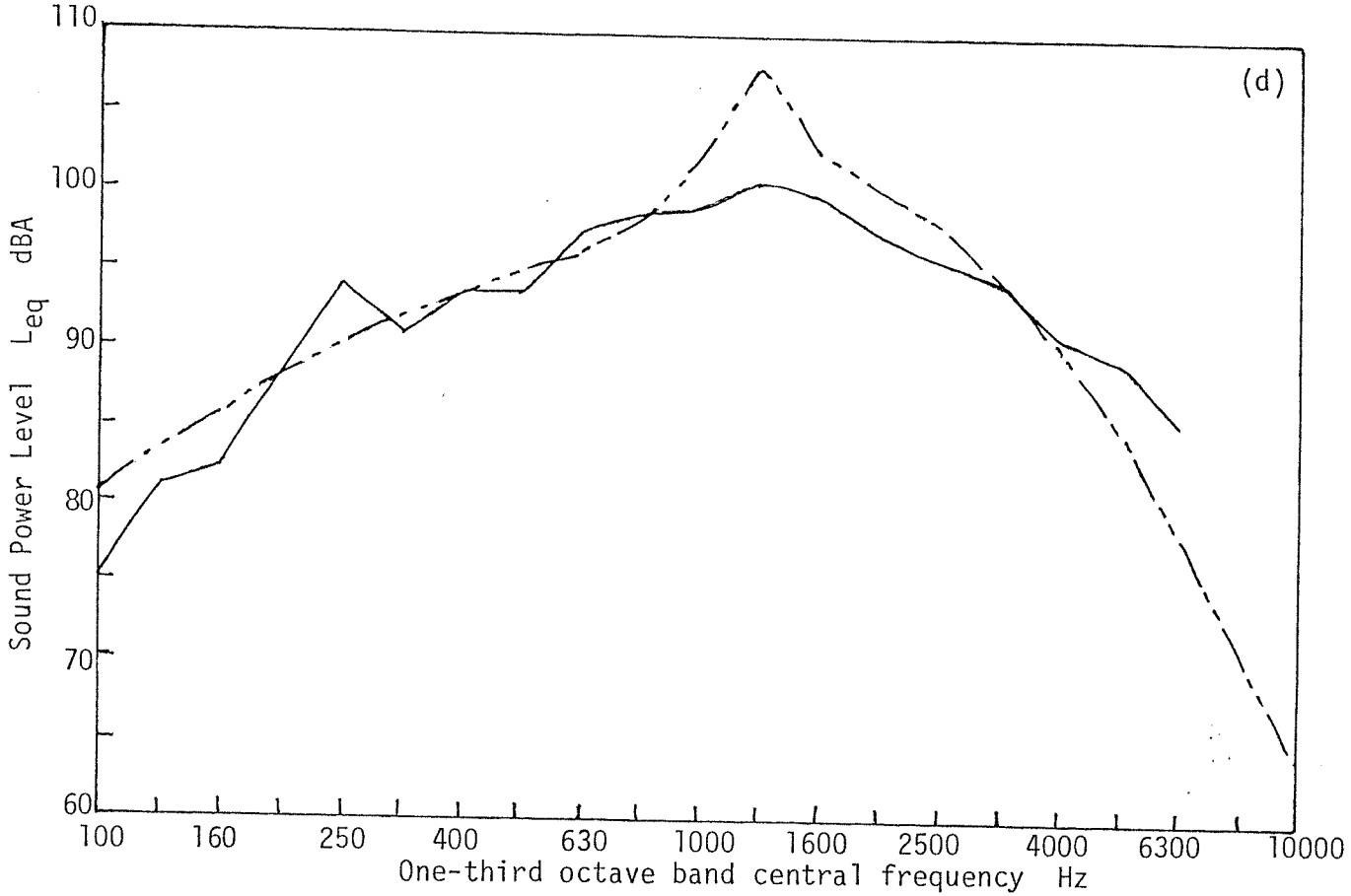

figure 5.10. Condition 1, phase 2: excitation through blocking mass, η_S = 0.02. (a) Structure point response (i) plate (ii) plate and blocking mass; (b) force pulse; (c) force derivative spectrum; (d) radiated A-weighted noise. ———, Measured; — .. —, estimated.

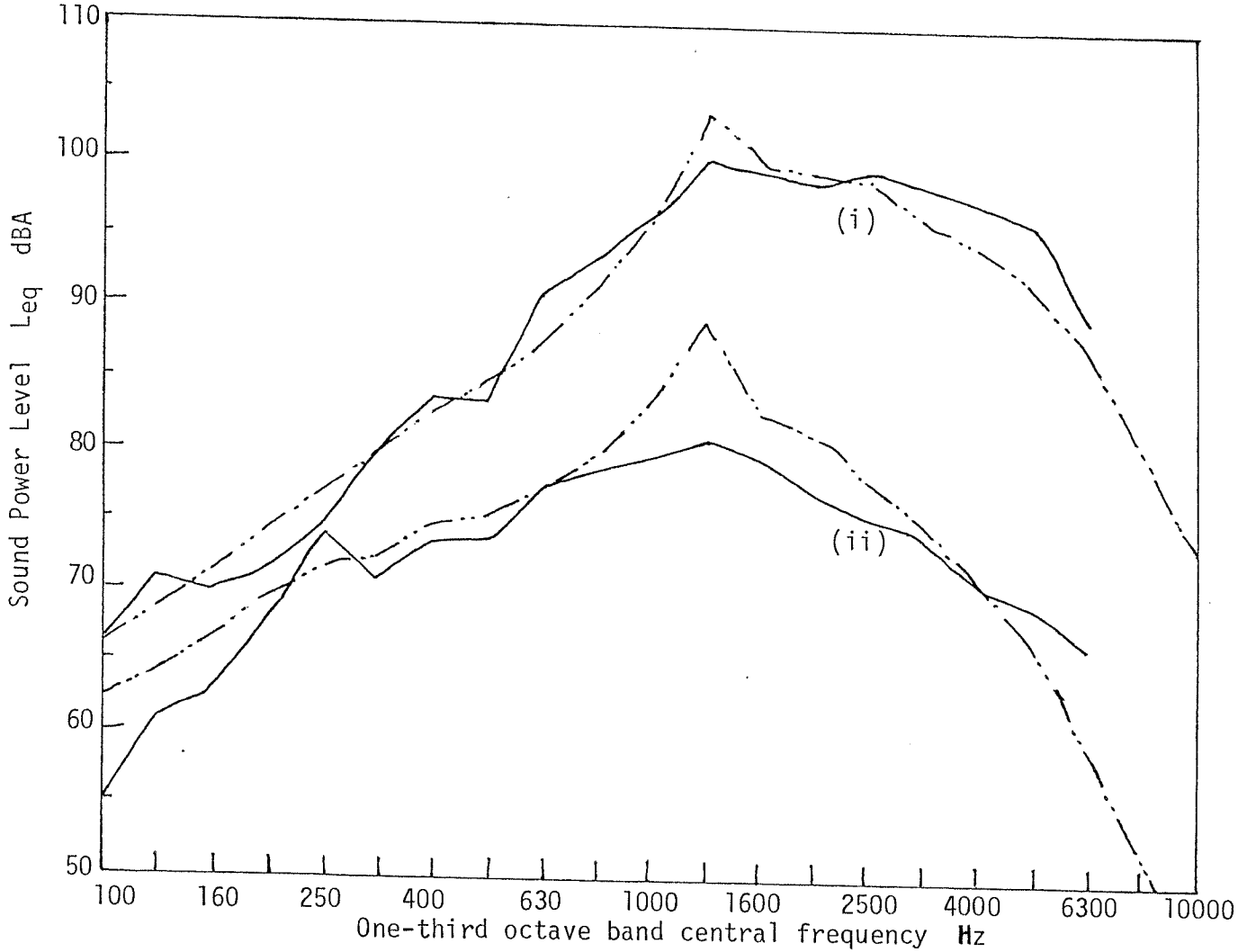

figure 5.11. Noise energy radiated for equal momentum change. (i) Plate directly excited; (ii) plate excited through blocking mass. ———, Measured; —— .. —, estimated.

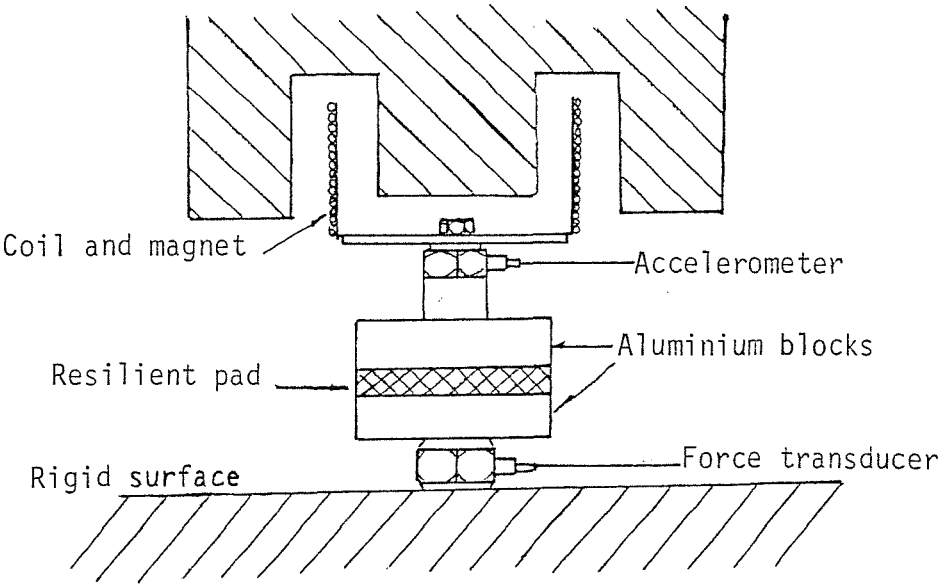

figure 5.12. Set-up to measure stiffness and loss factor of isolator

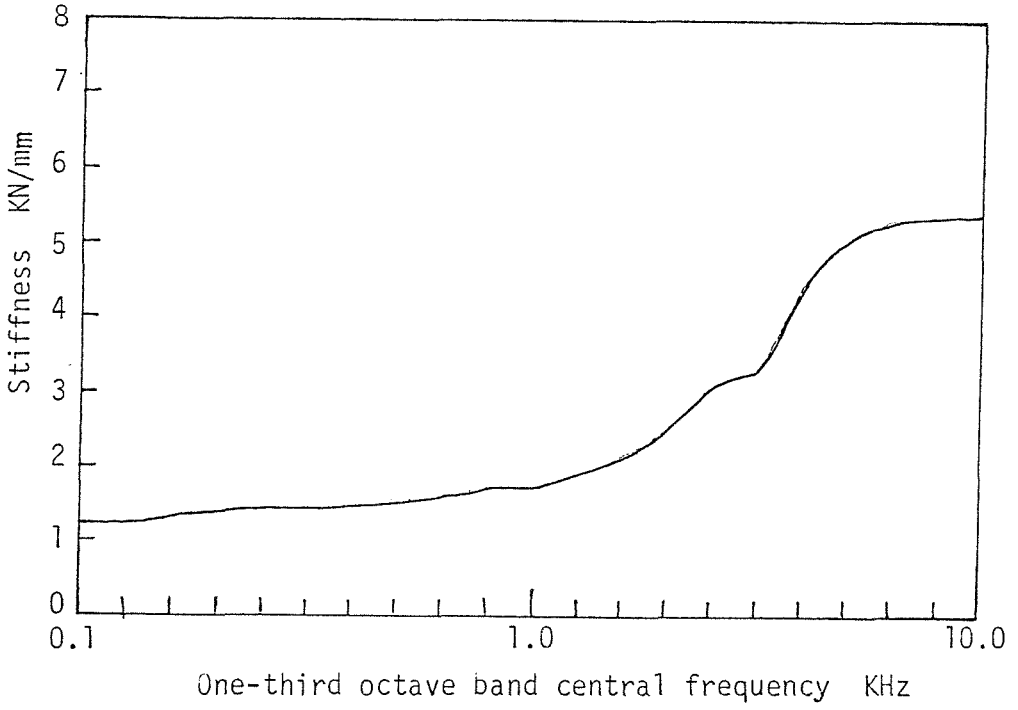

figure 5.13. Change of isolater stiffness with frequency.

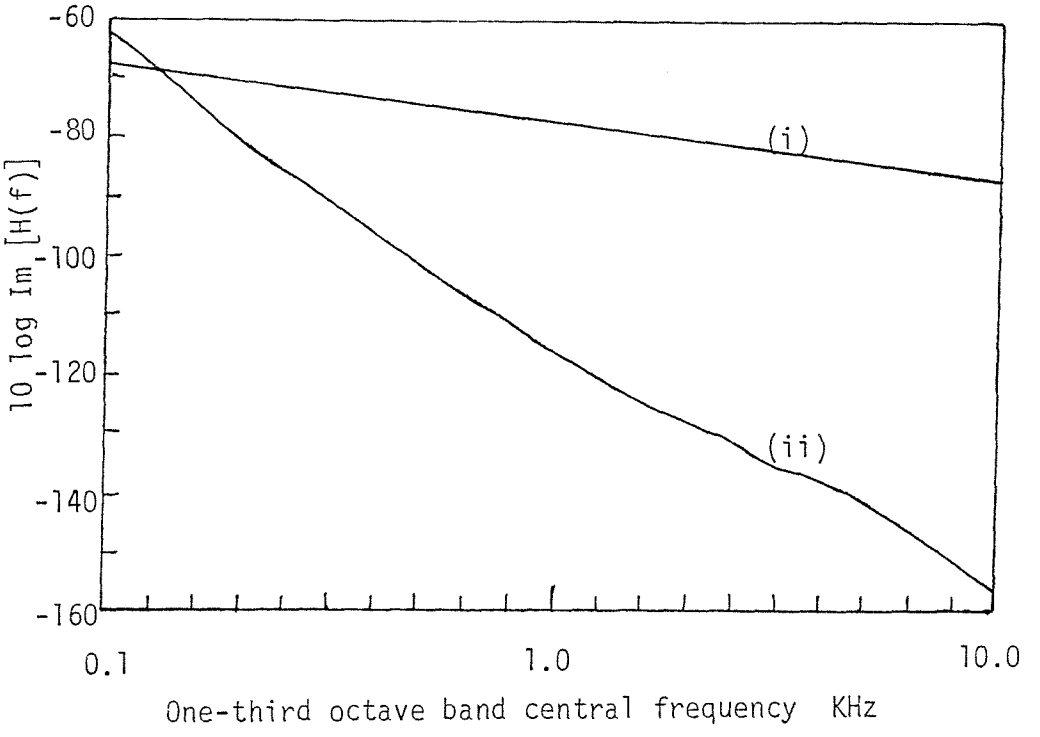

figure 5.14. Structure point response. (i) Plate; (ii) plate and blocking mass on resilient pad.

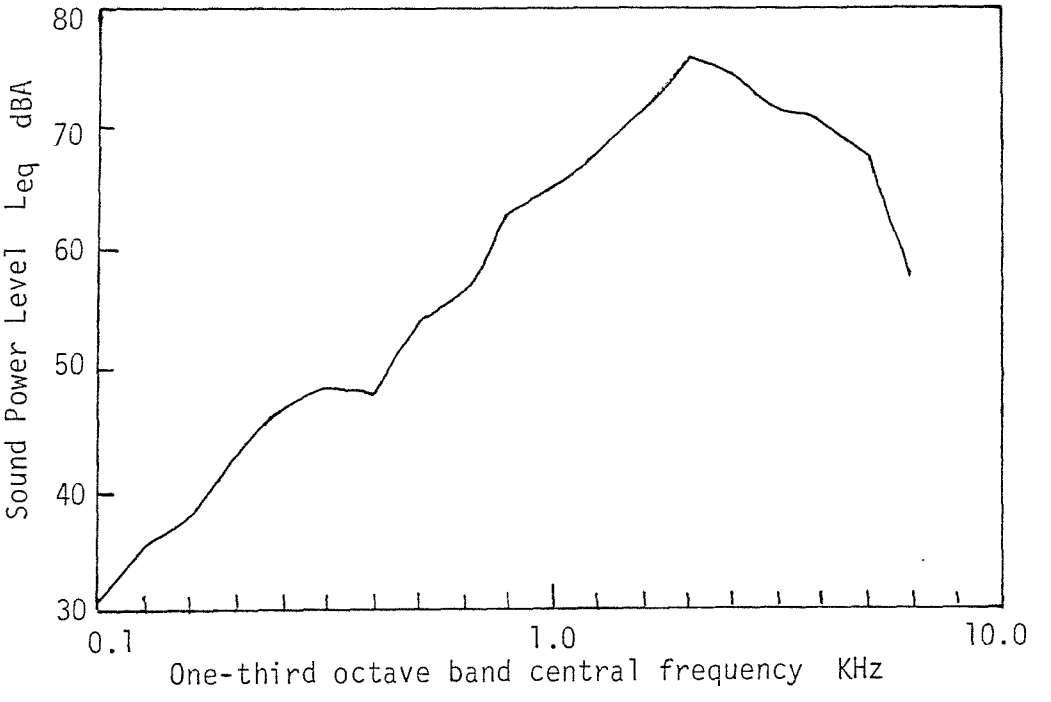

figure 5.15. Acceleration noise energy spectrum for 50 mm dia. sphere hitting block.

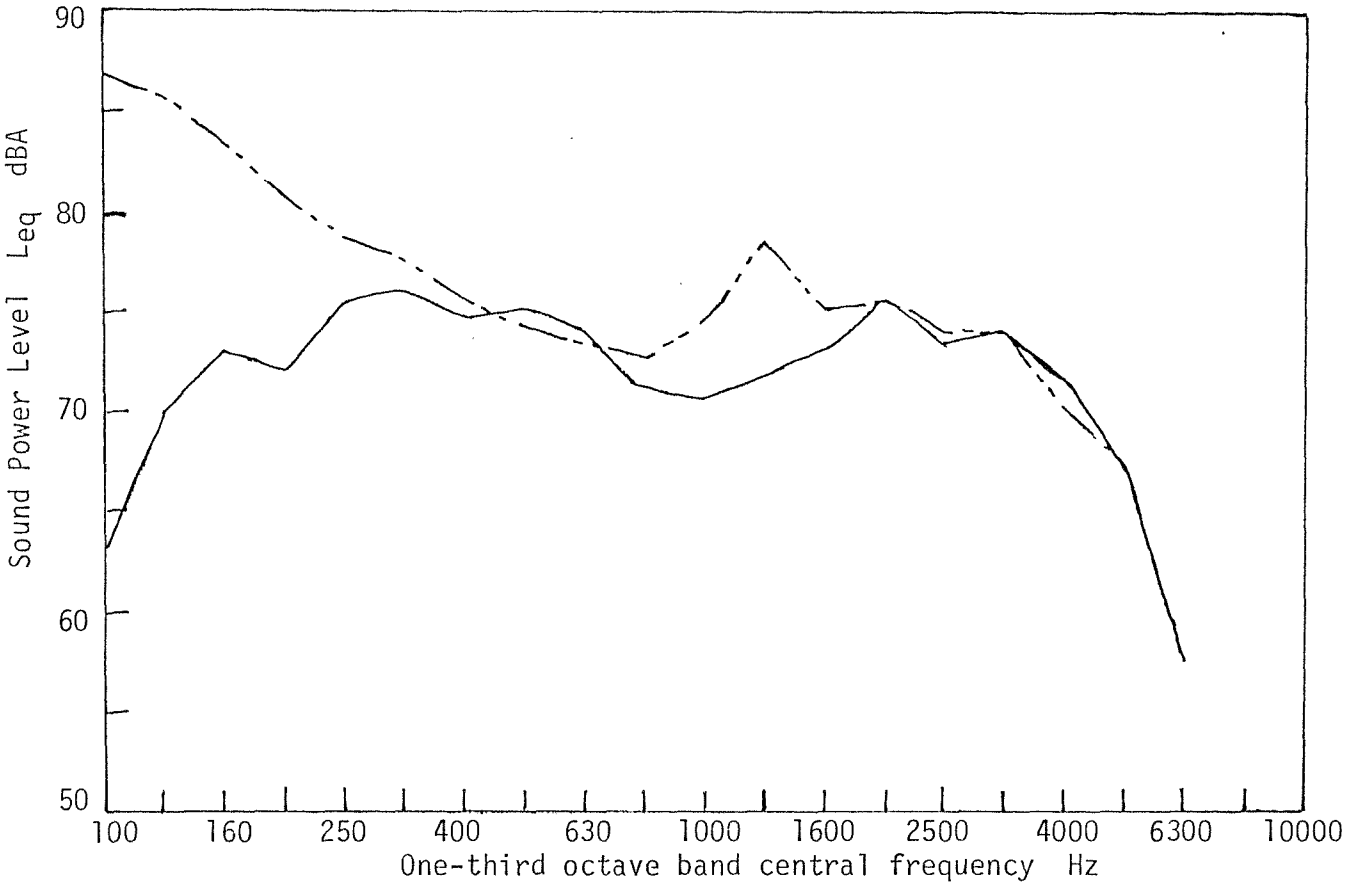

figure 5.16. Condition 2, phase 2: Excitation through blocking mass on resilient pad, n_S = 0.02. Radiated A-weighted noise. ———, Measured; —— ·· —, estimated.

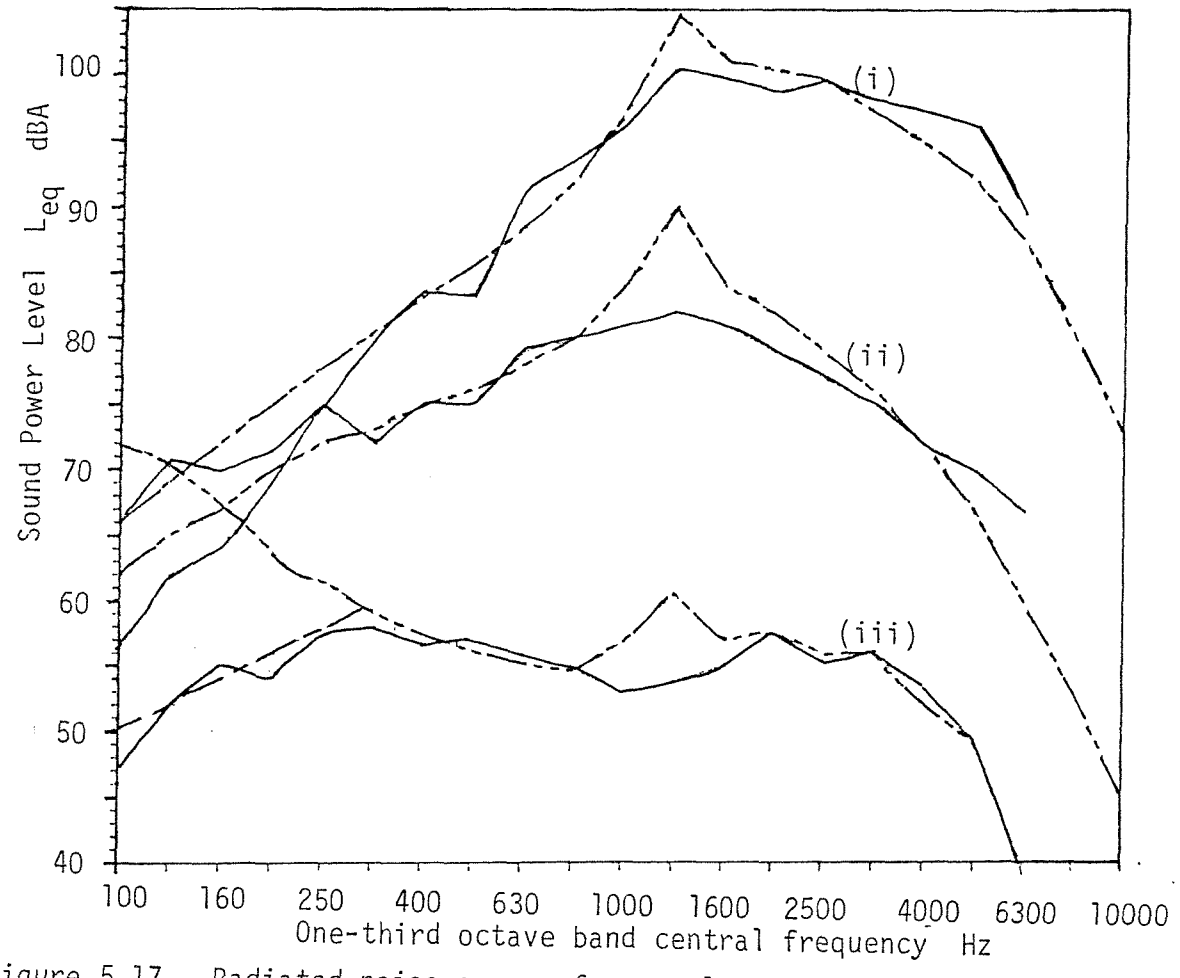

figure 5.17. Radiated noise energy for equal momentum change for different excitation of plate, showing the high attenuation due to the change in structure response. ——, Measured; — .. —, estimated. (i) Plate directly excited; (ii) excitation through blocking mass; (iii) excitation through blocking mass coupled to the plate via the resilient pad.

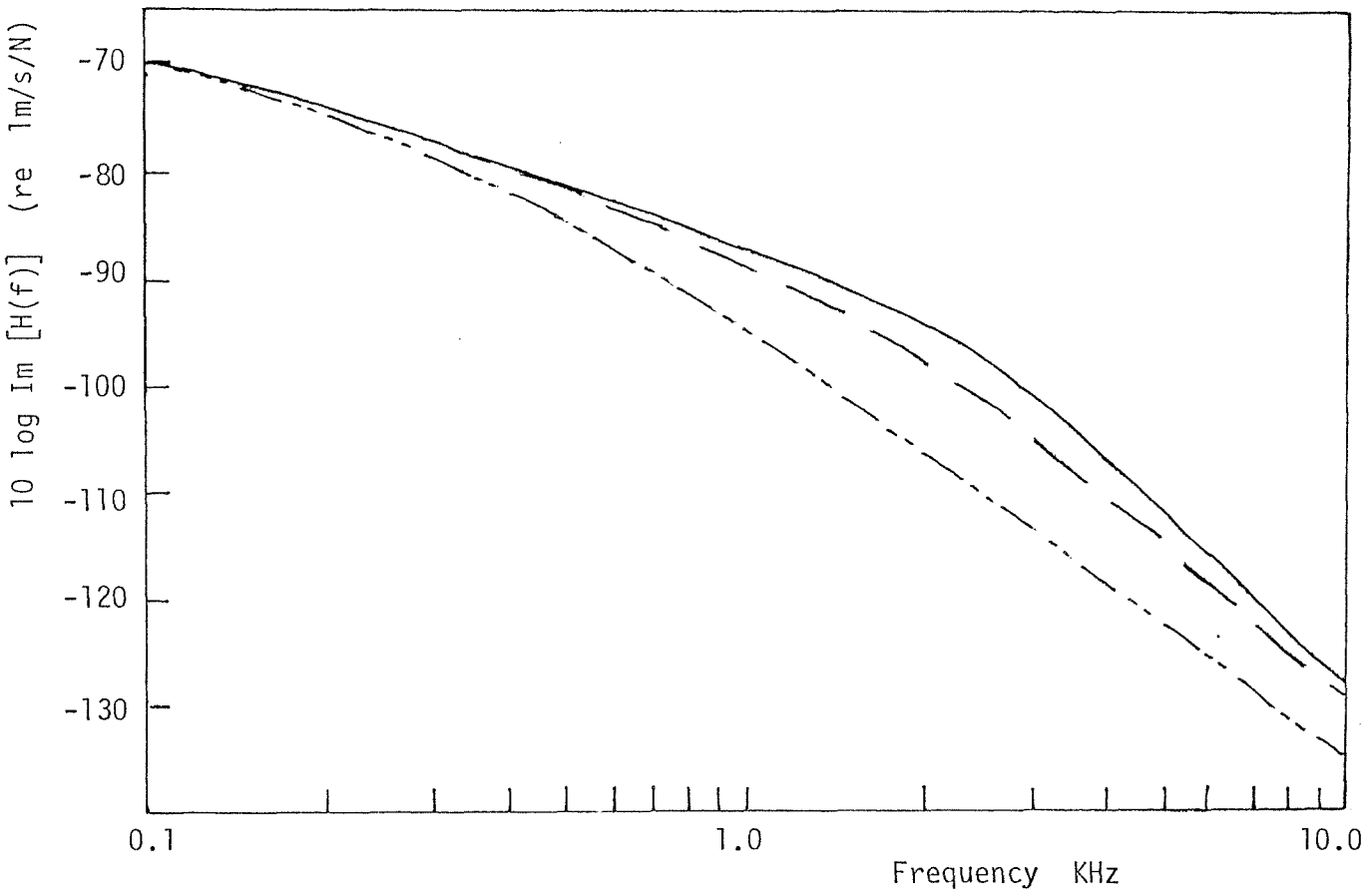

figure 5.18. Change in Im [H(f)] for a plate excited via a blocking mass and isolator with change in cos β. Combined natural frequency 2.2 KHz. ——, cos β = 1.0 (infinite plate); -----, cos β = 0.1 ; — ·· —, cos β = 0.01 .

CHAPTER VI

DIESEL ENGINE NOISE

VI. 1. Introduction

The noise radiated from a simple machine structure is investigated in the previous chapter where a comparison is made between the measured and estimated radiated noise using the "energy accountancy" concept. In this chapter, this concept is applied for a more practical type of structure.

The noise from other complicated structure types like cylindrical shells is investigated in reference [16]. In this case, the noise energy radiated when a bottle structure is impact excited is investigated with the aim of noise control in bottling lines.

The noise radiated from a diesel engine has been investigated by many specialised groups who have been working in this field for a number of years. Their methods, used for noise level measurement from different parts of the engine structure, have been fairly standard and the deductions made from these measurements for noise control purposes have been rather empirical.

The method used for noise estimates is to measure the spatial average velocity squared on the engine surface, $\langle\overline{V^2}\rangle$ and estimate the radiated noise from the expression

$$E_{rad} = \rho_o c \langle\overline{V^2}\rangle A\sigma_{rad} \qquad (6.1)$$

where A is the area of the surface. These estimates are verified by either using part covering methods, where the engine surface is covered by sheets of lead, lined with sound absorbing material and the noise radiated from a particular surface is obtained by removing the covering only over that surface; or by using an acoustic intensity meter [29]. The latter technique has only been recently developed and it consists of having two microphones situated very close to

the engine surface.

From these results, it has been concluded that if thin panels like the oil sump, the timing chain cover and the valve cover are treated, by increasing their damping and by isolating them from the rest of the engine structure, and also if other noise sources like the exhaust system and fan noise are treated with conventional methods, then most of the noise radiated comes from the vibrations of the crankcase [30]. The contribution to the total noise radiated, made by the cylinder head and inlet and exhaust manifold is generally small.

The modes of vibration of the crankcase were also studied by a number of people and the modal shapes can be found in papers dealing with engine noise and its control [31 - 33]. The work on noise control from the engine block dealt with the reduction of the level of vibration of these crankcase modes. It is shown that most of the noise emitted by the engine block is from the lower part of the engine structure, i.e., the crankcase side walls. Different forms of the crankcase are investigated and changes include the number of main bearings and the shape of the crankcase. If the number of bearings is increased, by including intermain bearings, the bending stiffness of the whole engine increases and therefore the first mode in bending occurs at a higher frequency. There are basically two different shapes of crankcase, the underslung crankshaft or the skirted crankcase (figure 6.1). These give different patterns of vibration and the level is higher for the skirted type [34]. This higher level is due to the larger span of the bottom part of the engine structure.

VI. 2. Sources of Vibration

The excitation in a diesel engine structure is mainly from two sources: combustion excitation due to the combustion pressures and mechanical excitation due to the backlash and clearances being taken up when there is a change in the force direction. One of the main contributions of the second type is piston slap. The strength of each source depends on the engine size, speed and load, (figure 6.2). The structural vibrations induced into the engine structure are then

transmitted through to the thin sections of the external faces of the engine.

The combustion noise is due to the high cylinder pressures and the rate of increase of this pressure. In a diesel engine, a distinctive knock can be heard, as compared to the petrol engine, which is due to the more rapid rate of change of pressure, which occurs after the ignition of the combustion charge. In a diesel engine, the fuel is injected into the cylinder during the "ignition delay period", which is the time between the beginning of fuel injection and the ignition of the injected fuel. The increase in the cylinder pressure and the rate of rise can be studied by detailed examinations of the combustion process. Generally speaking, the more fuel injected into the cylinder, the more rapid is the rate of change of pressure during combustion.

The rapid change of pressure inside the cylinder appears in the pressure spectrum as an increase at high frequencies. Thus to reduce noise due to combustion, either the pressure pulse is smoothed, i.e., a more gradual cylinder pressure development, shifting the pressure spectrum to lower frequencies where there is the combined effect of A-weighting and lower structure response; or the peak pressure of combustion is decreased. Sometimes, the combustion pressure can be smoothened by turbo charging, or indirect or pilot injection. The mechanics involved when using a turbo charger is that the charge entering the cylinder is at a slightly higher temperature, which makes the ignition delay period shorter resulting in a more gradual pressure rise at ignition. The rise in temperature of the charge varies with the speed of the engine and increases with an increase in speed. Therefore, turbocharging is effective at all speeds. With indirect injection the fuel can mix with a restricted volume of the charge, thus limiting the rate at which the combustion pressure rises. One drawback with indirect engines is that generally this smoothing occurs only at full load, and sharp rises in the pressure, detected by knocking noise, become more pronounced at part load and at idling conditions.

Piston slap excitation occurs because of impact of the piston

against the cylinder wall. Under the influence of the gas and inertia forces of the con-rod and piston, a transverse component of the force is developed which is balanced by the reaction of the cylinder wall on the piston. When this force changes direction, the reaction on one side becomes zero and the piston travels across the clearance under the influence of this transverse force. On reaching the opposite wall of the cylinder, the piston has a transverse velocity and it impacts the cylinder wall. The size of the impact depends on the velocity of the piston, which depends on the speed of the engine and the gas forces in the cylinder clearance.

The clearance between the piston and the cylinder cannot be eliminated because of the different expansion coefficients. The piston and cylinder block are made of different materials which result in different levels of expansion. Present methods of reducing noise due to piston slap are; one, to introduce an offset in the gudgeon pin on the thrust side, this is only effective at high speeds when the engine is hot; and two, to include devices which distort the piston skirt as it cools [35], thus reducing the clearance.

The impacts on the cylinder wall are transmitted to the outside of the engine via the decks above and below the water jacket. The excitation of the crankcase panels is usually due to impacts near bottom dead centre. The vibrational energy is transmitted via the lower water jacket deck or via the water jacket panels. The transmission of combustion excitation is along the con-rod, crank-shaft and engine bearings and appear at the crankcase panels. Since the vibrations from both sources appear on the same engine section, it is very difficult to separate the two on a running engine.

To reduce the noise due to the combustion pressure or piston slap, the method which has been suggested is to smoothen the sharp rises in the excitation forces. This is one method of solving the problem, but by changing the force pulse in a machine, the operation of which is inherently dependent on the shape of the pulse, like in this case, will result in diminished performance. Therefore different methods for noise control which modify other parameters of the engine, have to be sought. This can be done by using the energy accountancy concept and by identifying the energy flow paths. If this

concept can be used for such a complicated structure, then the results can be investigated for noise control measures.

VI. 3. Experimental Methods

VI. 3.1. Side Excitation

This chapter investigates the use of the energy accountancy concept to estimate the noise that an engine structure would radiate from combustion and piston slap excitation. Since it is not possible to separate the noise from each source on a running engine, simulation tests are done on a static engine, to measure the noise radiated from the engine frame due to each source.

The engine used in these tests is a Ford, 4 cylinder inline engine of 1.5 litre capacity. The crankcase is of the underslung crankshaft type and it has five bearings. It is a petrol engine but there is no difference in the block structure between a petrol and a diesel engine. The combustion pressure and piston slap are simulated and therefore, the difference in a running engine between a petrol and diesel engine does not affect the results.

Before investigating simulated combustion and piston slap noise, the engine structure is directly impacted on the side on one of the crankcase panels. The impact is from a calibrated hammer and the radiated noise is simultaneously measured with the impact force. The force-time history is shown in figure (6.3) and figure (6.4) shows the spectrum of the force first derivative. The straight line approximation, (Appendix A), is used to estimate the noise energy radiated from the engine structure. The same technique can be used to calculate the shape of the spectrum for the pressure pulse due to combustion.

The next term needed in the accountancy concept to estimate the noise radiated, is the structural loss factor. Measurement of the loss factor for an engine structure fully assembled, partially assembled and the engine frame on its own by Russell [31] shows that the cylinder head does not increase the loss factor (figure 6.5), contrary to the assembly of most other engine parts, like the pistons,

the con-rods, bearings etc. The loss factor for the engine under test is measured with different stages of assembly, particularly the effect of the cylinder head (figure6.6). These results show that the loss factor of the engine structure is very high, even with just one piston assembled and assembling all four pistons will not change the loss factor at all. The fixing of the cylinder head does not change the loss factor. This enabled combustion noise to be simulated by direct impact on the piston top with the cylinder head removed. This measurement of loss factor is used in all the tests.

To calculate the constant term in the accountancy equation, an average bulkiness of 1cm for the engine structure is assumed; Values for the density of air ρ_o of 1.23 Kg/m^3 ; the speed of sound in air c_o of 340 m/s ; and the material density of the engine structure ρ_m of 8.1×10^3 Kg/m^3 are taken. Analysis are done in one-third octave bands, thus $\Delta f/f_o$ is a constant of 0.23. Therefore, the value of the constant is -12.2 dB.

The remaining two terms which are to be determined are the structure response and the radiation efficiency. Although in previous work on the radiation efficiency of different structures, an estimate of the efficiency of an engine block is not given, it is shown that [15] the exact shape of the structure is not important. Only the order of the source, i.e., a dipole or higher order, depending on the mode of vibration and the size of the structure affect the radiation efficiency. The vibration of an engine structure has a complicated shape and therefore it must be a high order source. The main noise from the engine comes from the vibration of the crankcase, which is cylindrical in shape of about 200mm diameter. Thus the radiation efficiency of a cylinder of equal diameter, in flexural vibration is assumed (figure 6.7).

The structural response term is not easily estimated because of the complicated shape of the structure and because of the variation with frequency of the types of modes that are excited. Therefore, an estimate for the response is obtained by measurement at the point of impact. The interpretation of the measured results is very important. The response on the side of the engine is measured by the use of a

coil and magnet arrangement using white noise excitation. The first resonance of the structure occurs about 650 Hz, and the response below this frequency cannot be easily obtained because of the very low amplitudes and the very large mass of the structure.

Above the first ringing frequency, i.e., above 650 Hz, the response is that of a cylindrical shell of diameter 200mm and 12mm thickness. The rate of fall is of 5 dB per frequency decade as shown in reference [16], for a cylindrical shell below its circumferential resonance frequency. However, there is a discontinuity in the response at about 4 KHz. The individual panels of the engine block between bearings are of approximately 80mm in length and therefore, 4 KHz correspond to the fundamental ringing frequency of each panel. This gives the high level of the response above 4 KHz .

The response below the first ringing frequency of the block is estimated using the same technique as in chapter III, i.e., using the summation of modes method to calculate the response and then approximating for frequencies lower than the fundamental frequency. The response below the fundamental is given by

$$\text{Im}\left[H(f)\right] = \frac{\eta_s}{4\pi^2 M f_o^2} \qquad (6.2)$$

where M is the mass of the whole engine;
η_s is the structural loss factor of the final mode; and
f_o is the first ringing frequency.

Figure (6.8) shows the measured structure response, and for the estimate of noise in one-third octave bands the mean line through the measured curve is used.

Having computed all the parameters necessary to estimate the noise energy radiated, the noise from the engine frame is measured by using a system of nine microphones arranged in a parallelpiped, as in chapter V. The measured results are compared with the estimated ones and the agreement (figure 6.9), is within ± 3 dB. This shows that

the energy accountancy concept to estimate the radiated noise can also be used in the case of complicated structures. Thus noise control of the engine can now be investigated by looking at each parameter of the engine that contributes to the radiation of noise.

VI. 3.2. Combustion Noise

The second investigation considers an impact inside the engine structure. This is similar to the excitation due to the combustion forces inside the engine cylinder. Thus this experimental method investigates a form of simulated combustion; the engine is being excited by an impact on the piston top as if with the action of the combustion pressure.

The structural loss factor does not change with the assembly of the cylinder head; the only change that occurs is that the values of the structure resonances of the engine block shift slightly. This does not affect the simulation since the noise is estimated in one-third octave frequency bands. Therefore, to simulate the combustion pressure rise, an impact is given on the top of the piston, with the latter at T.D.C. The impact is not exactly similar in shape to the combustion pressure pulse, but if the noise can be estimated for this shape of impact, then the only difference that is to be considered in estimating noise due to combustion is the different frequency spectrum.

The engine is freely suspended and the impact is provided by a 50mm diameter steel sphere. The force pulse is measured by an accelerometer on the impacting sphere. The force-time history and the force derivative spectrum are shown in figures (6.10) and (6.11) respectively. The approximate level of the spectrum is again used to estimate the noise energy radiated from the engine.

The same value of the constant as in the first experiment applies and also the radiation efficiency does not change. The structural loss factor is also unaltered, since the engine is still fully assembled as in the first experiment. The loss factor values are not dependent on the position of any one of the pistons.

Therefore, the remaining parameter to be estimated or measured is the structure response term. In this case, the direct measurement of the response is not possible because the impact to the crankcase is internal. The vibrational energy is transferred from the top of the piston down to the con-rod, via the crankshaft to the crankcase where it is radiated as noise.

The structural response is estimated from measurements of the response of the different parts. It is assumed that the contact between the con-rod and the crankshaft, and the crankshaft and engine block are perfect; the contacts have been very well cleaned from grease and oil and also all the parts are bolted down to manufacturers specified torques. To estimate the response, a model which consists of three sections is considered (figure 6.12). The top section represents the piston and con-rod assembly; the middle section, the crankshaft; and the bottom section, the crankcase. Using mobility methods, the governing equations for the velocity and forces at different points on the model are given by:

$$V_2 = V_f + F_2 M_2 \tag{6.3}$$

$$V_2 = -F_2 M_{2'} - F_3 M_{2'3'} \tag{6.4}$$

$$V_3 = F_3 M_3 \tag{6.5}$$

$$V_3 = -F_3 M_{3'} - F_2 M_{2'3'} \tag{6.6}$$

$$V_1 = F M_1 + F_2 M_{21} \tag{6.7}$$

$$V_f = M_{12} F \tag{6.8}$$

and solving for V_1 and F_3 using these equations

$$\frac{V_1}{F} = M_1 - \frac{M_{21}\, M_{12}\, (M_3 + M_{3'})}{(M_2 + M_{2'})(M_3 + M_{3'}) - M_{2'3'}\, M_{3'2'}} \tag{6.9}$$

and the point response $H_1(f) = V_1(f)/\dot{F}(f)$

$$H_1(f) = \frac{1}{j\omega}\left[M_1 - \frac{M_{21}\, M_{12}\, (M_3 + M_{3'})}{(M_2 + M_{2'})\,(M_3 + M_{3'}) - M_{2'3'}\, M_{3'2'}} \right] \qquad (6.10)$$

The energy transferred from the crankshaft to the crankcase is given by

$$E(f) = \tfrac{1}{2}\, |\dot{F}_3(f)|^2\, \mathrm{Im}\,[H_3(f)] \qquad (6.11)$$

$$= \tfrac{1}{2}\, |\dot{F}(f)|^2\, \mathrm{Im}\,[H(f)] \qquad (6.12)$$

i.e. the structure response term used in the energy accountancy equation is given by

$$\mathrm{Im}\,[H(f)] = \frac{|M_{12}\, M_{2'3'}|^2}{|(M_2 + M_{2'})\,(M_3 + M_{3'}) - M_{2'3'}\, M_{3'2'}|^2}\ \mathrm{Im}\left[\frac{M_3}{j\omega}\right] \qquad (6.13)$$

where M_{12} is the transfer mobility between piston top and big end of con-rod ;

M_1 is the point mobility at top of piston con-rod assembly;

$M_{2'3'}$ is the transfer mobility from crankpin (where big end connects) to crankshaft journal ;

$M_{2'}$ is the point mobility at crackpin on crankshaft ;

M_2 is the point mobility at big-end of con-rod ;

$M_{3'}$ is the point mobility at crankshaft journal ;

M_3 is the point mobility at bearing on engine frame.

The measured values of these mobilities are shown in figure (6.13).

These measurements were done by using a force calibrated hammer and an accelerometer placed very close to the point of impact. The calculated response, equation (6.10), at the top of the piston when assembled is compared to the measured response (figure 6.14). The agreement between the two curves is reasonable, when considering the low levels of response and the number of computations involved. At some points, the level of accuracy of the computer was not enough to handle the large extremes of numbers being manipulated. Using equation (6.13), a curve for Im $[H(f)]$ is computed (figure 6.15). It is impossible to obtain the low frequency response because of the high noise to signal ratio at these low frequencies. Therefore, the level at low frequencies is calculated using the same technique as in section II. 3. The first resonance frequency of the block is about 650 Hz. This gives the same low frequency level as the response on the side of the engine. The response over all frequencies is verified using the alternative method described in section III. 2.

From the measurements of the response of the different engine parts, a model can be built up, which can be used to investigate modifications on the engine structure to obtain an overall lower response. The piston / con-rod assembly response (figure 6.13 (a)) is the same as that of a two mass system connected by a damped spring (figure 6.16). From the values of the resonance frequency, the anti-resonance frequency and the shape of the curve, the stiffness and loss factor of the spring can be estimated. In this case, for this particular engine, the loss factor is approximately 0.12 and the stiffness is 2.04×10^8 N/m. This is of the same order of magnitude as the static stiffness of the con-rod when considering an average cross-sectional area. Similarly, the response of the crankshaft is identical to that of a beam in flexure and an average thickness, width and length can be evaluated from the level of the curve and the first resonance frequency.

Another method to measure the response is to measure the spatial average velocity squared on the engine surface. The point response is related to the spatial averaged surface admittance (see section III.2)

and is given by

$$\text{Im}\ [H(f)] = \eta_s m \frac{\langle V^2 \rangle}{F^2} \qquad (6.14)$$

To measure the spatial averaged admittance, the piston is excited on the top when at top dead centre and the vibration level measured by an accelerometer fixed at different positions on the engine block surface. The response curve using this method is shown in figure (6.17), which also includes the mean level. The first resonance frequency is about 650 Hz. However, this method for measuring the response does not give any information on the energy flow path, and therefore no possible modifications can be deduced from this measurement.

The noise radiated from the engine is measured by an array of nine microphones in one-third octave frequency bands, and compared to the noise energy estimate using the energy accountancy equation (figure 6.18). There is good agreement betwen the measured and the estimated results. However, the agreement in the results depends very much on the interpretation of the structure response curves. At low frequencies, the acceleration noise from the impactor dominates the noise measured.

VI. 3.3. Piston Slap Noise

A similar investigation to estimate the noise radiated due to piston slap excitation is done using the energy accountancy concept. To increase piston slap noise on the test engine, the piston rings are removed to increase the clearance between piston and cylinder. The piston is moved from side to side by means of a shaker, applying a force at the gudgeon pin end of a second connecting rod which is fixed back to back to the con-rod attached to the piston (figure 6.19). All other bearings are well packed with grease to eliminate other backlash.

The force applied by the shaker is approximately the same as the force acting on the piston because of the symmetry of the two con-rods. The input signal to the shaker is in the form of a sawtooth which is very similar to the reaction force acting on the piston for a running engine [35], the frequency of the input signal being 12 Hz corresponding to a typical engine running speed of about 1600 r.p.m. (twice the speed, assuming a four stroke engine). When the piston moves from one side to the other, this does not result in a single impact but a series of impacts. Figure (6.20) shows the output signal from the force transducer, as compared to the input signal into the shaker (top trace).

Two accelerometers are attached on the inside surface of the piston. The output from these accelerometers contain both the bodily accelerations and the ringing of the pistons. If the low frequency content of this signal is filtered out, it can be seen that the two signals are completely out of phase, which show that the piston is moving from side to side, impacting the cylinder wall. One of the accelerometer signals together with a more detailed curve for the output from the force transducer are shown in figure (6.21).

To estimate the noise using equation (1.4), all the terms except the force derivative spectrum and the structure response remain the same. By considering the output from the force transducer, taking first one impact and then weighing the spectrum to account for the multiple impacts, the force derivative spectrum is obtained (figure 6.22). In weighing this spectrum for the multiple impacts, it is assumed that each impact can be considered seperately and energy escapes into the engine structure at each impact.

It is impossible to obtain an estimate for the structure response without a detailed model of the engine structure, because of the complex way in which the cylinder liner is attached to the cylinder block and crankcase. Thus an estimate for the response is obtained from the spatial averaged admittance (figure 6.23). Although this method does not give any information on the energy flow path, there is only one way that the energy can flow, i.e., from the liner via the upper and lower water decks to the engine crankcase. This is

because the only excitation is between the piston and cylinder.

The noise energy radiated is measured by an array of microphones and the measured noise in one-third octave frequency bands is compared to the estimated levels (figure 6.24). The agreement between the measured and estimated results is good to within ±3 dB. At low frequencies, the noise from the engine structure is masked by the acceleration noise from the shaker table, which moves with a similar acceleration pattern as the signal from the force transducer. This is why in figure (6.24) there is a very high level of low frequency noise when the first resonance frequency of the engine structure is about 600 Hz.

VI. 4. Design Considerations

From the results of this investigation, both combustion and piston slap noise can be related to different parameters of the engine structure. One of the parameters which can give large noise reductions if modified, is the structural response, like in the case of the blocking mass in chapter V. Therefore, a method to tackle engine noise would be to look for a way to lower the structural response i.e., to restrict the flow of vibrational energy.

In the case of combustion noise, the vibrational energy in this engine type travelled from the piston top via the con-rod and crankshaft to the crankcase. Therefore, to reduce the structural response, one can consider a radically new design for the shape of the con-rod. Tests were done on the response of a con-rod and compared to the responses of two other identical con-rods, but made of different materials; one of mild steel and the other of aluminium. From the results, (figure 6.25), it can be observed that the point response at the piston top and the transfer response between piston top and big-end, hardly change at all and therefore, it is not surprising that when tested on a running engine, the level of vibration of the crankcase did not vary. This shows that to get any results, more radical changes are needed in a new design of a con-rod.

Another method would be to use laminated bearing rings as suggested by Lyon [28] . In this case, the bearing rings are made with a resilient layer in between two layers of aluminium, to reflect some of the vibrational energy due to the structure change. In the model of the engine, (figure 6.12), a new spring mechanism is introduced between the beam and support, which will result in a lower response. To lower the response of the bearings, more massive main bearing stands can be used. However, this may involve some weight penalty which can be offset by reducing the weight of other non-stress bearing sections, since now the level of vibration will be lower.

In the case of piston slap noise, one way to reduce vibrational energy would be to isolate the cylinder liner from the engine structure. However, there are some problems here which have to be solved like the high temperatures involved and the contact with the engine head. These problems can be eliminated by new design of the engine block to house the cylinders. Alternatively, piston slap noise can be reduced by increasing the contact duration of the impact, that is, parts of the piston or cylinder are made of a softer material which is not heat affected to alter the clearance. Some design ideas for piston slap noise control are shown in figure (6.26).

Other structural modifications can be investigated and a technique which is very useful to develop structural modifications is to optimise the response of the engine structure when statically loaded and then apply these results for optimisation of the dynamic situation [33] . The use of static results is justified for small and medium sized engines because at low frequencies, lower than the fundamental frequency, the response of the structure is directly related to the static response. For small and medium sized engines, the fundamental ringing frequency occurs at mid and high frequencies and the combustion pressure pulse contains a large low frequency content, making the static response an important parameter.

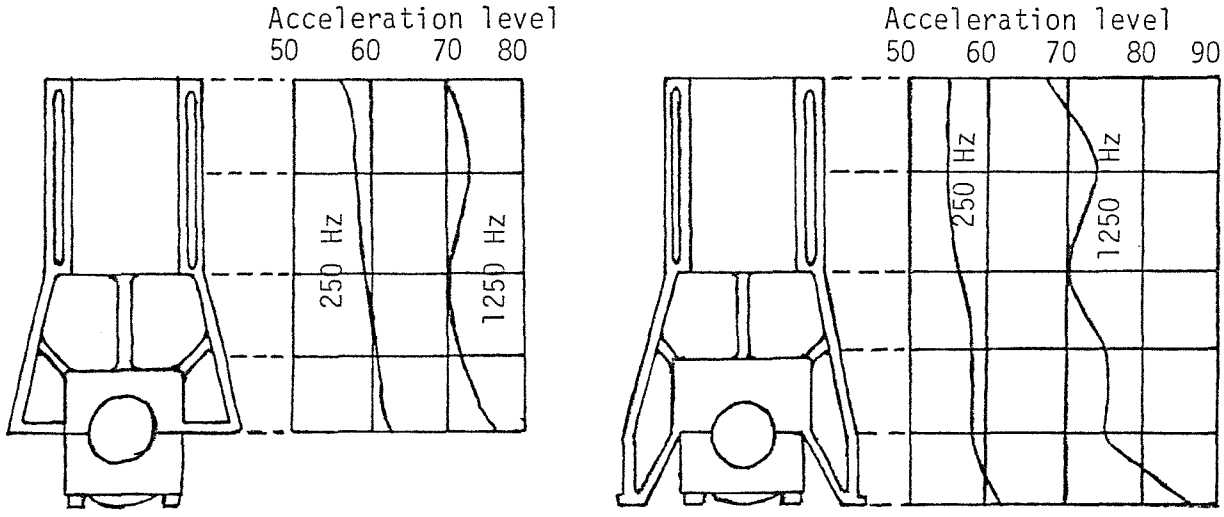

(i) Underslung crankshaft crankcase

(ii) Skirted crankcase

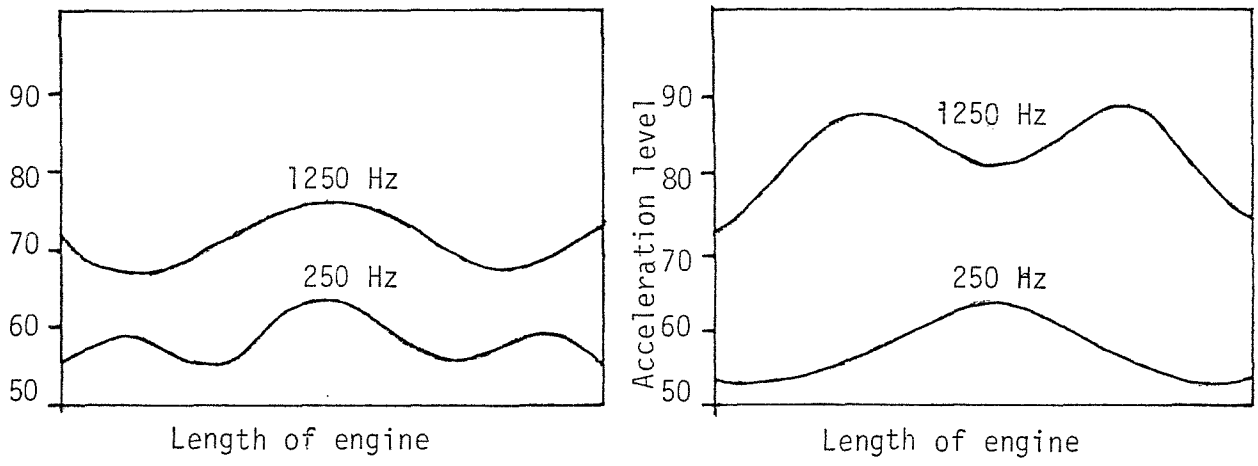

figure 6.1. Vibration levels of different types of crankcase, (i) underslung crankshaft; (ii) skirted. (Source ref.: 34).

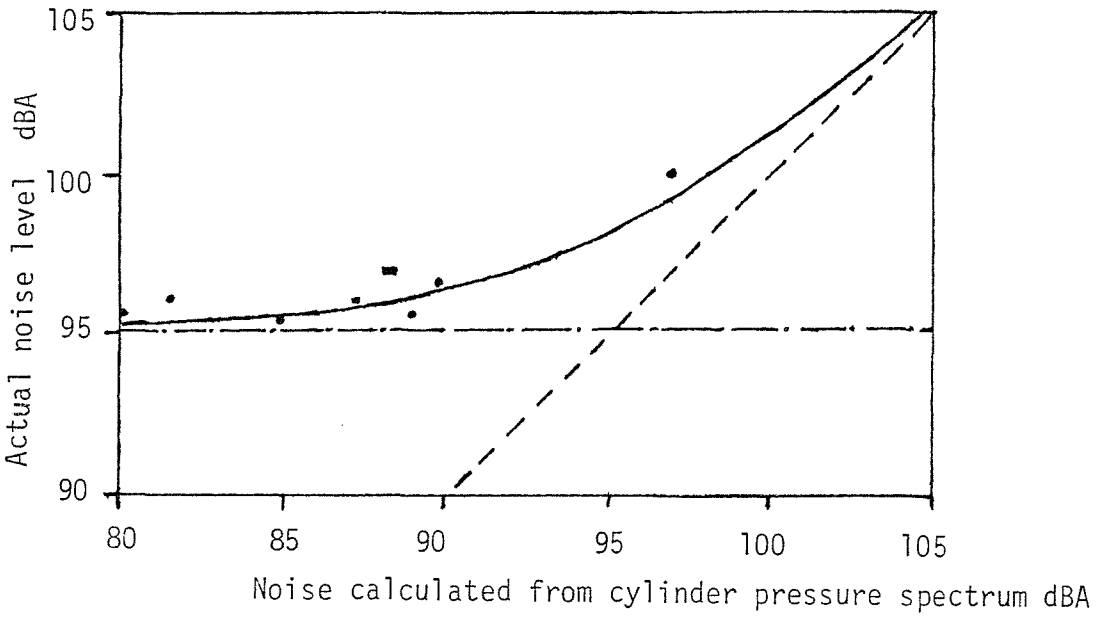

figure 6.2. Total noise due to combustion and mechanical impacts. -----, combustion noise only; — · —, mechanical noise only; ———, total noise = combustion + mechanical.
(source ref. : 32) .

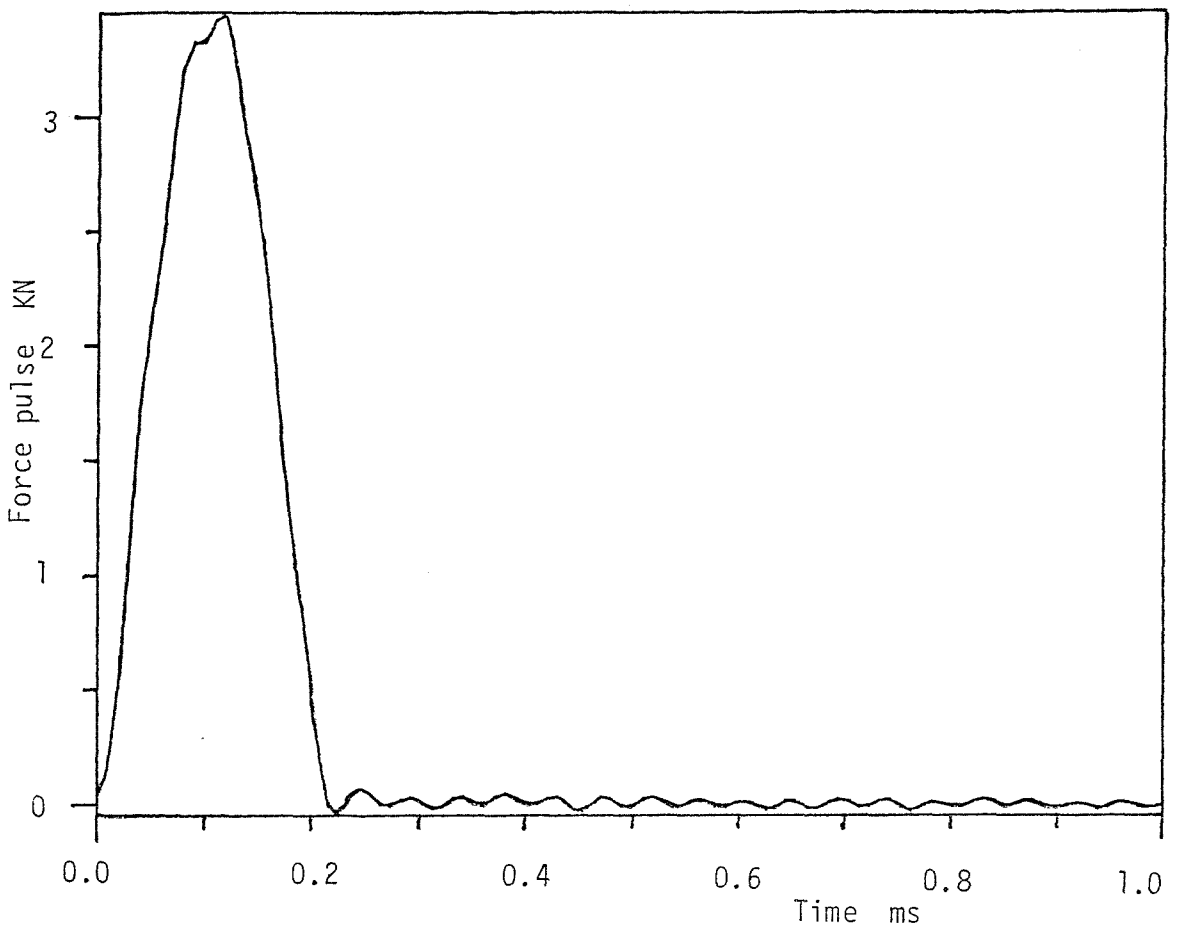

figure 6.3. Force-time history of excitation force on side of engine.

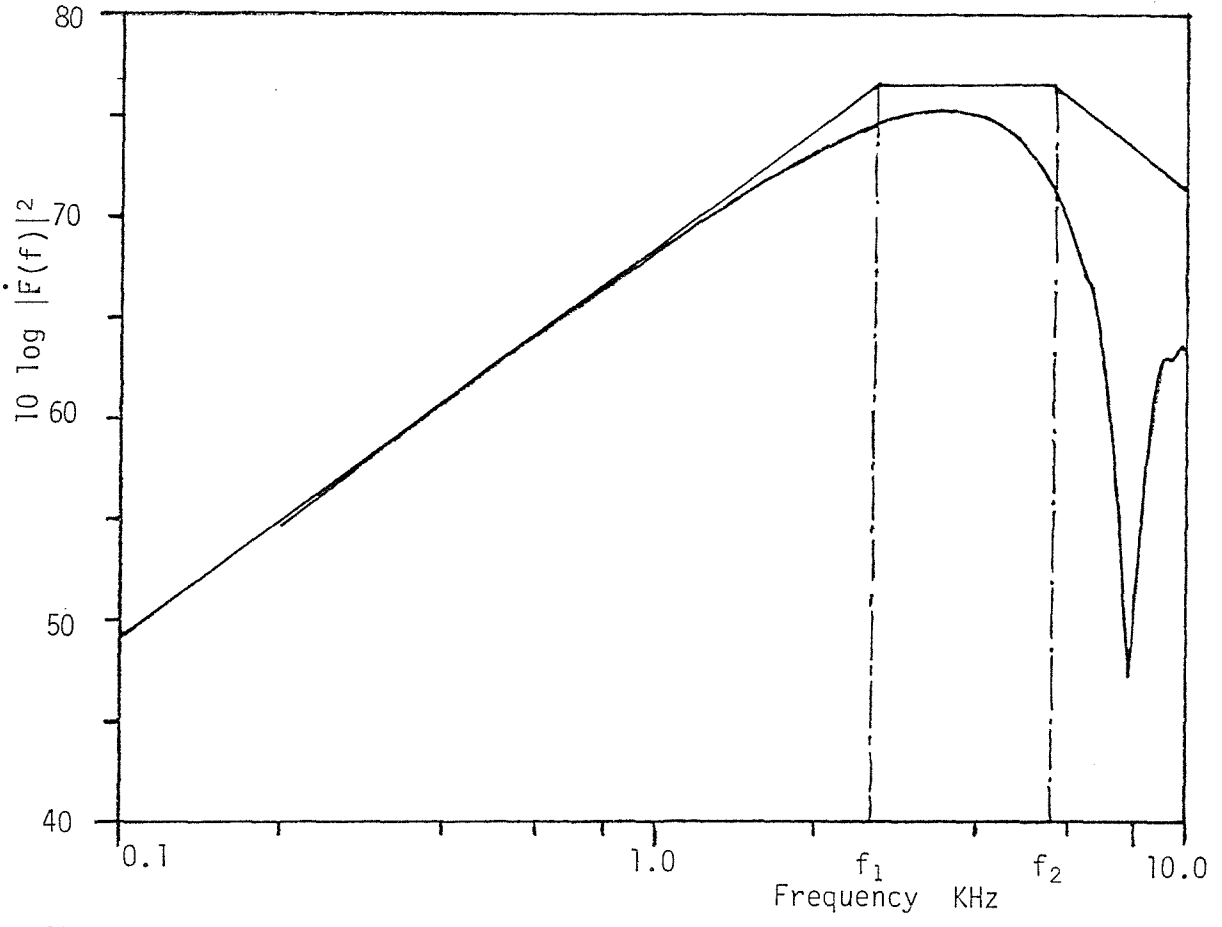

figure 6.4. Force derivative spectrum for force on engine side.

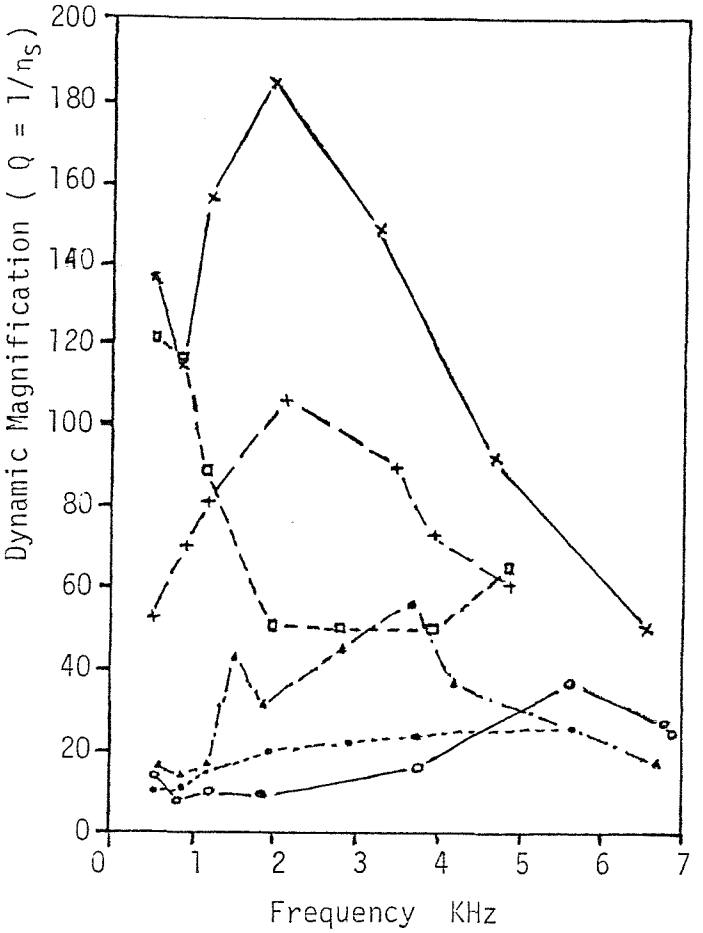

figure 6.5. Structural damping for a typical small diesel engine.

x — x, Bare crankcase; o — o, complete engine. Parts assembled to crankcase: □ — □, cylinder head only; + -- + sump only; ▲— · —▲, crankshaft only; ●---●, crankshaft, pistons and connecting rods.

(Source ref. : 31).

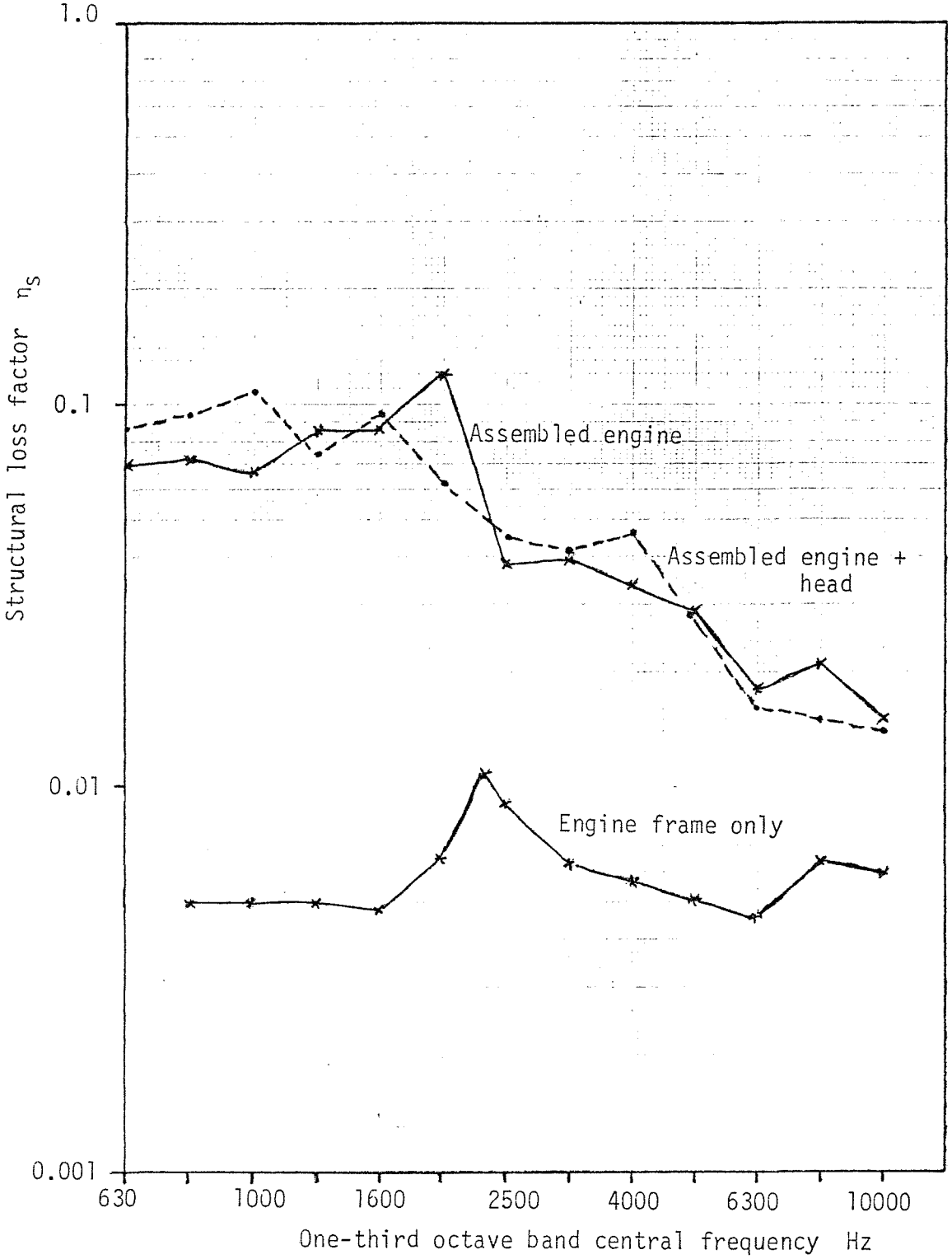

figure 6.6. Structural loss factor for engine under test.

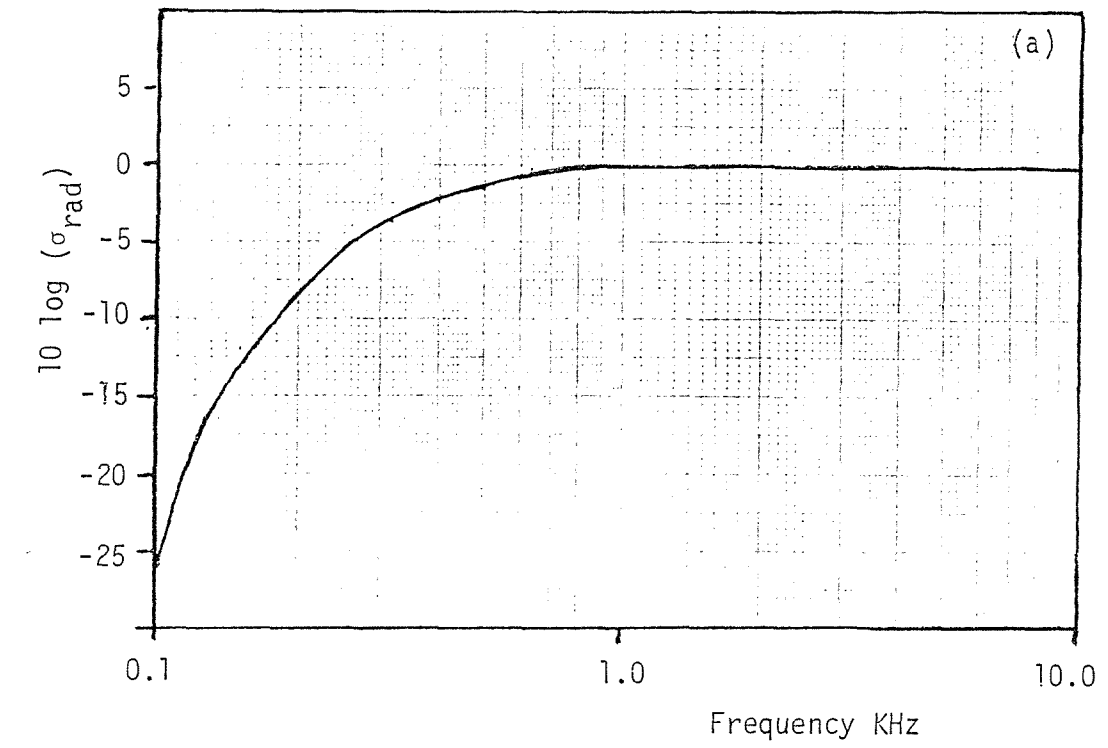

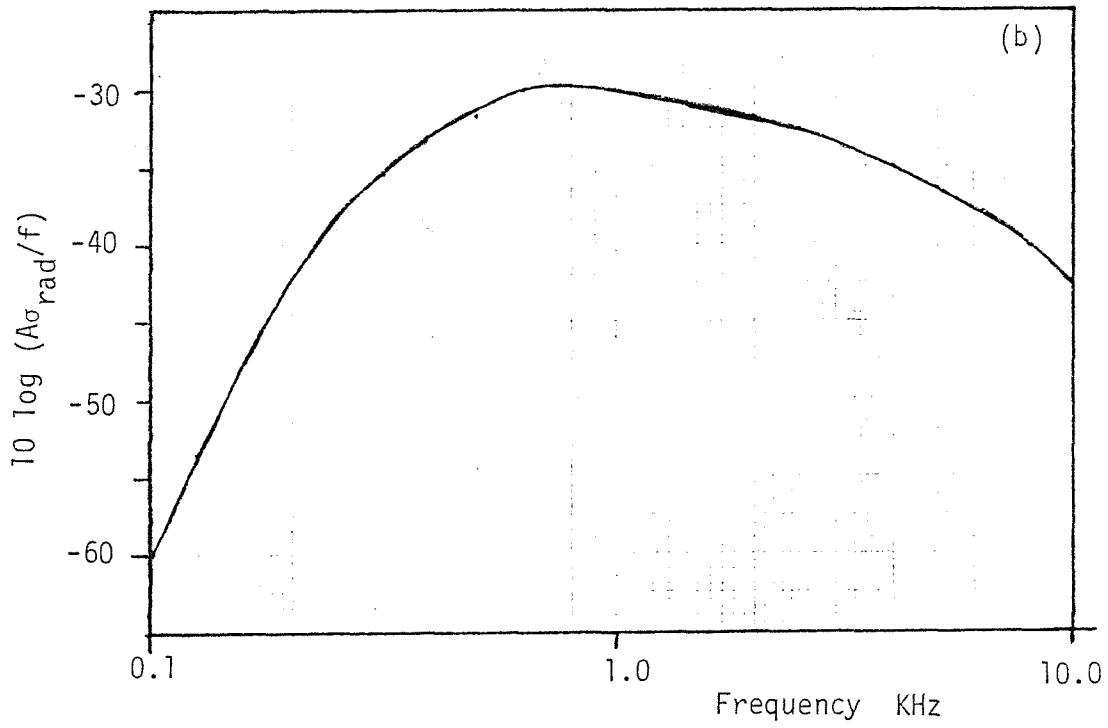

figure 6.7. Radiation efficiency curves for a rod in flexure dia. 200 mm. (a) 10 log (σ_{rad}); (b) 10 log ($A\sigma_{rad}/f$).

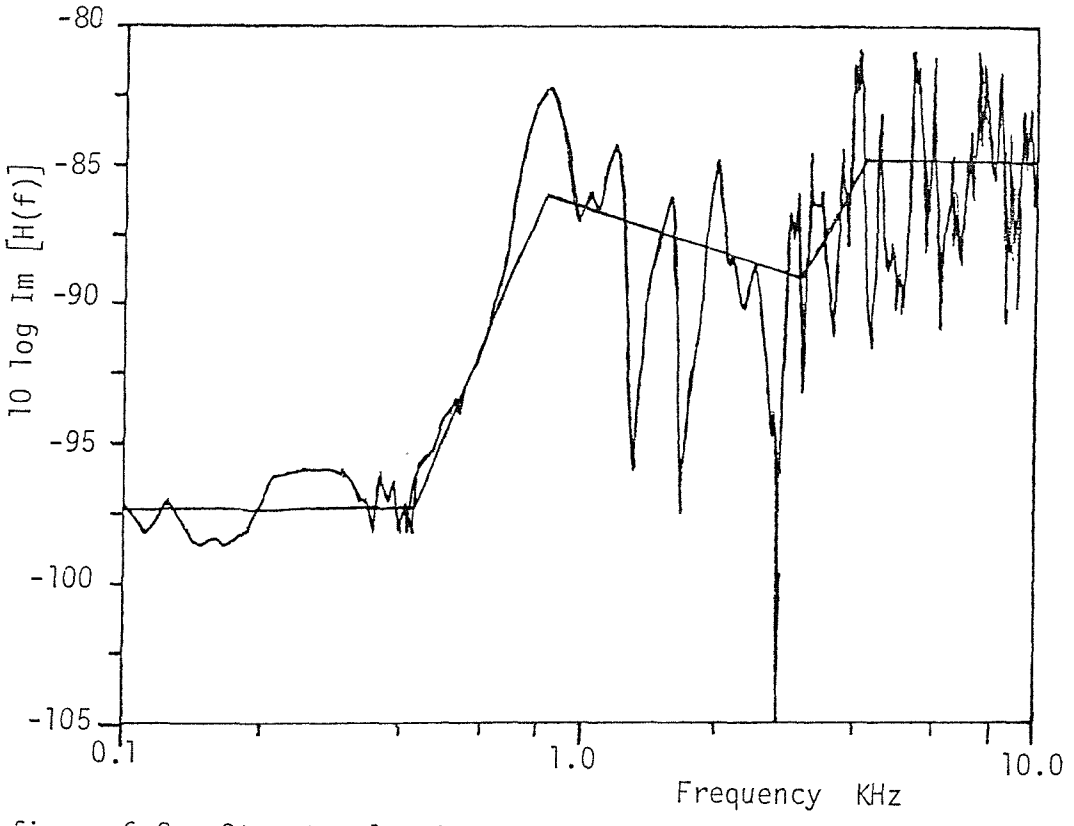

figure 6.8. Structural point response on side of engine frame.

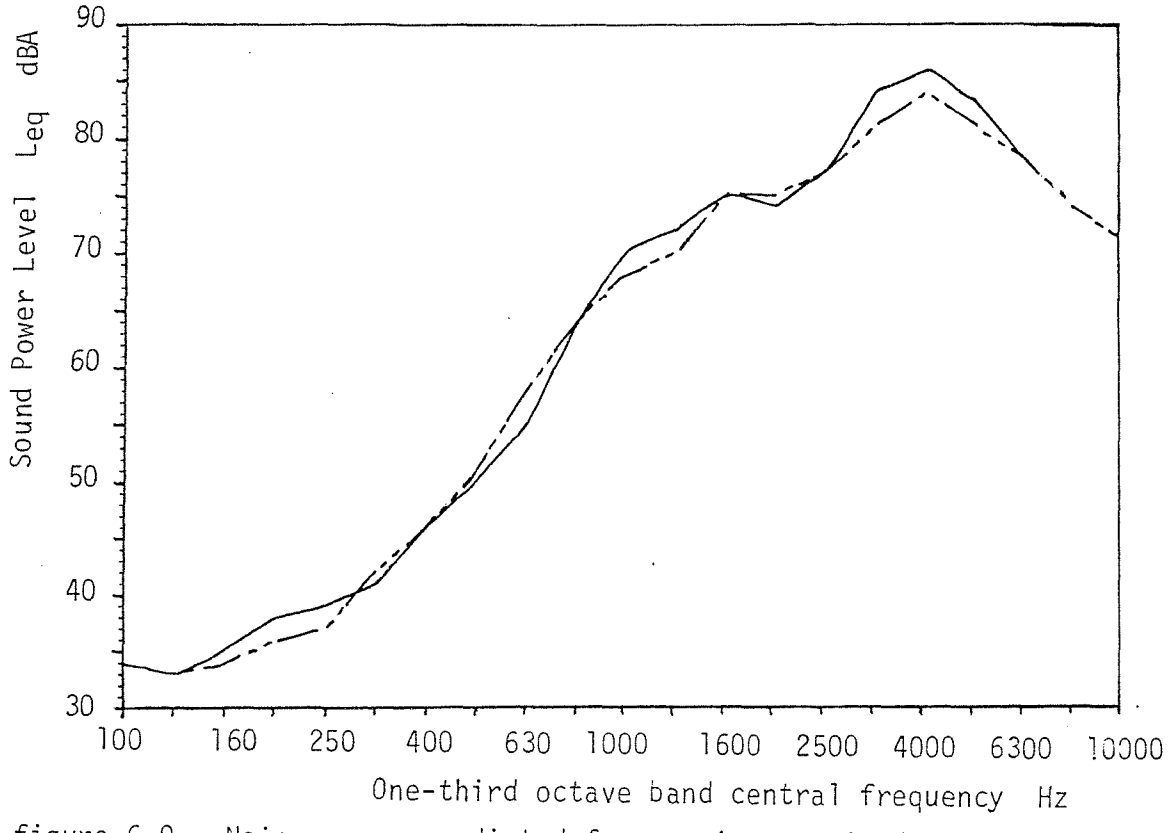

figure 6.9. Noise energy radiated from engine, excited on the side.
———, Measured; —— ·· —, estimated.

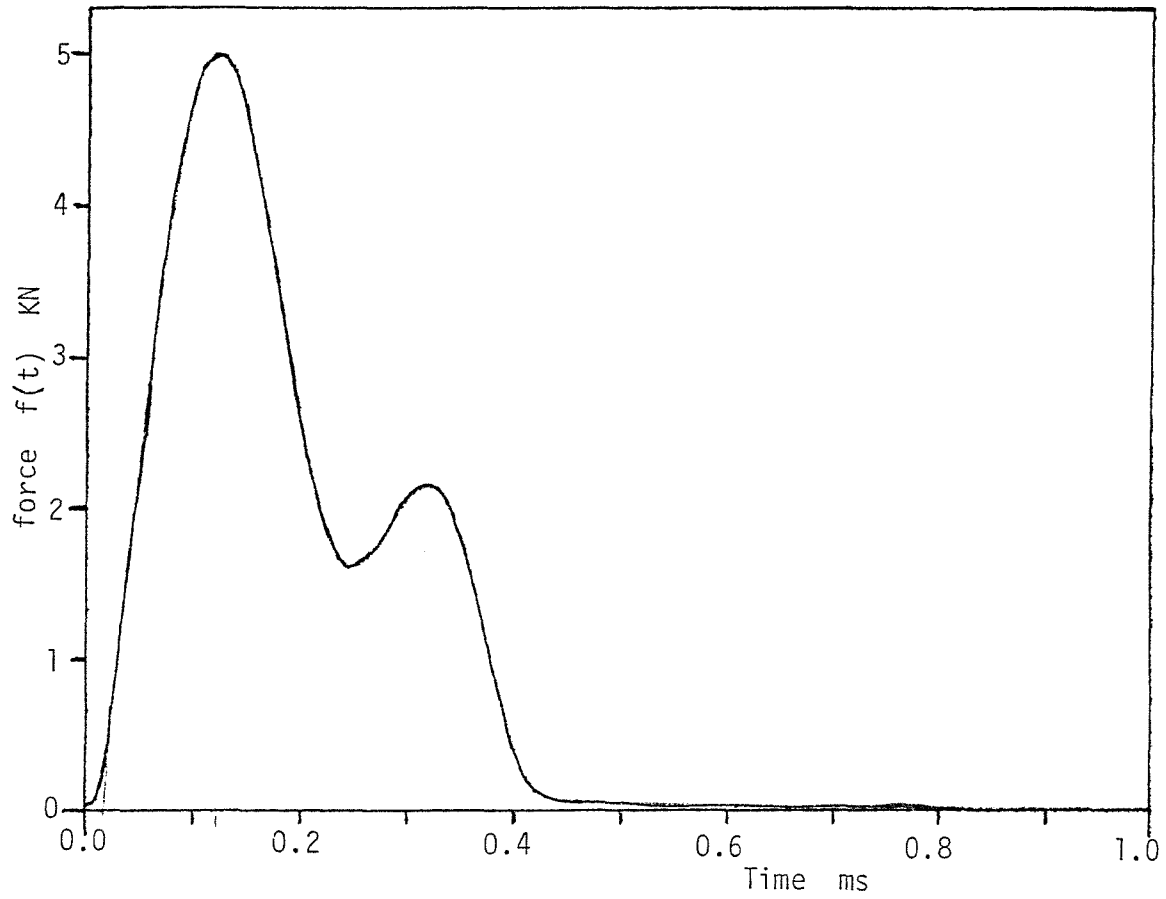

figure 6.10. Force-time history in simulated combustion excitation.

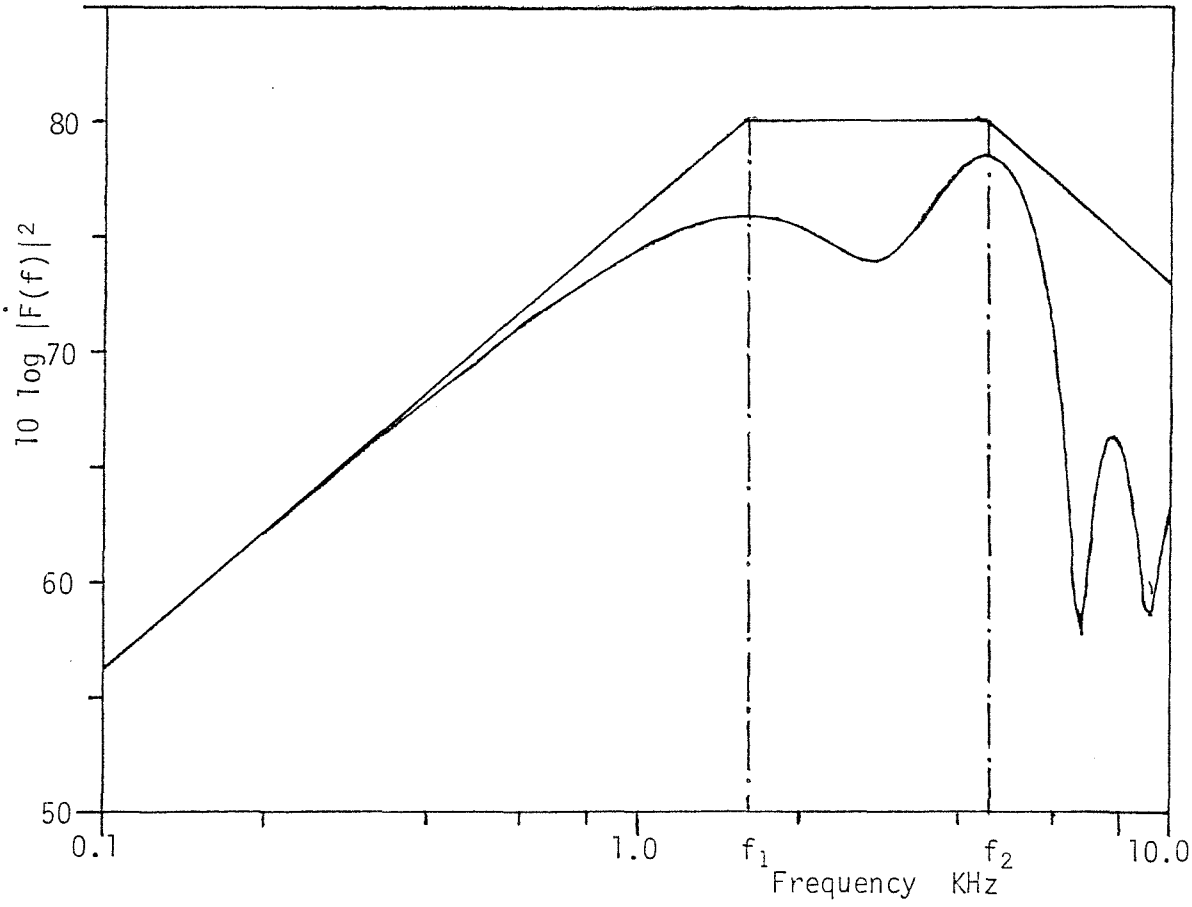

figure 6.11. Force derivative spectrum for excitation on piston top.

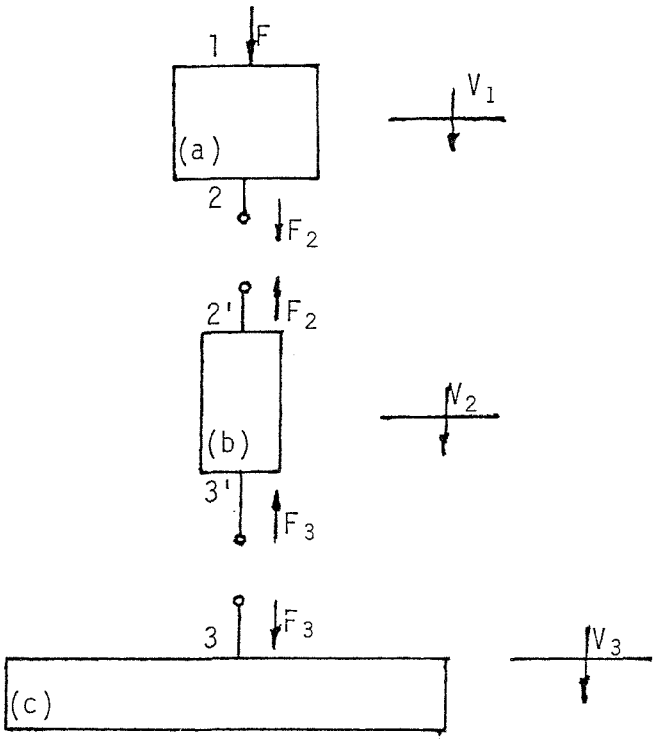

figure 6.12. Model to estimate response from measurements of the response at points on the engine frame and accessories. (a) Piston / con-rod assembly; (b) crankshaft; (c) engine frame.

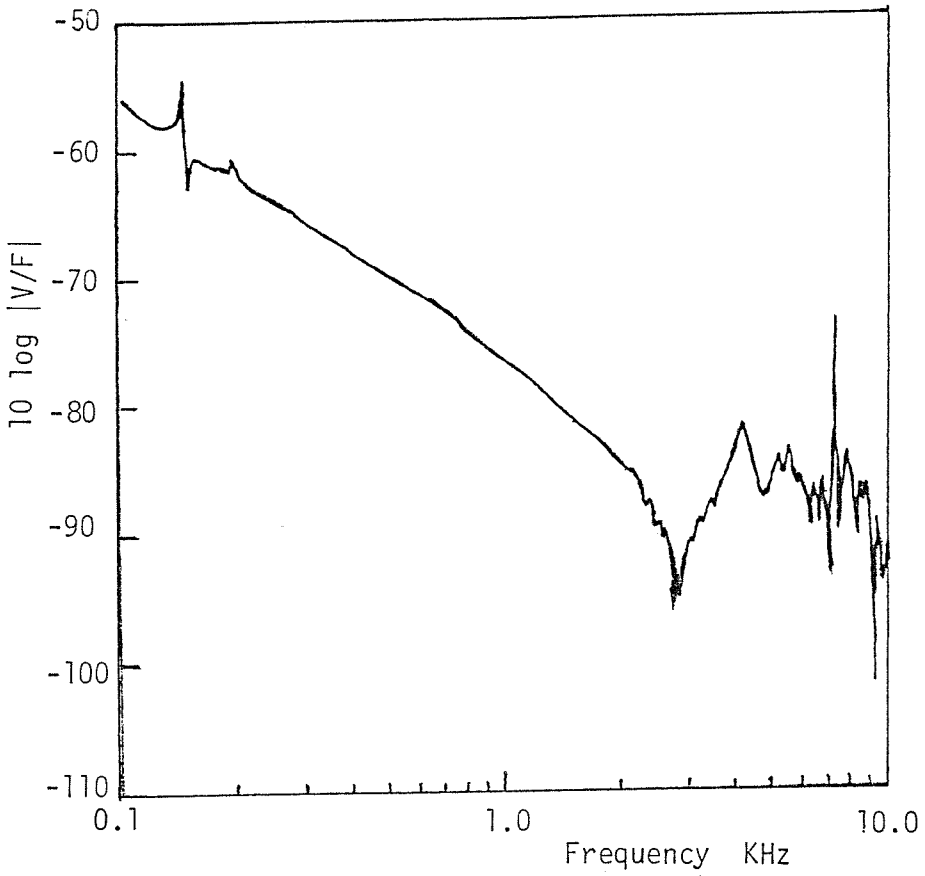

figure 6.13(a). M_2 : point response at big end on con-rod.

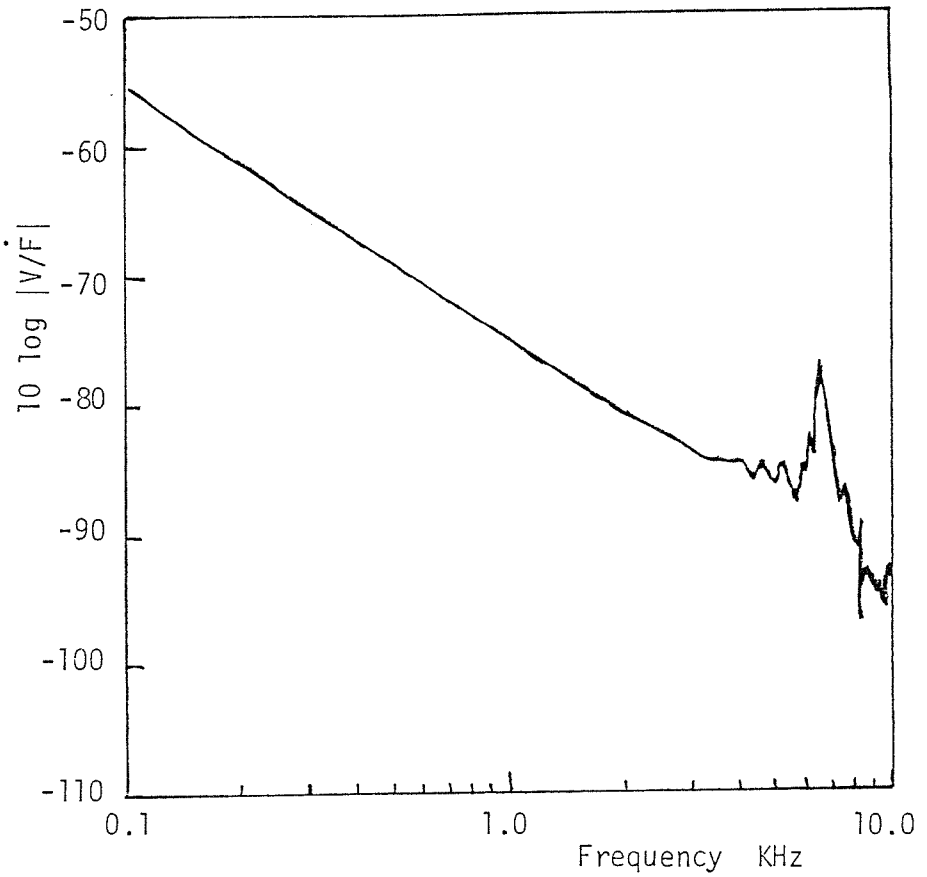

figure 6.13(b). M_{12} : transfer response between piston top and big-end on con-rod.

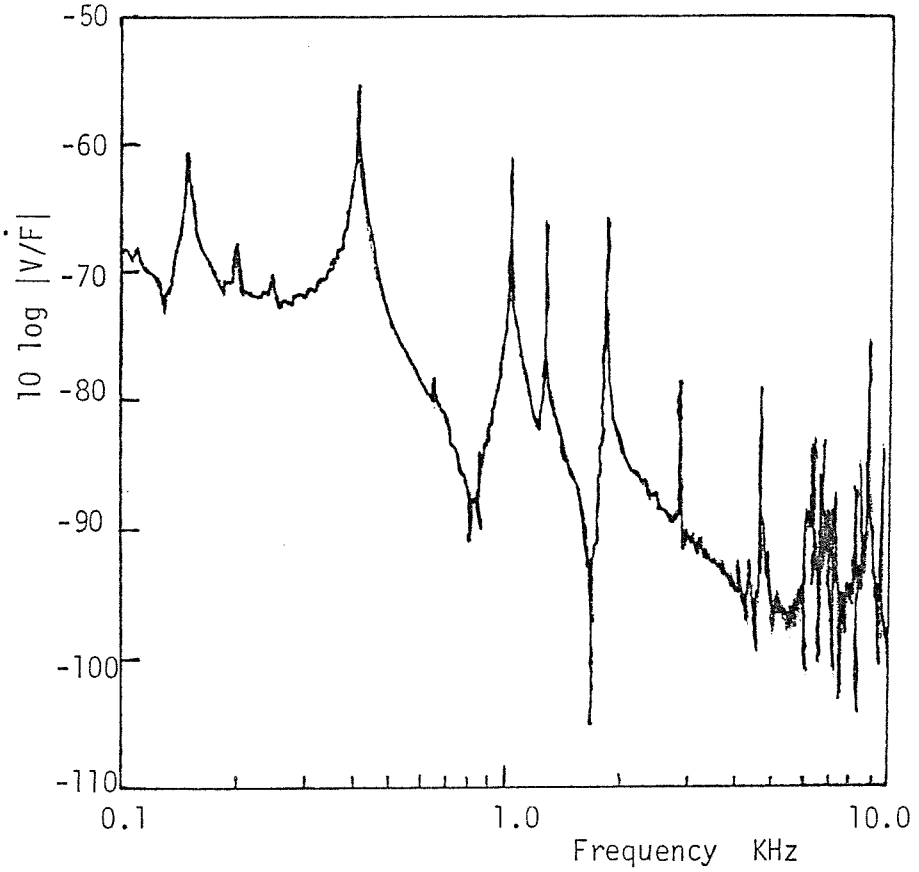

figure 6.13(c). $M_{2'}$: point response at crankpin on crankshaft.

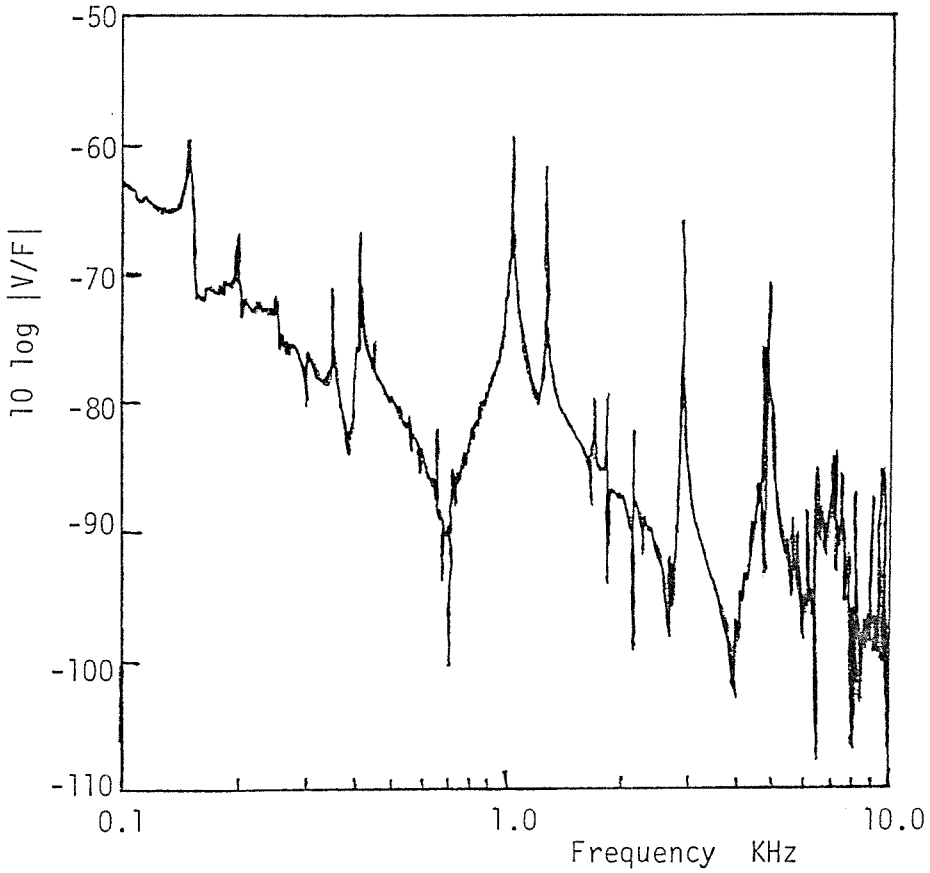

figure 6.13(d). $M_{3'}$: point response on crankshaft journal.

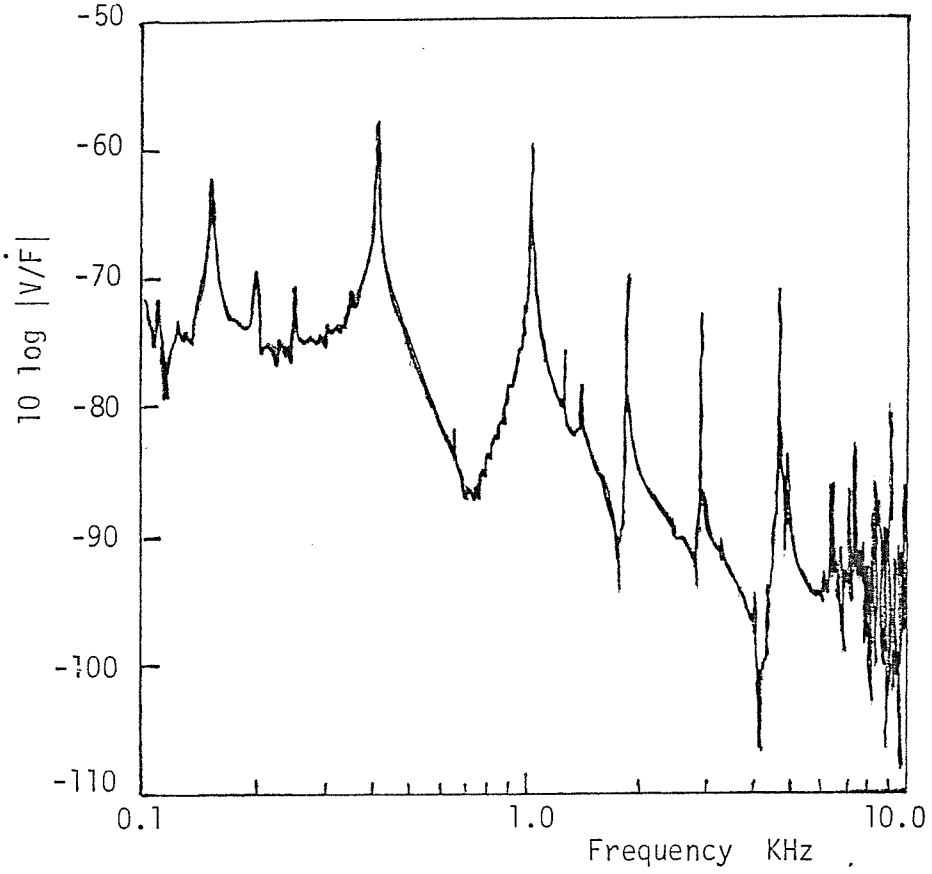

figure 6.13(e). $M_{2'3'}$: transfer response from crankpin (where big-end connects) to crankshaft journal.

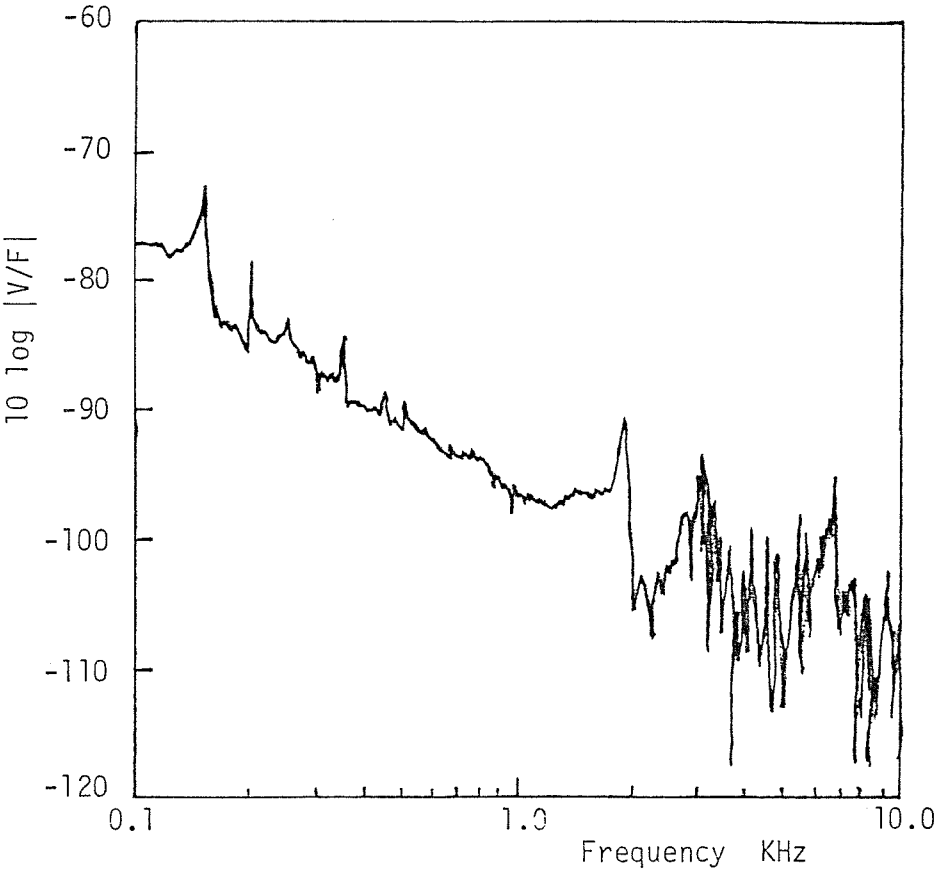

figure 6.13(f). M_3 : Point response at bearing on engine frame.

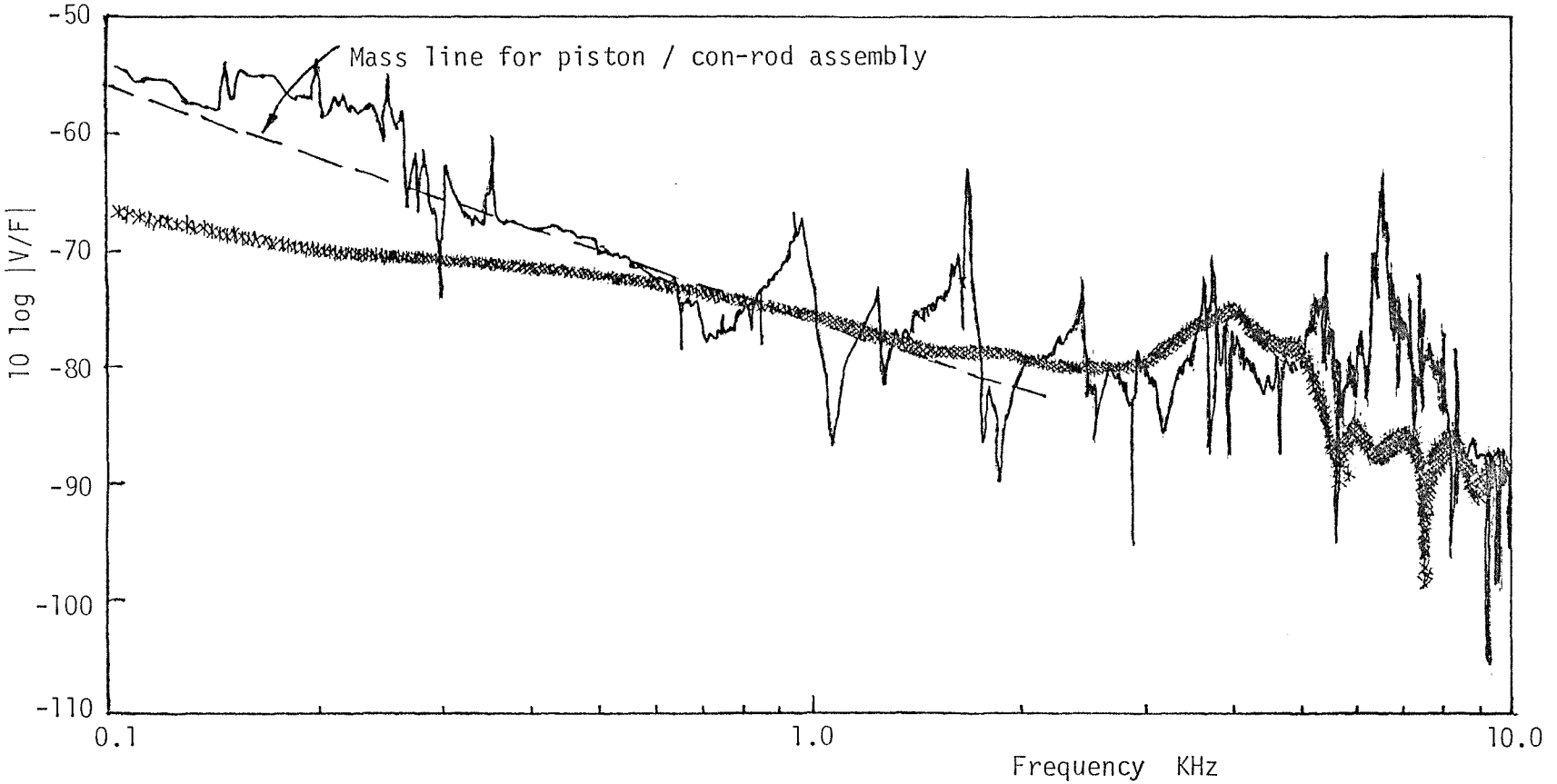

figure 6.14. Comparison between measured and estimated point response on piston top, with piston at T.D.C. ———, Estimated; *****, measured.

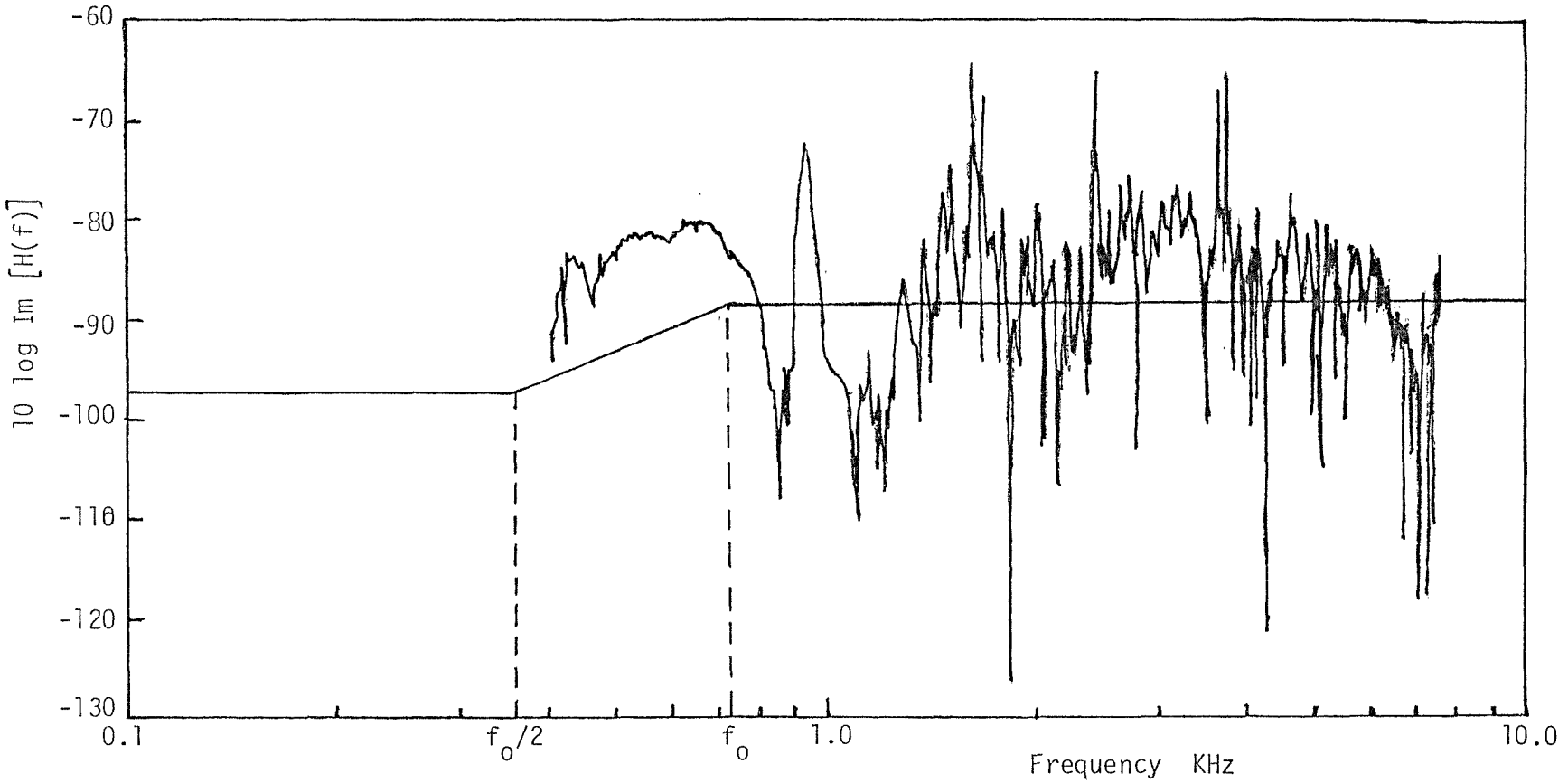

figure 6.15. Point response term estimated using equation (6.13).

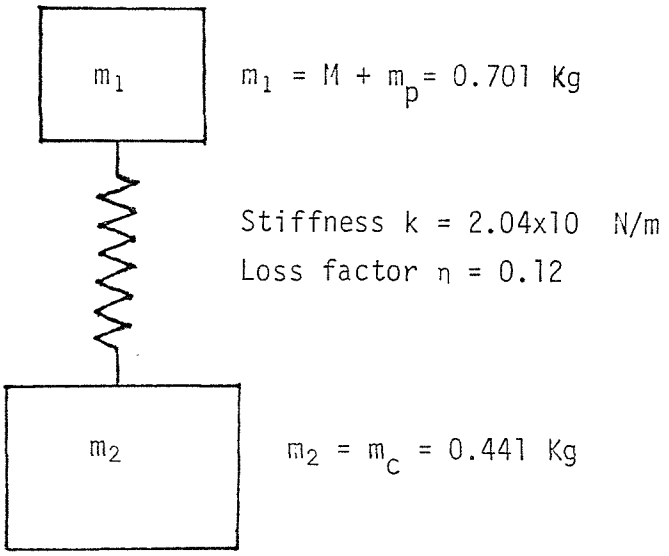

figure 6.16. Mass-spring-mass model for piston and con-rod assembly. M is the piston + gudgeon pin mass; m_p is the mass of con-rod at gudgeon pin; m_c is the mass of con-rod at big end.

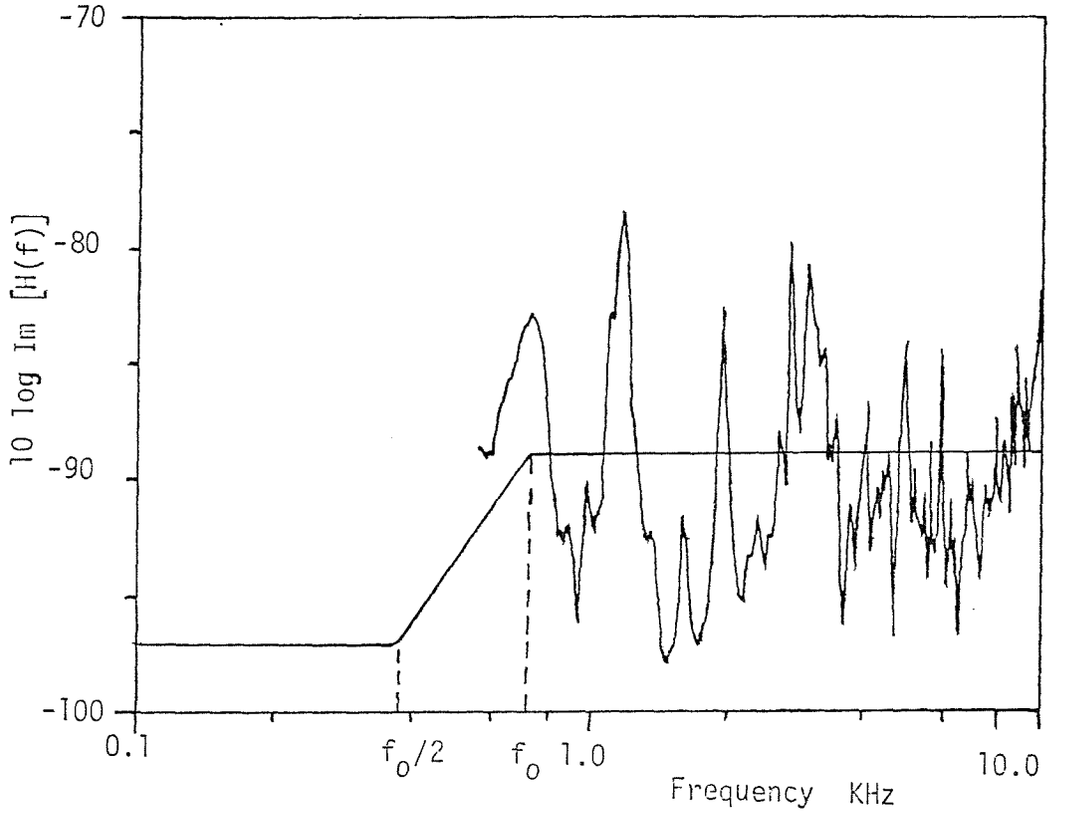

figure 6.17. Point response calculated from the spatial averaged admittance.

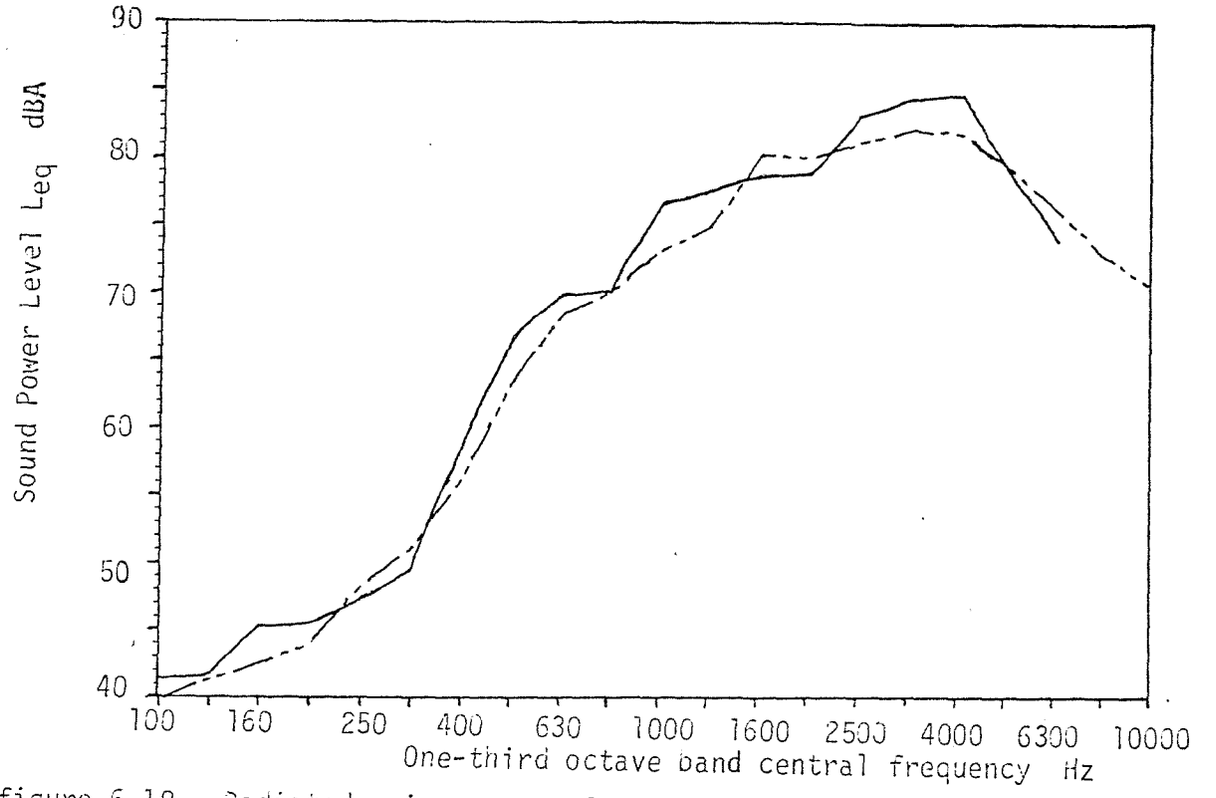

figure 6.18. Radiated noise energy from engine frame under simulated combustion. ——, Measured; —— .. —, estimated.

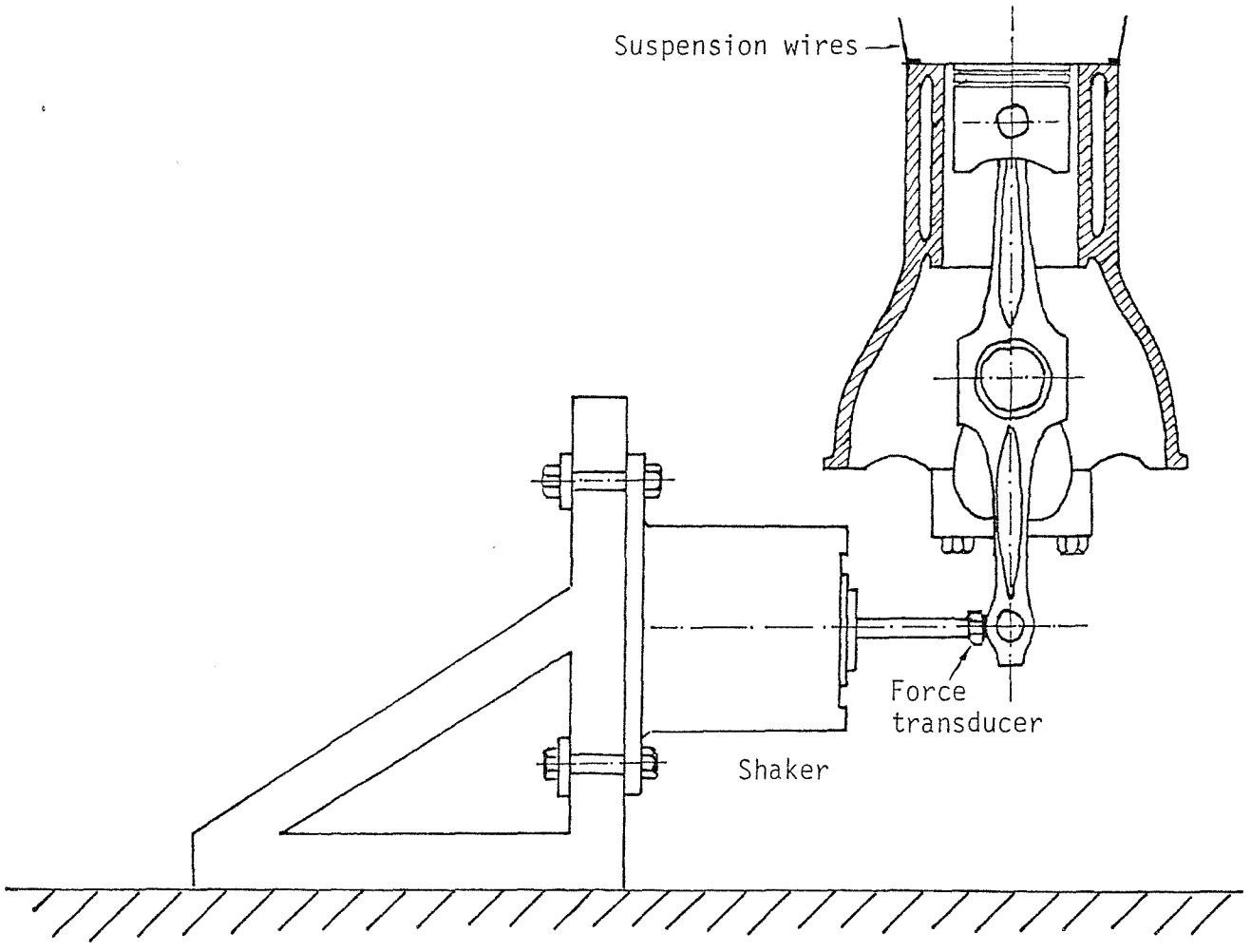

figure 6.19. Set-up to simulate piston slap.

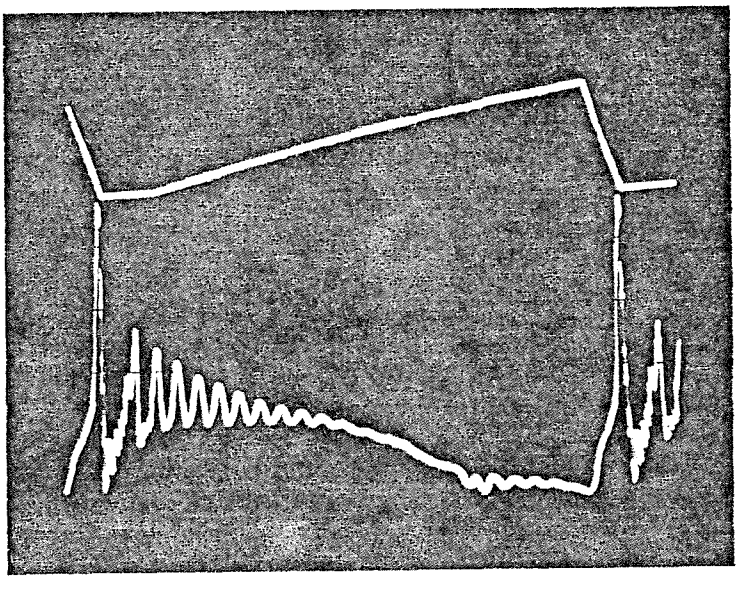

figure 6.20. Time history for (i) input to shaker; (ii) output of force transducer at bottom end of con-rod.

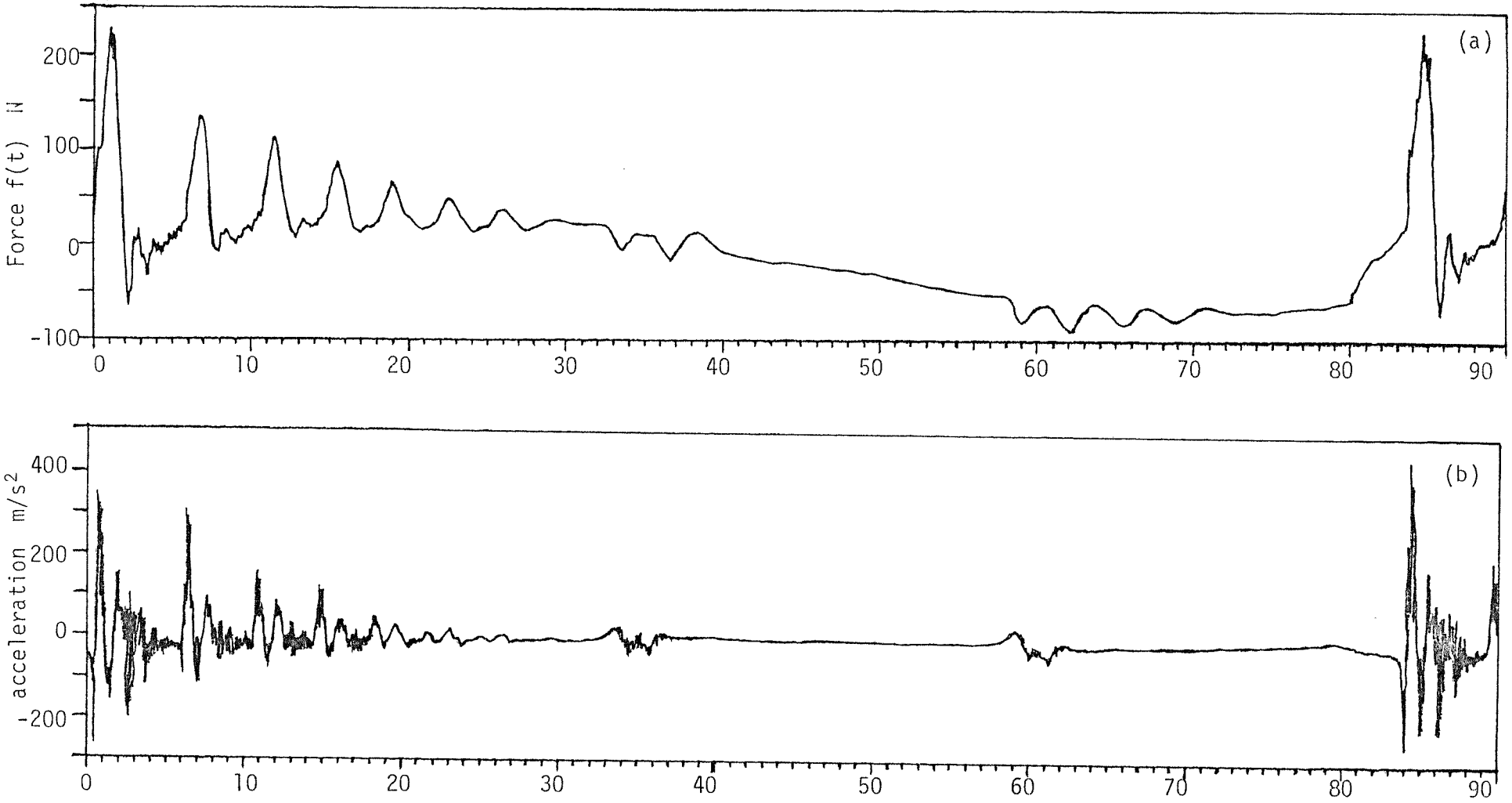

figure 6.21. Simulation of piston slap. (a) force-time history;(b) piston sideways acceleration.

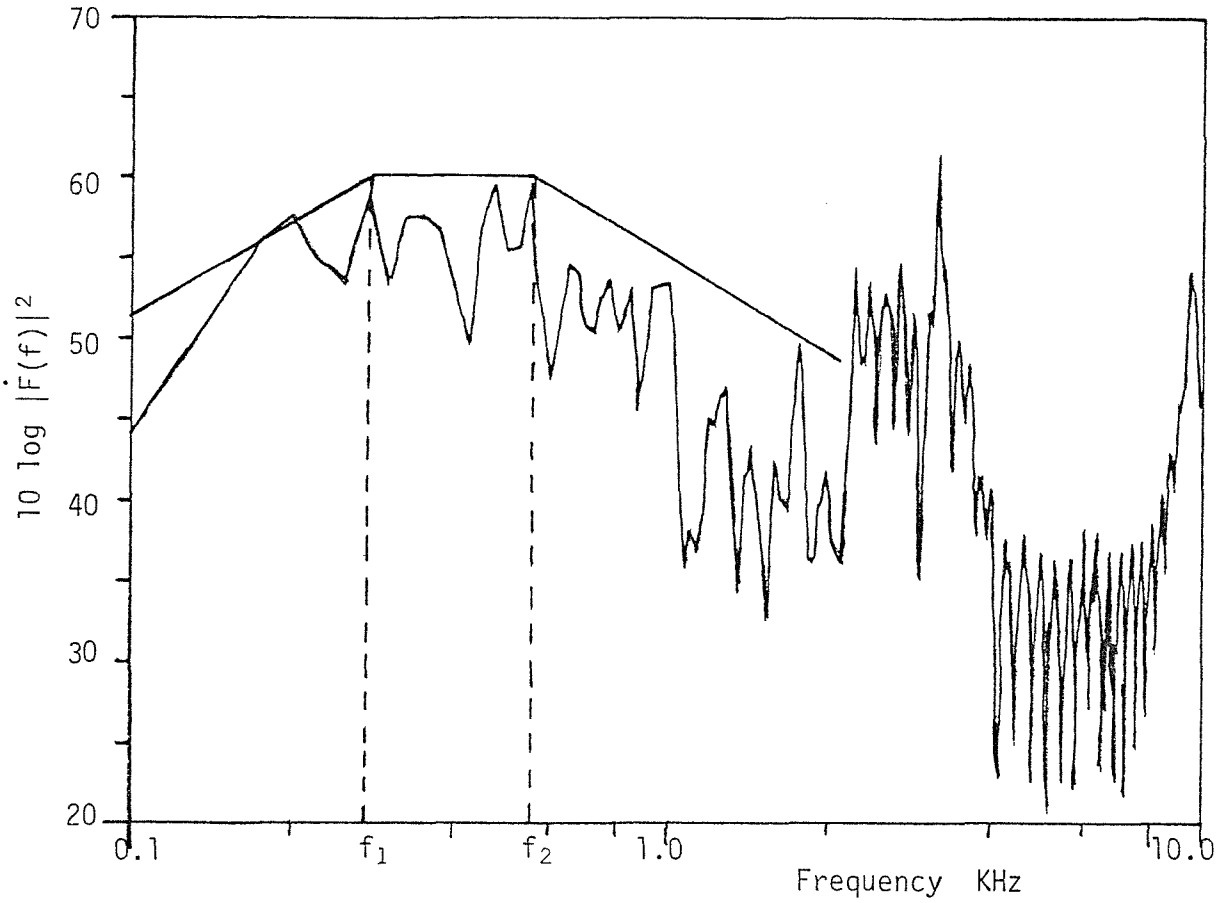

figure 6.22. Force derivative spectrum in piston slap simulation.

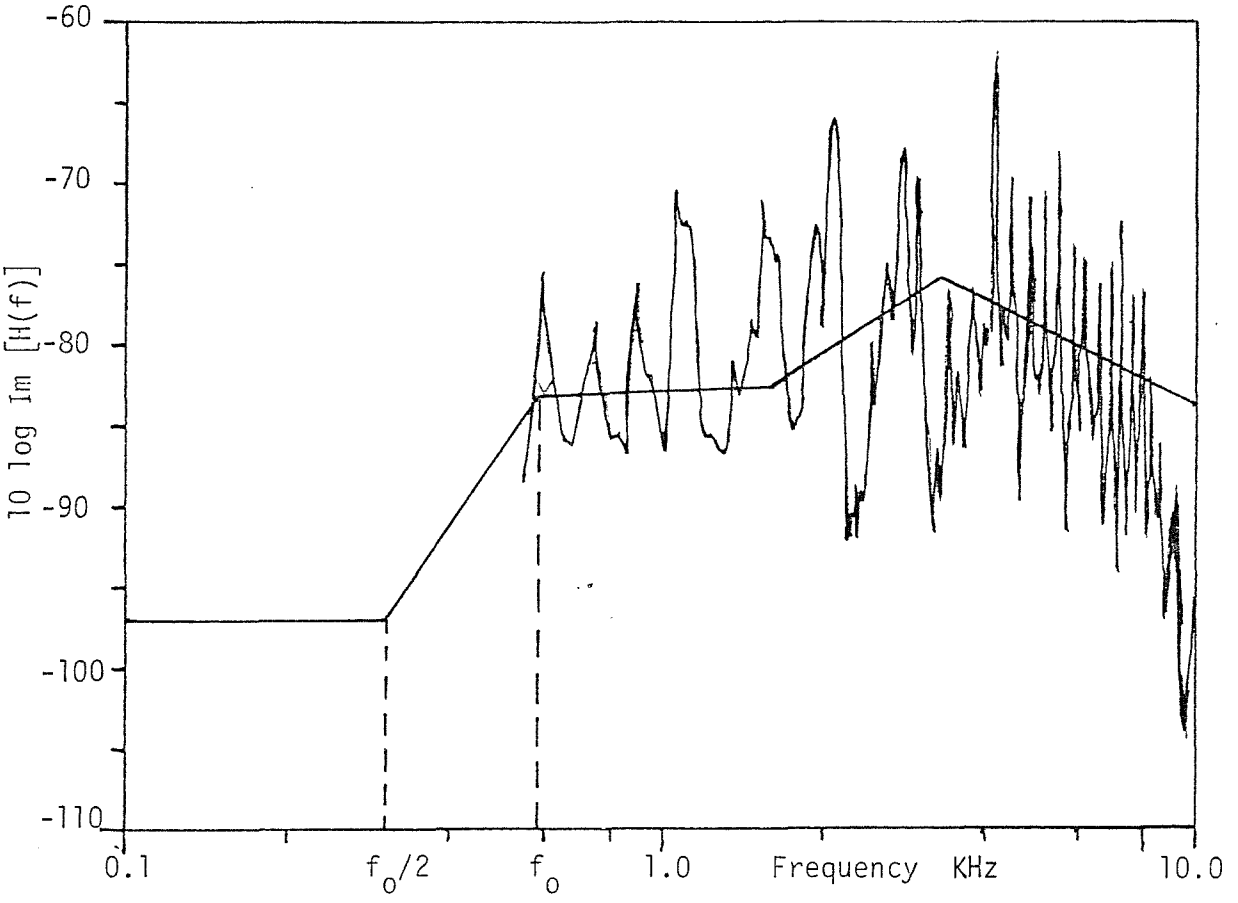

figure 6.23. Response term calculated from spatial average admittance.

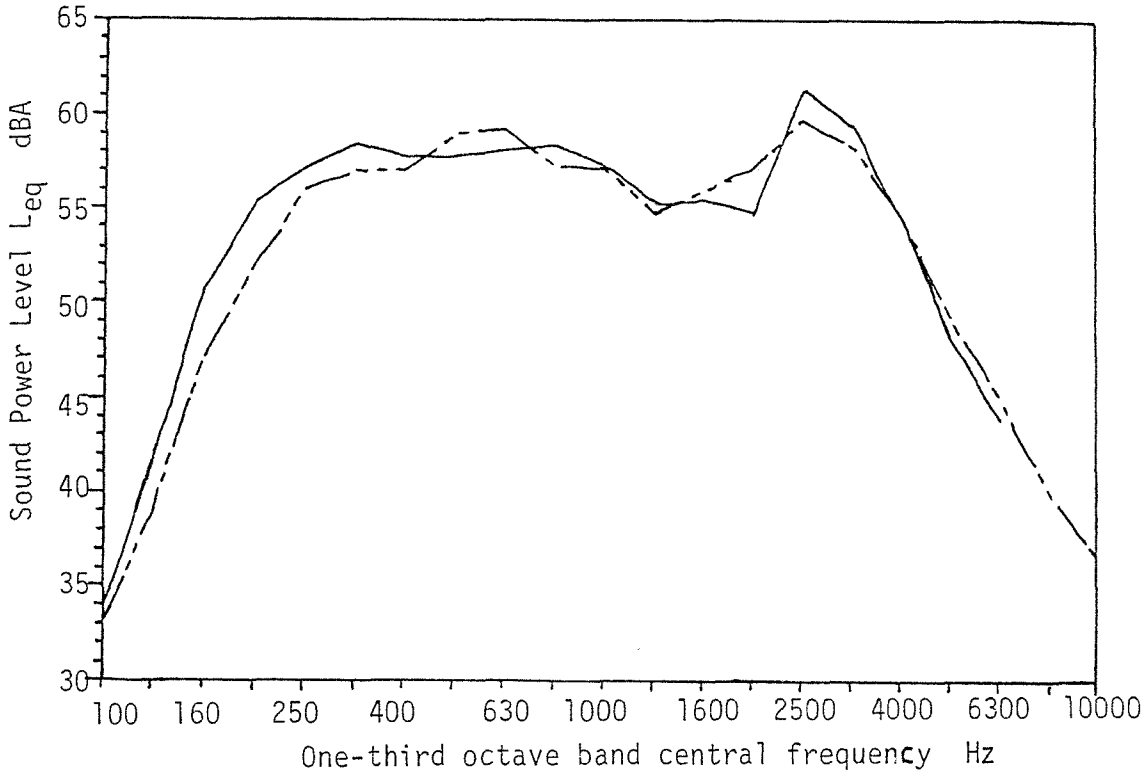

figure 6.24. Noise energy radiated from engine with simulated piston slap excitation. ——, Measured; — ·· —, estimated.

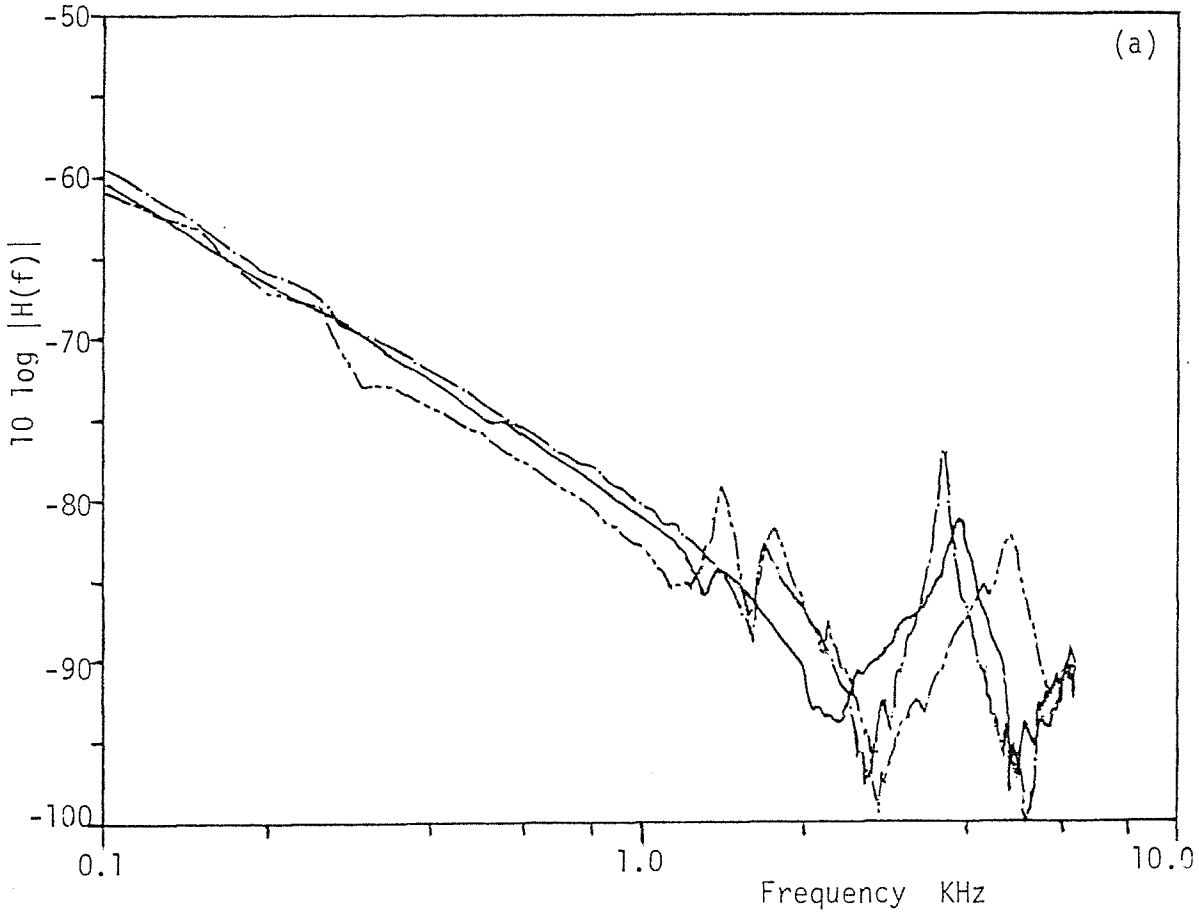

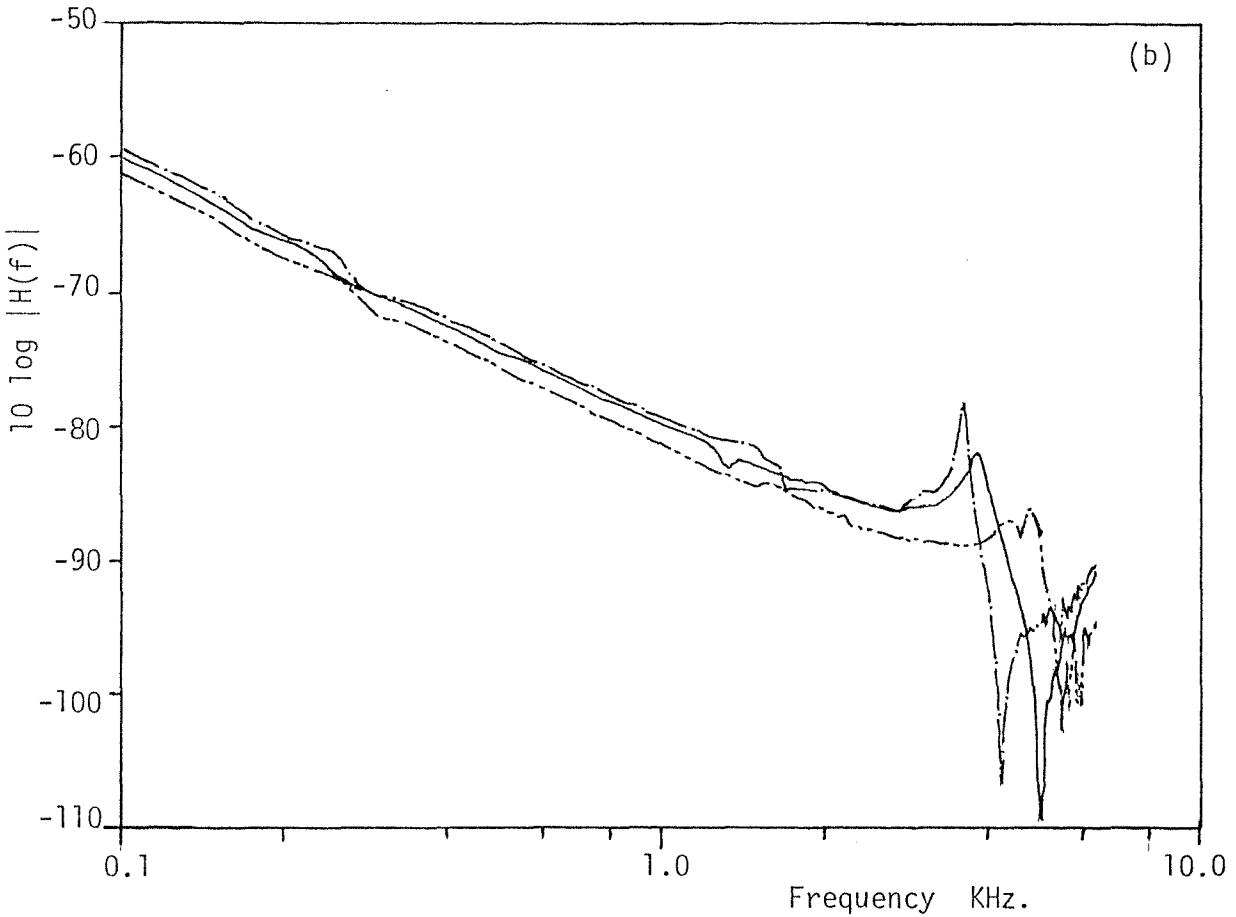

figure 6. 25. Response of a con-rod made of three different materials. (a) Point response at piston top; (b) transfer response. ——, Normal rod; — · —, aluminium rod; — .. —, steel rod.

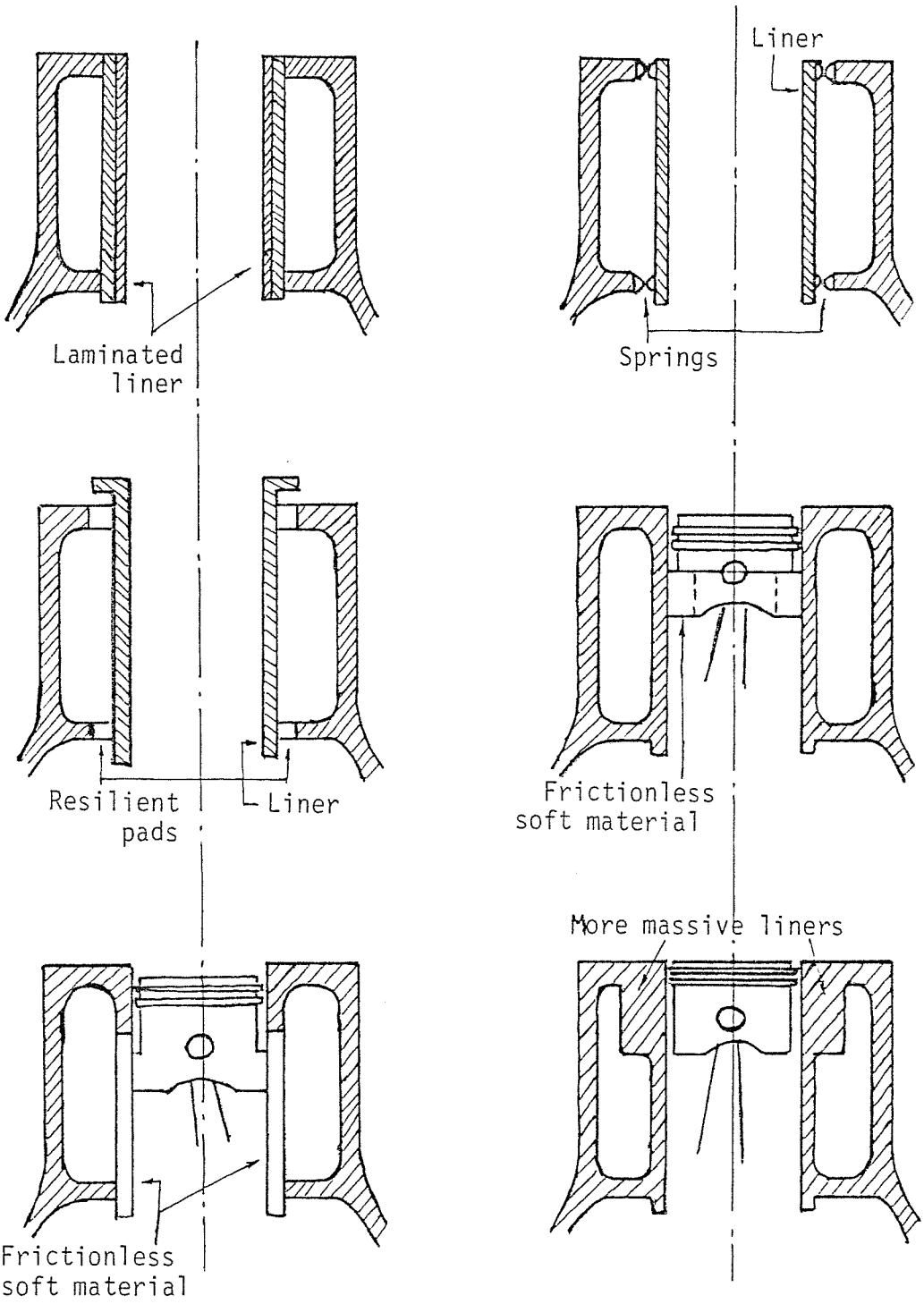

figure 6.26 Design ideas to reduce piston slap noise.

CHAPTER VII

ACTIVE FORCE CANCELLATION

VII. 1. Concept and Limitations

Different methods for noise control can be deduced from the energy accountancy equation, but sometimes all of these methods fail and other solutions for noise control have to be found. One method which may prove to be very effective is active control. Active noise control is now widely accepted, but the concept of active force or vibration is completely new. Like active noise systems, active force control systems cannot be regarded as some magic method which can be used even when no other noise design precautions have been taken. This method of noise control should only be used when all other methods have failed and this is because of the complexity of implementation.

The concept is similar to active noise control, but in this case the vibrations of the structure are controlled by actively cancelling the force excitation. Stress waves in a structure travel much faster than acoustic waves in air. Therefore, for an active system to be effective, its response must be very fast, faster than the response of the structure. This creates some problems in implementing such a system especially in impact situations. In this chapter, different methods are investigated to eliminate these problems and obtain some feel of the kind of noise control possible.

Active force control systems can take two forms depending on the duration of the impact force. If the force pulse is relatively of a long duration with sharp changes of the force, as in the case of the force-time history of a power press, then only the rapid changes need to be cancelled. However, for metal to metal impacts, such as the final forging blows in a drop hammer, that is , the force pulse is of very short duration, the cancellation of the whole pulse is necessary.

The type of system to be used in a particular situation can be decided by investigating the spectrum of the derivative of the force

pulse. Figure (7.1) shows the force-time history, the force derivative spectrum and the spectrum of the second derivative of the force for a single normal operation of a punch press. In the frequency range where the ear is most sensitive, i.e., between 100 and 10,000 Hz, the spectrum for the second derivative is almost flat. The level of this spectrum depends on the sharpness of the changes in the force pulse and therefore, to reduce the noise radiated from the excited structure, this level has to be reduced. Using an active force system, the sharp changes in the force must be cancelled. That is, the unloading of the press is slowed down (figure 7.2 (a)) so that the level of the second derivative spectrum is lowered (figure 7.2 (b)).

For very short pulses, the force derivative spectrum will have a peak in the frequency range 100 Hz to 10 KHz, as obtained in the metal to metal impacts of chapter V. Therefore, in this case the spectrum of any of the derivatives is not flat and thus the active control system must cancel the complete force pulse, rather than just the sudden changes.

The second type of control system is investigated in this chapter and a laboratory system is built to investigate how critical the system is on the various parameters. A description is also given on some system principles which although theoretically should work, are practically impossible to achieve. The reasons why these systems fail are also investigated. The type of system where the whole of the force is cancelled, is easier to implement in some situations, than the system where only the sharp force changes are cancelled. Infact, the hardware for the latter system is not yet available.

VII. 2. Other Uses

There are other uses for an active force cancellation system such as in naval defence. Ships or submarines are identified from the noise signature that they radiate, because of the machinery. If total cancellation of this noise is not possible, not even with an active system, then the latter can alternatively be used to change

the noise signature radiated at will. This can be done by altering some of the parameters like, the timing between the control force and the excitation force, the shape of the control force, making it different from that of the excitation force, so that it will have some other frequency content, etc. In the last case, cancellation will only occur at some particular frequency range. The implementation of such systems would be more complicated than the pure cancellation of all the excitation, but if it can be shown that it is possible, then such a system can be constructed.

VII. 3. Active Force Control

When using an active system, the best position to place the control force is as close as possible to the excitation force. If this is physically possible, then all the vibrations in the structure would be eliminated, that is, no vibrational energy escapes into the structure. However, this is not physically possible, especially in machine structures. In the case when the control force is an exact replica of the excitation force, a force additional to the excitation force is applied to the machine structure at some other point, so that the structure is now acted upon by two forces. Much of the success of the system will depend on the positioning of this control force and the magnitude and synchronisation of this force with respect to the excitation force. The purpose of the active system is to measure the vibration level of the structure and adjust the control force, so that the structure vibrates at a lower level at the measuring position.

In previous investigations [36-37] active force control systems are used for structures which are under constant or quasi-constant excitation. Those that dealt with step inputs, did not modify the initial transient vibration of the structure, but concentrated on decreasing the level of the vibration during the ringing of the structure, after the transient has occured. The structure is very lightly damped and these control systems usually deal with only one particular mode. In this case, the output from the measuring

transducer is fed to the control system which has time to compute and adjust the required control force, because of the long ringing time. The output signal from a control system always lags the input signal because of the components constituting the system. If the system to be controlled is continuous or quasi-continuous, this delay time in the control system is adjusted to be a whole number of cycles, provided that only one mode is treated.

Such a set-up is not practicable in the case of a highly damped structure which is impact-excited by a very short impact, where the ringing time is very short and most of the noise comes during the impact and right after the impact has occurred. A conventional active control system will be too slow to adjust the control force. In such cases, the control force must be exactly in synchronisation with the excitation force and both forces must be as identical as possible. That is, time compensation is to be applied in the control system to compensate for the time lag inherent in the system, mainly the amplification and the control force unit. This means that a phase advance system is needed such that a pulse is output from the control system prior to the pulse exciting the structure and thus the excitation force pulse and the control force pulse are synchronised. This is impossible practically because it implies that an infinite voltage is applied to the control force exciter which will load all practical electronic systems. Another form of an active force control system for machines which are impact excited when hit with a hammer blow is to measure the position of the hammer well before the impact. Assuming a constant time of flight of the hammer, the control system is given enough warning time so that the control force occurs at the same time as the impact. Both these methods are investigated in the case of a plate-like structure.

VII. 4. Multiple Impacts

Active force control would be a very useful method to cancel the vibrations from the principal source of excitation. In many situations the excitation from the principal source will cause other secondary

impacts to occur at interfaces and bearings within the machine when backlash and clearances are taken up. These secondary sources of excitation cannot be controlled by an active system because a system will be needed for each impact and placed at each source point. However, these secondary impacts should be eliminated by the cancellation of the main source of excitation.

In the case of a machine mounted at several points, active control can be used with no problem at all. The positions where the impacts occur are of a finite number and very well defined. Active control systems can be designed for each individual mounting point by taking into consideration the excitation force at that mount.

VII. 5. Experimental Investigation

An active force control system is built to control the vibrations of a plate structure excited at the centre by an impact force. This system is investigated to find which parameters influence the system and what tolerances are allowed. An equal and opposite control force is applied to the plate on the opposite side of the excitation force and although the vibrations are not completely cancelled, the mode of vibration of the plate is changed from flexural or bending waves to dilational waves, which occur at a much higher frequency and are of a much lower amplitude. Thus, in this case, the escape energy into the structure is limited because of the lower response due to the different type of vibrations in the plate.

If a plate is transversely excited by a point force, the plate sets itself into bending vibrations. Since there is nothing to oppose the transverse force at the point of impact, a localised moment is introduced into the plate which bends the plate and creates flexural waves (figure 7.3). Since the impact is usually very short, the energy of the pulse is distributed evenly with frequency and thus most of the plate modes would be excited. If an equal and opposite force is applied to the plate at the same point of impact, no vibrational energy escapes into the plate, and the plate remains stationary. However, it is impossible to apply a force at the exact

point of impact; thus, if the control force is applied on the opposite side of the plate, synchronised with the impact, the plate will be compressed at that point (figure 7.4). In this case, the excitation force is opposed by the control force and therefore there is no moment present to excite the plate in bending modes. However, the plate is compressed at the point of impact and longitudinal waves are excited in the plate. It would be expected that the first mode of the plate in this type of vibration will happen when the thickness of the plate corresponds to half a wavelength. The speed of compression waves in an infinite plate is given by [32] .

$$c = \left(\frac{E}{\rho(1 - \nu)^2}\right)^{\frac{1}{2}} \qquad (7.1)$$

where E is Young's modulus;
ρ is the material density; and
ν is Poisson's ratio.

Therefore, for a 1cm thick plate, the first modal frequency is about 370 KHz, which is outside the audible frequency range. Thus, theoretically, by setting this type of waves instead of bending waves, the reduction in noise due to the ringing of the structure is very high.

The requirements are that a similar and equal in magnitude control force is applied to the structure at exactly the same time as the excitation force. This was one of the major problems encountered in setting up this system. It is a drawback in the application of an active control system for machine structures because of the short duration of the impact, seldom longer than a fraction of a millisecond. That is, the control system must have a very high speed response. Also, all the components, especially mechanical linkages, must be very reliable and accurate. Their operation must be repeatable within a fraction of a millisecond.

As a first system, an electronic phase advance box is used to

condition the signal of the force pulse measured when the impactor hits the plate. This phase advanced signal is fed to the control system (figure 7.5). This system works on the principle that two identical pulses with a time difference in their occurence, if transformed to the frequency plane will have the same magnitude but will have a phase difference between the two transforms. If this phase difference is compensated for by an electronic phase advance box, the two pulses can be synchronised. However, an initial infinite voltage is needed for such a system to function.

This system was investigated to ascertain its impracticality. The phase lag of the control system was measured and the right transform computed for the compensation of this delay. An electronic system with this transform was built and tested, but when included in the control circuit it had two problems, as envisaged from the theoretical conditions. The first was that because of the finite value of the output voltage the phase advance provided was not enough to compensate for the lag of this system. The second was that a phase advance system is effectively a high pass filter and the amplification at high frequencies is very high, making the system very noisy and unstable at high frequencies. The amplification was so high that it overloaded the whole of the control system and gave a very high level of background noise. Thus a phase advance system to compensate for the lag of the force control system is not practical.

The second system is of the type where the force pulse is prerecorded. Two pulses are recorded on magnetic tape, the first pulse triggers a mechanism that releases the impactor and the second pulse which is identical, i.e., of the same duration and magnitude as the force pulse from the impactor, serves as an input to the control system. The spacing in time between the two pulses is adjusted so that the second pulse, when output from the control system, is synchronised with the impact. The first pulse is gated off from the input to the control system so that only the second pulse is input into the system (figure 7.6). The problem with this set-up is that since the separation on tape between the two pulses

depended on the time of flight of the impactor, the time had to be very precise and constant to within a fraction of a millisecond which was not possible without continuous minor adjustments in the system, which are not possible with this set-up. The hinging mechanism was not smooth and the magnet release was not constant due to varying collapse of the magnetic field, resulting in changes in the time of flight of the same order of magnitude as the impact duration, making the system unreliable. Also, too many operations were necessary to operate the system which made it impractical.

The third system built sought to improve all these problems. The hinging mechanism of the impactor was changed from a greased packed bearing to a knife edge support. This reduced the friction at the bearings to a minimum. The magnet release support structure was stiffened so that any fluctuations in the length of the flight path were eliminated. The electro-magnet core which held the impactor before release was covered with a thin layer of nylon so that it reduced friction and thus gave a more constant release. The impactor is released by switching off the current to the magnet manually and an infra-red sensor locates the position of the impactor before it hits the plate. The pulse from the infra-red sensor triggers off a pulse generator, which gives a pulse after a preset delay time. This delay time is adjusted so that the pulse from the impactor (excitation force) and the force pulse from the control system are synchronised (figure 7.7). The use of the pulse generator allowed easy adjustment of the delay time in the system. The amplification is adjusted so that the excitation force and control force are of the same magnitude.

VII. 5.1. Experimental Results

The noise and surface acceleration wereinvestigated for the case of a 1 metre square plate, 1cm thick, both with and without a control force. The duration and magnitude of the control force were adjusted to be as close as possible to the excitation force. Figure (7.8) shows the force pulses for the excitation and the

control; (a) is the control force pulse and (b) the pulse from the impactor, the excitation force pulse. Superimposed on the excitation pulse are the vibrations of the impactor, but as can be observed in curve (c), which shows an alternative measurement of the force pulse from the impactor, it is a smooth pulse of approximately half sine in shape of duration 0.35 ms. Curve (d) is a measurement of the excitation force as measured on the impactor which was used for calibrating the system.

There is a high reduction in the average surface acceleration of the plate with the application of the control system, both when expressed as a time signature (figure 7.9) and when expressed as a frequency spectrum (figure 7.10). Note that in figure (7.10 (a)), the spatial average acceleration spectrum using the control system, the vertical scale is ten times the scale of the spectrum for the case of no control system. Similar results are obtained for the noise energy radiated by the plate with the control system, both when expressed in the time domain (figure 7.11), and when given in one-third octave bands. The decrease in the noise level is very high, the overall reduction being of about 14 dB, which is constant throughout the whole frequency range (figure 7.12).

VII. 5.2. Analysis of Results

The reduction in noise when the two forces act on opposite faces on the same point is lower than expected. If the results are studied carefully, it can be observed that the noise energy spectrum in the two cases is the same, only with an average of 14 dB difference in the level. This suggests that the reduction is not complete. The elimination of the bending vibrations is not total. An active force control system will give a reduction in the level of noise energy radiated but much depends on perfect matching of the excitation and control force, both in the time domain and in their frequency spectrum. In the case of the cancellation of only the sharp changes of the force, the extent of the cancellation at each frequency band will depend on the matching of the spectra of

the sharp force changes of the excitation and the control system. It can be observed in figure (7.11) that the control force is not an exact replica of the excitation force and this may be the reason why the vibrations are only partially cancelled. The theoretical maximum reduction in noise that can be achieved if the two forces are exactly the same is not easy to obtain. However, because of the type of waves that are present under this form of excitation, the reduction must be very high. Therefore, in setting up a second generation of active force control systems, an improvement in the matching of the force pulse must be further investigated.

VII. 6. Effect of Separation between Excitation Force and Control Force

It is not always physically possible to have the controlling force at exactly the same location as the excitation force or on the opposite side, as in the case of the flat plate experiments. Therefore, the two forces can be some distance apart. The effect of this separating distance is investigated, in the case of the flat plate, by traversing along the plate the position of the control force, keeping the excitation force at a fixed location. These results are then generalised for other types of structures.

The response of a plate structure away from the point of excitation is given by the empirical formula [18]

$$M_t = M_c \qquad kr \leq 0.63$$

$$= M_c \sqrt{(2/(\pi kr))}\, e^{-j(kr - \pi/4)} \qquad kr \geq 0.63 \qquad (7.2)$$

where M_c is the characteristic mobility of the plate given by $M_c = (8\sqrt{B\rho_s})^{-1}$;

B is the bending stiffness;

ρ_s is the surface density;

k is the bending wave number; and

r is the distance from the point of excitation.

If the structure is acted upon by two forces with opposite direction with respect to one another, as in the case of an active control system, the two forces are completely coupled only if the separation between the point of application of the two forces satisfies the relation $kx \lesssim 0.63$ where x is the separation distance. Then, in this case, the plate structure would be excited by a torque of magnitude (Fx), where F is the excitation force. Outside this range, $kx > 0.63$, the coupling between the two forces diminishes as x increases, until the two forces are completely independent of each other. Then the structure can be considered to be under the excitation of two totally independent forces, i.e., twice as much energy escapes into the structure as compared to the excitation of only one force.

The condition $kx \lesssim 0.63$ is frequency dependent, and therefore the extent of the coupling for a set separation will depend on the frequency of excitation. In impact situations, the excitation force is a pulse of finite duration, and therefore its frequency spectrum contains components of different magnitude at all frequencies. Thus, for a certain separation, the two forces are coupled up to the frequency where $kx = 0.63$. The variation of this frequency with x/α, the separation in terms of the number of wavelengths of the structure, ($\alpha \sim$ wavelength λ and $\alpha^4 = Eh^2/(12\rho(1 - \nu^2))$ for a flat plate), is shown in figure (7.13).

In the case of torque excitation, the structural response of a flat plate is independent of frequency, while the response for point force excitation has a slope of -10 dB per frequency decade. Thus, the input energy per unit force under torque excitation will be higher than that for the point force, above a certain frequency. This frequency is dependent on the bulkiness of the structure and the separation distance between the two forces, if the torque is given by Fx. Figure (7.13) also shows the variation of this frequency with x/α.

Thus in the case of two forces, acting in opposite direction and separated by some distance, the noise radiated from the plate increases at 6 dB per doubling of the separation distance, if the

two forces are completely coupled. However, in practice, the two forces are not exactly identical, as in the experimental results obtained in this investigation. In such circumstances, the noise radiated would be a combination of the noise due to the difference in the force and the noise due to the torque excitation. This result is observed in the noise radiated in one-third octave bands from the plate, with the changing separation distance (figure 7.14). At zero separation, the noise radiated can be assumed to be the contribution due to the difference between the excitation force and the control force. The contribution due to the torque excitation with the increase of separation, should follow the dotted line shown in figure (7.14). This dotted line intersects the level of noise that the plate radiates if excited by only one point force at the separation given by curve (i) in figure (7.13). In figure (7.14) the curves for four representative one-third octave bands are shown. In other bands the same general results are obtained. However, as the separation increases, kx becomes greater than 0.63 and the two forces will not be completely coupled. Thus, the noise radiated will not increase by 6 dB per doubling of separation, but increases more slowly, reaching a maximum and then decreases again to approach a level 3 dB higher than the noise radiated, had the plate been excited by a single force. This condition corresponding to no coupling between the two forces.

Generalising these results for any structure, the effect of separation distance on the performance of an active force cancellation system will be that its performance is reduced as compared to the case where the control force is applied at the same location as the excitation force. However, up to a certain separation, which is structure dependent, the introduction of an active force control system can still be an improvement in noise control over the original set-up. At a given frequency, the separation at which kx is equal to 0.63 is usually less than the separation for which the torque response is equal to the point force response. Thus any distance which is less than this latter critical separation will give a reduction in the noise radiated. Because of the lower coupling

between the two forces at this critical separation, the performance of an active force control system will be an improvement in noise control even for a slightly less separation than the critical distance.

These results also apply if the excitation is not at discrete frequencies and the excitation spectrum ($10 \log |\dot{F}(f)|^2$) has a maximum level. In this case, the frequency of highest excitation can be taken as the frequency of interest. Figure (7.15) shows the total noise radiated by the plate with changing separation distance. The curve has the same features as the curves for the one-third octave bands, and the critical distance corresponds to the frequency of maximum excitation.

Figure (7.13) holds only for plate-like structures of varying thickness. For other types of structures, similar curves can be obtained by equating the point force response and the torque response. If in such cases, the separation distance given by $kx = 0.63$ is greater than the critical distance, the performance of the control system at separation distances very near to the critical distance will be very poor. In all cases, the control force must be located as close as possible to the excitation force.

VII. 7. Conclusion

The conclusions from this investigation are that the performance of an active force control system is very critical on the timing of the two pulses; the separation distance of the control force and excitation force; and the exact shape of the force pulse or its spectrum where cancellation is required. The need for good synchronisation of the force pulse is because of the highly damped nature of machine structures, where the vibrations die down very quickly. With two pulses which are not synchronised, the noise radiated from the structure may increase. Different time durations, or in the case where only the sharp changes are being cancelled, the force changes are not identical; the spectra of the control and the excitation will have different levels at different frequencies and cancellation occurs only in some frequency ranges, while other

frequencies are not affected at all.

In this investigation and set-up of a force control system, the synchronisation of the two forces proved to be one of the major problems since the time of flight of the impactor varied from the triggering point to the instant of impact. This is bound to happen in ordinary machinery, the impact occuring within a certain time limit. Thus to implement an active force control system in a machine, it may be that, not only the inclusion of the system is necessary, but also modifications in the machine, especially its running sequence, are needed to eliminate the problems of synchronisation.

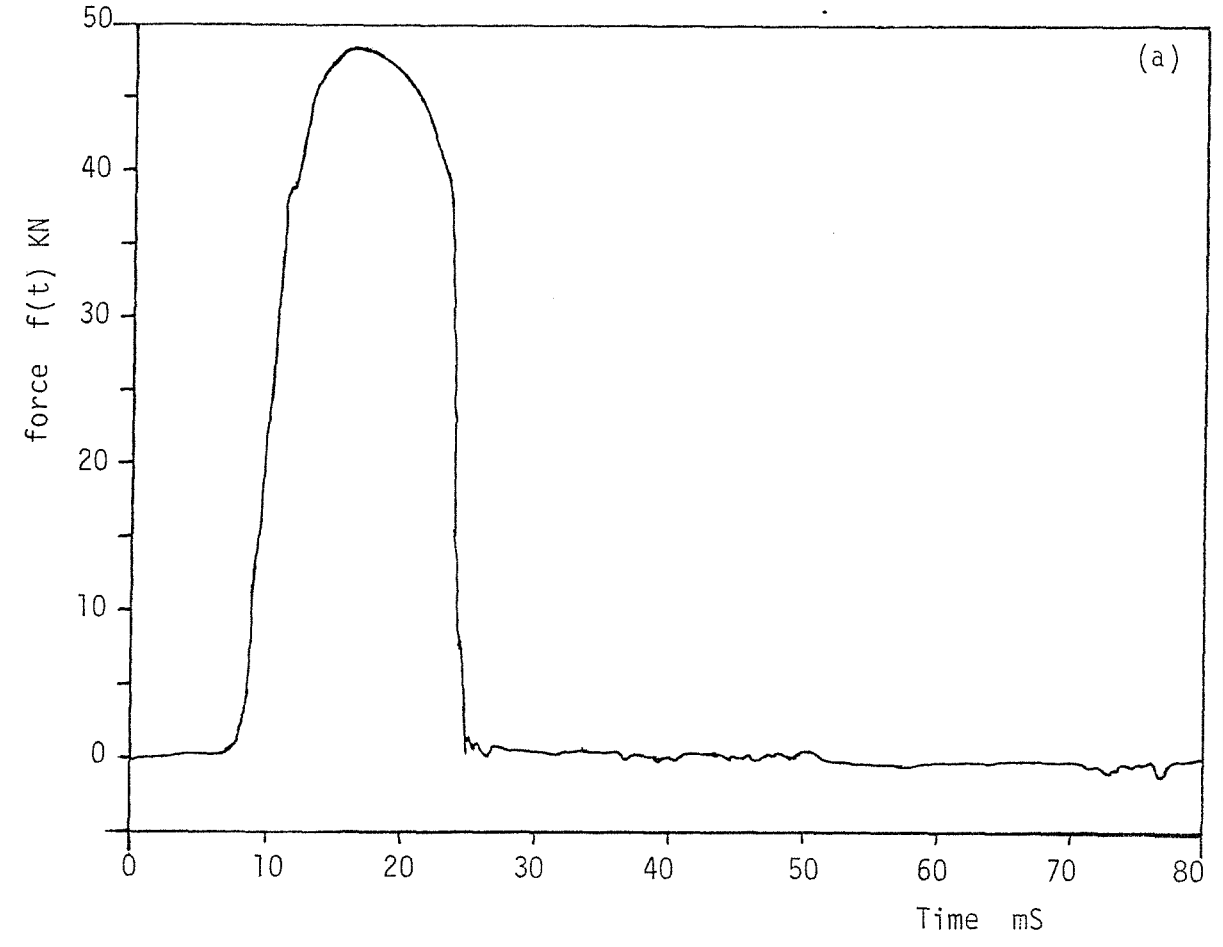
(a)
force f(t) KN
50
40
30
20
10
0
0
10
20
30
40
50
60
70
80
Time mS

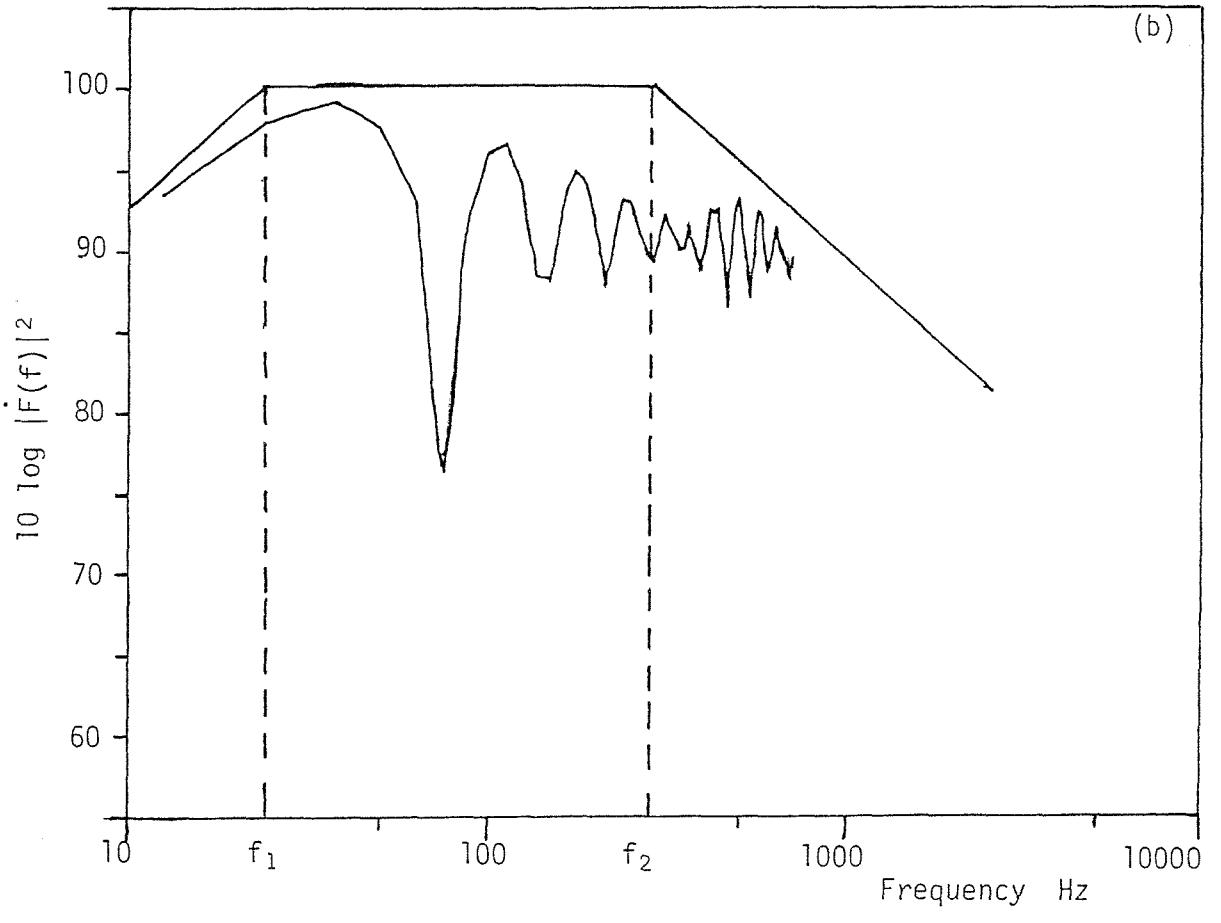
(b)
10 log |F(f)|²
100
90
80
70
60
10
f1
100
f2
1000
10000
Frequency Hz

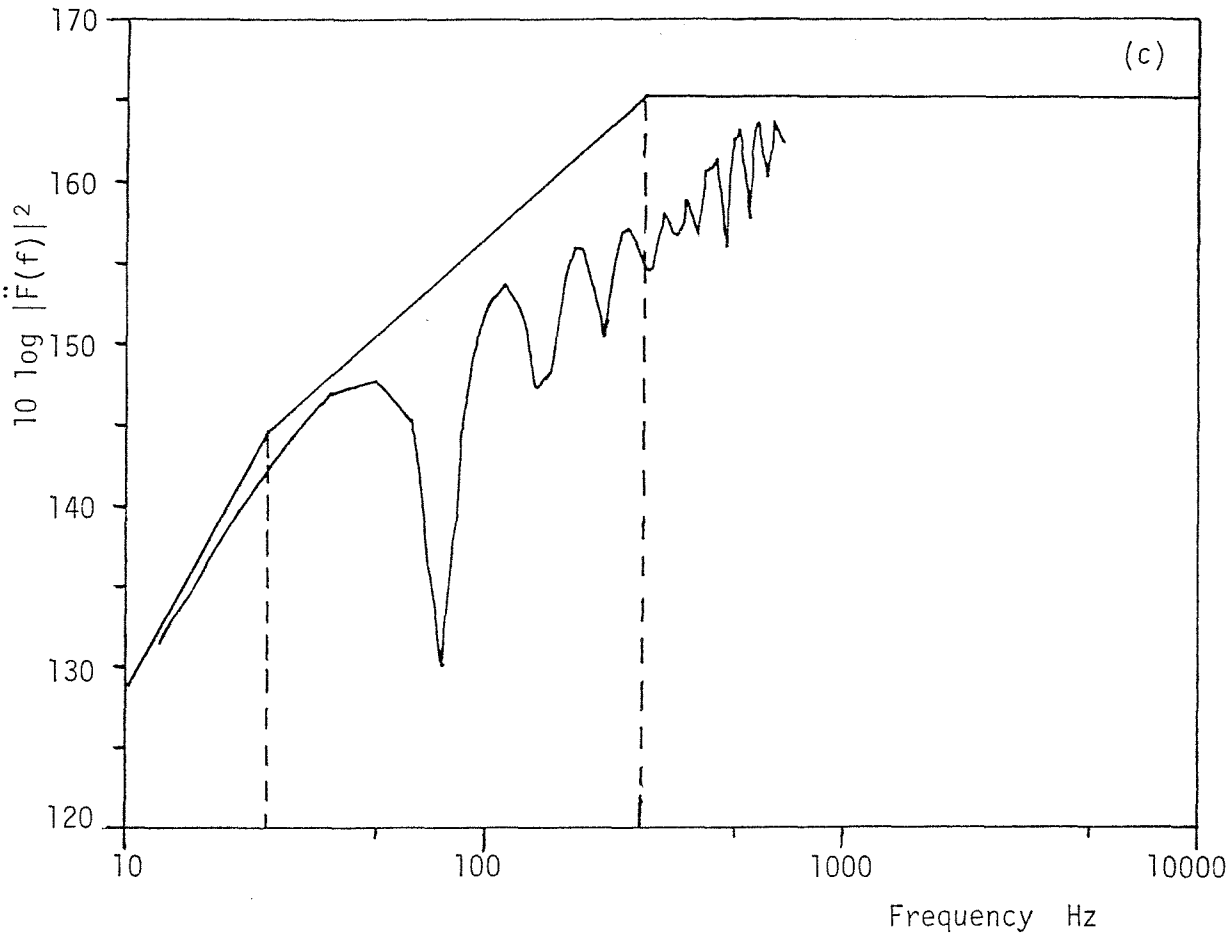

figure 7.1. Fracture force pulse for the normal operation of a power press, showing the very sharp unloading on fracture. (a) force-time history; (b) first derivative spectrum; (c) second derivative spectrum.

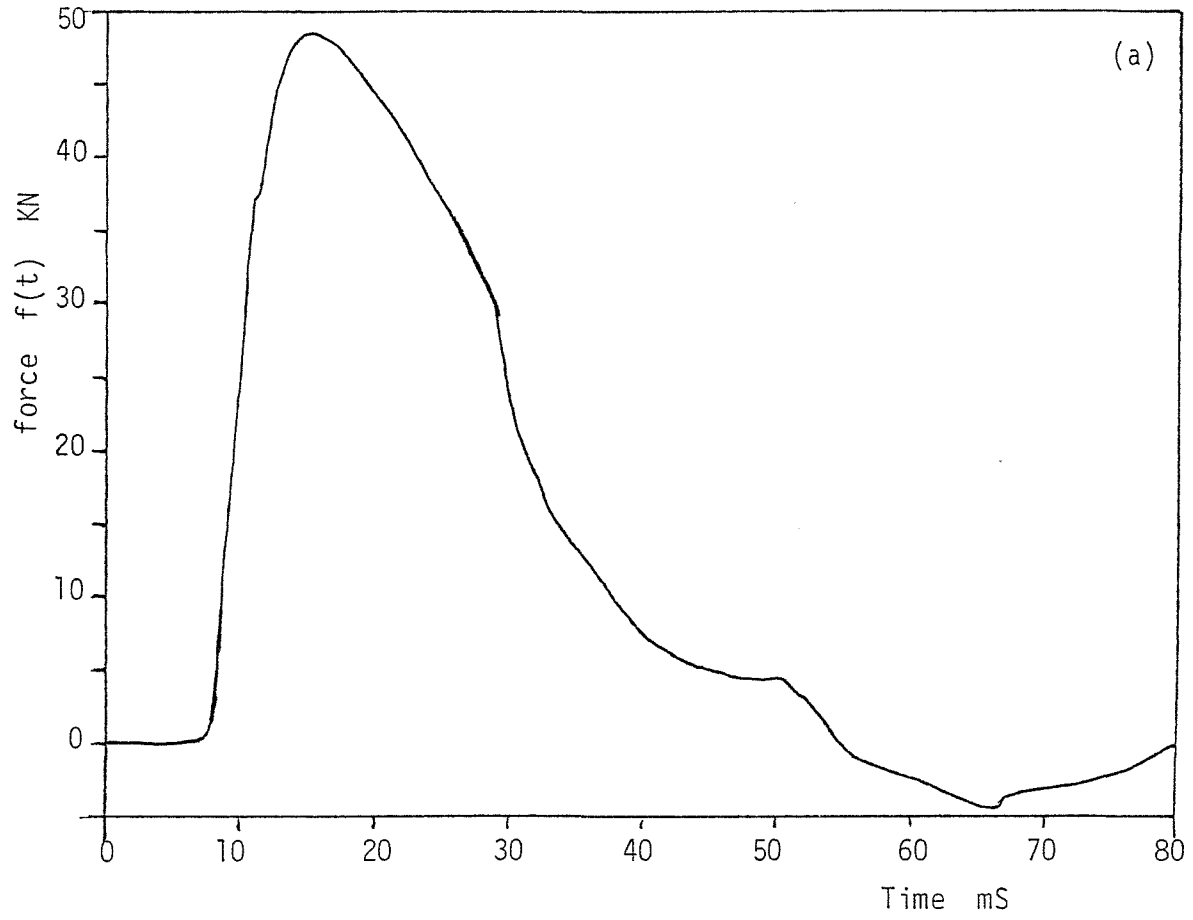
(a)
force f(t) KN
50
40
30
20
10
0
0
10
20
30
40
50
60
70
80
Time mS

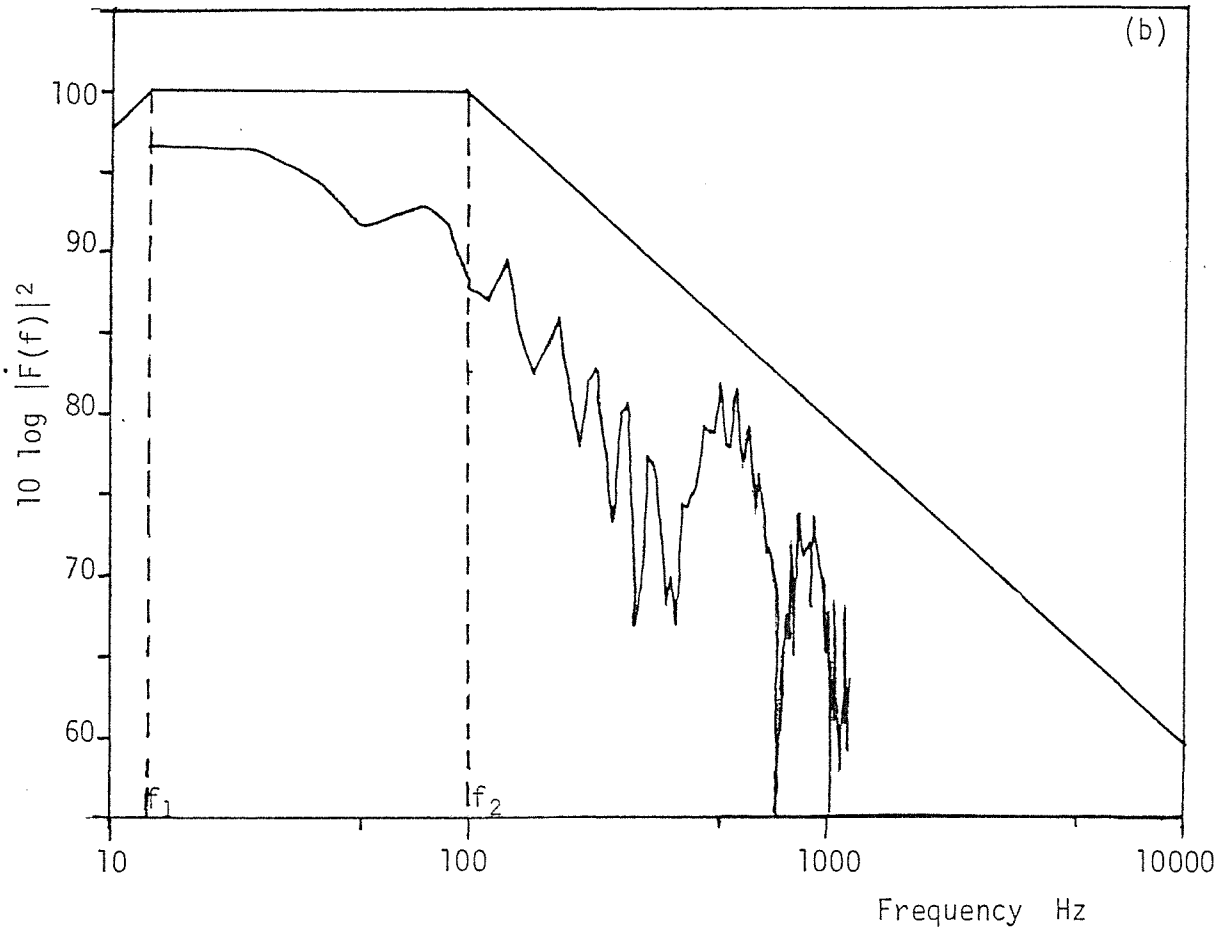
(b)
10 log |Ḟ(f)|²
100
90
80
70
60
f1
f2
10
100
1000
10000
Frequency Hz

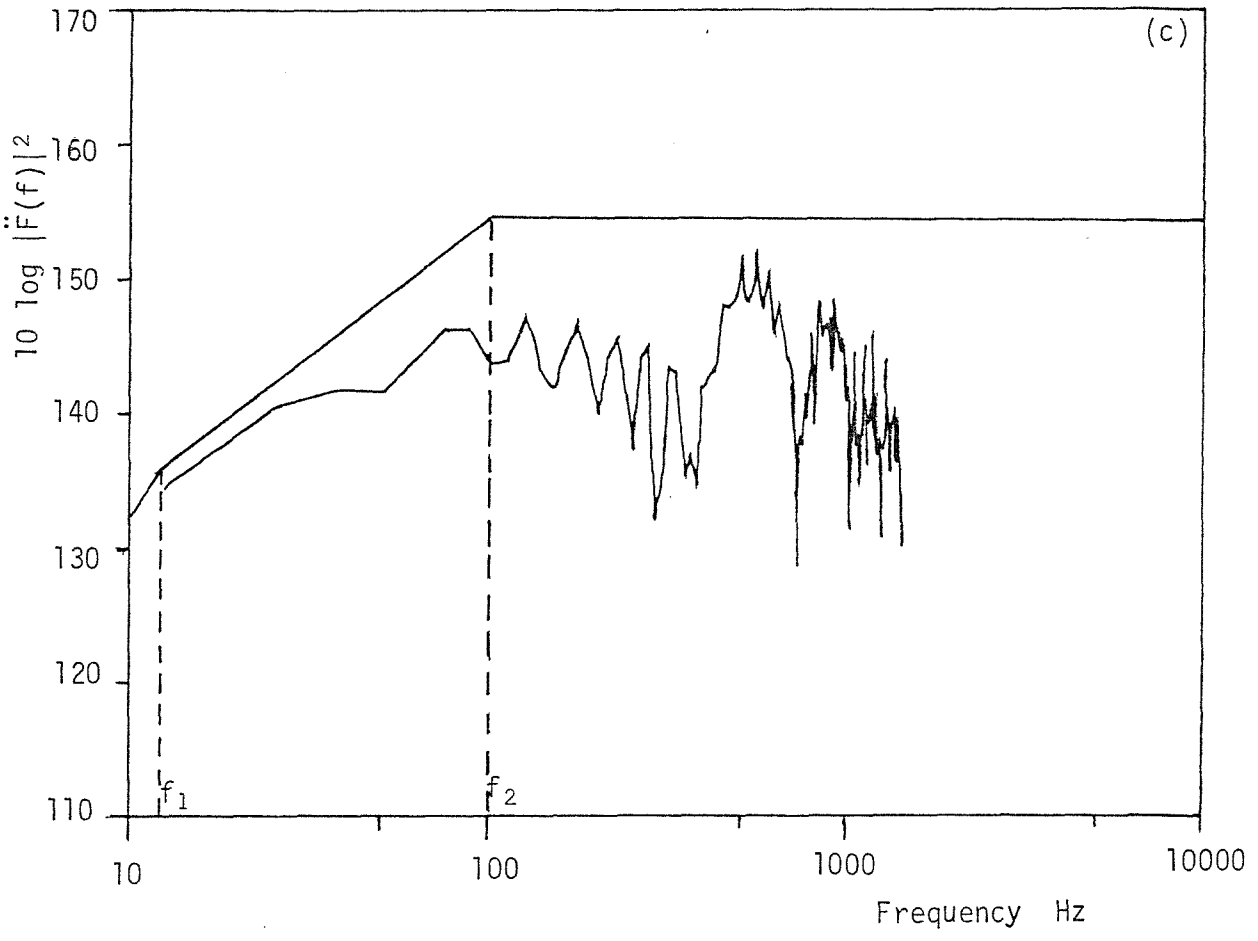

figure 7.2. Modified fracture force for a power press, where the sharp unloading is controlled. (a) force-time history; (b) first derivative spectrum; (c) second derivative spectrum.

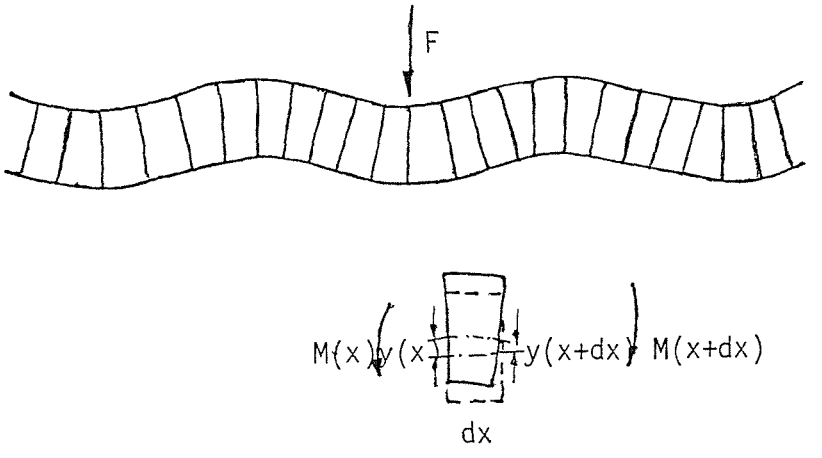

figure 7.3. Bending waves in a plate structure.

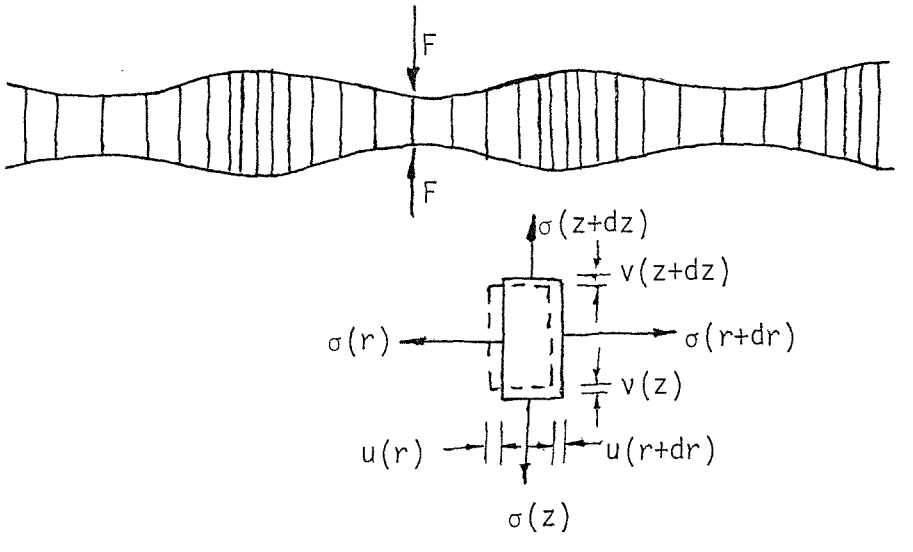

figure 7.4. Compression waves in plates.

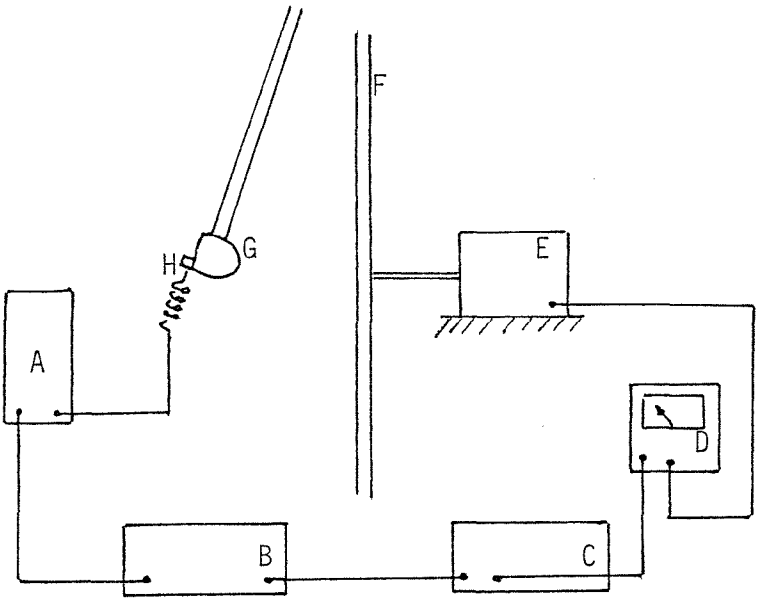

figure 7.5. Test set-up using Phase advancing. A, charge amp; B, phase advance box; C, power amp; D, Ammeter; E, shaker; F, plate; G, impactor; H, transducer.

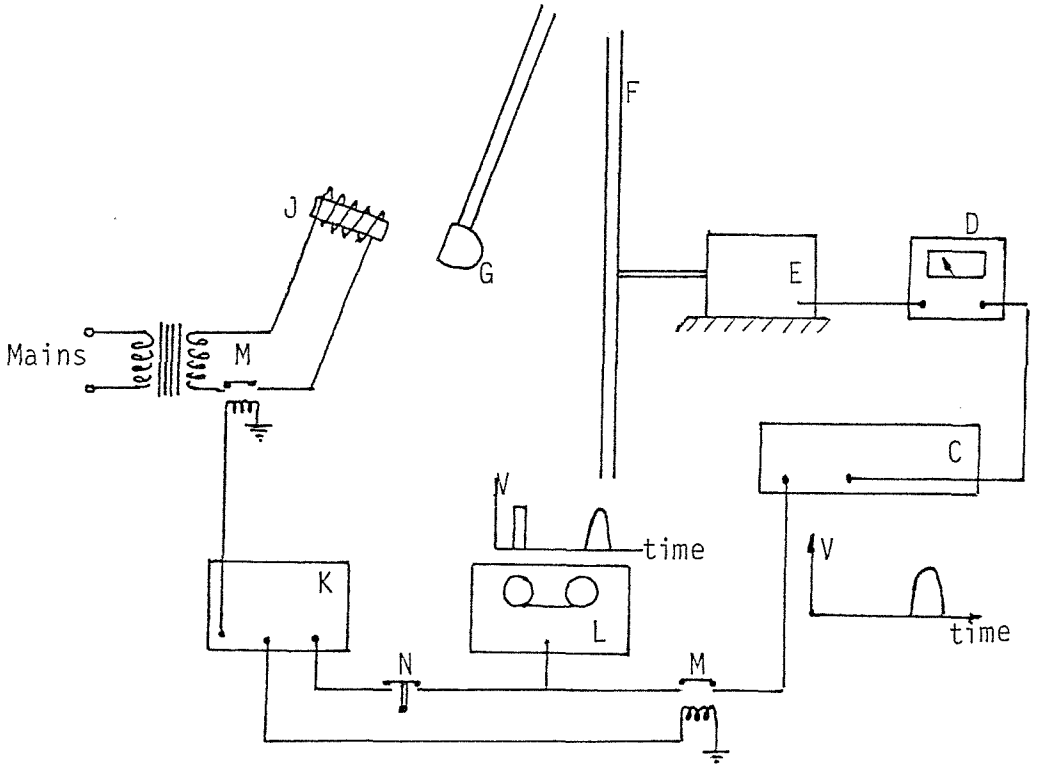

figure 7.6. Set-up using prerecorded trigger signal. C,D,E,F,G, same as in figure 7.5.; J, electromagnet; K, pulse generator; L, tape-recorder; M, relay switches; N, spring switch.

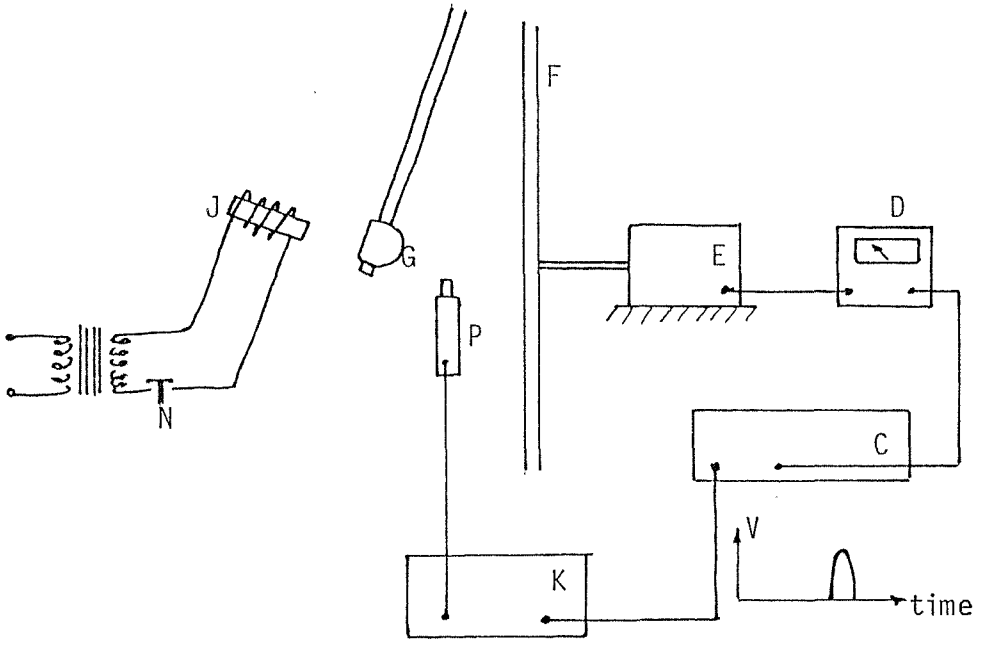

figure 7.7. Experimental set-up. C,D, E,F,G,J,K,N, same as in figure 7.6. ; P, infrared detector.

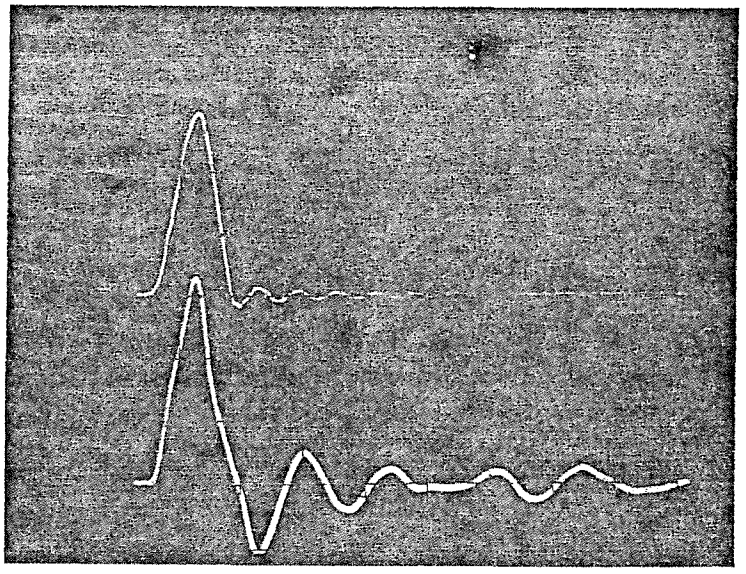

(a)

(b)

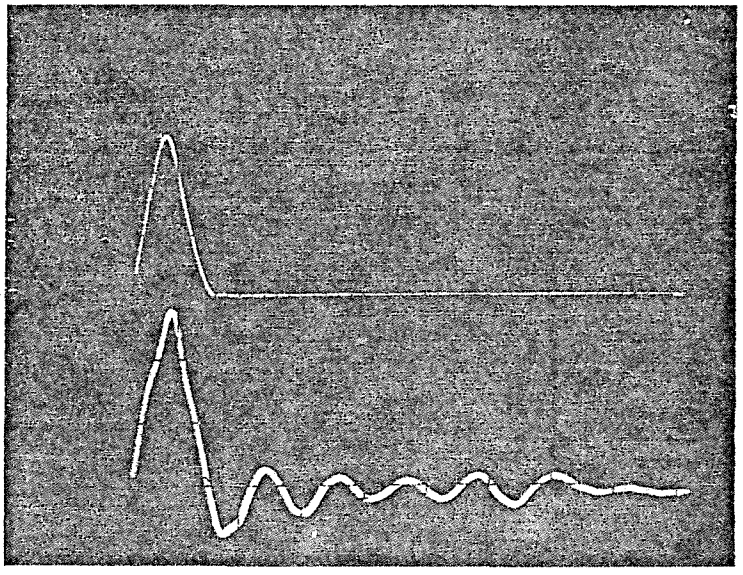

(c)

(d)

figure 7.8. The excitation and control force pulses applied to the plate. (a) control pulse from shaker; (b) excitation pulse from hammer; (c) hammer pulse measured by force transducer; (d) same as (b).

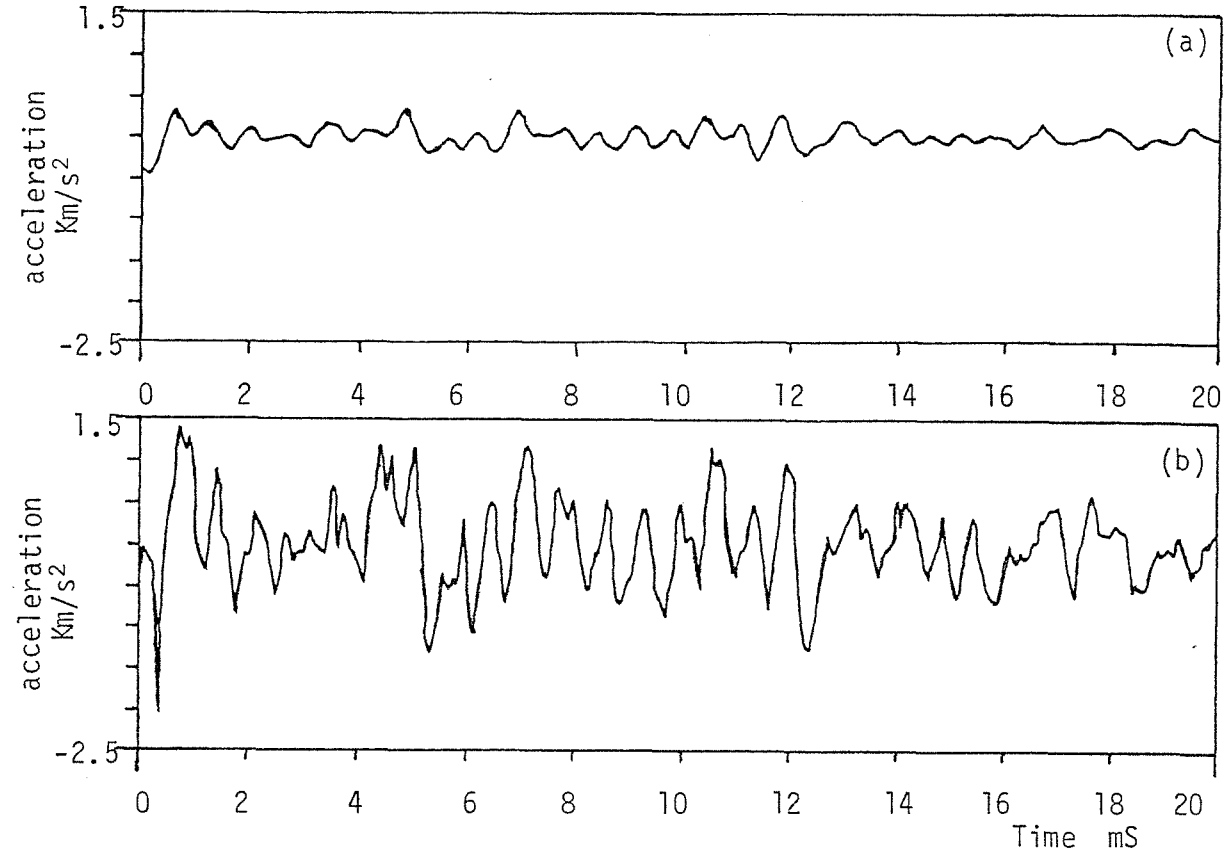

figure 7.9. Surface acceleration signature. (a) With active force cancellation; (b) without active system.

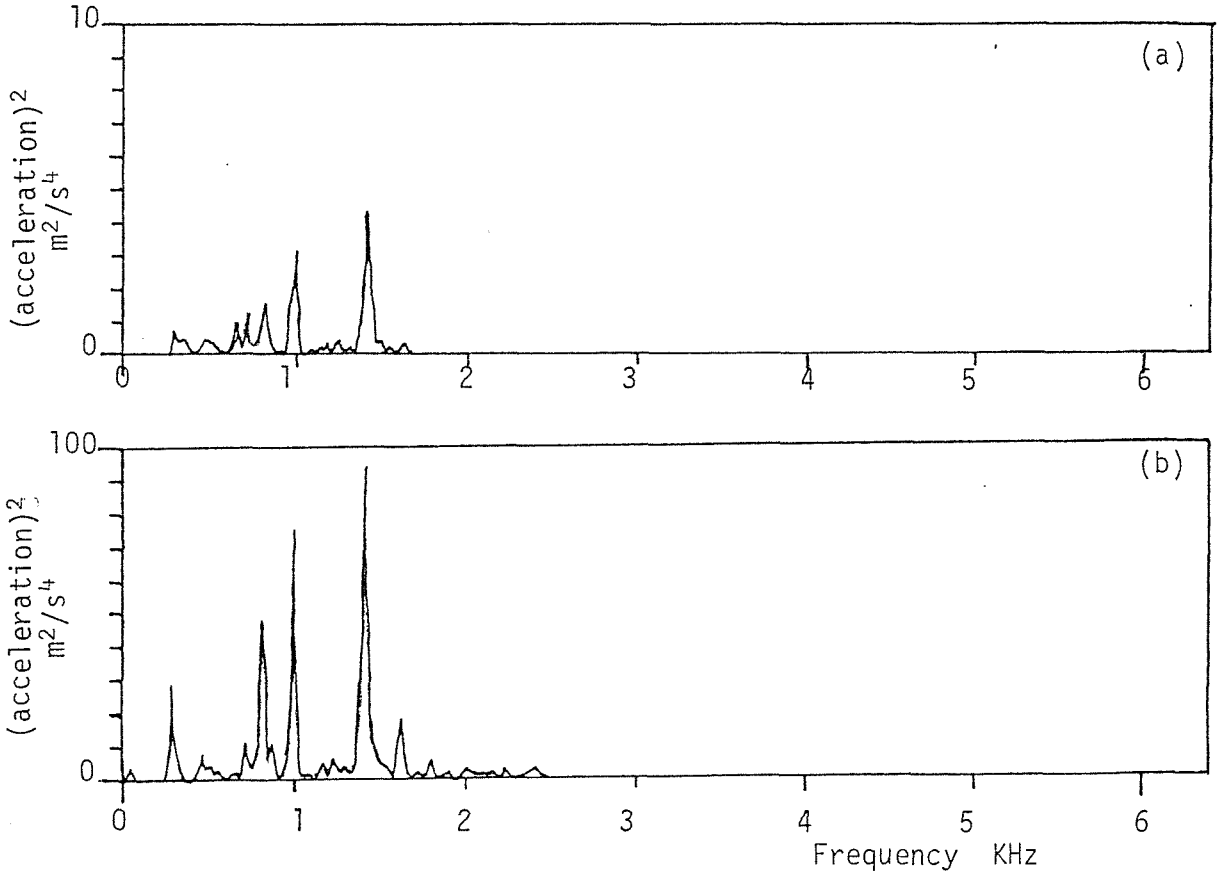

figure 7.10. Frequency spectrum of plate surface acceleration. (a) with active system; (b) without active system.

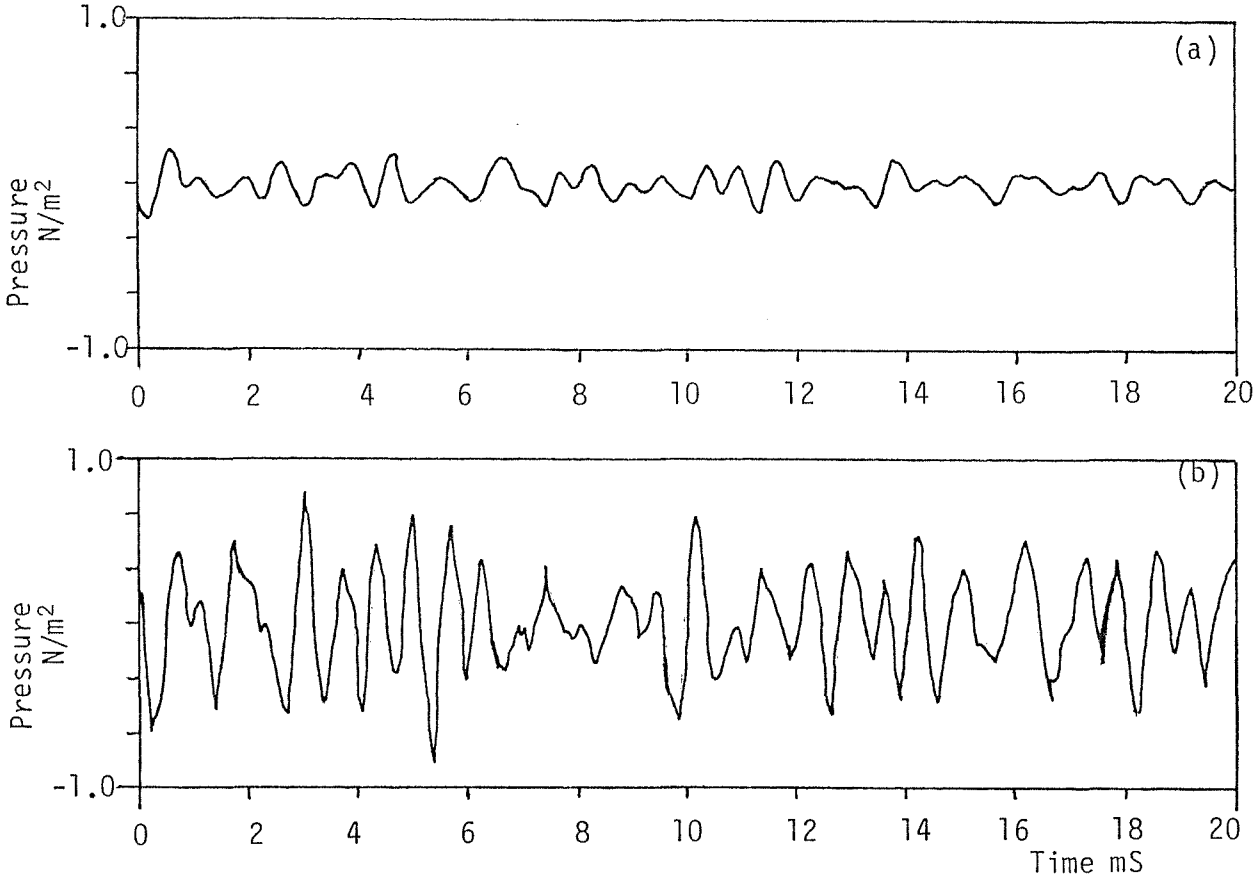

figure 7.11. Noise signature radiated from plate.(a)with control system; (b) without control system.

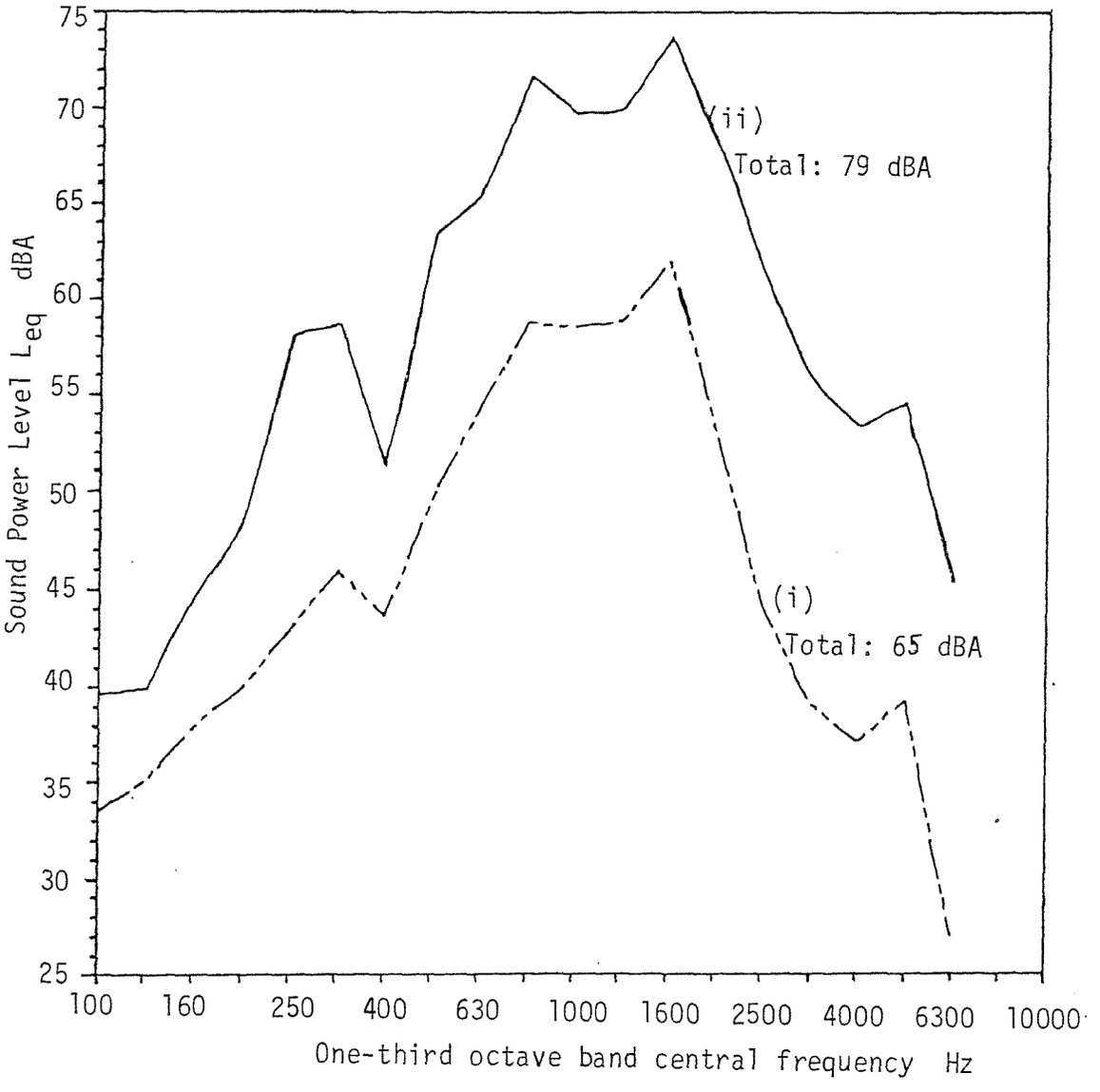

figure 7.12. Radiated noise in one-third octave frequency bands.
(i) with control system; (ii) without control system.

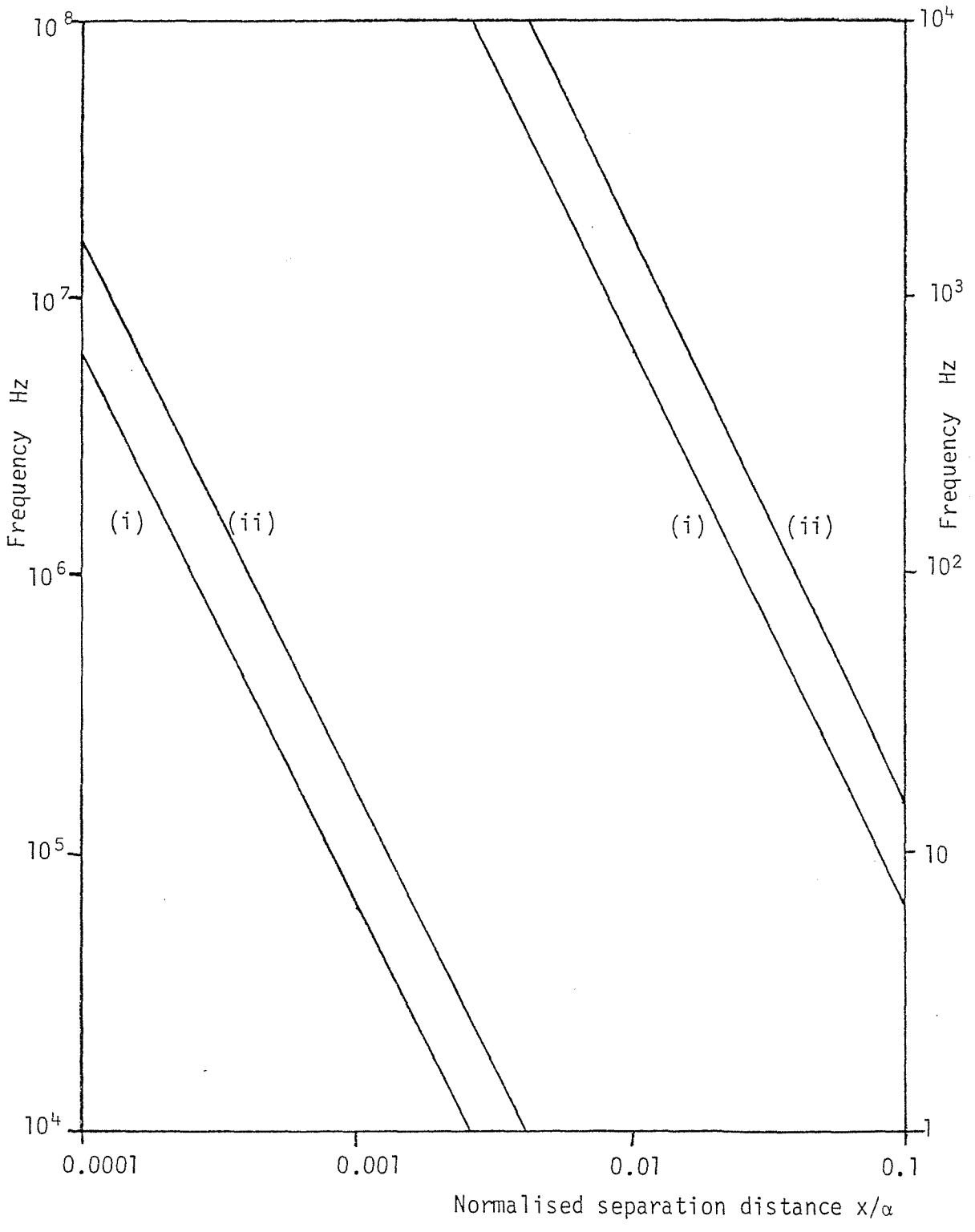

figure 7.13. Change of frequency with separation distance.
(i) kx = 0.63; (ii) frequency at which torque response is equal to point response for a plate.

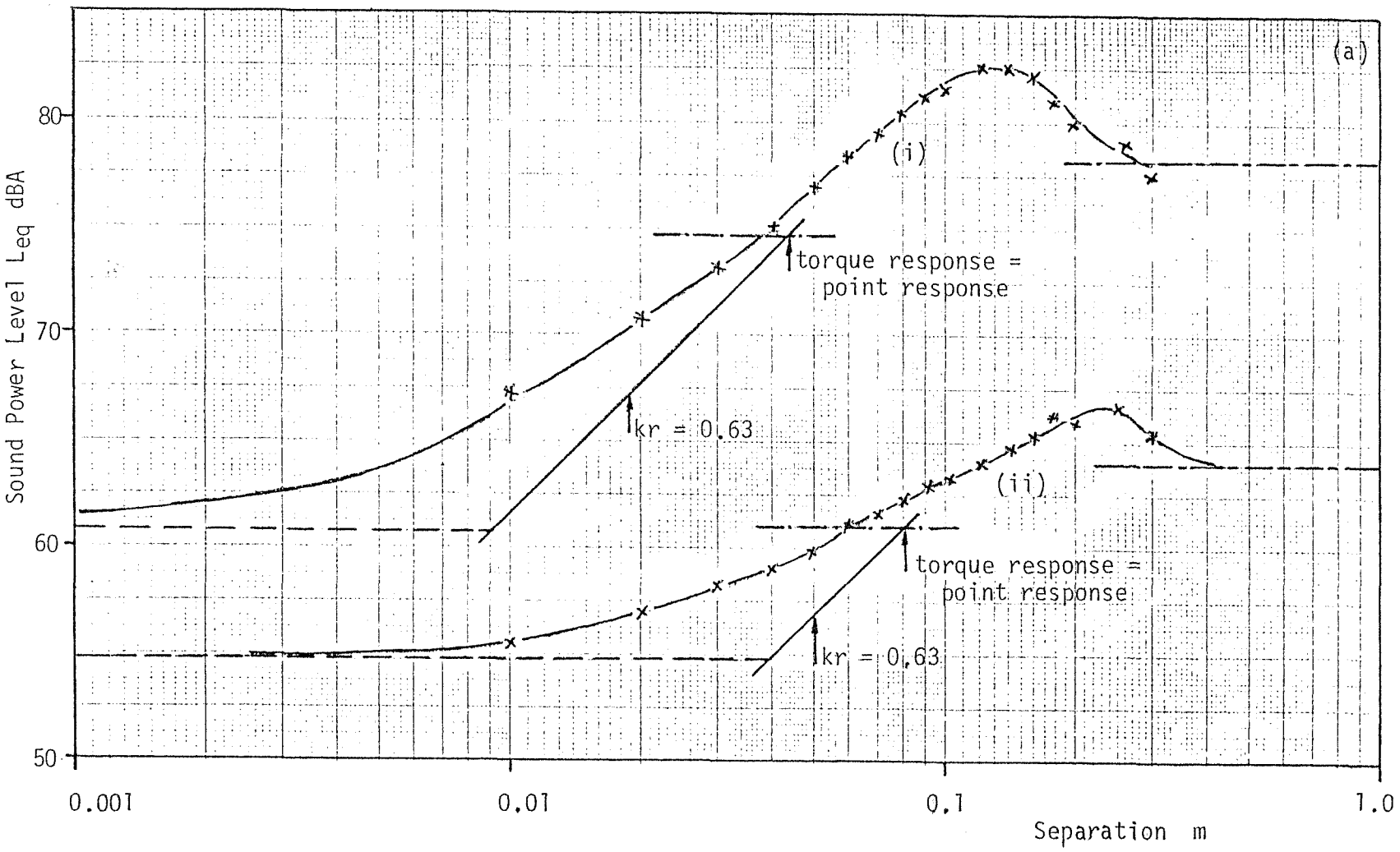
(a)
80
70
60
50
Sound Power Level Leq dBA
(i)
torque response =
point response
kr = 0.63
(ii)
torque response =
point response
kr = 0.63
0.001
0.01
0.1
1.0
Separation m

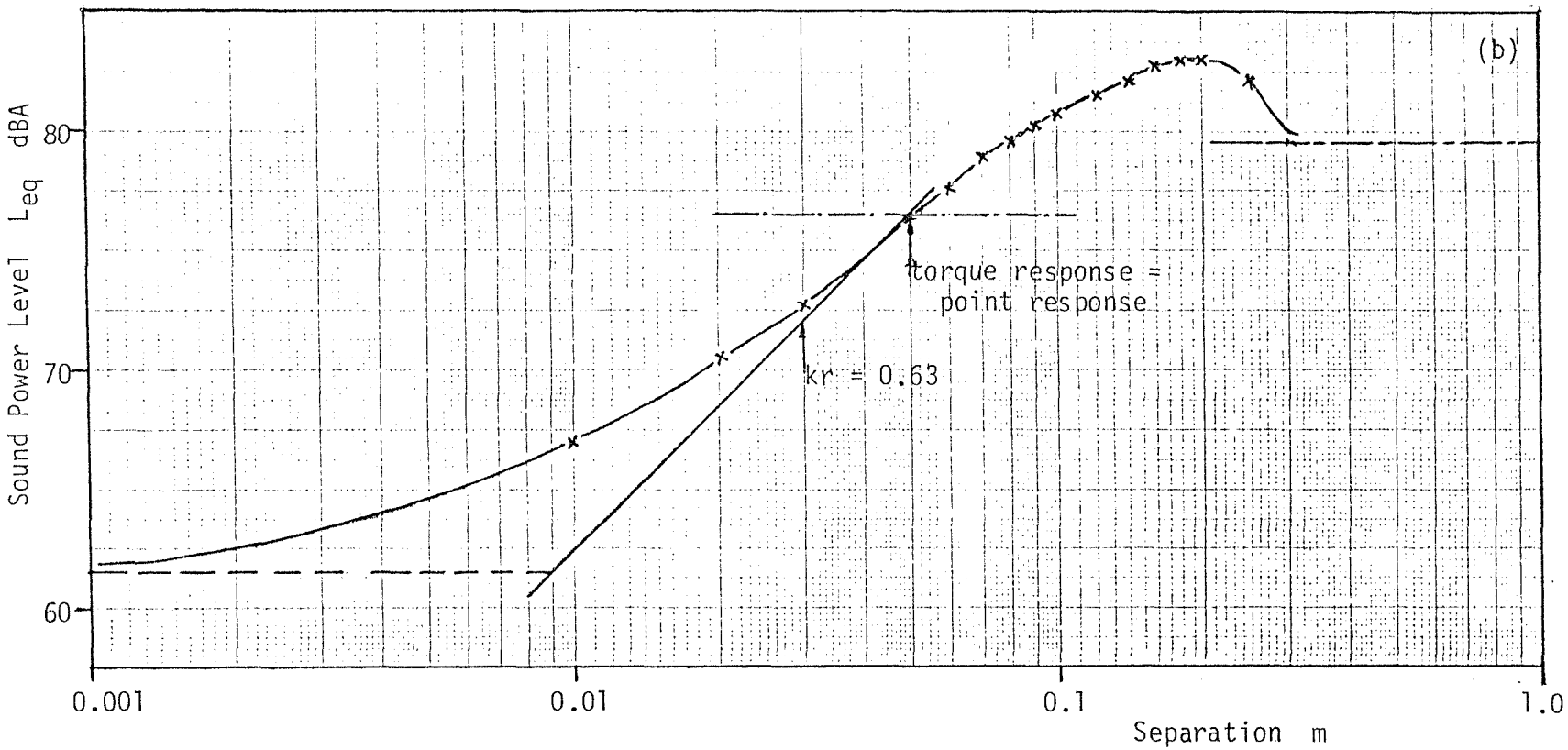
(b)
Sound Power Level L_{eq} dBA
80
70
60
0.001
0.01
0.1
1.0
Separation m
torque response =
point response
kr = 0.63

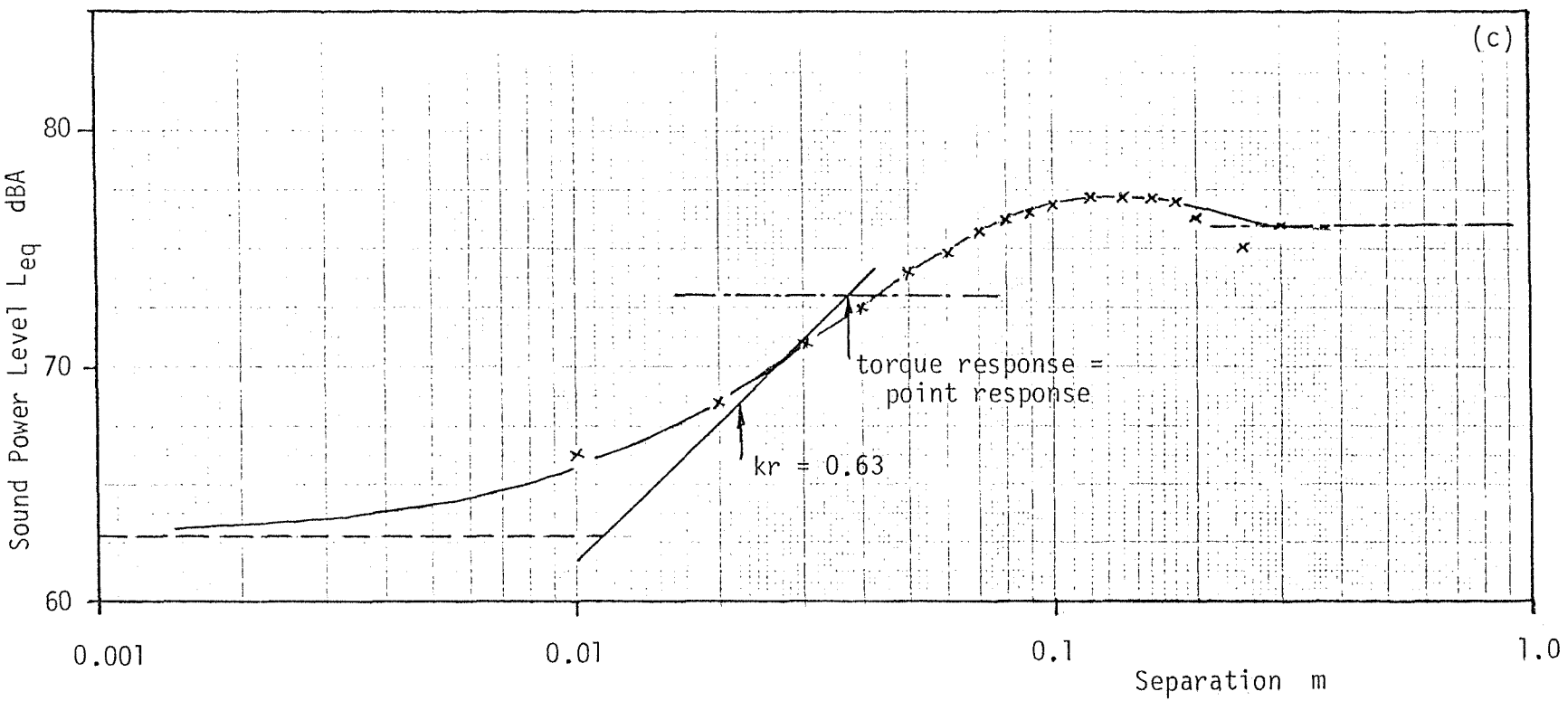

figure 7.14. Change of noise radiated with changing separation distance in one-third octave bands. –x–x–, measured; ----, noise level due to excitation at same point; – · –, noise level due to single force excitation; — -- —, noise level due to two independent forces; ——, increase of noise due to torque excitation with separation, (6dB per doubling of distance). (a) (i) 1.25 KHz; (ii) 400 Hz; (b) 1 KHz; (c) 2 KHz.

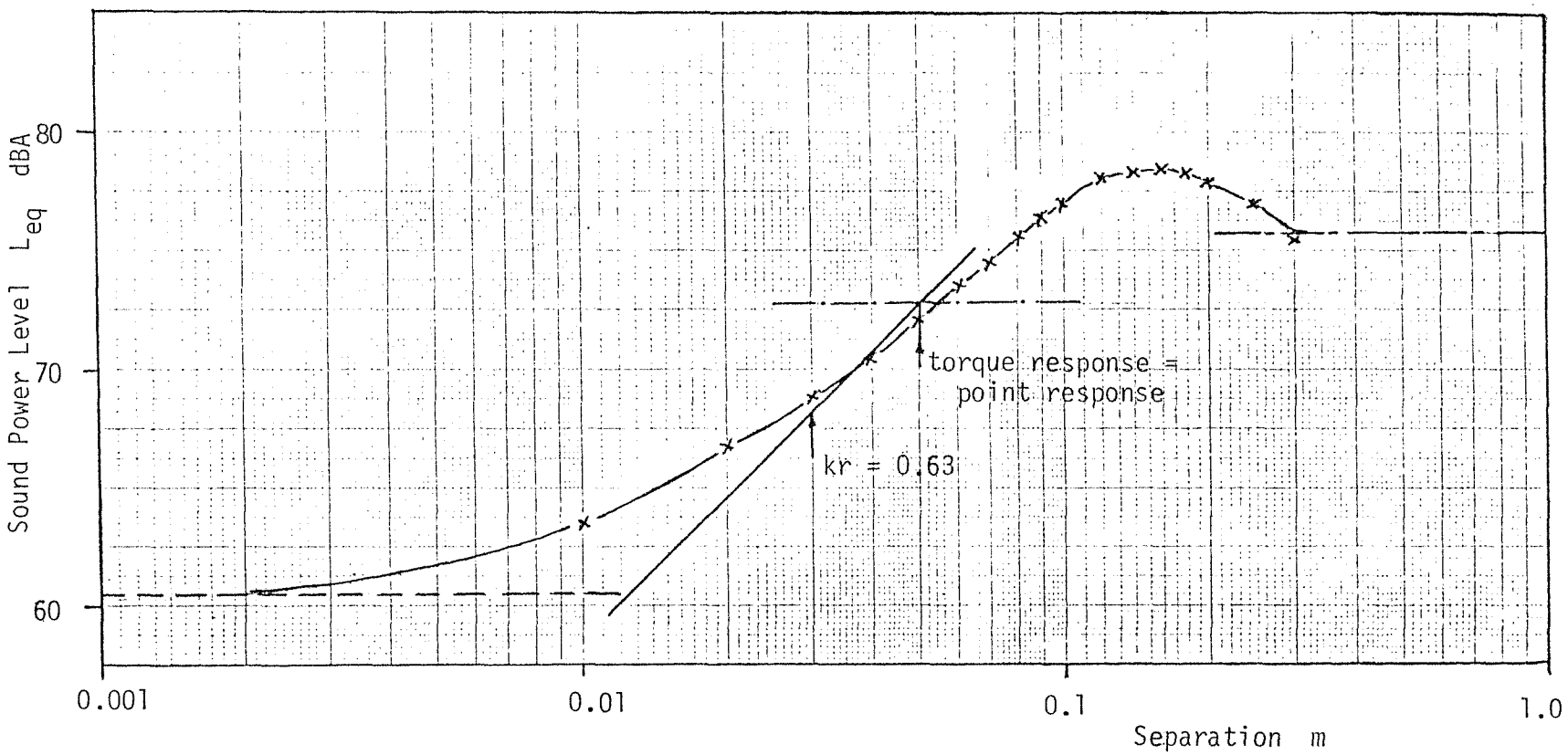

figure 7.15. Change of total noise radiated with separation distance. Maximum excitation at 1 KHz. —x—x—, measured; ----, noise level due to excitation at same point; — · —, noise level due to single force excitation; — -- —, noise level due to two independent forces; ——, increase of noise due to torque excitation with separation.

CHAPTER VIII

ENGINEERING DESIGN

VIII. 1. Introduction

In the previous chapters, it is shown that the noise energy radiated from a structure, impact excited, is given by the relation

$$L_{eq}\,(A,f,\Delta f) = 10 \log N + 10 \log |\dot{F}(f)|^2 + 10 \log \mathrm{Im}\,[H(f)] + 10 \log \left(\frac{A\,\sigma_{rad}}{f}\right) - 10 \log d - 10 \log n_s + 10 \log \left(\frac{\rho_o c}{2\pi^2 \rho_m} \cdot \frac{\Delta f}{f}\right) \qquad (8.1)$$

The terms in this equation are defined in Chapter I.

This equation gives the contribution that each of the structure parameters has on the radiated noise. Thus, it can be used as a diagnostic tool to analytically investigate which parameters can be modified for noise control. In this Chapter, the diagnostic use of this relation in engineering design, together with its limitations, is investigated.

Two of the structure parameters which are shown to be very effective for noise control measures are the force spectrum and the structural point response, that is, the parameters that control the escape energy into the structure. By tailoring of the force spectrum or the structure response, to reduce the level of escape energy into the structure, more energy remains in the impact which is neither dissipated nor destroyed. Thus, before such modifications can be used, the question of where the energy goes must be answered.

It is not possible to give a generalised answer to this question. Each problem of what happens to the impact energy has to be studied individually, with consideration of how the impact is created. In

this Chapter, the problem of where the energy goes is considered in general terms, and where generalisations are not possible, particular cases are investigated to demonstrate the problem and its effect.

The term $10 \log |\dot{F}(f)|$ represents the excitation of the structure. It is not necessary, in the noise estimation process, to use the first derivative of the force spectrum. Other orders of the derivative can be used depending on the most convenient to represent the excitation. This term controls the level and frequency content of the excitation energy. That is, by changing the duration of the impact, the excitation energy is shifted to low or high frequencies when the impact is lengthened or shortened respectively. The level of the energy depends on the magnitude of the excitation. This excitation energy is accepted by the structure, at different levels at different frequencies, depending on the shape of the point response of the structure. That is, the $10 \log \text{Im} [H(f)]$ term gives the fraction of the excitation energy that the structure accepts at each particular frequency band.

In tailoring the $|\dot{F}(f)|^2$ term, the excitation energy to the structure is channelled into frequency ranges, where the other terms of equation (8.1) do not complement to increase the total level of the noise energy radiated. Similarly, in tailoring $\text{Im} [H(f)]$, the structure is made to accept the excitation vibrational energy at frequency ranges where other terms are at a minimum in their contribution to the total radiated noise level.

The structural loss factor term $10 \log \eta_S$ is the only term in equation (8.1) which reduces the noise directly by dissipation of the vibrational energy, which would otherwise be radiated as noise. All the other terms in the equation, when modified, reflect rather than dissipate the vibrational energy, and if no other precautions are taken, no noise control may be possible by modifications of these terms. However, for high damping loss factor structures, the increase of the loss factor may not always be practical.

The A-weighting term included with the radiation efficiency of the structure becomes very important when the noise energy radiated is shifted to low or high frequencies by the tailoring of the impact force or structure response, because of the lower response of the ear at low and high frequencies. If A-weighting is not included, then

when the radiated noise is shifted to low frequencies, the total level of the noise will not be reduced, only its frequency content is changed. The radiation efficiency has a similar effect. If excitation is shifted to frequencies lower than the coincidence frequency, then the radiated noise level is reduced, provided that the structure has structural damping.

If the impact does not occur directly on the structure which is the most efficient noise radiator, then the radiated noise can be controlled by restricting the flow of the vibrational energy from the point of impact to the noise radiation efficient structure. In this case, equation (8.1) does not hold for the whole structure, provided that the reflected energy at the discontinuity is not reflected back unattenuated by the structure boundary. The point response of the structure at the point of impact does not change with the introduction of the structural discontinuity away from the point of impact and thus equation (8.1) estimates no reduction in the radiated noise, which is not true if localised losses are included between the impact point and the discontinuity. However, equation (8.1) holds for the part of the structure which is radiation efficient, that is, the noise radiated is controlled by the reduction of the escape energy to this part of the structure. A blocking mass at the point of impact, does not follow this general behaviour since lumped masses cannot store vibrational energy at audible frequencies.

In the solution of most noise problems, different methods of noise control can be used, each with its own advantages and disadvantages. From the accountancy equation (8.1), the structural modifications or tailoring of the impact mechanics, which are needed to reduce the noise where levels are high, can be deduced. The implications of these changes on the machine operation and on the machine structure have to be accurately assessed.

Chapter VII of this thesis, shows an alternative method of tailoring the impact shape and structure response by the use of active cancellation. To control the radiated noise, the method used to tailor the impact and the structure response, depends very much on the shape of the impact. As shown in Chapter VII, if the impact is

very short, then the force spectrum, in the frequency range where the ear is most sensitive, will depend on the total shape of the pulse, while, for relatively long impacts, the spectrum will only depend on the sharp changes in the force pulse. Hence, to control the noise throughout the whole frequency range, the whole of the pulse must be tailored for short impacts, while only the sharp changes need to be tailored for relatively long impacts. That is, for sharp impacts, an equal amount of energy as that of the impact or the work of the machine has to be generated to cancel the vibrations of the structure. This makes this method very inefficient and not very practical.

For very sharp impacts, the use of structural modifications and resilient inserts, to tailor the structure response and the impact respectively, are very effective as shown in the flat plate experiments of Chapter IV. Blocking masses and the softening of the impact give a very high reduction of the radiated noise energy especially at high frequencies. Thus, this is a better solution than active cancellation.

Using an active system in the case of the cancellation of the rapid changes in the impact, or the sudden unloading of the structure as in the case of a power press, the amount of energy needed is much less compared to that for the operation of the machine. Thus, an active system will be suitable in this case. Considering the noise radiated from a punch press due to the sudden unloading when material fracture occurs, if the press is unloaded more slowly by the use of the active system, activated only during fracture, large noise reductions are obtained.

The advantage of using an active system in this case is that, while structural modifications are possible, such as mass loading of the press frame so that the vibration of the frame will be at a lower level and lower frequency, these modifications will have to be very bulky to be effective and therefore will be impractical. Also, if mass loading is used, the increase in mass has to be on the top part of the frame, which will make the press frame unstable.

In the case of the power press, although only the sharp changes are cancelled, and the power needed is much less than that compared to the capacity of the press, the force loading on the frame is very high. Thus, to control the force changes, a high power system is necessary. A hydraulic system will give the necessary power, and it is more practical than an electro-dynamic system, because, the latter is bulkier. However, the response of a hydraulic system may be too slow as compared to the fast response of the press structure. Stimpson [38] is investigating methods of eliminating this delay in the response of a hydraulic system for a 25 Ton power press.

VIII. 2. Energy Considerations

When tailoring the force pulse and the structure response, the physical implication is that less energy escapes into the structure, that is, more energy remains in the impactor. If the force pulse is due to the impact from a hammer, more energy will be left in the hammer, which may bounce back. To obtain reductions in the radiated noise energy, it is important that multiple impacts do not occur, otherwise the same amount of energy will be transferred to the receiver structure over a number of impacts. If the noise energy radiated is expressed in an equivalent level averaged over a period of time, then with multiple impacts, the same noise level will result.

In the case where the impact is not due to metal to metal clashing or other impacts, but due to a pressure pulse like in combustion excitation of a diesel engine, this problem of multiple impacts will not arise. The energy that escapes into the structure from a pressure pulse is a fraction of the energy stored in the combustion charge, which, if not allowed to escape into the structure, will not be dissipated in this way but is left available to do useful work. Therefore, in this case, by restricting the escape of vibrational energy, no other problems would arise.

One method of tailoring the force pulse is to soften the impact, that is, the contact duration is longer. When softening the impact by the use of resilient material, the energy of the impactor is stored

in the resilient material during the first part of the impact. Some of this energy is transferred to the structure. The magnitude of the force acting on the receiver structure is lower than that for metal to metal impact and also acts over a longer period of time, thus less energy and of a lower frequency content escapes into the structure. The energy that is left in the resilient material is transferred back to the impactor during the second part of the impact. Thus, the impactor regains some of its original energy and therefore bounces back.

A note on the estimation of the force derivative spectrum when the pulse is of relatively long duration. As shown in the Appendix, the accuracy of the approximation method, used to estimate the noise in the cases investigated for the plate and the engine block, deteriorates with the increasing order of the derivative. Therefore, in the case of fairly long impacts with sharp changes at the front and trailing edges of the pulse, the approximate envelope for the force derivative will give an overestimate. If this approximate level is used to estimate the noise energy radiated, an overestimate in the result is obtained. The overestimate of the force second derivative spectrum is shown in figures (7.3) and (7.4) and a better approximation for the spectrum will be to use the initial value theorem as indicated in Appendix A.

The noise estimates obtained in Chapters V and VI are for very short impacts, where the approximation was within 1dB of the true force spectrum in the frequency range where the spectrum had a maximum level. Thus, in these cases, the estimates obtained do not give an overestimate of the noise energy. If the initial value theorem is used in case of hard impacts, there is an underestimate in the frequency range where the spectrum has a maximum level. For soft impacts, the second derivative spectrum of the force is mostly flat in the region where the ear is most sensitive to noise and therefore, the initial value theorem will be more appropriate. This method still relates the level of the spectrum to measurements in the time domain, as shown in Appendix A, and similar analysis to tailor the impact can be done as in the case of hard blows.

In the case of structural tailoring to reduce the escape energy, the response level of the structure per unit force is reduced, that is, the structure is made more rigid. If the rigidity of the structure is increased, a point is reached when the structure will be completely rigid and in this case, no energy escapes into the structure. If the impact is due to the blow of a hammer, the hammer strikes a surface which is completely rigid, then no energy will be transferred from the hammer, and the latter will bounce back with exactly the same velocity as the impact velocity. In practical structures, impact surfaces are seldom completely rigid and therefore, some energy will escape into the structure, but this energy can be controlled by making the structure more rigid, that is, reducing the structure response. In the case of impacts due to hammer blows, the same will happen as in the case of the softening of the impact, that is, multiple impacts may occur and the same amount of energy will be transferred over a period of time. If multiple impacts do not occur, very high reductions in the radiated noise are possible, such as the reductions of the radiated noise from the plate when structural tailoring is done at the impact point.

When the flow of the escape energy is restricted by structural changes away from the point of impact, that is, including a mobility mismatch along the path of energy flow, in general, some of the escape energy will be reflected back at the structural discontinuity. In the case of an infinite structure, with vibrational energy flowing in one direction, a structural discontinuity will reflect some of the vibrational energy and this energy will propagate away from the discontinuity. Since the structure is infinite, the reflected energy will not return towards the discontinuity. However, for a finite structure, the reflected energy will meet the structure boundary and is reflected again to return to the discontinuity. If there are no losses in the structure between the discontinuity and the boundary where there is the input of energy, then, the reflected energy from the first incidence on the discontinuity will continue to be reflected back and forth between the discontinuity and the structure boundary without any attenuation, until all the energy is transferred through the discontinuity.

In this case, applying equation (8.1) to the noise radiation efficient part of the structure, N does not only represent the number of impacts that occur per second but also includes the number of reflections. However, one is not able to quantify this, although, if no losses are present, reflections will continue to occur to transfer all the available energy.

This is similar to the case of multiple impacts and therefore, the same level of noise will be radiated. However, if losses are included in the structure between the discontinuity and the structure boundary, then some of the reflected energy will be dissipated and thus less vibrational energy will be available each time the flow of energy is reflected in consecutive incidences.

The reduction of the escape energy expected will depend on the discontinuity included in the structure, but also on the localised losses between the discontinuity and the structure boundary. Only if localised damping is very high, so that none of the reflected energy comes back, will the full attenuation, due to the discontinuity, be obtained. Different discontinuities give different levels of attenuation, and expressions for the attenuation possible, in the case of no return of the reflected energy, are found in reference [1] .

The difference of a structural discontinuity as compared to discontinuities for the transmission of acoustic waves in ducts is that, in the latter case, the wavelengths are relatively short and the discontinuity can be placed such that the reflection interacts with the generated noise to cancel part of the radiated noise energy. In structural problems for longitudinal vibrations, the wavelengths are much longer, thus making an analogous solution impractical.

However, what exactly happens to the escape energy will depend on the type of structural discontinuity present. In the case of the impact excitation of the plate investigated in Chapter V, the level of energy that escapes into the plate is reduced by the addition of the blocking mass and the blocking mass and the resilient pad. In the former case of the blocking mass directly fixed onto the plate, the escape energy is reduced because the structure is made more rigid at the point of impact, especially for high frequencies. The mass itself does not store any energy, since its first natural frequency of ringing is about 26 KHz.

In the case of the blocking mass fixed onto the plate via the resilient material, the level of energy that escapes into the plate is lower than that for the mass directly fixed on the plate. The resilient material acts as a structural discontinuity to further restrict the flow of vibrational energy. However, since the lumped mass does not store any energy, the problem of multiple incidences does not occur, in fact, the structure response level is reduced at the point of impact, and thus less energy actually escapes at the impact point. The loss factor of the resilient pad does not affect the amount of energy that escapes into the structure. Figure (8.1) shows that the frequency averaged point response for a blocking mass fixed onto a plate via a resilient material is independent of the loss factor of the resilient pad, except at the combined natural frequency of the mass, resilient pad and receiver structure. That is, less energy flows into the plate , not because energy is dissipated within the resilient pad. The loss factor of the resilient material will only reduce the level of escape energy to the plate, if energy can be stored in the system where the impact occurs.

In this case, the mass does not store any energy and energy can only be stored in the mass-spring system composed of the blocking mass and the resilient pad, and thus, the loss factor is effective in restricting the level of escape energy only near the natural frequency of this system. At this frequency, the level of the response is inversely dependent on the loss factor of the resilient pad. For the stiffness of the resilient pad and mass used in the experiments of Chapter V, this natural frequency is about 100 Hz. The curves in figure (8.1) for the different values of the resilient pad loss factor differ only at frequencies near 100 Hz.

A physical explanation for the restriction of the vibrational energy flow for the case of a lumped mass mounted onto a resilient pad is that, because of the inertia of the blocking mass, the high frequency energy is not transmitted. The low frequency energy that is transferred by the mass, when moving as a rigid body, is stored in the resilient material. Some of this stored energy is transferred to the receiver structure, some is dissipated due to the resilient pad loss factor and some is transferred back to the mass which is then

transmitted to the impactor.

If the structure which receives the impact (source structure) does not behave like a rigid mass, that is, the source structure can store vibrational energy, then during the impact, energy is transferred to the source structure. The inclusion of the resilient interlayer between the source structure and the receiver structure may not reduce the total vibrational energy that will flow into the receiver structure. The reduction of energy flow will only occur if there are losses in the resilient pad and the source structure, since multiple incidences will occur in this case, at the structural discontinuities.

VIII. 2.1. Results in Practice

The above energy considerations can be observed in some results obtained in the control of radiated noise from an engine structure due to combustion and piston slap excitation, where only $|\dot{F}(f)|^2$ and Im $[H(f)]$ terms are modified. In Chapter VI, it is shown that the flow of energy due to combustion excitation is through the con-rod, via the crankshaft and into the engine frame. Therefore, if a discontinuity is inserted along this energy flow path, some of the vibrational energy due to the combustion forces should be reflected back. A change in the cross-sectional area of the con-rod will act as a structural discontinuity (figure 8.2).

Setting up an experiment to verify this, a ring of lead is melted onto one of the con-rods of the engine used in Chapter VI. The noise energy radiated from the engine frame with the modified con-rod, when impacted on the piston top is compared to the results for the normal con-rod. The transmission loss, due to the change in cross-sectional area when the ring of lead is fitted onto the rod, is shown in figure (8.3), that is, a reduction of 8 to 9dB at high frequencies. However, this transmission loss is for the propagation of vibrational energy in an infinite structure, that is, when the reflected energy does not return towards the discontinuity in the structure.

Comparing the noise radiated in the two cases, there is no change at all. Figures (8.4) and (8.5) show the noise radiated by the

normal con-rod and the noise radiated by the modified rod. The total noise radiated is exactly the same, with also the narrow band noise energy very much alike. There is a slight difference of the high frequency peak in the narrow band spectrum due to the fact that the ring is of a different material and also because it is not an integral part of the con-rod. The reason for the fact that no change at all occurs in the radiated noise is due to the multiple reflections as explained above, and there are no losses to dissipate the reflected energy.

From the response of the piston/con-rod assembly (figure 6.13(a) in Chapter VI), the con-rod behaves like a rigid mass up to about 2KHz. Thus, no energy is stored in the con-rod below this frequency. Also from figure (6.13(a)), the con-rod/piston assembly has its first natural ringing frequency at about 4KHz, that is, energy will be stored within this assembly at this resonant frequency. Hence, energy from the impact will be transmitted through the rod above the first natural frequency and by the rod moving as a rigid body, at frequencies below this natural frequency, where the rod behaves like a solid mass. To reduce this latter transmission of energy and therefore, the noise energy radiated, an increase in mass is necessary. With the addition of the ring on the con-rod in the experiment, the increase in mass is less than 0.5 Kg, thus the decrease expected due to this increase in mass will be minimal. The energy that is transmitted through the rod will be reflected at the structural discontinuity. However, if there are no losses between the discontinuity and the piston-top, the reflected energy will be reflected back and forth between discontinuity and structure boundary until all the energy is finally transmitted. That is, the transmission loss as given by figure (8.3) will not be real.

To reduce the transmission of energy in this case, a loss mechanism must be included in the structure. On the experimental rod, some wire is wound round the top part of the con-rod, between the discontinuity and the piston top, to create frictional losses. Measuring the noise energy radiated by the engine frame, with the piston again impacted on the top (figure 8.6) and comparing the results to those obtained in the previous cases, there is a slight

change in the level of noise at high frequencies, which is less than that suggested by the transmission loss. The full transmission loss will only be attained if the losses dissipate all the reflected energy. However, comparing the narrow band spectra for the noise energy radiated in all these cases, the high frequency peak is completely removed, that is, this resonance decreases in level by about 8dB , which is equal to the transmission loss as given by the change of cross-sectional area. Hence, it can be concluded that to reduce the noise energy radiated, a structural discontinuity will not give any reductions unless a dissipative mechanism is included in the structure before the discontinuity.

If the localised damping between the discontinuity and the piston top is very high, the noise reduction is only at very high frequencies, the low frequencies are not affected at all. However, for much larger engines, the con-rod will be longer and the response will not be mass controlled up to high frequencies, as obtained in these experiments. For large con-rods, the introduction of a structural discontinuity of the right size, together with a dissipative mechanism, will also affect the medium range frequencies. Also, in this case, more than one discontinuity can be included with a dissipative mechanism in between. This will be particularly useful to cancel the transmission of energy at a particular frequency range by tuning the separation and size of the discontinuities.

From the response curves, the piston, con-rod, crankshaft and engine frame system is equivalent to the plate with the blocking mass directly fixed, as in Chapter V, since the response of the piston/con-rod is mass controlled up to relatively high frequencies. Therefore, to obtain large noise reductions similar to the reductions obtained in the plate experiments, either the piston/con-rod is made more massive, or, resilient material is included between the con-rod and the crankshaft at the bearings. The increase of mass of the piston/con-rod is investigated for a slight increase in mass of the piston crown.

The conclusion, that no change will occur in the radiated noise due to a change in the con-rod, can also be obtained by considering

the equation for the response Im [H(f)] , (equation (6.13)). The piston/con-rod response is mostly mass controlled, and to change the level of equation (6.13), the mass must be increased substantially. The increase of the damping of the con-rod reduces the peak of the first natural frequency, but the mean level of the response does not change at all. Therefore, the energy transferred, due to this peak, is reduced, as obtained in the measured narrow band noise results, but the general level of the response is only slightly affected, which results in the level of the noise hardly changing. The reduction is of about 1.5dB, due to the removal of the resonant peak by the increased con-rod loss factor.

If the piston-top is made more rigid, by increasing the piston crown mass, the response level will decrease, although again only slightly because the increase in mass is very small. Figure (8.7) shows a comparison between the noise energy radiated form the engine frame with a normal piston and that with a loaded piston. At low frequencies, there is no change at all because the increase in mass is only of 0.2 Kg , but at high frequencies, near and above the con-rod first resonant frequency, there is a 2dB reduction in noise. The energy stored in the con-rod at these frequencies is reduced, due to the increased rigidness at the point of impact, thus less energy flows into the rod during the impact. This energy is not allowed to escape into the structure, that is, in the experimental tests it will remain in the impactor, while on a running engine, this energy will remain in the combustion charge to do useful work. In this case, no dissipative mechanism is needed because unlike the loaded con-rod, the energy is not reflected within the system, but is reflected before or, in other words, not allowed to enter the structure.

Multiple impacts due to the rattling of pistons are investigated for the case of piston slap excitation. If the cylinder liner is made of a softer material, when the piston impacts the liner, energy will be stored in the liner. Some of this energy escapes into the engine structure. However, the first impact of the piston will be of a lower magnitude and a longer duration, thus the escape energy into the engine structure will be at low frequencies. The energy left stored

in the liner will be transferred back to the piston during the second part of the impact. At the same time, the piston is acted upon by other sideway forces due to its inertia, and the force exerted on the piston will be a combination of these two forces. When the inertia force decreases, the piston leaves the liner with a higher velocity as compared to the case where only the inertia forces are present, thus the impact on the other side will be of the same magnitude as that of metal to metal, but at a lower frequency. Thus, in the steady running of the engine, the same amount of energy will be transferred, although this escape energy will be at a lower frequency. Hence the engine will radiate more low frequency noise. In practice, the resilient material will usually have a high loss factor such that some of the energy stored in the liner will be dissipated.

An experiment is set up where the normal liner is removed and instead an isolated liner, mounted on rubber pads at the top and bottom water decks, is used. The inserted liner is made out of mild steel. The noise radiated from the engine frame is measured when the piston is moved from side to side, as in the experimental set-up shown in figure (6.19) of Chapter VI. One of the first observations is that, since the liner is more resiliently mounted, the force of the piston on the cylinder is completely different. The sharp impacts, as obtained with the normal liner, disappear to a much lower frequency impact except for very shallow peaks, due to the initial metal to metal impact. Figure (8.8) shows a comparison between the piston sideway impacts for a normal liner and for the isolated liner. In the latter case, the liner was tested both undamped and with the addition of damping tape. Increasing the liner damping slightly, decreased the sharpness of the piston impacts. However, the level of the sideways force does not change at all in these situations. This is because the resilient liner will soften the impact, but does not change the amplitude of the impact, as for a liner made of resilient material.

During the piston impact, the liner will mainly store energy in its resonant modes, and this energy will be transferred to the engine structure at these frequencies if no losses are present. The resilient material will have some losses, and thus some of the energy

will be dissipated. However, to obtain a reasonable reduction in the radiated noise energy, more energy has to be dissipated than just that in the resilient mountings. Figure (8.9) shows the response for the normal liner and the damped and undamped isolated liner. The normal liner has a high value of loss factor due to the fact that energy transfers directly to the rest of the engine frame. The response for the isolated liner shows a resonant frequency at about 300 Hz which corresponds to the whole bodily movement of the liner on the resilient pads. The resonance at about 1.5 KHz is the first ringing frequency of the liner.

Taking into consideration the shape of the impact and the resonant frequencies of the liner, the noise radiated with the isolated liner is expected to be lower at some frequencies, although the decrease in the noise energy radiated is not expected to be high for the undamped liner due to the fact that there are no losses. Some reduction in noise energy radiated will occur because of the change in the sideway force. Figure (8.10) is a reproduction of figure (6.24) for a normal liner, with the acceleration noise from the shaker table removed, and figure (8.11) is the noise energy radiated with the undamped isolated liner.

The first observation is the high levels of noise that occur at the resonant frequencies of the liner, which can be seen both in the narrow band spectrum and the one-third octave band spectrum. However, the noise energy radiated is not entirely from the engine frame and the high levels of noise at these frequencies are not entirely due to the fact that more energy is transferred to the engine frame at these frequencies. The radiated noise with the isolated liner is higher than the noise radiated with the normal liner, although the increase in noise depends very much on the alignment of the piston inside the liner. Most of the increase in the noise energy is due to the direct noise radiated from the ringing of the liner itself, which in the experimental set-up is not covered at all, unlike in a running engine. In this case, the liner will be covered by the oil sump underneath and by the cylinder head on top.

If a screen is fitted on the top and bottom of the engine to cut

off the direct noise from the liner, the radiated noise energy from the engine frame is obtained (figure 8.12). The resonances are still apparent since the energy stored in the liner at these resonant frequencies will be transferred through, due to multiple incidences. There are no other losses except those due to the resilient pads. At low frequencies, the level of the noise increases due to the higher low frequency excitation and because the combined natural frequency of the liner, resilient pad and engine frame occurs within the frequency range of interest. The reduction in noise is mainly due to the change of the shape of the impact.

The change in radiated noise is verified by measurement of the surface velocity of the engine frame. The level of the surface velocity is lower when excitation is through the isolated liner (figures 8.13 and 8.14), except at the natural frequencies of the liner. This is the same as the measured radiated noise energy. At low frequencies, the level of the surface velocity with the isolated liner is higher due to the higher low frequency excitation and the combined natural frequency.

If the isolated liner is damped, then losses which should dissipate some of the reflected energies will be included, especially at the resonances of the liner. Figure (8.15) shows the surface velocity of the engine frame when excited by an impact of the damped isolated liner. The high levels at the resonances of the liner are removed, only the low frequency combined natural frequency remains, and this is unchanged in level since the loss factor of the resilient material is not altered.

Therefore in this case, the noise energy radiated should be lower. However, in making the noise measurements. the same problem as before is encountered, that is, the direct noise from the liner predominates the noise radiated. Figure (8.16) shows the radiated noise and there is still the influence of the liner resonances, due to the fact that the noise includes the direct noise from the liner. If covers are fitted onto the engine to cut off the direct radiated noise (figure 8.17), the total noise energy radiated by the engine frame is reduced by about 10dB as compared to the normal liner, and the distinct resonance frequencies of the liner are very much reduced.

These experiments verify the energy considerations as discussed in the beginning of this section. The energy transferred during the impact is not dissipated at all in the case of the undamped isolated liner and the loaded con-rod. There are no dissipative mechanisms to dissipate the reflected energy. In the case of the isolated undamped liner, the only noise reduction is due to the change in the impact force shape. Comparing the impact force for the normal liner to that of the undamped isolated liner (figure 8.8(a) and (b)), the magnitude of the sharp impact is reduced to about one-third, but the low frequency content increases. Thus, the noise reduction expected will be of about 4dB or slightly less due to the increase of the low frequency. In the measured results, the reduction in noise is of 2.5dB.

With the introduction of the damping in the liner and the friction losses on the con-rod, the energy that is reflected due to the structural discontinuity is dissipated. This results in a reduction of the total escape energy into the engine frame with a corresponding reduction in the radiated noise. With the isolated damped engine liner, energy is dissipated within the liner. The increase in damping of the damped liner is about five times over that of the undamped liner. In this case, the reflected energy is a large portion of the incident energy. Thus, the noise reduction with the addition of the dissipative mechanism will be very close to the increase of the loss factor of the liner. Therefore, the noise reduction expected will be about 4dB due to the change in the impact force, which is similar to the undamped liner, and about 6dB due to the increase in the liner damping. However, there is a slight increase of noise at low frequency. Hence, the total reduction will be of 10dB or less. The measured reduction of the noise energy radiated in this case is of 8.5dB.

VIII. 3. Future Work

Two areas of work that follow from this parametric study are: (1) To use this new method to estimate the noise energy radiated, to completely redesign an existing machine structure which is too noisy.

Modifying the existing version of the machine cannot give the desired attenuations in the noise energy radiated. Although the study of the existing version will give the necessary insight into the machine characteristics and operational demands, large enough reductions of noise cannot be obtained by modifications alone. The noise radiated from most machines has to be drastically reduced because of the high propability of legislation to regulate the maximum radiated noise levels of machines. Also, in todays environment, the noise reductions must be very high because of the continuous increase of noise due to the larger size of machinery. The investigation for a complete redesign should also include the understanding of what happens to the energy that is not allowed to escape into the structure.

(2) The development of an active force cancellation system, especially a system whereby different portions of the excitation force can be controlled, thus making the active system more efficient and practical. The practical application of an active force control system to control the radiated noise from a structure will then follow.

Another area of work is the understanding of the structural loss factor. In this investigation, the structural damping has been either assumed or measured. Thus, it was not possible, because of the lack of understanding , to optimise the structural damping in the whole or parts of the frequency range of interest. To make this possible, a complete understanding of the different damping mechanisms like friction, air pumping, fluid pumping, etc., must be obtained together with knowledge of the interaction of the different mechanisms, when more than one is present in a structure. The different mechanisms give a high structural loss factor at different frequency ranges. Thus, it will then be possible for noise control purposes, not only to tailor the structure response or the pulse shape, but also to tailor the structural loss factor. Also, the question of how a mechanism can be changed from one type to another with changing frequency, needs to be investigated.

Other areas for future work are the application of similar analysis to the problem of fatigue failure and stress levels induced in a structure due to vibrational motion, and the development of the energy accountancy concept to be applied in cases where the interaction between the structure and the surrounding medium cannot be neglected.

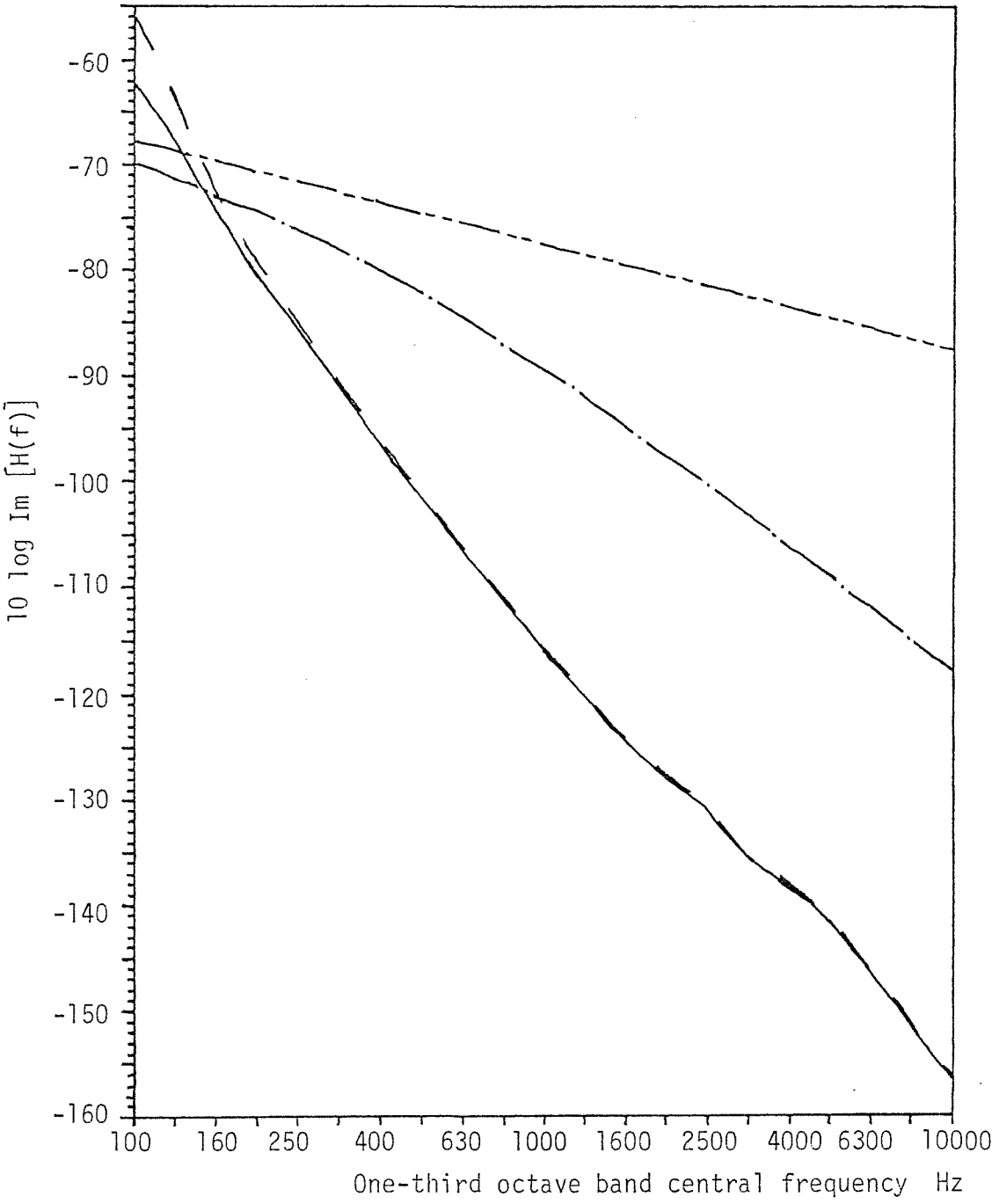

figure 8.1. Structure point response for a 1cm thick plate with different structural tailoring at the point of impact. — -- —, Plate; — · —, plate with blocking mass (3.5 Kg); ——, plate with blocking mass on resilient pad with loss factor of pad $\eta = 0.25$; ---, plate with blocking mass on resilient pad with no loss factor, $\eta = 0$

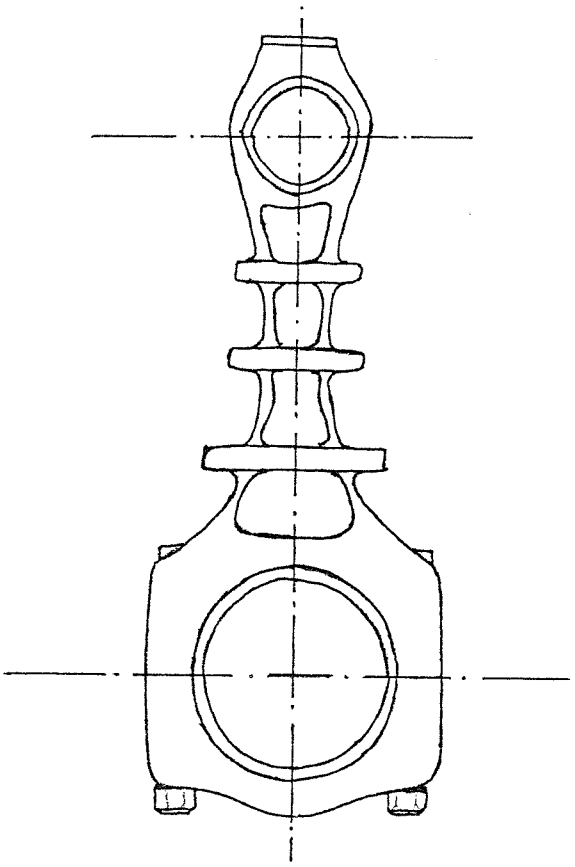

figure 8.2. Con-rod design for cobustion noise control.

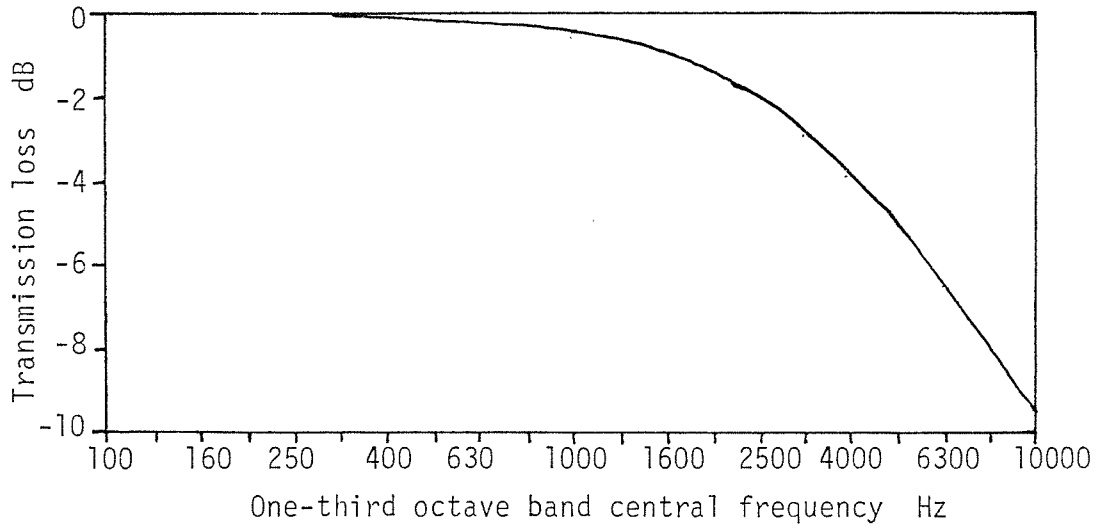

figure 8.3. Transmission loss for the change in cross-sectional area of experimental rod.

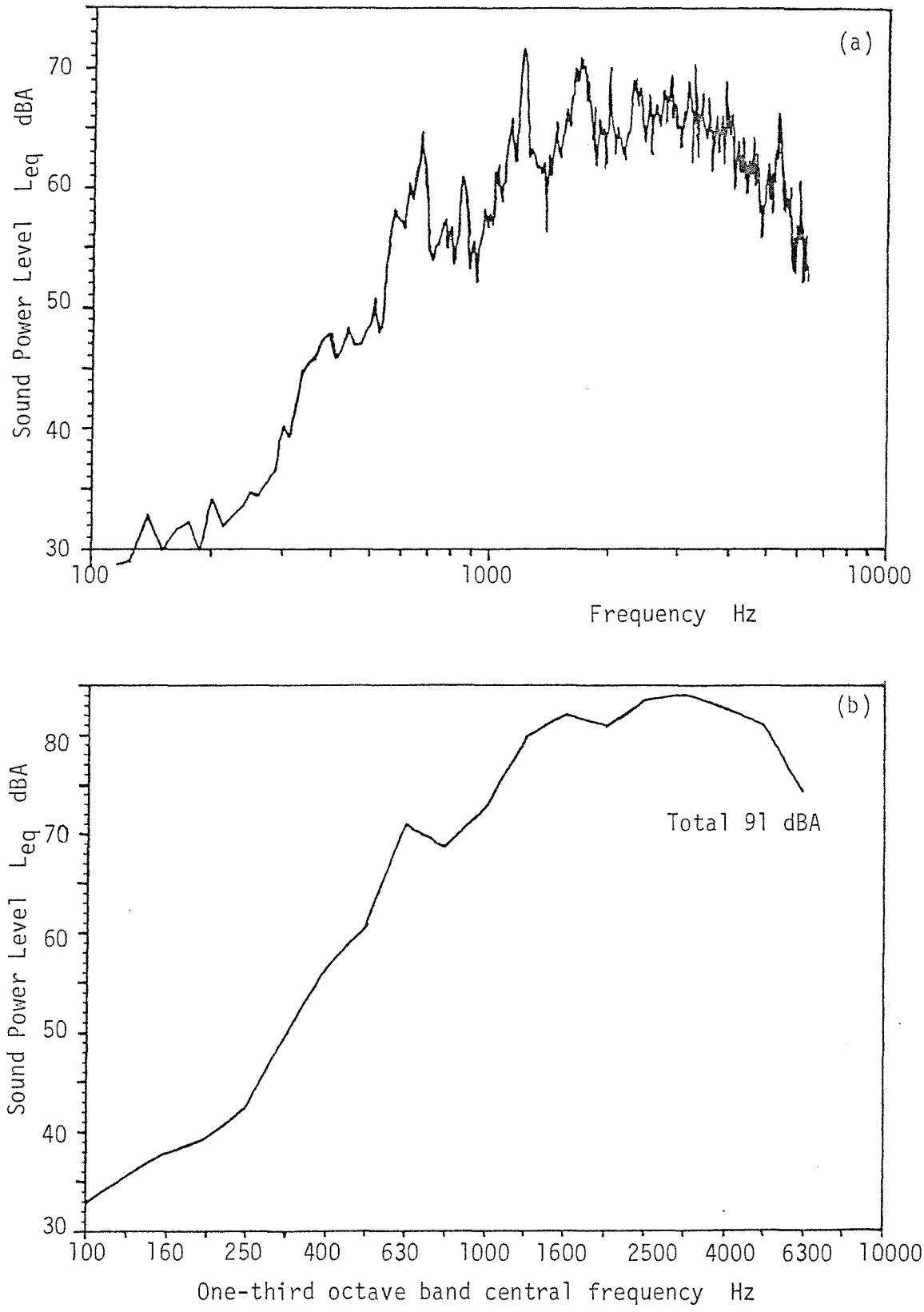

figure 8.4. Noise energy radiated by engine block with the normal con-rod under simulated combustion forces.
(a) narrow band; (b) one-third octave bands.

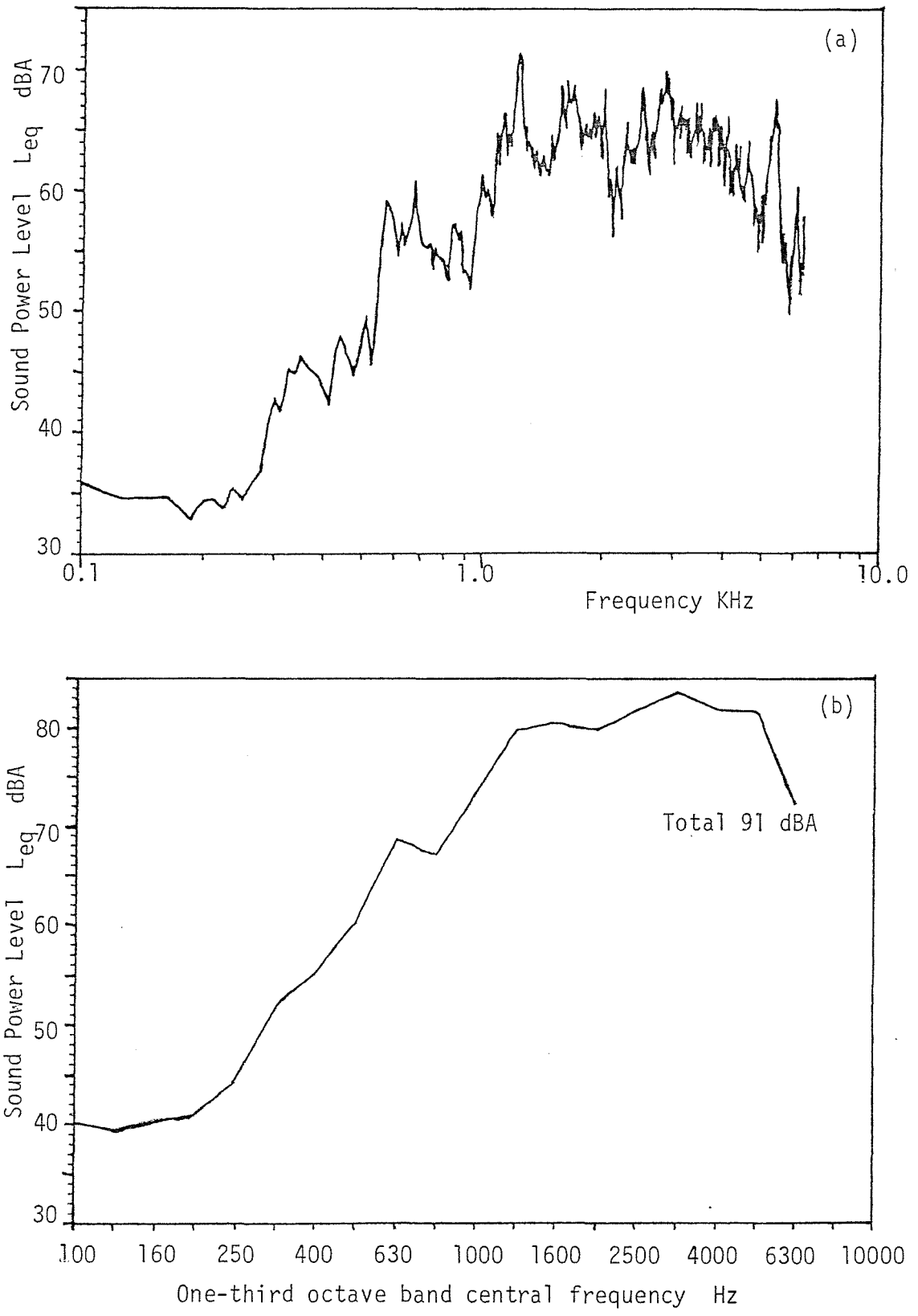

figure 8.5. Noise energy radiated by engine block with experimental con-rod. (a) Narrow band; (b) one-third octave bands.

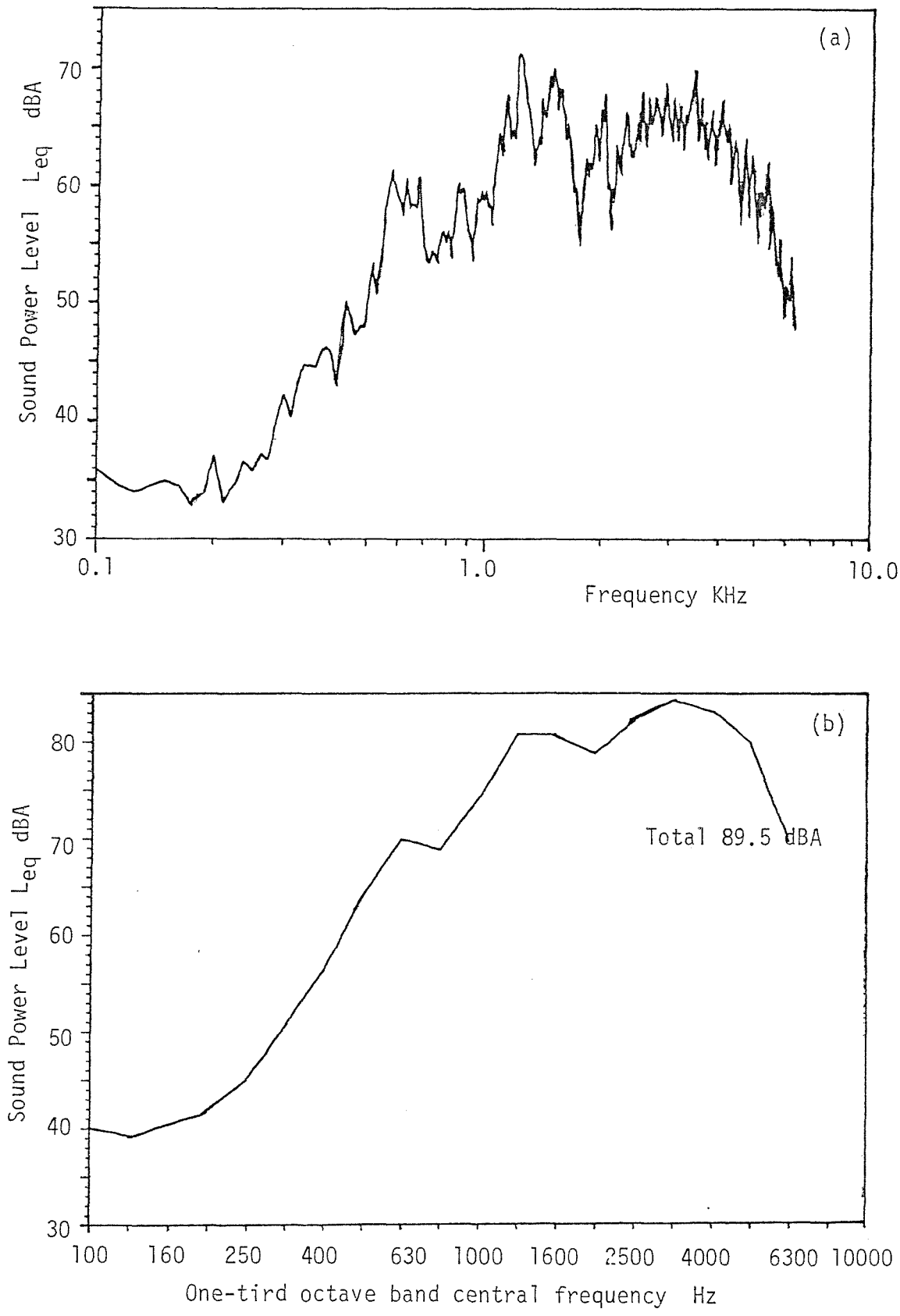

figure 8.6. Noise energy radiated by engine block with experimental con-rod with a damping mechanism between discontinuity and piston top. (a) Narrow band; (b) one-third octave bands.

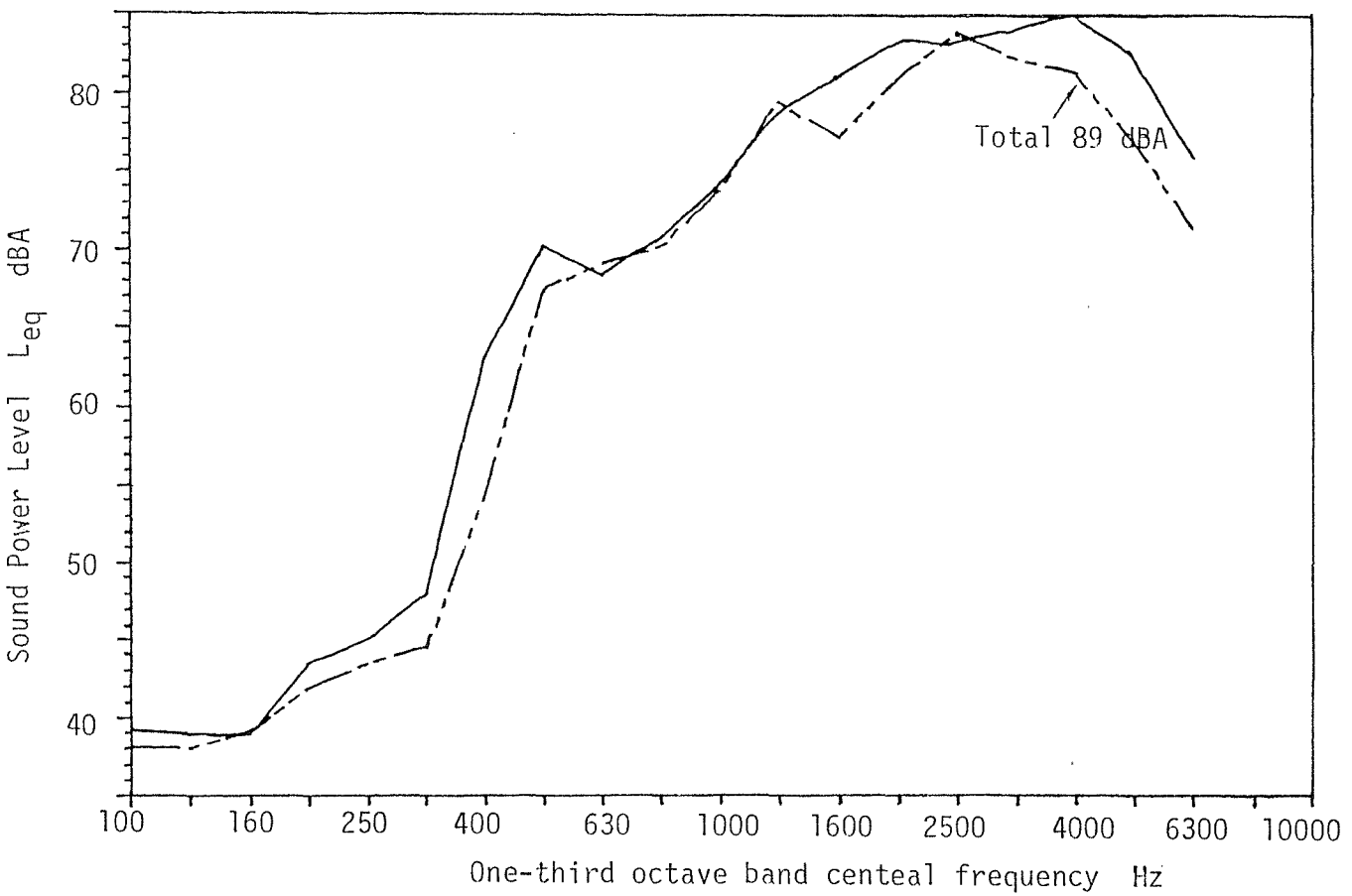

figure 8.7. Noise energy radiated by engine block under simulated combustion excitation: ——, with normal piston; — -- —, with an increase in mass of the piston crown, increase of 0.2 Kg.

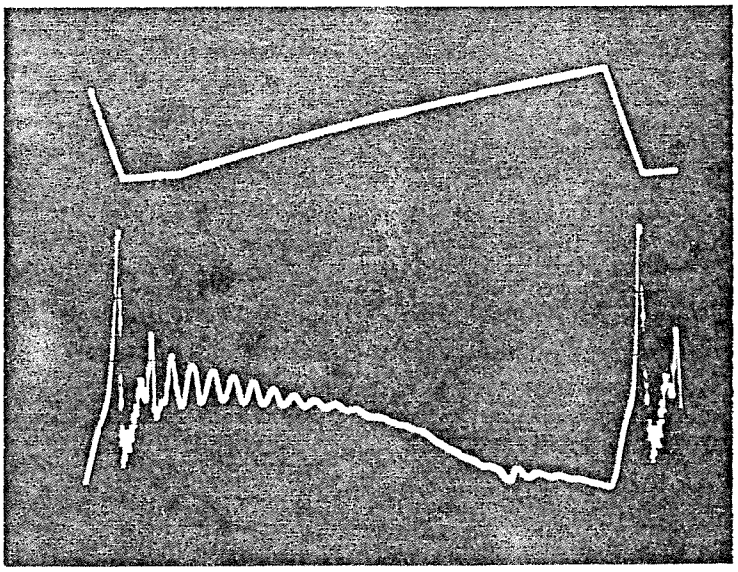

(a)

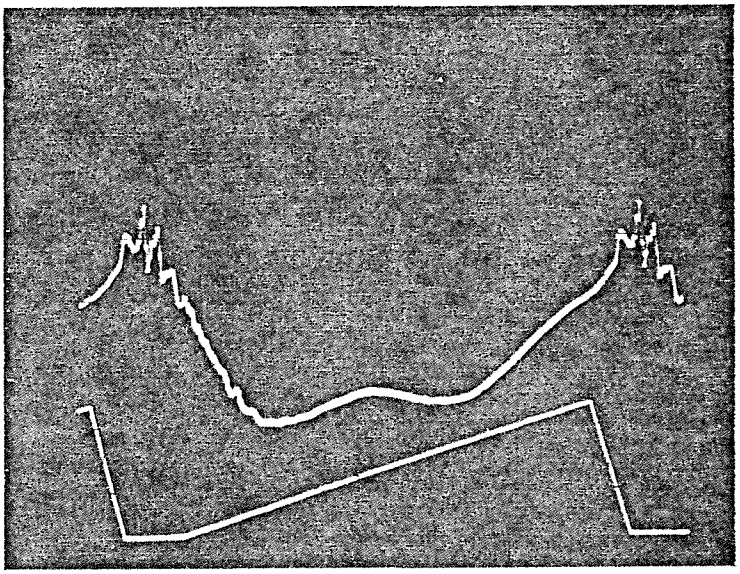

(b)

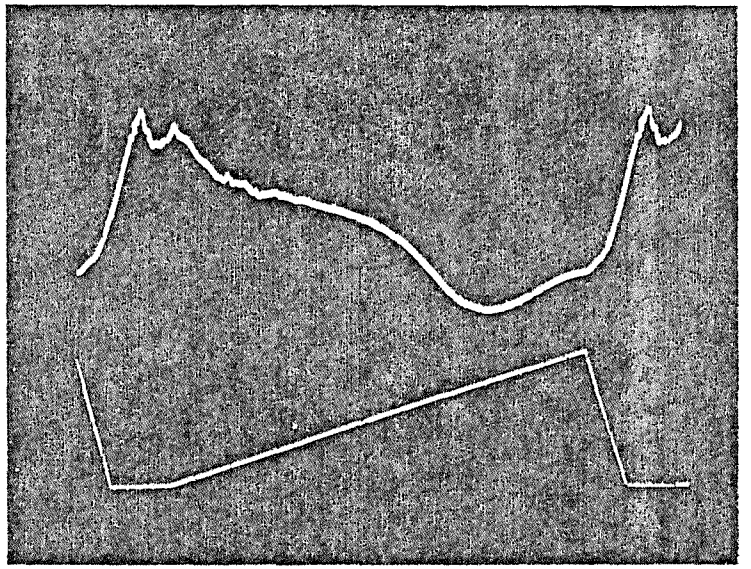

(c)

figure 8.8. Side excitation of piston onto cylinder liner in simulated piston slap. (a) Normal engine liner; (b) isolated liner; (c) isolated liner + damping on liner. The sawtooth waveform is the input to the exciter.

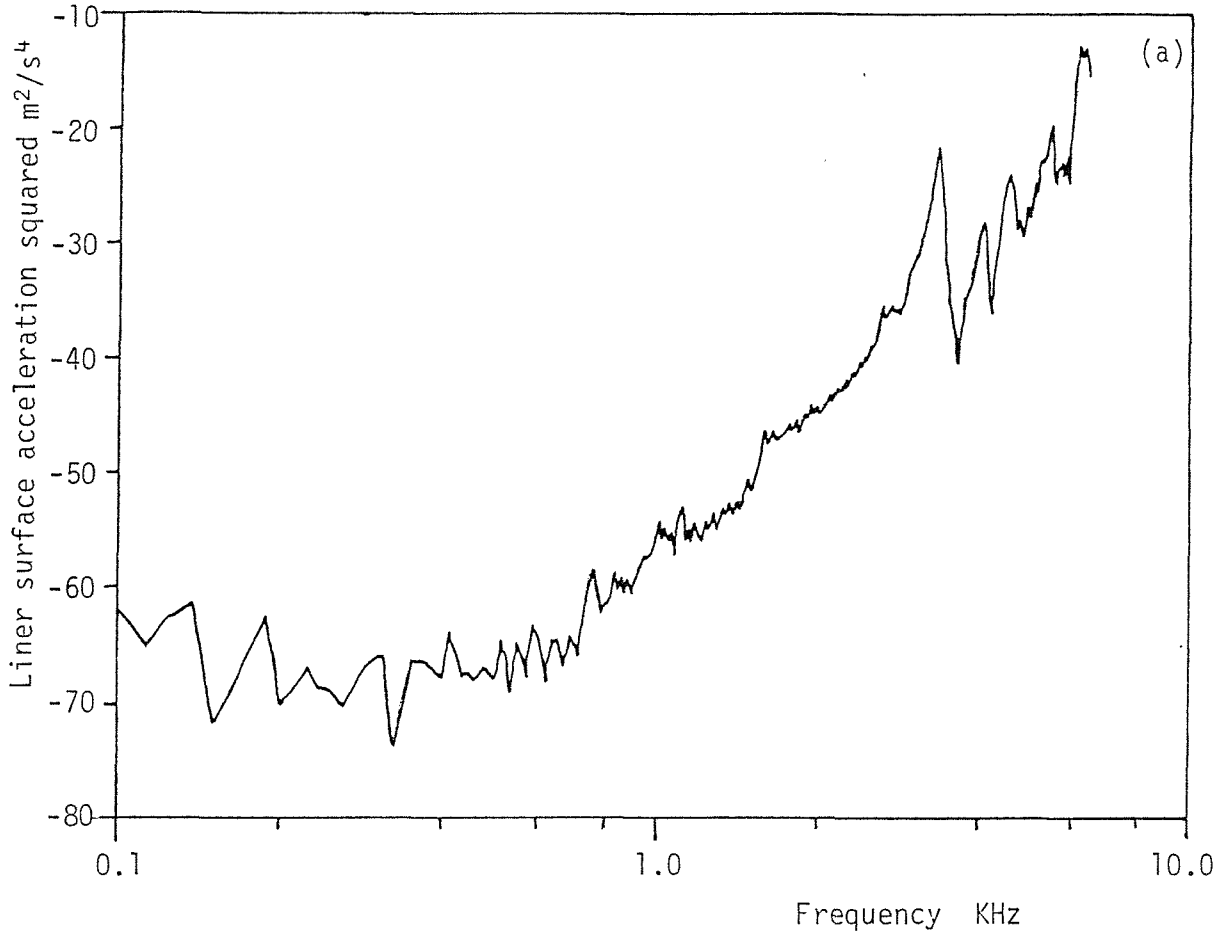
(a)
Liner surface acceleration squared m²/s⁴
-10
-20
-30
-40
-50
-60
-70
-80
0.1
1.0
10.0
Frequency KHz

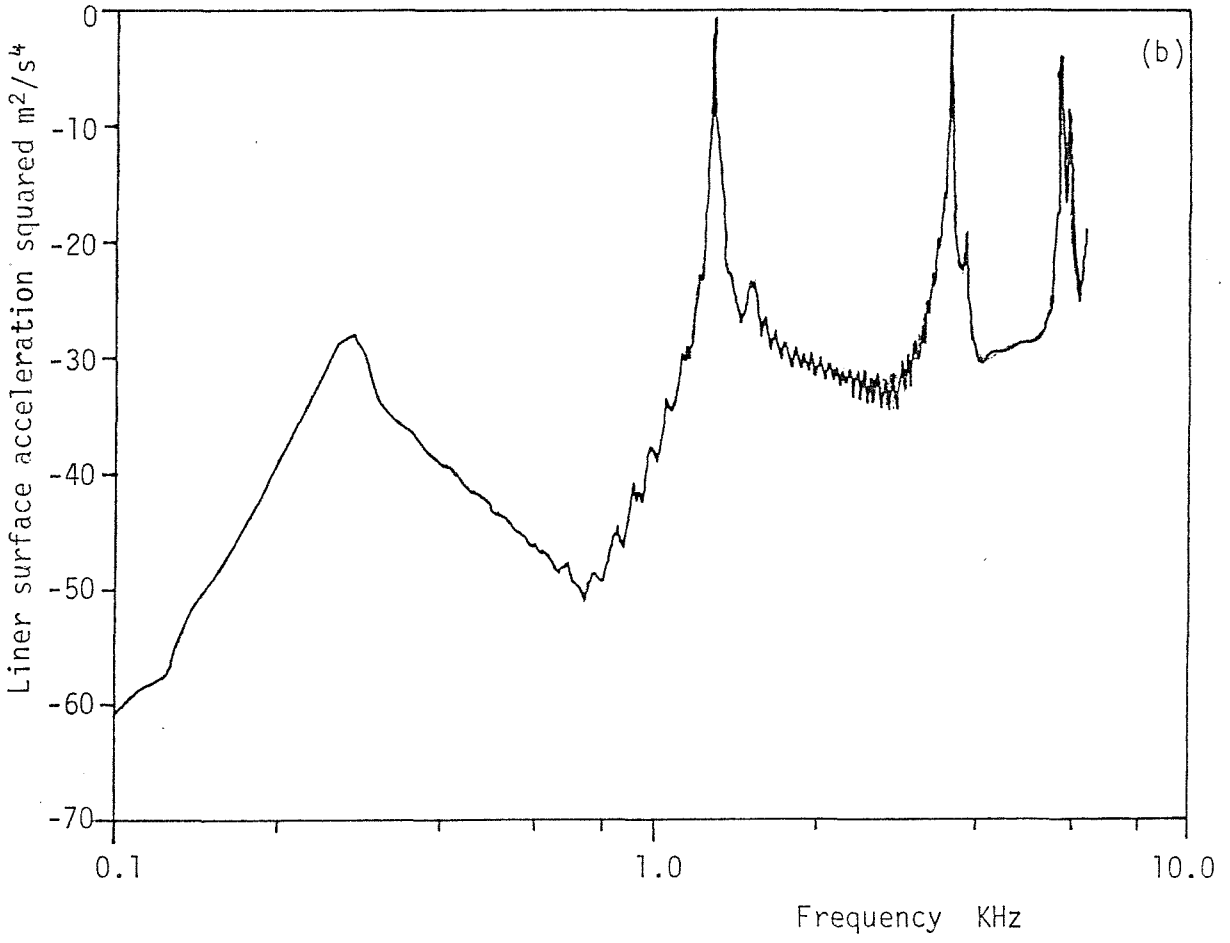
(b)
Liner surface acceleration squared m²/s⁴
0
-10
-20
-30
-40
-50
-60
-70
0.1
1.0
10.0
Frequency KHz

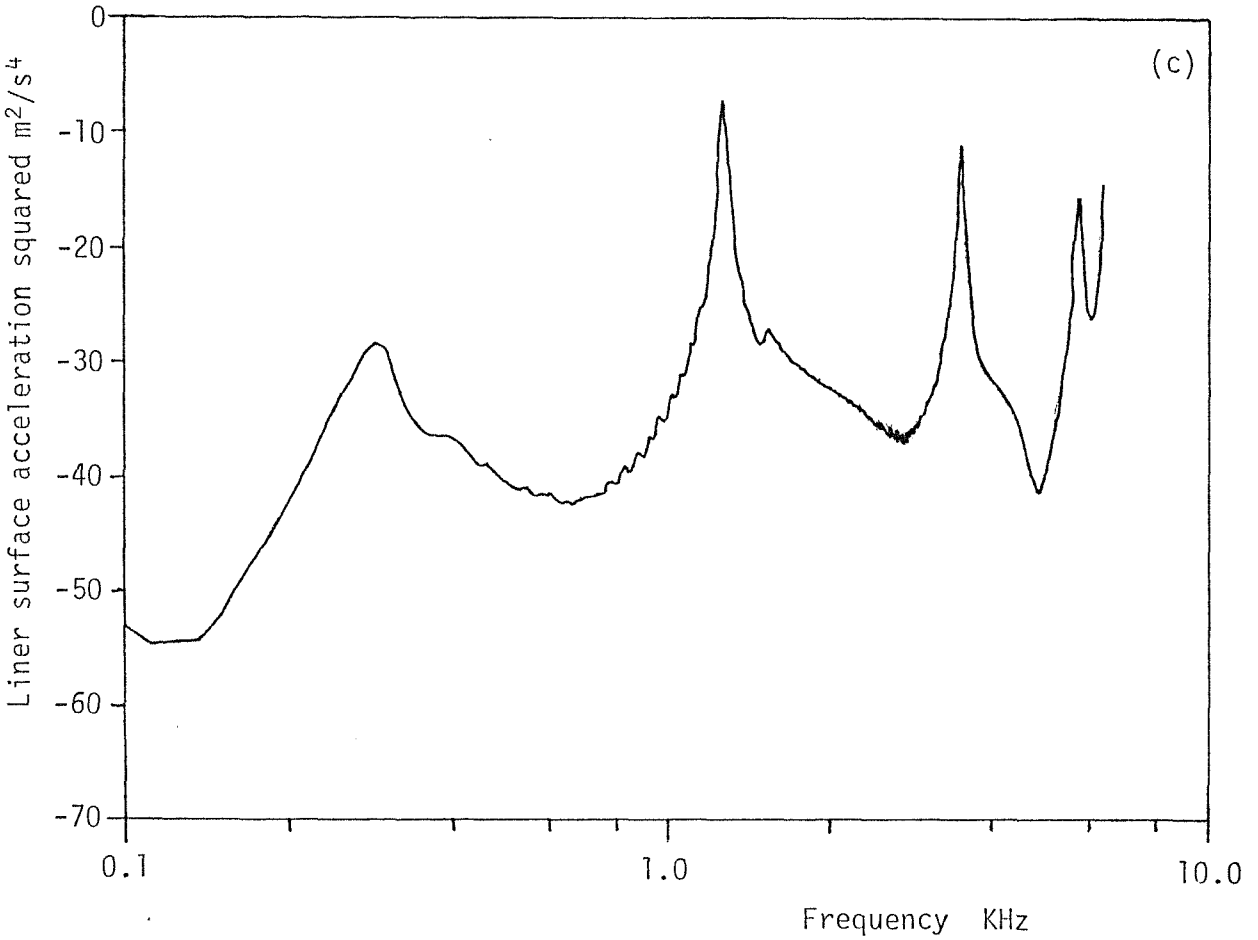

figure 8.9. Acceleration energy spectrum of the engine cylinder liner. (a) Normal liner; (b) isolated steel liner; (c) isolated damped liner.

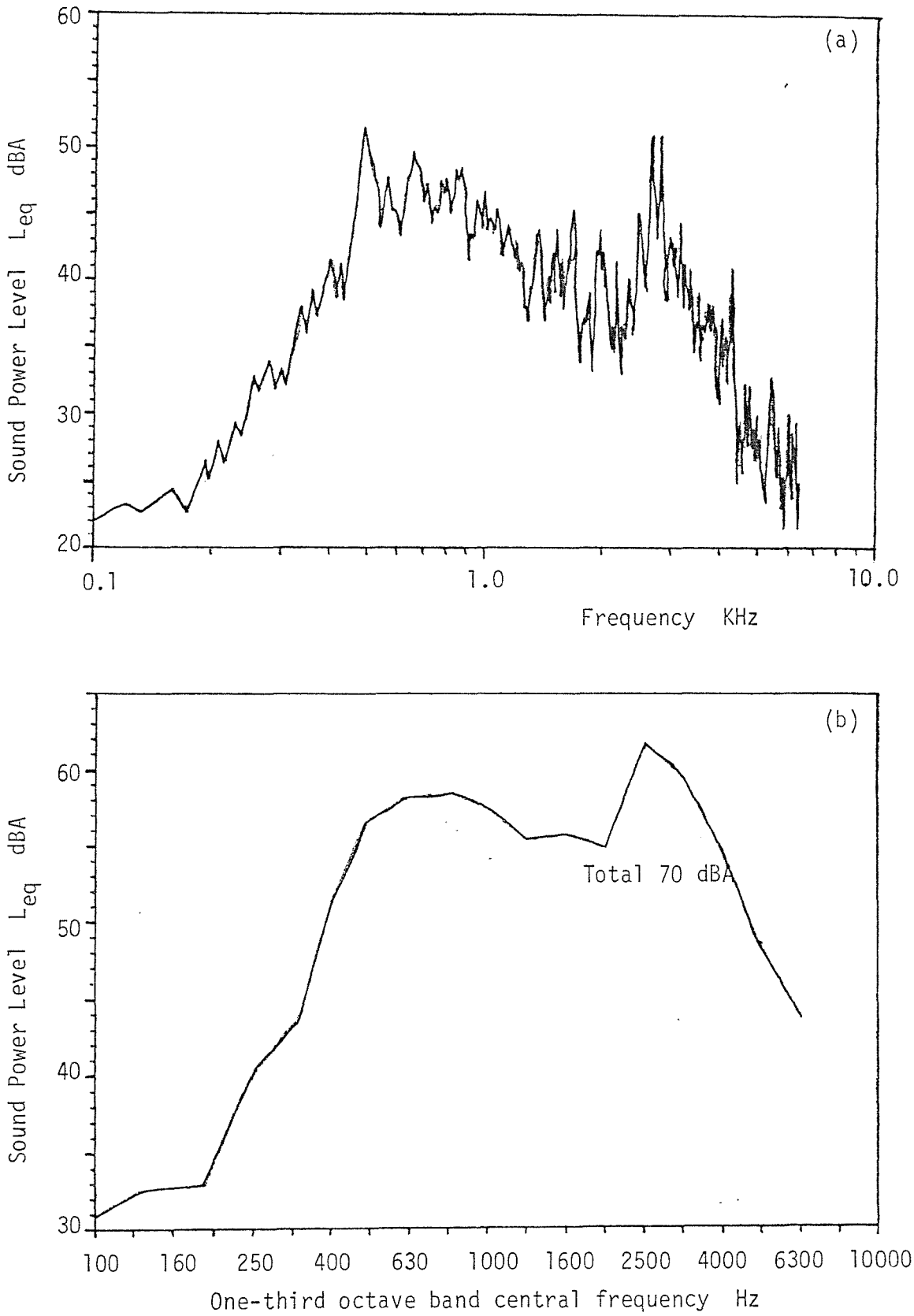

figure 8.10. Noise energy radiated from engine frame with simulated piston slap for a normal liner. This is a reproduction of figure(6.24.) with the acceleration noise due to shaker table removed. (a)Narrow band; (b) one-third octave bands.

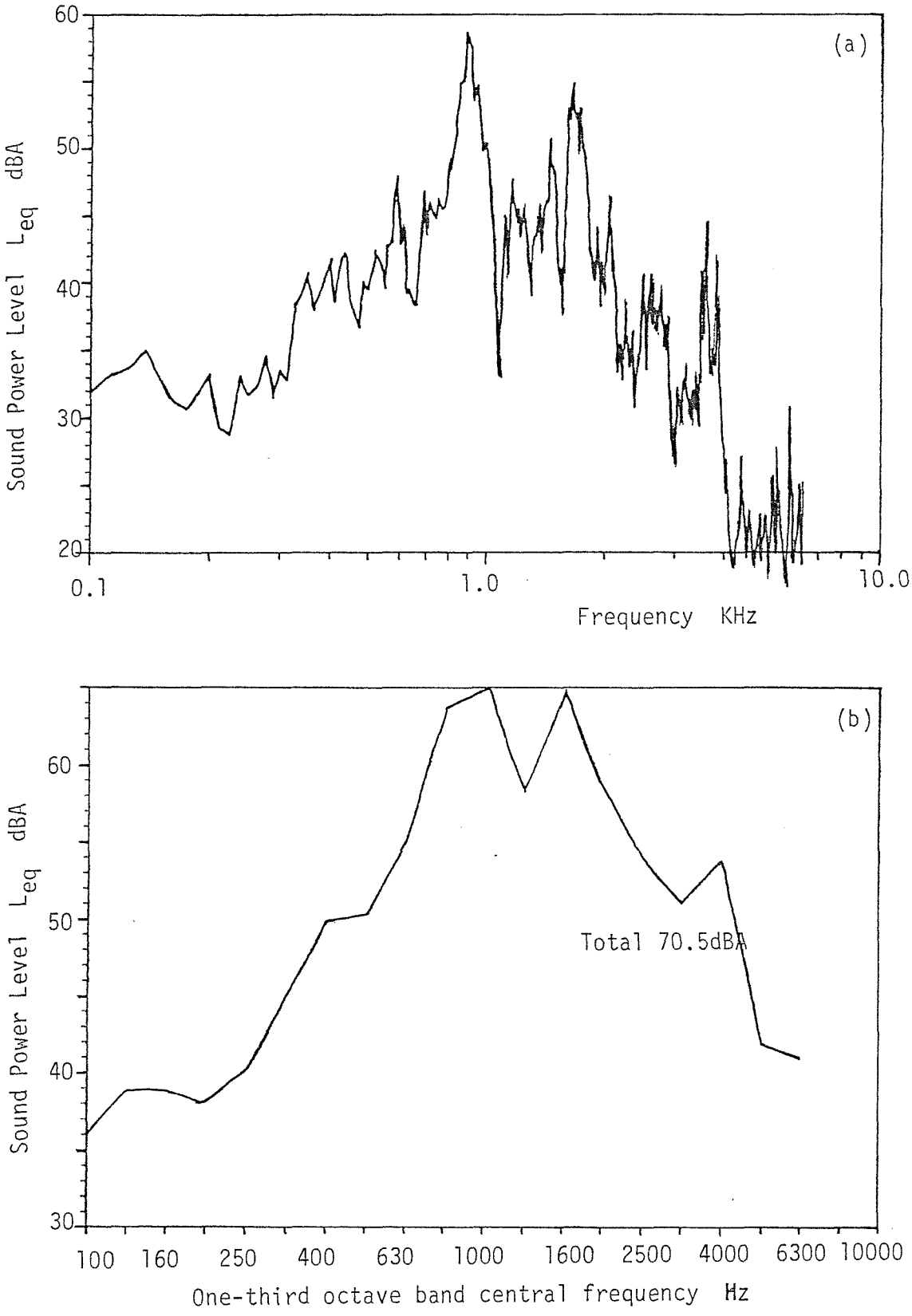

figure 8.11. Noise energy radiated with simulated piston slap for the isolated undamped liner. (a) Narrow band; (b) one-third octave bands.

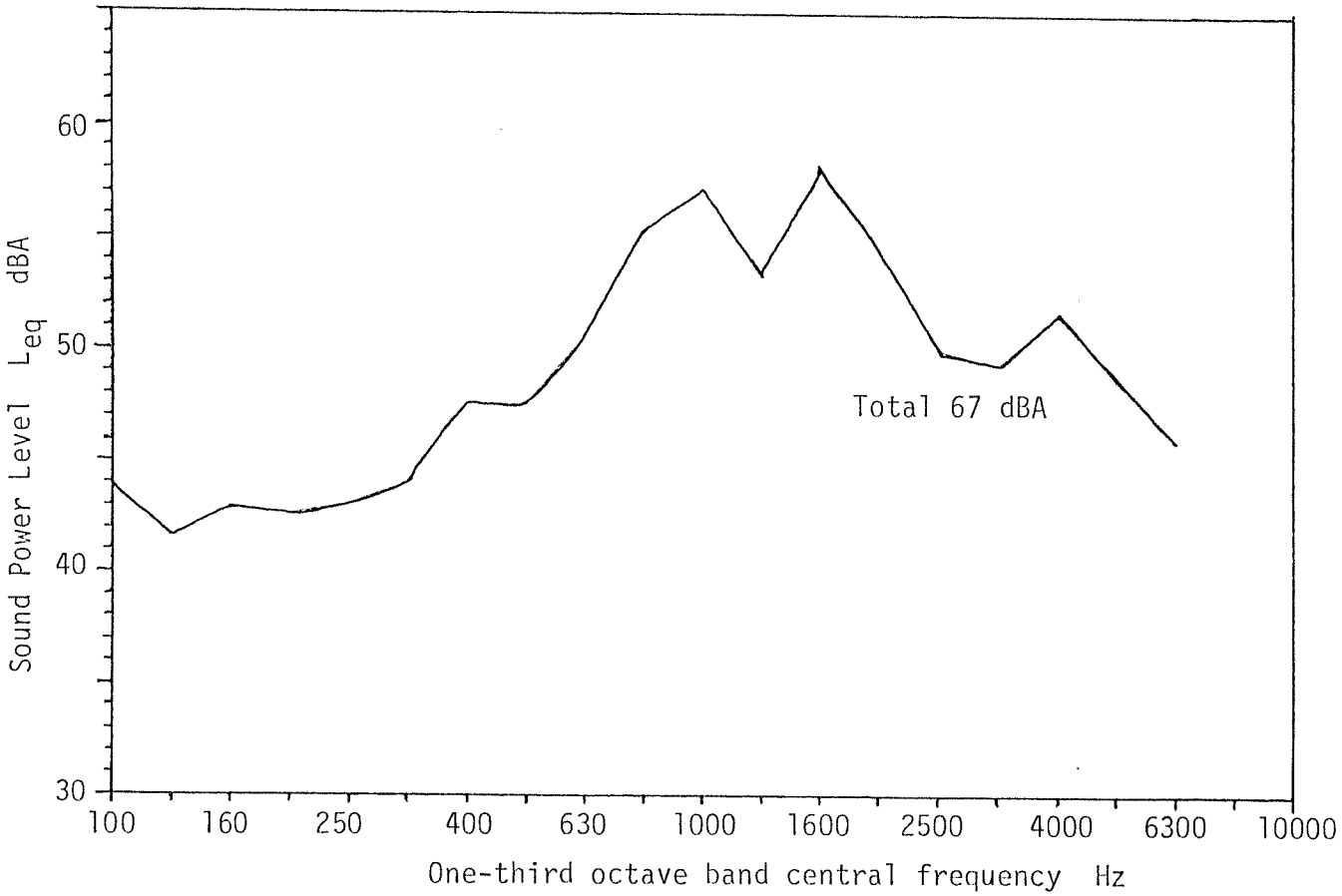

figure 8.12. Noise energy radiated from engine frame with simulated piston slap for the isolated undamped liner with screens fitted to remove the direct noise from the ringing of the liner.

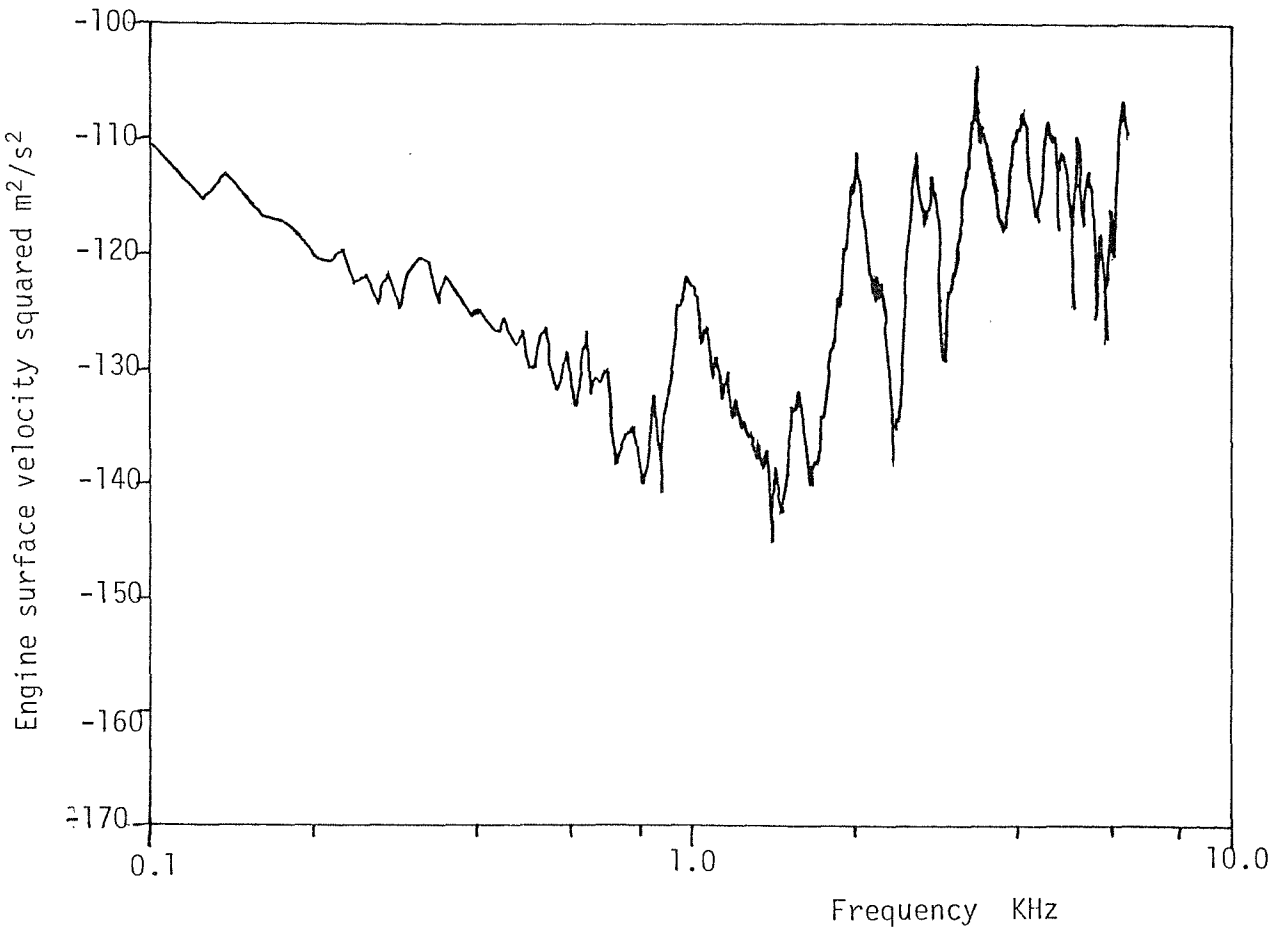

figure 8.13. Engine frame surface velocity squared with excitation of a normal liner.

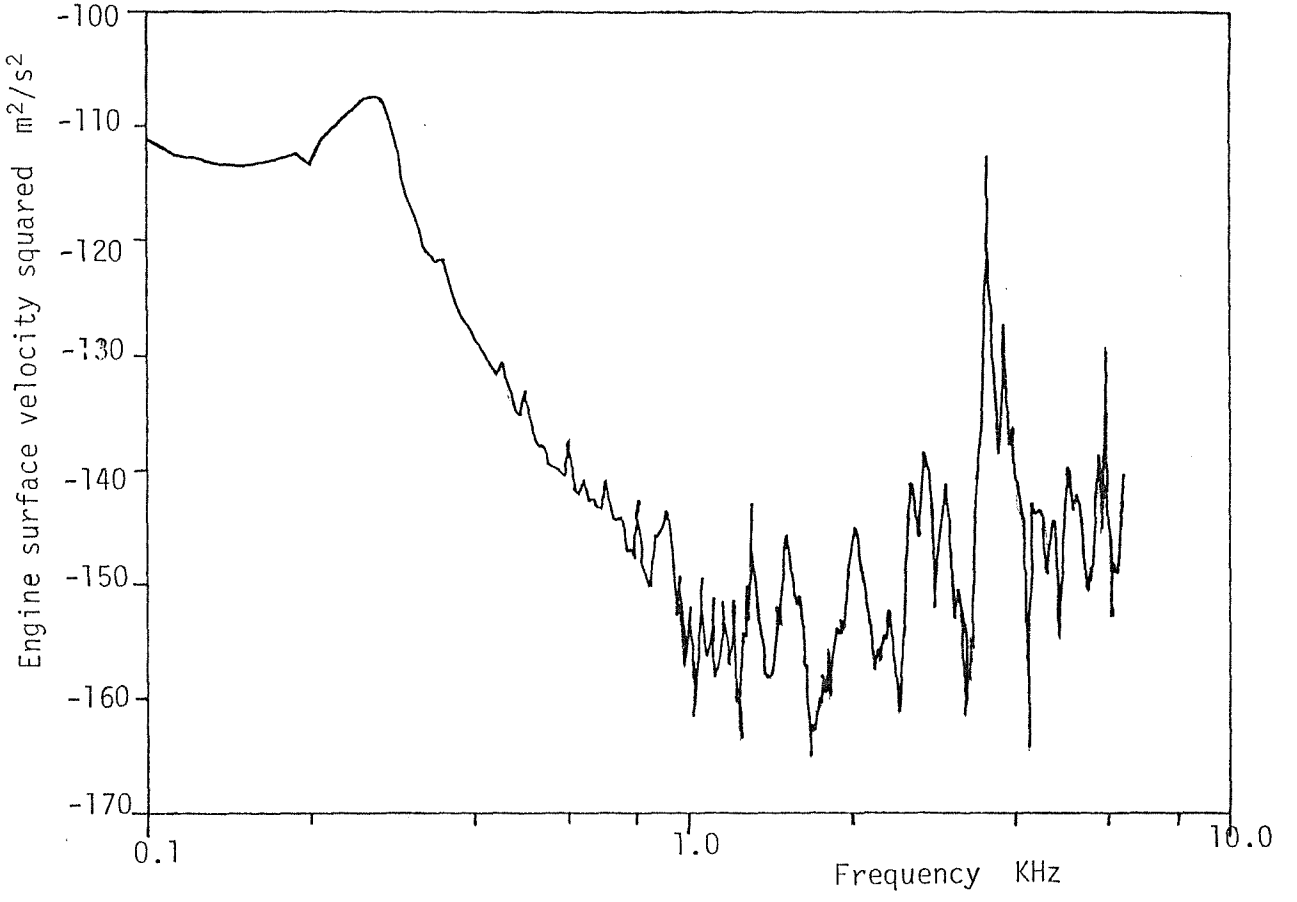

figure 8.14. Engine frame surface velocity with excitation of the undamped isolated liner.

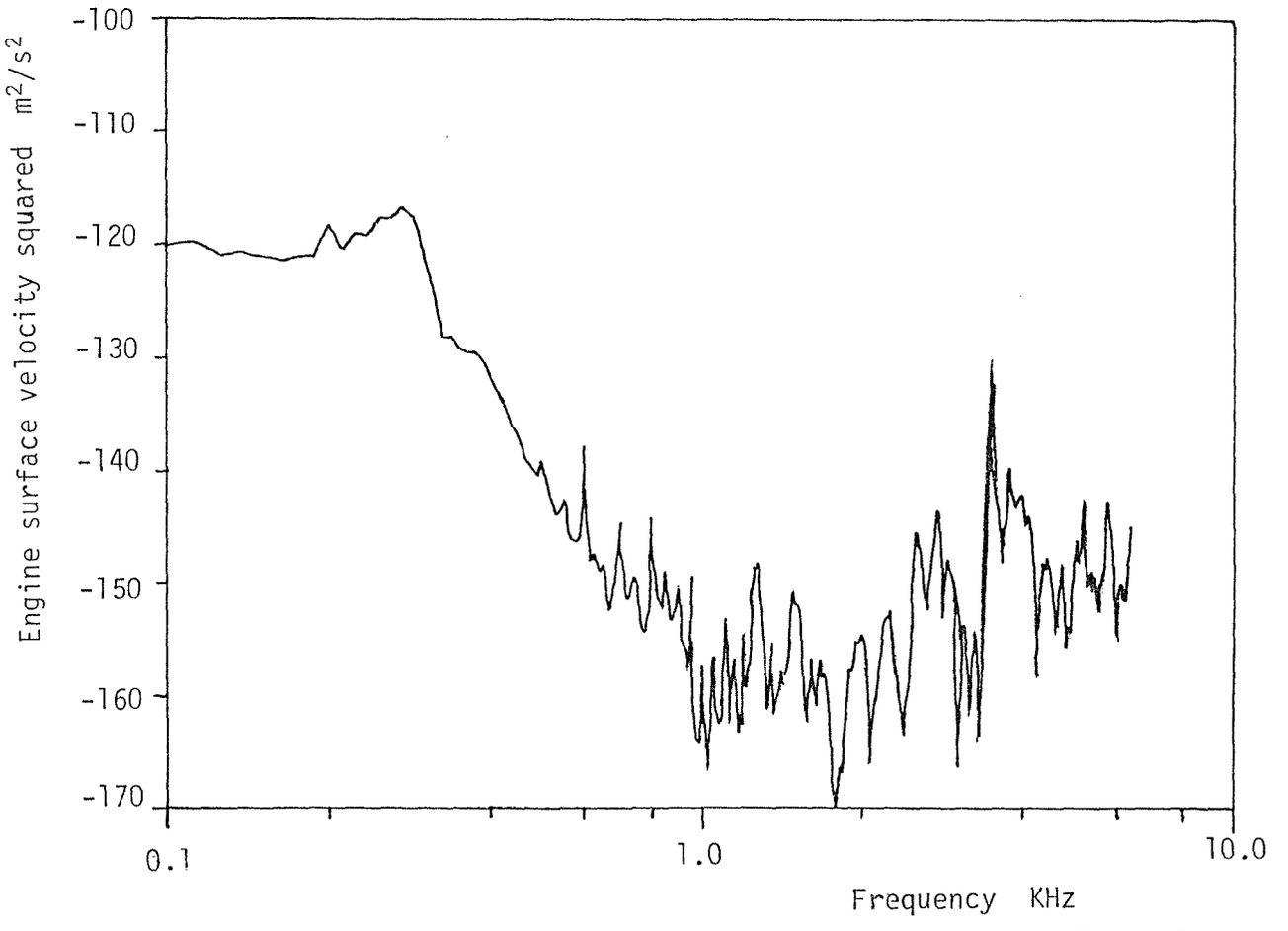

figure 8.15. Engine frame surface velocity squared for excitation of damped isolated liner.

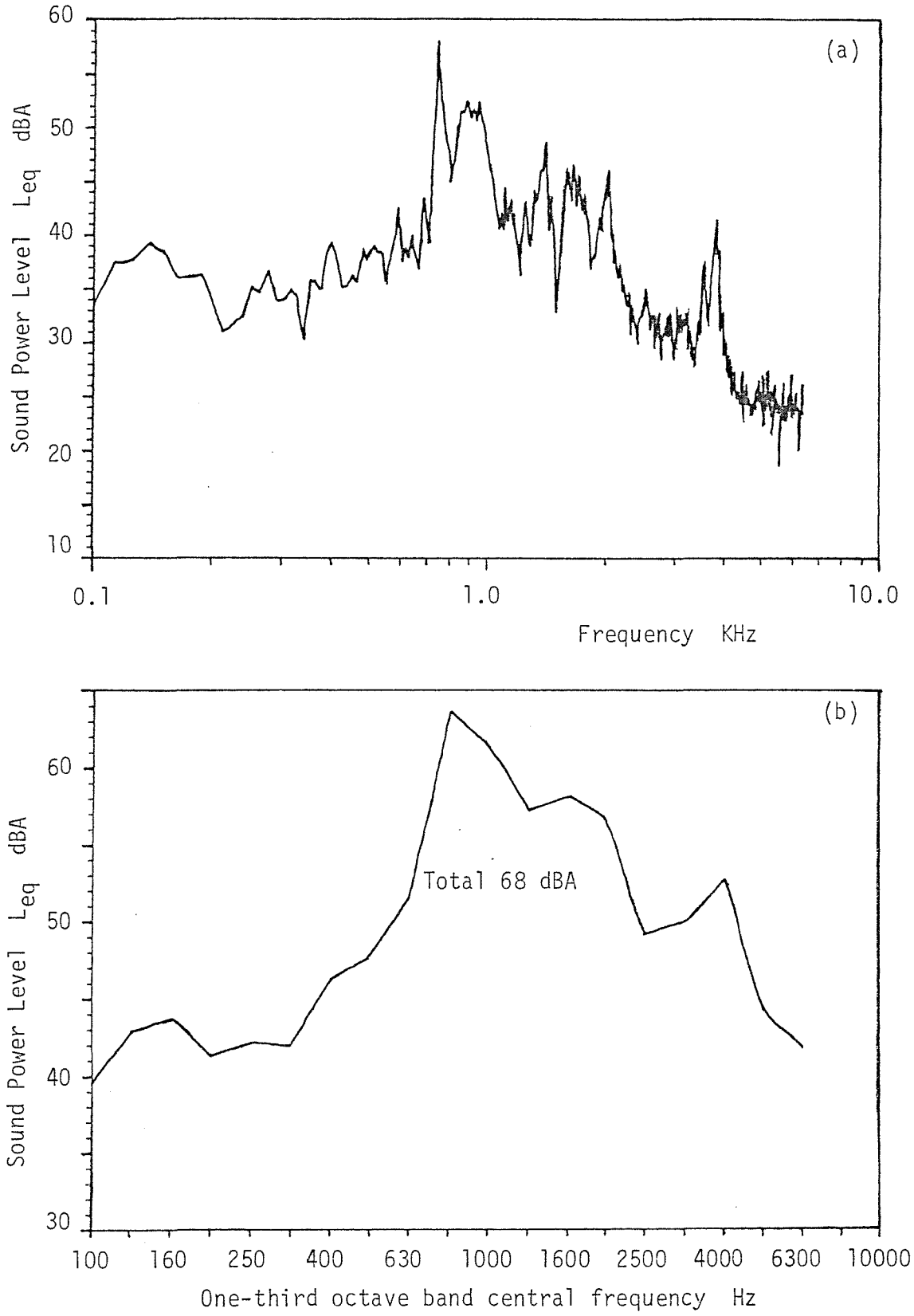

figure 8.16. Noise energy radiated with simulated piston slap for the isolated, damped liner. (a) Narrow band; (b) one-third octave band.

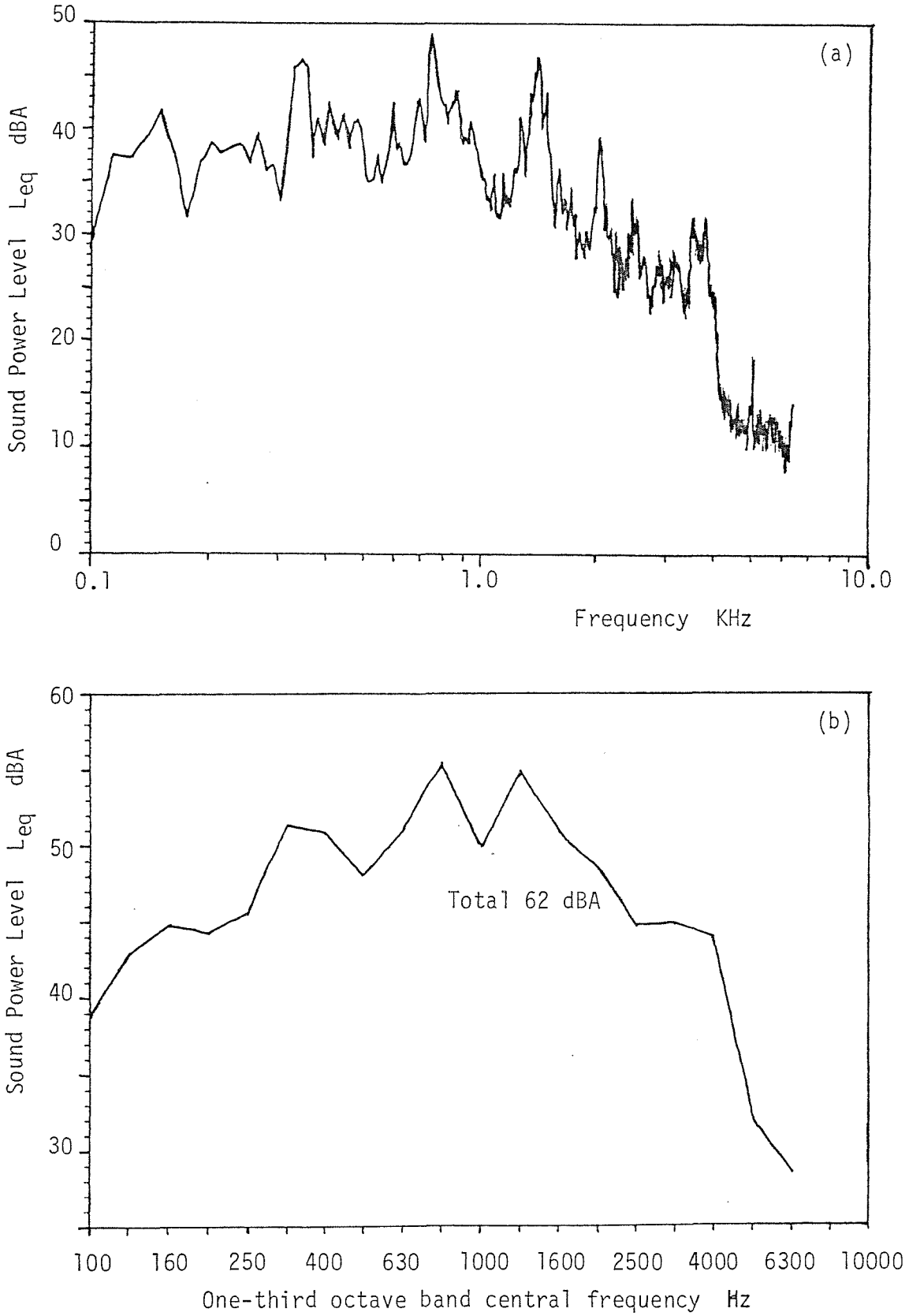

figure 8.17. Noise energy radiated from engine frame with simulated piston slap for the isolated, damped liner, with screens fitted to remove the direct noise from the ringing of the liner. (a) Narrow band; (b) one-third octave band.

APPENDIX A

APPROXIMATION FOR THE FOURIER TRANSFORM OF A PULSE

The transform of a pulse, of any shape, when plotted on a dB-log frequency scale will usally consist of a main lobe and other side lobes. The fall-off rate of the maxima of the side lobes depends on the shape of the pulse. An envelope of the transform curve can be drawn consisting of straight lines, with successive lines having a slope difference of -20 dB per frequency decade, (figure A.1).

The corner frequencies f_1, f_2, f_3, ..., f_n, and the level of each line can be computed by considering the pulse and its derivatives in the time domain. Consequently the largest fall off rate and number of corner frequencies depends on the continuity of the pulse function and its derivatives in the interval (including boundaries) between which the function is defined. Some examples follow:-

(i) A rectangular pulse - there is a discontinuity at the initial and end of the pulse. Therefore the rate of fall off for the transform is -20 dB per frequency decade and there is only one corner frequency.

(ii) Triangular pulse - the second derivative is not completely defined throughout the pulse interval, therefore the largest fall off rate is -40 dB per frequency decade.

(iii) Cosine pulse - defined by $\cos^{\alpha}x$. This is a family of pulses depending upon the parameter α; α being a positive integer. The continuity of any of the derivative functions depends on the value of α; the larger the value of α, the higher the derivative which remains continuous. Therefore, the fall-off rate is larger, the bigger the value of α, say for $\alpha = 2$ (Hanning window) the pulse has a discontinuity in the second derivative and the rate of fall-off is therefore -60 dB per frequency decade.

The corner frequencies and level of the envelope are computed

from measurements in the time domain. The Fourier transform for a function $g(t)$ which is defined in the interval $0 \leq t \leq T$ (for a rigorous analysis one must state that $g(t)$ must satisfy the Dirichlet conditions in the interval $0 \leq t \leq T$), is $G(f)$, i.e.,

$$G(f) = \int_0^T g(t)e^{-j2\pi ft}dt, \tag{A.1}$$

$G(f)$ being generally a complex quantity. Using inequalities defined for complex numbers, if z_1 and z_2 are two complex numbers, then

$$|z_1 + z_2| \leq |z_1| + |z_2| \tag{A.2}$$

i.e. ,

$$|G(f)| = \left| \int_0^T g(t)e^{-j2\pi ft}dt \right| \tag{A.3}$$

and using the inequality

$$|G(f)| \leq \int_0^T |g(t)|dt \tag{A.4}$$

or

$$|G(f)|_{max} = \int_0^T |g(t)|dt \tag{A.5}$$

The right hand side of equation (A.5) is the summation of the

magnitude of the areas enclosed by the pulse, i.e. ,

$$|G(f)|_{max} = \sum_{n} A_n \qquad (A.6)$$

where A_n are the areas under the curve (figure A.2).

It follows that, for the q'th derivative

$$|G^q(f)|_{max} = \int_o^T |g^q(t)|dt$$

$$= \sum_{n=o}^{n=q} A_n^q \qquad (A.7)$$

where A_n^q are the successive areas under the curve for the q'th derivative. Also,

$$|G^q(f)| = 2\pi f|G^{q-1}(f)| \qquad (A.8)$$

Therefore the corner frequencies are given by;

$$f_q = \frac{1}{2\pi} \frac{\sum_{n=o}^{n=q} A_n^q}{\sum_{m=o}^{m=q-1} A_m^{q-1}} \qquad (A.9)$$

For the pulse shown in figure (A.2), the second derivative has a discontinuity at $t = 0$, thus the maximum fall-off rate is -60 dB

per frequency decade. The corner frequencies are given by:

$$f_1 = \frac{A_0^1 + A_1^1}{2\pi A_0^0} \tag{A.10}$$

$$f_2 = \frac{A_0^2 + A_1^2 + A_2^2}{2\pi (A_0^1 + A_1^1)} \tag{A.11}$$

and

$$f = \frac{(A_0^3 + A_1^3 + A_2^3 + A_3^3)}{2\ (A_0^2 + A_1^2 + A_2^2)} \tag{A.12}$$

The levels of the lines are given by equation (A.7). From the above equations it follows that the first corner frequency, f_1, depends on the maximum slope per unit of the pulse amplitude, and f_2, the second corner frequency, depends on the change of slope per unit amplitude of the pulse, etc. Thus the sharper the rise in the pulse the higher is the first corner frequency, and f_2 increases the larger the change in slope.

This method gives a good approximation for the Fourier transform of any pulse or its derivatives. The accuracy of the approximation depends on the order of the derivative. The approximate transform over-estimates the actual transform, and the overestimation increases as the transform of a higher derivative is computed. Comparing this method with the initial value and final value theorems; from the final value theorem, which gives the asymptote of the curve at low frequencies, there is no difference between the two; from the initial value theorem, which gives the asymptote at high frequencies, the value in this case is different. The initial value theorem gives;

$$\lim_{t\to 0} |g^q(t)| = \lim_{f\to\infty} |G^{q+1}(f)| \qquad (A.13)$$

This is the maximum level for $|G^{q+1}(f)|$ against frequency, that is $|G^{q+1}(f)|_{max}$, but from the approximation method

$$|G^{q+1}(f)|_{max} = \sum_{n=o}^{n=q} A_n^{q+1} \qquad (A.14)$$

and from the initial value theorem,

$$|G^{q+1}(f)|_{max} = A_o^{q+1} \qquad (A.15)$$

The error will be of about 3 dB maximum. The initial value and final value theorems will not give a good approximation to the actual transform near the first corner frequency, which for most pulses will lie in a frequency range of maximum radiated noise energy.

The Fourier transform of the first derivative of the pulse, by the approximation method, has a flat portion between the first and second corner frequencies. If the analysis carried out is within this frequency range, it is very convenient to assume a constant spectrum, the magnitude of which corresponds to the amplitude of the pulse. However, this frequency range is limited even for the very short of pulses.

Considering a typical force pulse for a mass impacting a plate:

$$\begin{aligned} f(t) &= 0, && t < 0,\ t > \tau \\ &= X_o e^{-ht} \sin\left(\frac{\pi t}{\tau}\right), && 0 \leq t \leq \tau \end{aligned} \qquad (A.16)$$

where h is a constant depending on the plate mechanical impedance and Young's modulus;

X_o is another constant depending on the pulse duration, velocity of impact and Young's modulus;

τ is the pulse duration.

The curves for $f(t)/X_o$, $\dot{f}(t)/X_o$, $\int_o^\tau f(t)/X_o \, dt$ are given in figure (A.3). $f(t)$ has a discontinuity at $t = 0$, thus the maximum fall-off rate for $|\dot{F}(f)|^2$ is -20 dB per frequency decade. Using a value of $h = 212.1 \ s^{-1}$, and a pulse duration of 2 ms, the two corner frequencies are: $f_1 = 251$ Hz and $f_2 = 511$ Hz and $|\dot{F}(f)|^2_{max} = 4.3$ dB. The Fourier transform obtained using an FFT programme, with sampling rate of 51200 samples per second and the number of samples being 8192 points, is compared with the approximation transform in figure (A.3(d)).

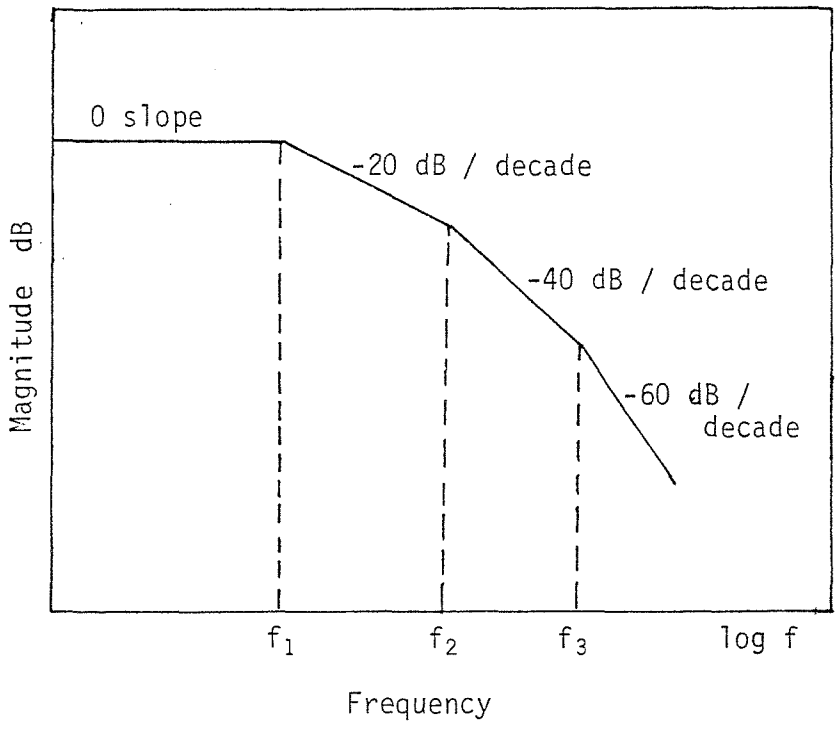

figure A.1. Envelope for the fourier transform of a pulse.

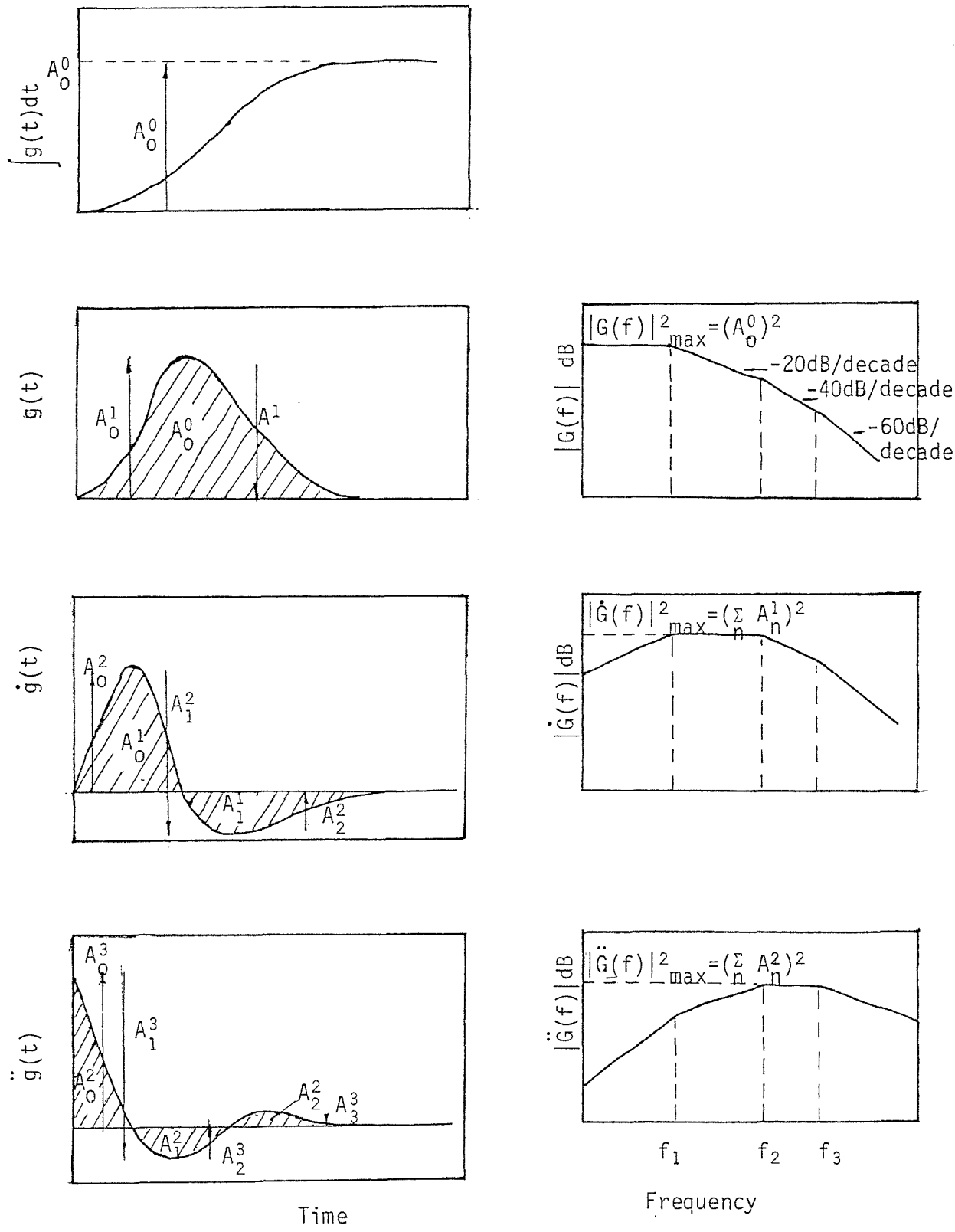

figure A.2. Relation between envelope and measurements in the time domain.

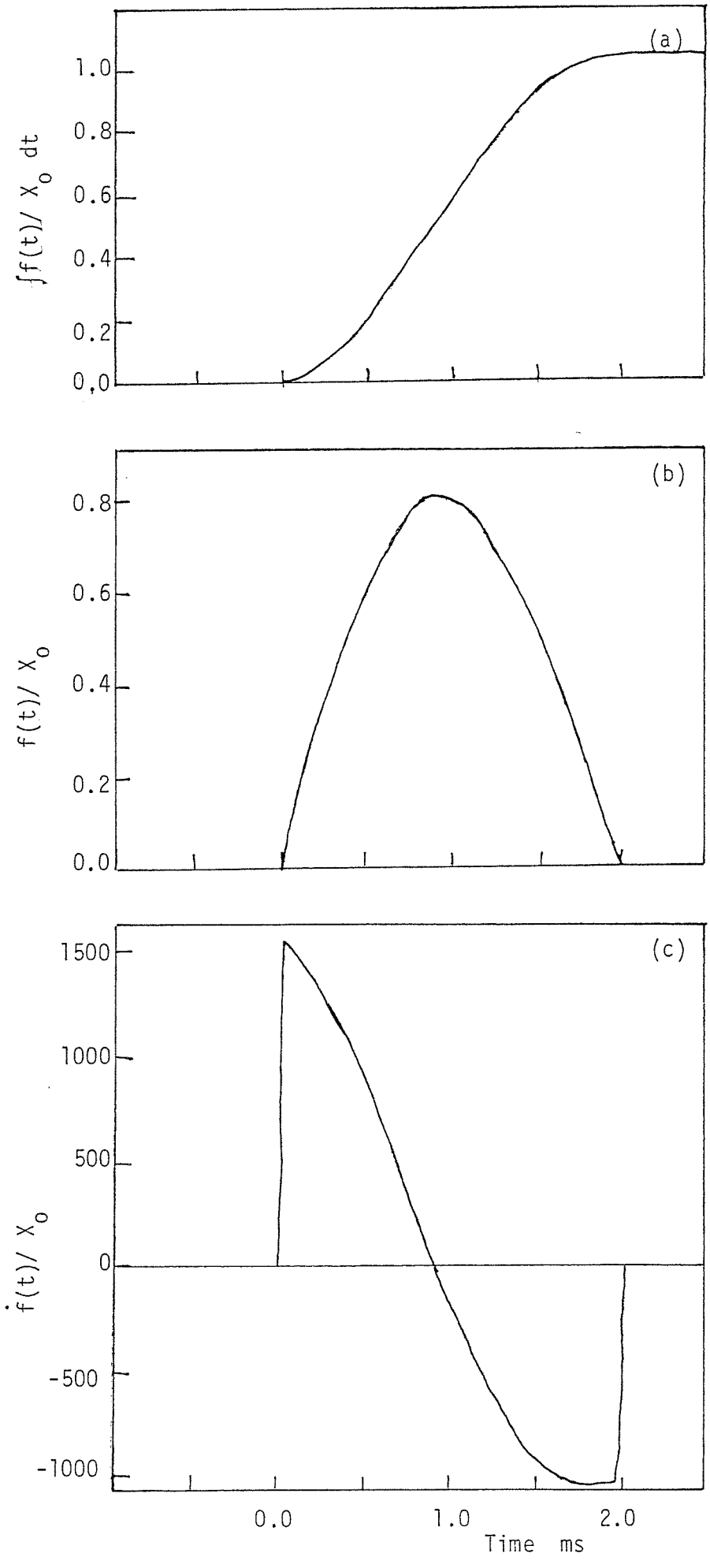
(a)
1.0
0.8
0.6
0.4
0.2
0.0
∫f(t)/ X_o dt
(b)
0.8
0.6
0.4
0.2
0.0
f(t)/ X_o
(c)
1500
1000
500
0
-500
-1000
ḟ(t)/ X_o
0.0
1.0
2.0
Time ms

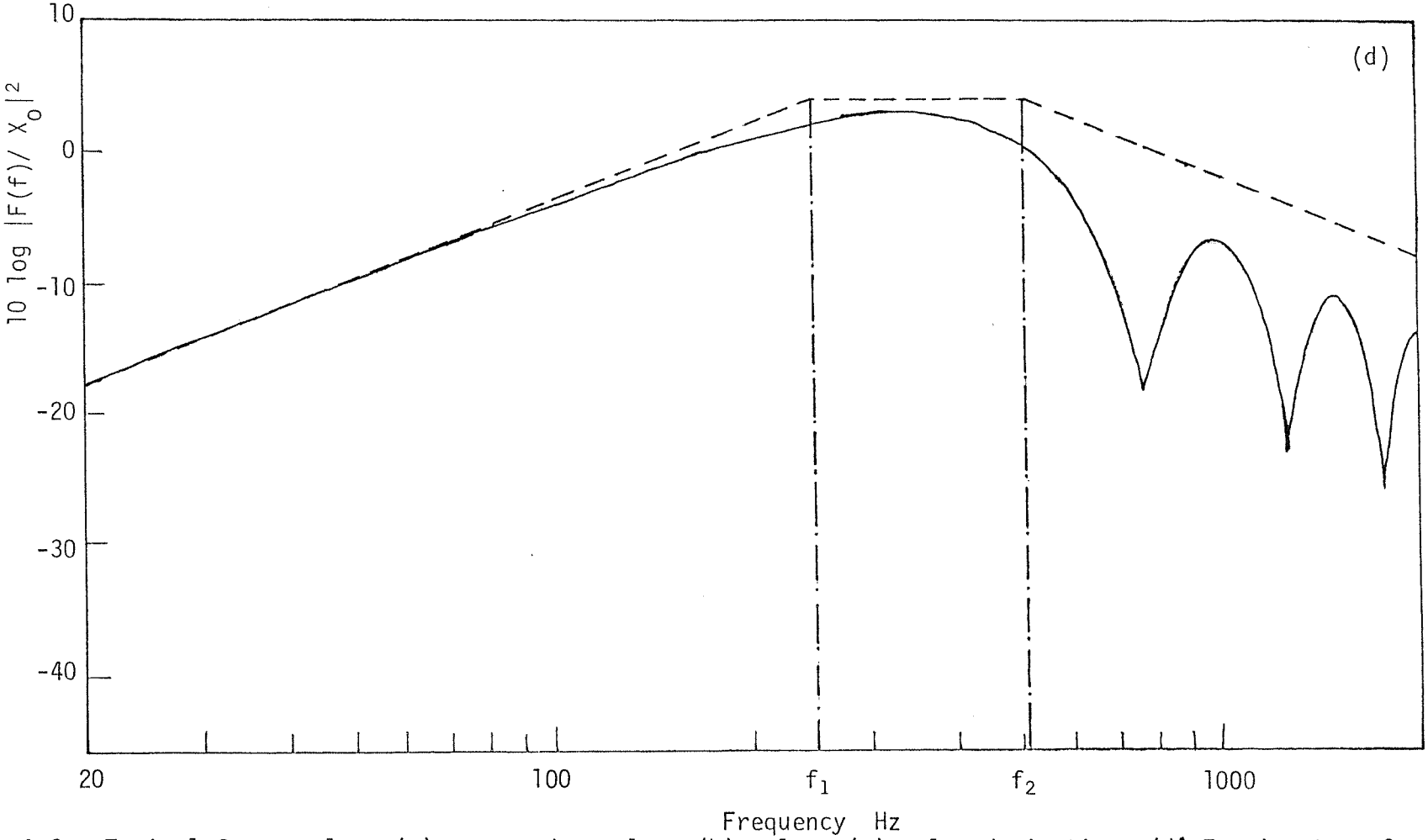

figure A.3. Typical force pulse: (a) area under pulse; (b) pulse; (c) pulse derivative; (d) Fourier transform of pulse. ——, Exact; ----, by approximate method.

APPENDIX B

COMPUTER PROGRAMMES TO EVALUATE CANTILEVER BEAM RESPONSE

B. 1. Imaginary part of response: $|V(f) / \dot{F}(f)|$

SO INPUT FILE (NAME = BEAM)

```
-----
      PROGRAM BEAM
      DIMENSION BMDBLOG (5000), FREQ (5000)
      DIMENSION X (5002), Y (5002)
      COMPLEX CWN, ARG, RESP, VAL
      INTEGER XTITL (5), YTITL (6), GTITL (6)
      DATA XTITL / 13H FREQUENCY HZ /
      DATA YTITL / 17H LOG IM(V/F) DB /
      DATA GTITL / 18H CANTILEVER BEAM 1 /
      CALL PLOTS (0, 0, 10)
      READ (8, 10) RHO, AREA, ALEN, E, SHON, QITA
 10   FORMAT ( 1PE 10.4, E11.4, 0PF6.0, 1PE9.2, E11.4, E9.2)
      L=0
      FACTOR = ((E*SHON)/(RHO*AREA))**0.25
      DO 12 I = 1, 5000
      FREQ (I) = 0.05*I
      W = FREQ (I)*2*3.1416
      SW = DSQRT (W)
      Q04 = QITA/4
      VAL = CMPLX (1.0, -Q04)
      CWN = (SW/FACTOR)*VAL
      ARG = CWN*ALEN
      RESP = (CWN/(W**2*RHO*AREA))*(((CDSINH(ARG)*CDCOS(ARG))-
     1  (CDCOSH(ARG)*CDSIN(ARG)))/((CDCOSH(ARG)*
     2  CDCOS(ARG))+1))
      RESPIM = REAL(RESP)*(-1)
      RESPRL = IMAG(RESP)
      BMDBLOG(I) = (LOG 10 (RESPRL))*10
```

```
      L = L + 1
      IF (L-1) 22, 16, 22
   22 IF (L-41) 18, 24, 24
   24 L = 1
   16 WRITE (9, 20)
   20 FORMAT (73 H 1      FREQUENCY HZ   REAL RESPONSE    IMAG
    1 RESPONSE    DBLOG (IMAG RESPONSE) 111)
   18 CONTINUE
      WRITE (9, 14)I, FREQ(I), RESPRL, RESPIM, BMDBLOG(I)
   14 FORMAT (1H, I4, F10.2, 1PE17.3, E16.3, 0PF18.3)
      X(I) = FREQ(I)
      Y(I) = BMDBLOG(I)
   12 CONTINUE
      CALL PLOT(0.0, 4.0, -3)
      CALL SCALG (X, 20.0, 5000, 1)
      CALL LGAXS ( 0.0, 0.0, XTITL, -13, 20.0, 0.0, X(5001), X(5002))
      CALL AXIS (0.0, 0.0, YTITL, 17, 20.0, 90.0, -80.0, 5.0)
      Y(5001) = 80.0
      Y(5002) = 5.0
      CALL LGLIN (X, Y, 5000, 1, 0, 17, -1)
      CALL SYMBOL (2.0, 10.0, 0.42, GTITL, 0.0, 18)
      CALL PLOT (30.0, 0.0, 999)
      STOP
      END
+++++
SONEWFILE (NAME = BEAMPLOT)
SOSAVEFILE (BEAMPLOT)
SOASSIGNFILE (LNAME = ICL9LF 10, NAME = BEAMPLOT, ACCess = W)
SOLP (LNAME = ICL9F9, DESC = *STDFORT)
SOASSIGNFILE (NAME = *STDADF, LNAME = ICL9LF8)
SOFORT (INPUT = BEAM, LIBRARIES = CALCOMPF1, DEF = FALSE)
-----
8.1000E+03 1.9200E-04 0.944 2.19E+11 5.7600E-10 1.99E-3
+++++
```

```
SOPLOT (NAME = BEAMPLOT)
ENDJOB
+++++
```

B. 2. Spatial average transfer admittance: $\langle|V(f)|^2\rangle / F(f)^2$

```
SOINPUTFILE (NAME = BEAM2)
-----
      PROGRAM BEAM2
      DIMENSION SAA(5000), FREQ(5000), FACTOR(5000)
      DIMENSION X(5002), Y(5002)
      INTEGER XTITL(5), YTITL(10), GTITL(6)
      COMPLEX ARG, CWN, VAL
      DATA XTITL / 13H FREQUENCY HZ /
      DATA YTITL / 31H (AV. TRANSFER ADMITTANCE)**2 DB /
      DATA GTITL / 16H CANTILEVER BEAM /
      CALL PLOTS (0, 0, 14)
      READ (12, 20) RHO, AREA, ALEN, E, SHON, QITA
      READ (12, 34) N
20    FORMAT(1PE10.4, E11.4, 0PF6.0, 1PE9.2, E11.4, E9.2)
34    FORMAT (I3)
      L = 0
      CONST = ((E*SHON)/(RHO*AREA))**0.25
      Q04 = QITA / 4
      DO 22 I = 1, 5000
      FREQ(I) = 0.05  *I
      W = FREQ(I)*2*3.1416
      SW = DSQRT(W)
      VAL = CMPLX(1.0, -Q04)
      CWN = (SW/CONST)*VAL
      ARG = CWN*ALEN
      SUM-= 0.0
      DO 24 J = 1,N
      SUM = SUM+(ABS((CDCOSH(ARG*J/N)-CDCOS(ARG*J/N))*(CDSINH(ARG)+
```

```
     1  CDSIN(ARG))-(CDSINH(ARG*J/N)-CDSIN(ARG*J/N))*(CDCOS(ARG)+
     2  CDCOSH(ARG))))**2
    24  CONTINUE
        AHOD = ((ABS(CWN/(2.0*W*RHO*AREA*(1+CDCOSH(ARG)*CDCOS(ARG)))))**2
        FACTOR(I) = AHOD*SUM
        SAA(I) = (LOG10(FACTOR(I)))*10
        L = L+1
        IF (L-1) 36, 26, 26
    36  IF (L-41) 28, 38, 38
    38  L = 1
    26  WRITE (13, 30)
    30  FORMAT(63H I    FREQUENCY HZ   AVERAGE ADMITTANCE   10LOG(AVRG ADM
     1  ITTANCE) 111)
    28  WRITE (13, 32) I, FREQ(I), FACTOR(I), SAA(I)
    32  FORMAT(1H, I4, F9.2, 1PE20.4, E23.4)
        X(I) = FREQ(I)
        Y(I) = SAA(I)
        CALL PLOT (0.0, 4.0, -3)
        CALL SCALG (X, 20.0, 5000, 1)
        CALL LGAXS (0.0, 0.0, XTITL, -13, 20.0, 0.0, X(5001), X(5002))
        CALL AXIS (0.0, 0.0, YTITL, 31, 20.0, 90.0, -90.0, 5.0)
        Y(5001) = -90.0
        Y(5002) = 5.0
        CALL LGLIN(X, Y, 5000, 1, 0, 17, -1)
        CALL SYMBOL (2.0, 10.0, 0.42, GTITL, 0.0, 16)
        CALL PLOT (30.0, 0.0, 999)
        STOP
        END
+++++
SONEWFILE(NAME = BEAMPLOT 2)
SOSAVEFILE (NAME = BEAMPLOT 2)
SOASSIGNFILE (LNAME = ICL9LF14, NAME = BEAMPLOT 2, ACCESS = W)
SOLP ( LNAME = ICL9LF13, DESC = *STDFORT)
SOASSIGNFILE (NAME = *STDADF, LNAME = ICL9LF12)
SOFORT (INPUT = BEAM2, LIBRARIES = CALCOMPF1, DEF = FALSE)
-----
```

```
8.1000E+03 1.9200E-04 0.944 2.19E+11 5.7600E-10 2.00E-3
40
+++++
SOPLOT (NAME = BEAMPLOT 2)
ENDJOB
*****
```

BIBLIOGRAPHY

1. CREMER, L. and HECKL, M. (1973) Structure-borne Sound. Heidelberg, Berlin, New York, Springer-Verlag.

2. BERANEK, L.L. (1971) Noise and Vibration Control, Chapter 11. McGraw Hill, New York.

3. MAIDANIK, G. (1962) Journal of the Acoustic Society of America 34, 802-826. Response of Ribbed Panels to Reverberant Acoustic Fields.

4. MORSE, P.M. and INGARD, K.U. (1968) Theoretical Acoustics. McGraw Hill, New York.

5. EVENSEN, H.A. (1980) Journal of Sound and Vibration 68, 451-463. A Fundamental Relationship between Force Waveform and the Sound Radiated from a Power Press during Blanking or Piercing.

6. BENEDETTO, G., SPAGNOLO, R. and MARINGELLI, M. (1980) Journal of Sound and Vibration 69, 157-161. Transient Sound from the Impact of a Sphere on a thin square Plate.

7. BOLGOV, V.M. and NIKIFOROV, A.S. (1980) Soviet Physics Acoustics 26, May-June. Transient impact-excited flexural Vibrations of an infinite Plate.

8. ENDO, M., NISHI, S., NAKAGAWA, M. and SAKATA, M. (1981) Journal of Sound and Vibration 75, 285-302. Sound Radiation from a Circular Cylinder subjected to Elastic Collision by a Sphere.

9. HOLMER, C.I. and LAGACE, A. (1972) American Industrial Hygiene Association Journal, January. Effect of Structural Damping on the Sound Radiated from impacted Structures.

10. GOYDER, H.G.D. and WHITE, R.G. (1980) Journal of Sound and Vibration 68, 59-117. Vibrational Power Flow from Machines into built up Structures. Parts I, II, III.

11. PINNINGTON, R.J. and WHITE, R.G. (1981) Journal of Sound and Vibration 75, 179-197. PowerFlow through Machine isolators to Resonant and Non-resonant Beams.

12. SKUDRZYK, E. (1980) Journal of the Acoustical Society of America 67. The Mean-value Method of Predicting the Dynamic Response of Complex Vibrators.

13. RICHARDS, E.J., WESTCOTT, M. and JEYAPALAN, R.K. (1979) Journal of Sound and Vibration 62, 547-575. On the Prediction of Impact Noise I: Acceleration Noise .

14. RICHARDS, E.J., WESTCOTT, M., and JEYAPALAN, R.K. (1979) Journal of Sound and Vibration 65, 419-451. On the Prediction of Impact Noise II: Ringing Noise.

15. RICHARDS, E.J. (1981) Journal of Sound and Vibration 76, 187-232. On the Prediction of Impact Noise III: Energy Accountancy in Industrial Machines.

16. RICHARDS, E.J., LENZI, A. and CUSCHIERI, J.M. (1983) Journal of Sound and Vibration 90. On the Prediction of Impact Noise VI: The Frequency Distribution of Acceleration Noise.

17. NAYAK, P.R. (1970) Journal of the Acoustical Society of America 47. Line Admittance of Infinite Isotropic Fluid Loaded Plates.

18. SKUDRZYK, E. (1968) Simple and Complex Vibratory Systems. Pensylvania State University Press.

19. IRIE, T., YAMADA, G. and KOBAYASHI, Y. (1982) Journal of the Acoustical Society of America 71. The Steady-state Response of Internally Damped Double Beam System Interconnected by Several Springs.

20. CLARKSON, B.L., RANKY,M.F. and ABOUTORABIAN, M.T. (1982) Institute of Sound and Vibration Research, Technical Report 5. Modal Density of Honeycomb Plates.

21. HECKL, M. (1980) DAGA'80 VDE-VERLAG, 827-830. Eine Einfache Methode zur Abschätzung der Mechanischen Impedanz.

22. RICHARDS, E.J., CARR, I. and WESTCOTT, M. (1983) Journal of Sound and Vibration (to be publised) On the Prediction of Impact Noise V: The Noise from Drop Hammers.

23. CUSCHIERI, J.M. and RICHARDS, E.J. (1983) Journal of Sound and Vibration 86, 319-342. On the Prediction of Impact Noise IV: Estimation of Noise Energy Radiated by Impact Excitation of a Structure

24. EWINS, D.J. and GRIFFIN, J. (1981) Journal of Sound and Vibration 78, 197-222. A State of the art Assessment of Mobility Measurement Techniques - Results for the Mid- Range Structures (30-3000 Hz).

25. KINSLER, L.E. and FREY, A.R. 1962 Fundamentals of Acoustics, 2nd Ed. New York, Wiley and Son.

26. WHEELER, P.D. (1980) Noise and Vibration Advanced Course Notes Chapter 26. Southampton, Institute of Sound and Vibration Research.

27. WESTCOTT, M.E. (1980) M.Phil. Thesis, University of Southampton, Institute of Sound and Vibration Research. Impact Noise from Drop Hammer - an Experimental Investigation.

28. LYON, R.H. (1976) Proceedings for the EPA - University Noise Seminar, 153-157. Designing Diesel Engines for Reduced Noise.

29. REINHART, E. and CROCKER, M.J. (1982) Noise Control Engineering, May-June 84-92. Source Identification on a Diesel Engine using Acoustic Intensity Measurements.

30. THOMPSON, J.W. (1973) Society of Automotive Engineers, Paper number 730713. An Engineering Approach to Diesel Truck Noise Reduction.

31. RUSSELL, M.F. (1972) Society of Automotive Engineers, Paper number 720135. Reduction of noise Emissions from Diesel Engine Surfaces.

32. RUSSELL, M.F. (1979), Lucas Engineering Review 7. Automotive Diesel Engine Analysis, Diagnosis and Control.

33. LALOR, N. (1980) Society of Automotive Engineers, Paper number 790364. Computer Optimised Design of Engine Structures for low Noise.

34. PRIEDE, T., GROVER, E.C. and LALOR, N. (1969) Society of Automotive Engineers, Paper number 690450. Relation between Noise and Basic Structural Vibration of Diesel Engines.

35. AUSTEN, A.E.W. and PRIEDE, T. (1965) Society of Automotive Engineers, Paper number 1000A. Noise of Automotive Diesel Engines: Its Causes and Reductions.

36. ROORDA, J. (1980) Solid Mechanics Archives 5. Experiments in Feedback Control of Structures.

37. SANKAR, S. and GUNTUR, R.R. Shock and Vibration Bulletin 51. Pneumatic Vibration control using Active Force Generators.

38. STIMPSON, G. (1982) Proceedings of the Institute of Acoustics, Autumn Conference F3. Damping and Cancellation Devices to Reduce Punch Press Noise.

39. HARRIS, F.J. (1978) Proceedings of the Institute of Electrical and Electronic Engineers 66, 51-83. The Use of Windows for Harmonic Analysis with the Discrete Fourier Transform.

40. MEIER-DORNBERG, K.E. (1969) VDI Verichte 136 Die Bescheibung von Stossvergangen Durch ihre Zeitsfunctionen, Fourier und Shockspectrum.